FULLY OVERLAPPED ROLLED HOLLOW SECTION WELDED JOINTS IN TRUSSES

Thesis submitted to the University of Nottingham
for the degree of Doctor of Philosophy

by

ANTONY PHILIASTIDES, B.Sc

Department of Civil Engineering
University of Nottingham
May 1988

To my mother and father

SYNOPSIS

The designer of lattice trusses has been traditionally encouraged to avoid extra joint bending moments by ensuring 'noding' of member centre lines. This can however cause problems in the design of RHS trusses with small (economical) branch members by causing large gaps at joints with undesirable flexibility for slender chord walls. 100% overlap joints overcome this problem while still maintaining economic single cut branch ends.

The research programme set out first to highlight the difference in behaviour of trusses with large gap noding and completely overlapping joints. Two similar trusses - one gap, the other lap - with matched sections were tested to failure. It was concluded that the gap joint truss (branch/chord width ratio = 0.4) was much less efficient than the corresponding 100% overlap truss despite the large eccentricities. The collapse load of the latter was some 35% greater, while the stiffness properties were better, and remained linear for a substantial proportion of the loading. On the other hand the gap joint truss soon became non-linear, with large overall deflections. Local connecting chord wall deflections were quite small in the lap joints while appreciable deflections occurred at gap joints under service loads.

Elastic frame analyses were carried out for all the six test trusses (one gap and five lap). For the overlap trusses, axial forces and bending moments could be predicted fairly accurately but a non-linear analysis was required for the gap jointed truss even at fairly modest loads. The effects of β ratio, chord slenderness and branch angle were all examined within the parameter range tested. The advantages of truss continuity moments as well as plastic redistribution of moments have been observed to reduce the occurrence of the local chord buckling mode of failure (L7), compared with previous isolated joint tests.

Results obtained from tests on isolated joints can give good agreement with those obtained from truss tests, both with respect to strength and failure mode. However, as the isolated joint testing cannot always reproduce the support conditions in a truss, the failure modes (and hence strengths) can differ.

The current CIDECT design strength equations and recommendations for gap and overlap joints are largely based on the results of isolated joint testing. The suitability of the CIDECT strength equations and recommendations for designing RHS lattice trusses has been reviewed. Consequently, for the 100% overlap joint trusses a

simple design method has been presented in conjunction with practical design recommendations. The problems associated with the analysis and design of the gap joint truss are described in detail.

ACKNOWLEDGEMENTS

The author expresses his sincere gratitude to the following :

The Science and Engineering Research Council (SERC), and the British Steel Corporation (BSC), Tubes Division, Corby for their generous financial support to this project.

Professor P.S. Pell, Head of Department of Civil Engineering, for the provision of the excellent facilities in the Department.

Dr G. Davies and Dr. M.G. Coutie, for their constant help, guidance , criticism and encouragement throughout this investigation.

Messers. N.F. Yeomans and T.W. Giddings of the Structural Engineering Department, BSC Tubes Division for taking active interest and providing valuable knowledge and advice.

Messrs. N. Hardy, D. Oakland, and M. Langford, for their assistance in conducting the experimental investigation. Their knowledge, advice, and co-operation were essential ingredients, ensuring experimental results of the highest quality.

CONTENTS

VOLUME I **THESIS**

VOLUME II **APPENDICES**

VOLUME I

CHAPTER 9

CONCLUSIONS AND RECOMMENDATIONS

VOLUME II

LIST OF TABLES

LIST OF FIGURES

CHAPTER 7

LIST OF PHOTOGRAPHS

SYMBOLS

Symbol		Title
A_{ei}	:	Effective cross sectional area of member i.
A_i	:	Measured cross sectional area of member i, (i=0, chord; i=1, tie; i=2, strut; i=3, post).
C	:	Effective width factor.
C_m	:	Mean perimeter of branches in a K or N joint, (= $b_1+h_1+b_2+h_2$).
C_1, C_2	:	Constants.
E	:	Modulus of elasticity.
F_i	:	Axial force in member i, (prior to the attainment of truss ultimate load). (i=0, chord; i=1, tie; i=2, strut; i=3, post)
F_{op}	:	Axial pre-load in the chord, (prior to the attainment of truss ultimate load).
$F_{0(1\%b_0)}$	:	Force to produce normal deflection of the chord connecting face of $1\%b_0$.
I_i	:	Second moment of area of member i, (i=0, chord; i=1, tie; i=2, strut; i=3, post).
K_{01}	:	Ratio $\sigma_{e0}t_0/\sigma_{e1}t_1$.
K_{02}	:	Ratio $\sigma_{e0}t_0/\sigma_{e2}t_2$.
K_{12}	:	Ratio $\sigma_{e1}t_1/\sigma_{e2}t_2$.
K_{21}	:	Ratio $\sigma_{e2}t_2/\sigma_{e1}t_1$.
L	:	Length.
L_1	:	(see Fig. 3.4).
L_2	:	(see Fig. 3.4).
M_i	:	Measured bending moment in member i, (prior to the attainment of truss ultimate load; i=0, chord; i=1, tie; i=2, strut; i=3, post).
M_{ui}	:	Measured bending moment in member i, (at truss ultimate load; i=0, chord; i=1, tie; i=2, strut; i=3, post).
N_i	:	Measured axial force in member i, (at truss ultimate load).
N_{b1}	:	Measured buckling load for a compression branch.
N_{fq}	:	Reduced axial load capacity of the chord in the presence of shear, (see Table I1 - Appendix I).
N_k	:	Characteristic strength of joint.
N_q	:	Shear strength of chord cross section, (see Table I1 - Appendix I).
N_{qp}	:	Punching shear capacity of the chord wall, (see Table I1 - Appendix I).
N_u	:	Ultimate strength of joint.
N_{ik}	:	Characteristic strength of joint in terms of axial force in member i, (i=0, chord; i=1, tie; i=2, strut; i=3, post).
N_{im}	:	Predicted mean ultimate strength of joint expressed as an axial force in member i, (i=0, chord; i=1, tie; i=2, strut; i=3, post).
N_q	:	Shear strength of chord in the gap of a K or N joint.
Q	:	Shear force.
R	:	Linear potentiometer reading, (see Fig. 4.14).
R_i^{mean}	:	Mean value of two Linear potentiometer readings for member i, (see Fig. 4.14).
R_{exp}	:	Measured ram failure load.
R_{pi}	:	Predicted ram failure load derived using analytical method i, (see Chapter 7).
T_1	:	Thickness of 'overlapped' branch member.
T_2	:	Thickness of 'overlapping' branch member.

Symbol		Title
X_e	:	Experimental elastic axial force coefficient for a member.
X_1	:	Theoretical elastic axial force co-efficient for a member derived from pin-jointed frame analysis, (Model P).
X_2	:	Theoretical elastic axial force co-efficient for a member derived from Model GS (for gap joint truss) or Model S1 (for a 100% overlap joint truss).
X_3	:	Theoretical elastic axial force co-efficient for a member derived from Model GK (for gap joint truss) or Model S2 (for a 100% overlap joint truss).
X_4	:	Theoretical elastic axial force co-efficient for a member derived from Model Y.
X_5	:	Theoretical elastic axial force co-efficient for a member derived from Model K.
Z_i	:	Elastic section modulus of member i, (i=0, chord; i=1, tie; i=2, strut; i=3, post).
a	:	Chord wall shear span.
b_e	:	Effective width.
b_{eih}	:	Effective width of the heel of branch member i, (i=1, tie; i=2, strut).
b_{eit}	:	Effective width of the toe of branch member i, (i=1, tie; i=2, strut).
b_{ep}	:	Effective width for punching shear.
b_i	:	Width of member i, (i=0, chord; i=1, tie; i=2, strut; i=3, post),
b_1^*	:	$(b_1+h_1)/2$
e	:	Eccentricity of joint centre-line noding, (see Fig. 1.2).
g	:	Gap between branches in a K or N joint, (see Fig. 1.3).
g_1	:	Gap divided by chord wall thickness, (g/t_0).
h_{co}	:	Effective depth of chord sidewall.
h_{ei}	:	Effective depth of member i, (i=0, chord; i=1, tie; i=2, strut; i=3, post).
h_i	:	Depth of member i, (i=0, chord; i=1, tie; i=2, strut; i=3, post).
j	:	Joint.
l	:	Distance of Linear Potentiometer from the chord face. (see Fig. 4.14)
L_1,L_2	:	Length of shear plane in 'overlapped' and 'overlapping' branch members, respectively, (see Fig. 3.4).
l_w, l_t	:	Leg length, and throat thickness of fillet weld, respectively.
m	:	Member.
n_1	:	Ratio h_1/b_1.
n_2	:	Ratio h_2/b_2.
q	:	Length of overlap between branches of a K or N joint at the chord face, (see Fig. 1.2).
t_i	:	RHS wall thickness, (i=0, chord; i=1, tie; i=2, strut; i=3, post).
t_p	:	Thickness of chord flange reinforcing plate.
x, y, z	:	Tolerances, (see Fig. 3.3).
Δ_1,Δ_2	:	Support settlements, (see Fig. 4.12).
Δ_c	:	Truss central deflection relative to the supports, (see Fig. 4.12).
Δ_c'	:	Truss central deflection relative to the ground, (see Fig. 4.12).
Γ	:	Axial stiffness of connecting element in Models S1 & S2, (see Fig. 7.3).
Γ_1, Γ_2	:	Axial stiffnesses of connecting elements in Model GS, (see Fig. 7.3).
β	:	Width ratio between branches and chord = $(b_1+b_2)/2b_0$.
β^*	:	Ratio of average perimeter of branches to chord width, $(b_1+h_1+b_2+h_2)/4b_0$.
β_1	:	Width ratio between compression branch and chord.
β_2	:	Width ratio between tension branch and chord.

Symbol		Title
$\gamma_m\gamma_c$	:	Material or joint partial safety factors.
δ	:	Normal deflection of connecting chord face at a 100% overlap joint, (see Fig. 4.14).
δ_1, δ_2	:	Normal deflection of the connecting chord at a gap joint, (see Fig. 4.14).
ε	:	Measured surface strain.
ε_i^{mean}	:	Mean value of two strain gauges at one end for member i.
η_i	:	Efficiency of member i at ram failure load, ($N_i/A_i.\sigma_{ei}$; i=1, tie; i=2, strut; i=3, post).
θ_i	:	Acute angle between branch member i and the chord face.
λ	:	Member Slenderness ratio.
μ	:	Joint strength reduction factor due to presence of chord end load, (see Eqn. 8.1).
ν	:	Poisson's ratio.
σ	:	Axial stress.
σ_E	:	Effective stress.
σ_e	:	Minimum yield stress, (established from tensile test coupon).
σ_0	:	Direct stress on shear plane A-A, (see Fig. 8.5).
σ_1, σ_2	:	Principal stresses, (see Fig. 8.5).
σ_{ei}	:	Minimum yield stress of member i, (established from tensile test coupon; i=0, chord; i=1, tie; i=2, strut; i=3, post).
σ_0	:	Maximum axial stress in the chord.
σ_{0p}	:	Stress in the chord due to pre-load F_{op}.
σ_{ui}	:	Ultimate tensile stress of member i, (established from tensile test coupon; i=0, chord; i=1, tie; i=2, strut; i=3, post).
τ	:	Shear stress.
τ_0	:	Shear stress on plane A-A, (see Fig. 8.5).
τ_{max}	:	Maximum allowable shear stress based on Von Mises stress field, (see Fig. 8.5).

ABBREVIATIONS

C.I.D.E.C.T	:	Comite International pour le Developpement et l'etude de la Construction Tubulaire.
C.H.S	:	Circular Hollow Section.
R.H.S	:	Rectangular Hollow Section.
DG	:	Dial Gauge.
ERSG	:	Electrical Resistance Strain Gauge.
LC	:	Load Cell.
LP	:	Linear Potentiometer.
LVDT	:	Linear Variable Differential Transformer.
TCPL	:	Thermo-couple.
T1	:	Gap joint truss, (see Fig. 3.3 & Appendix A).
T2	:	100% overlap joint Warren truss, (see Fig. 3.3 & Appendix A).
T2/2	:	Shortened version of truss T2, (see Fig. 3.3 & Appendix A).
T3	:	100% overlap joint Warren truss, (see Fig. 3.3 & Appendix A).
T4	:	100% overlap joint Warren truss, (see Fig. 3.3 & Appendix A).
T5	:	100% overlap joint Pratt truss, (see Fig. 3.3 & Appendix A).
T6	:	100% overlap joint Warren truss, (see Fig. 3.3 & Appendix A).

ANALYTICAL MODELS

GS	:	Gap joint truss, spring model.
GK	:	Gap joint truss, rigid frame model.
P	:	Pin jointed frame model.
S1	:	100% overlap joint truss, spring model-type 1.
S2	:	100% overlap joint truss, spring model-type 2.
Y	:	100% overlap joint truss, rigid frame model.
K	:	100% overlap joint truss, simplified rigid frame model.

TERMS

Connecting chord face : Chord face to which the branches are connected.

Joint deformation : Deformation of the connecting chord face in a direction perpendicular to the face.

Truss deflection : Deflection of the tension chord at midspan in the direction of the applied load.

Heel face : Face of branch member which makes an acute angle with the connecting chord face.

Toe face : Face of branch member which makes an obtuse angle with the connecting chord face.

Sidewalls :Walls (of branches or chord) which are parallel to the plane of the truss.

Strut : Compression branch.

Tie : Tension branch.

Gap : Distance measured along the face of the chord between the toe faces of the strut and tie members.

Overlap joint : Joint where one branch member overlaps the other.

Squash force : Force in a member equivalent to measured cross-sectional Area x measured yield stress.

Member efficiency : $\frac{\text{Measured axial force at ram failure load}}{\text{Squash force}}$

TRUSS JOINT, MEMBER AND STRAIN GAUGE NUMBERING SYSTEMS

The referencing system used for the joints, members and strain gauges is presented in this section :

Joints	:	Figure S1
Members	:	Figure S2
Strain gauges	:	Figure S3

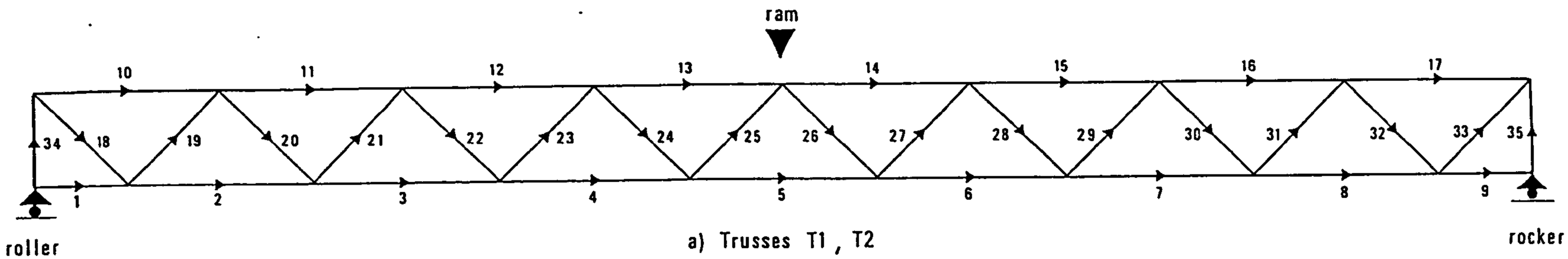

a) Trusses T1 , T2

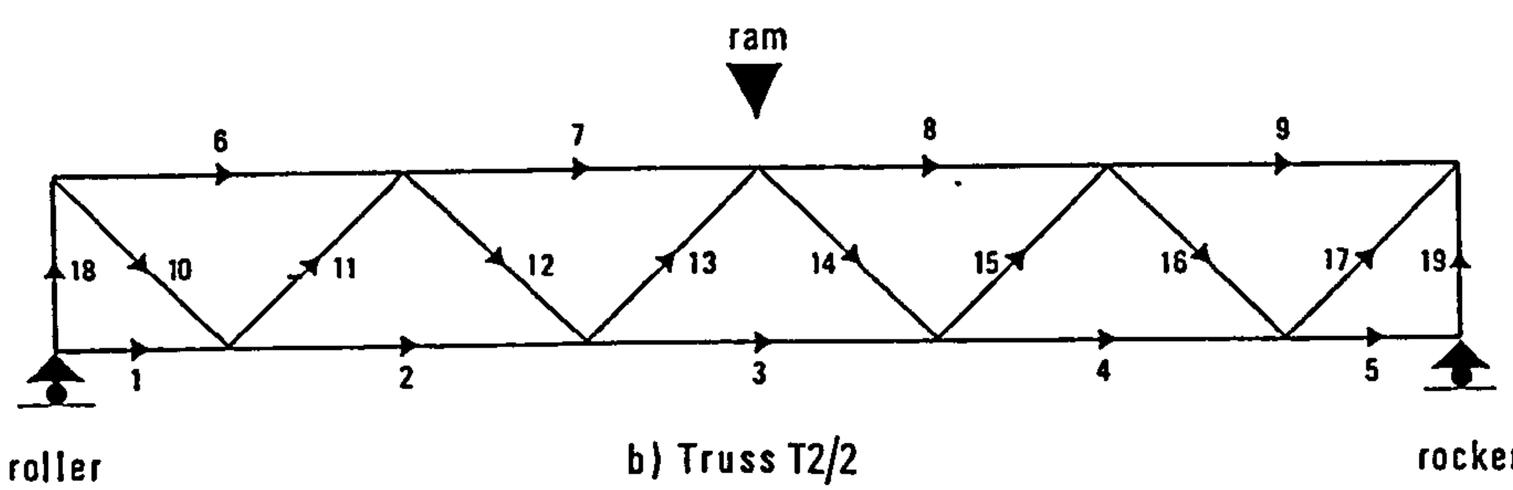

b) Truss T2/2

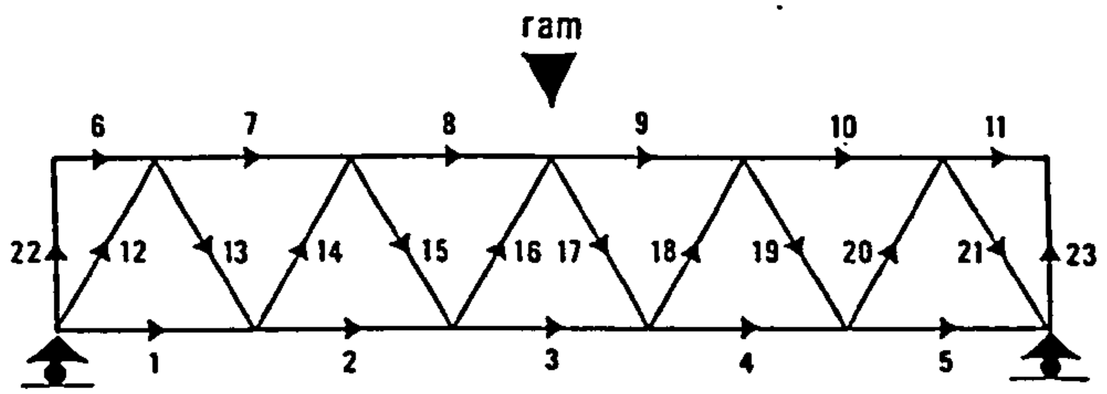

c) Trusses T3 , T4

Note

► defines local x-axis direction of member and the relative position of end 1 to end 2 such that :- 1 ——→—— 2

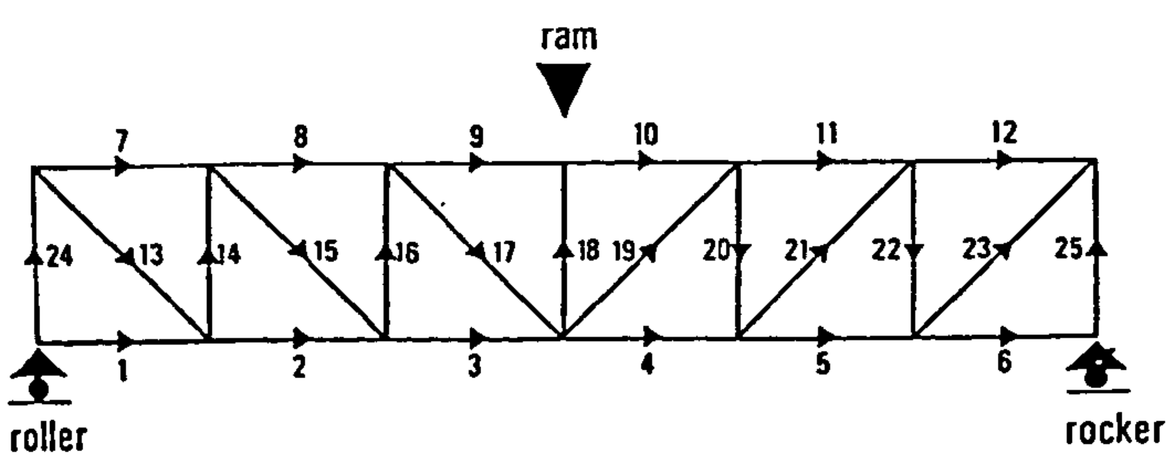

d) Truss T5

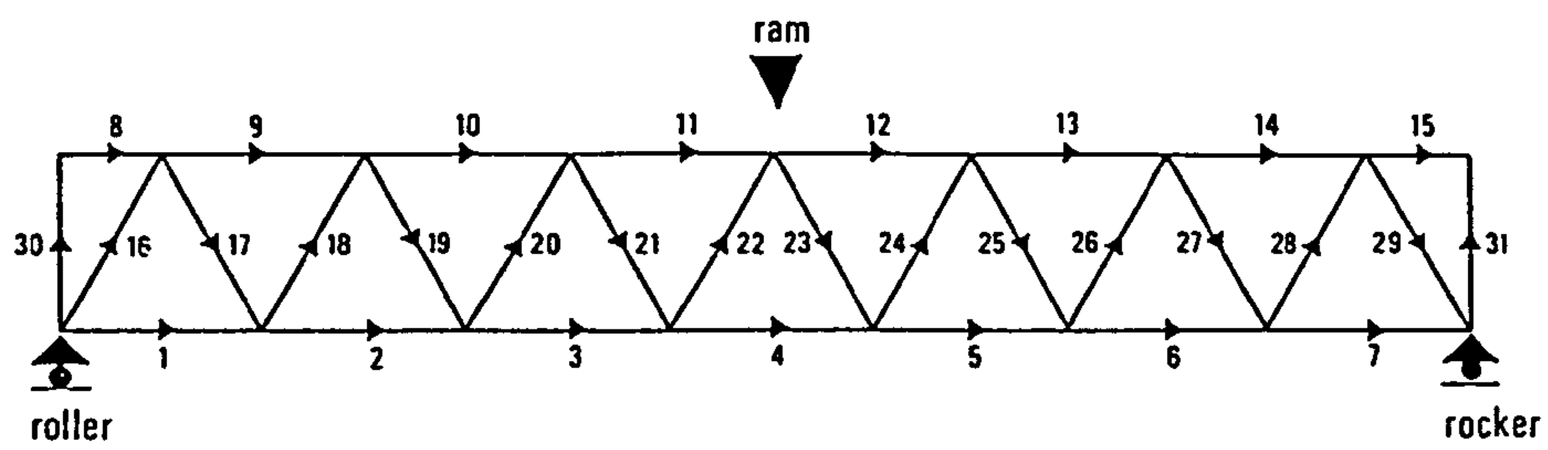

e) Truss T6

Fig S1 Member numbering systems.

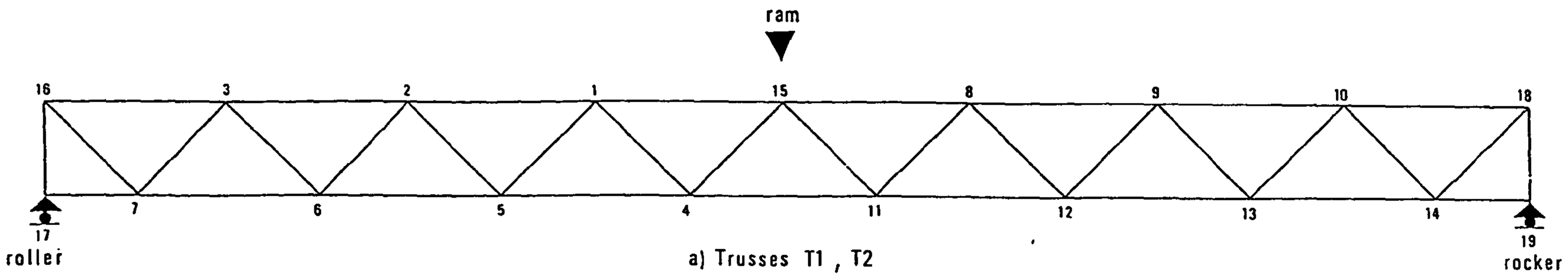

a) Trusses T1 , T2

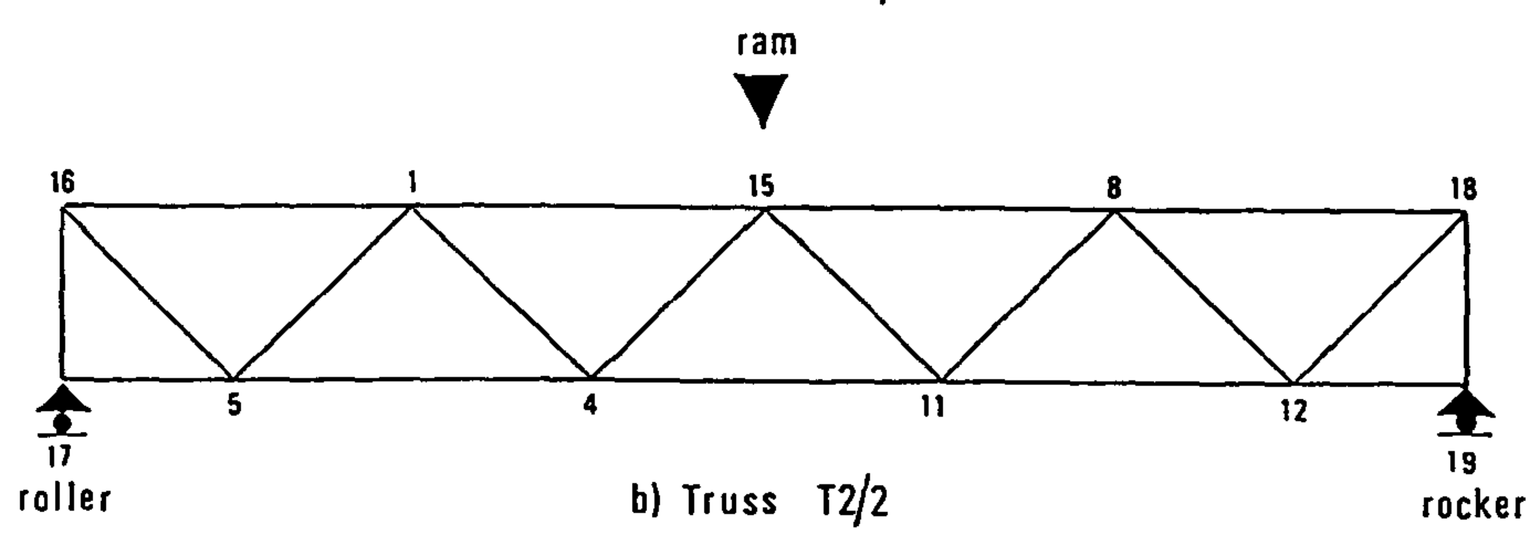

b) Truss T2/2

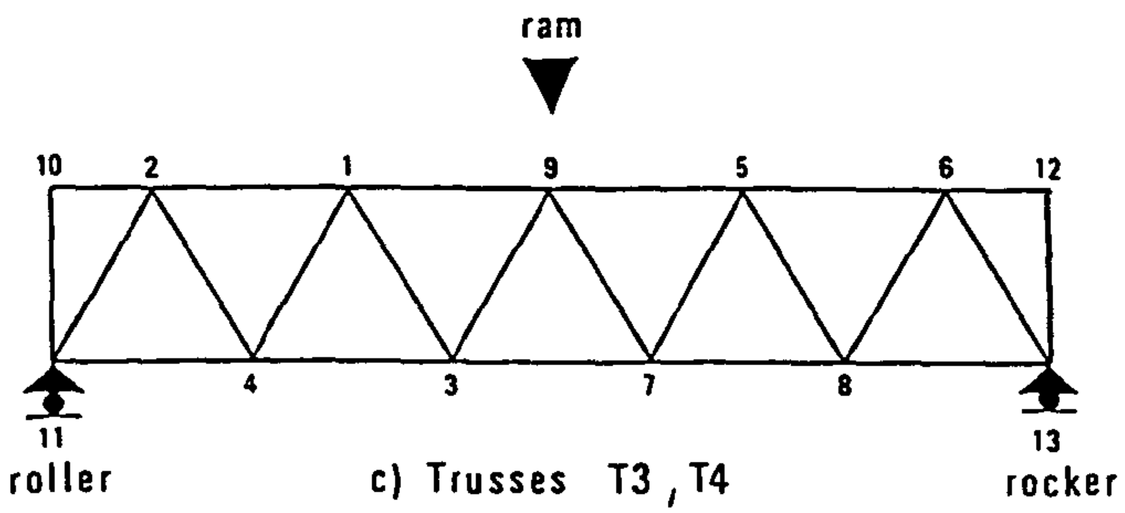

c) Trusses T3 , T4

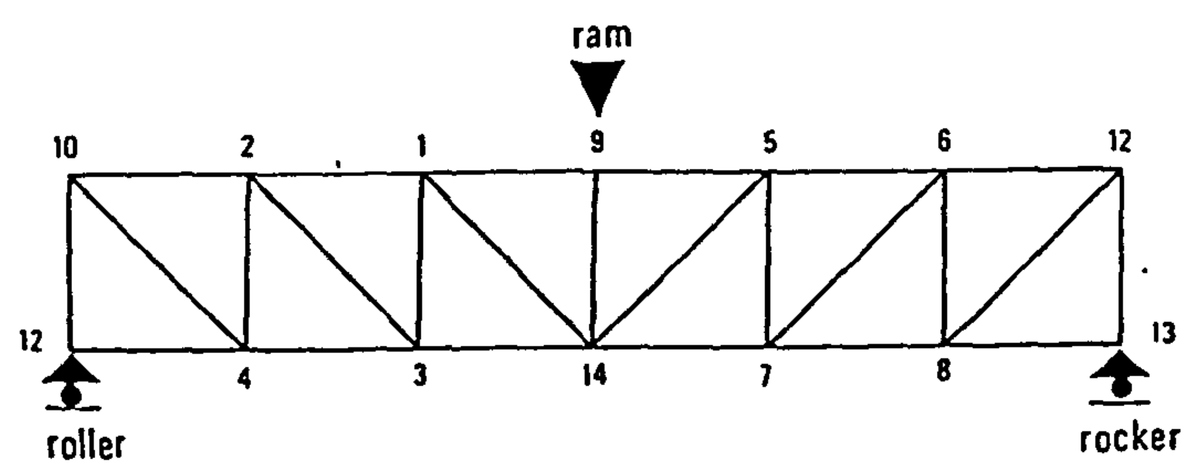

d) Truss T5

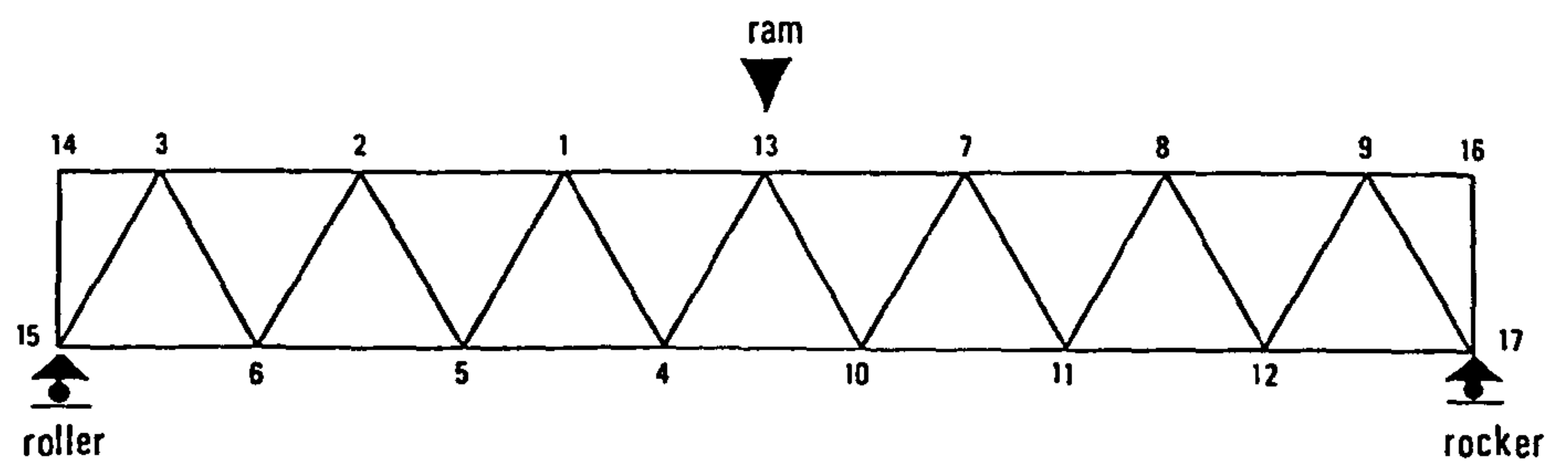

e) Truss T6

Fig S2 Joint numbering systems.

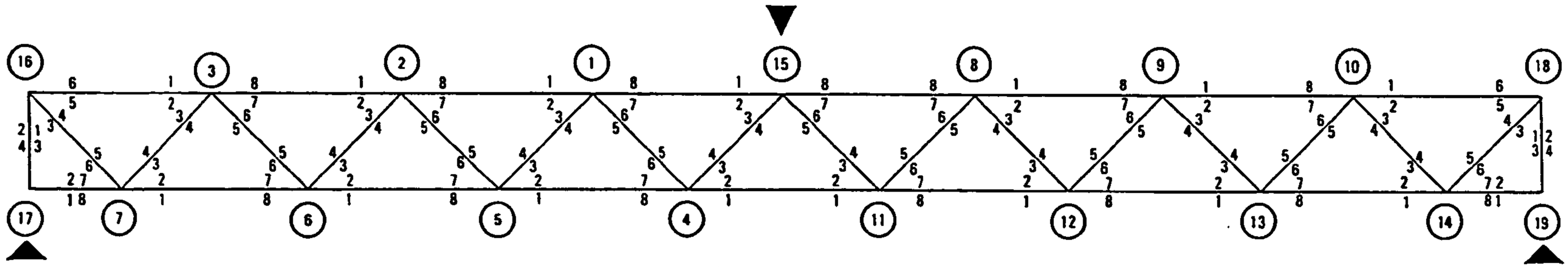

a) Trusses T1 , T2

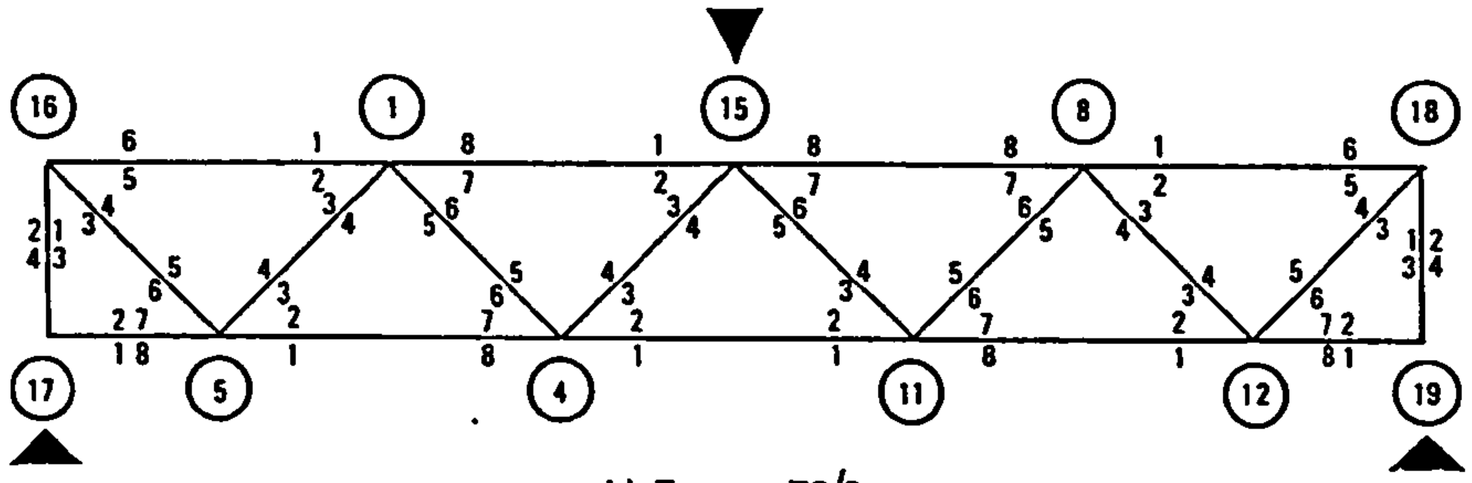

b) Truss T2/2

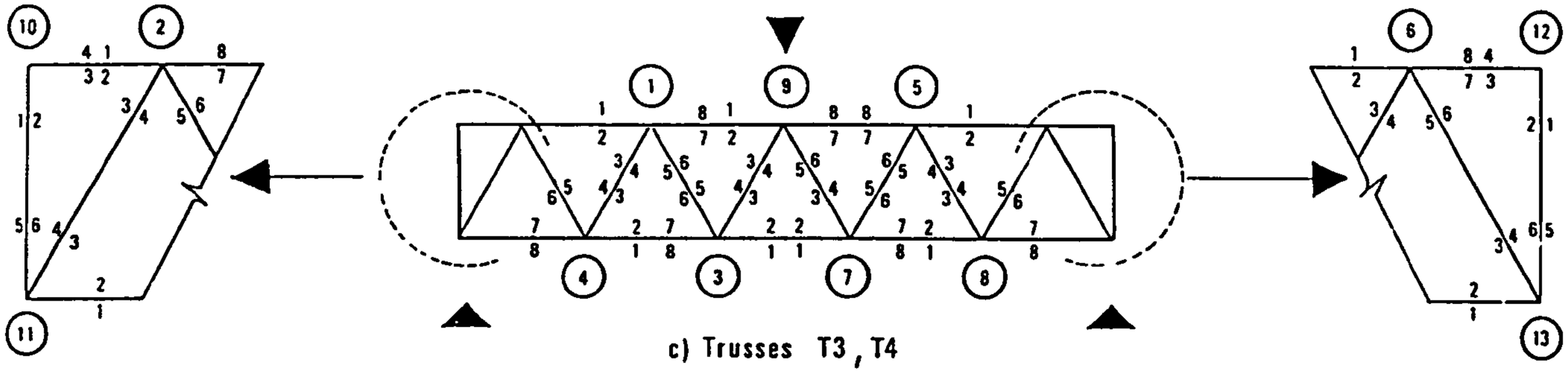

c) Trusses T3 , T4

Fig S3 Strain gauge reference systems for trusses T1, T2, T2/2, T3, and T4.

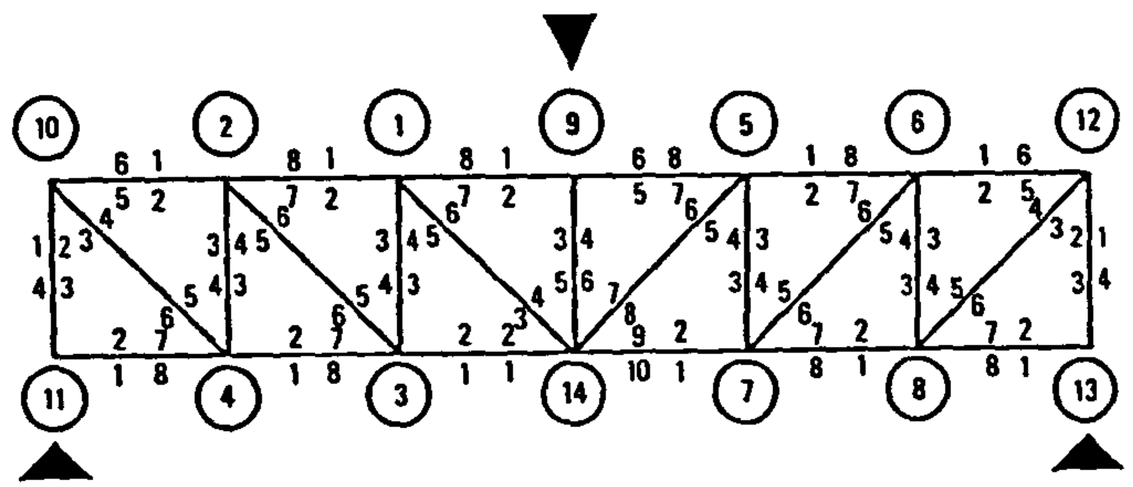

d) Truss T5

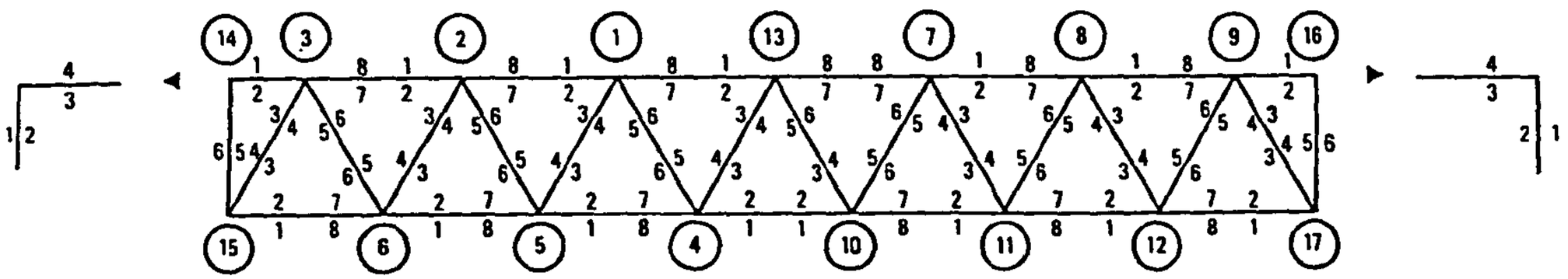

e) Truss T6

Fig S3 Strain gauge reference systems for trusses T5, and T6.

CHAPTER 1
INTRODUCTION

1.1 Introduction

The first Structural Hollow Sections (SHS) were produced by Stewarts and Lloyds in 1952. Since then their popularity has increased considerably world-wide due to the increased publicity and knowledge about their structural behaviour and design.

A common application of SHS is in parallel chord lattice trusses for reasons of pleasing aesthetics, structural efficiency and economy. Tubes are often much stronger than open section members of the same weight, but the economic advantage gained from this is offset by the connection costs which can be high. The cost of joint fabrication can be reduced by minimizing the number of joints in the structure, and therefore an initial economy can be achieved in tubular trusses by designing as a 'Warren' rather than a 'Pratt' or 'N' truss. Furthermore, to avoid profile-shaping Circular Hollow Section (CHS) members, Rectangular Hollow Sections (RHS) were developed to simplify jointing. RHS joints only require straight cutting of the branch member ends.

1.2 Terminology

1.2.1 Overlap

Partial overlap joints necessitate the double shaping of either one or both of the branch members as shown in Fig. 1.1. Authors in different countries have used different methods for defining the amount of overlap at a joint. In Britain, the percentage overlap, as seen in Fig. 1.2, is expressed as (BC/AC)x100, and this is the same as the CIDECT[43] definition.

The simplest form of overlap joint is the 100% overlap as shown in Fig. 1.3. In this type of joint the branch member ends can be formed from straight cuts.

1.2.2 Eccentricity

For ease of design, members are usually arranged so that all centre-lines are noding. If a specific gap or overlap of branch members is required then noding may not occur in which case a moment on the joint can be produced by the eccentricity.

Eccentricity from the chord centre-line towards the outside of the truss is termed positive. Thus gap joints often have a positive noding eccentricity and overlapped joints, a negative eccentricity (see Fig. 1.2).

1.2.3 Gap

A Gap joint is one in which there is a gap between the branch members on the chord face, the nominal gap (g*) as shown in Fig. 1.3 is reduced to a smaller actual weld gap (g) because of the fillet welds around the branch members.

1.3 The relative merits of gap and 100% overlapped joints

Lattice truss joints in RHS are most economically formed using member ends with straight saw cuts ,which favour gap or 100% overlap joints; the former being more commonly used. The latter however exhibit many structural advantages which would be beneficial to exploit.

Gap joints have an inherent flexibility that can lead to low joint strengths (particularly if the width ratio between branch and chord is low). The 100% overlap joint has the advantage of great stiffness, but apparent disadvantage of a large centre-line eccentricity. The results of 100% overlap joint testing[27, 28, 29, 30] generally indicate however, that the strength is not in fact reduced by this eccentricity.

1.4 Limitations of isolated joint testing

The majority of testing to date has been on isolated joints. Joint testing, must necessarily reflect the structural behaviour in a complete structure, and there is evidence to suggest that some tests on isolated overlapped joints[4, 6] have shown strengths well below those obtained in corresponding trusses[5, 32]. This could be accounted for by the difficulty in correctly simulating in a joint test the boundary conditions which determine the true force and moment combination. Axial force is particularly difficult to apply in a joint test as the jacks, or other loading devices interfere with the joint behaviour.

1.5 Objectives of the research programme

Six full-scale lattice trusses were fabricated and tested. One of these was fabricated from noded gap joints, and the remainder from 100% overlap joints. All the

test specimens were fabricated from square RHS. To supplement the truss testing a number of isolated joints were also tested at the Tubes Division of the British Steel Corporation in Corby[37] and at Nottingham University[38].

The research programme was specifically concerned with the behaviour of 100% overlap joint trusses. However, the structural behaviour of the gap joint truss has also been reviewed in detail. The objectives of the project were:

(i) To establish whether the eccentricity of the 100% overlap joint is detrimental to the strength and efficiency of the connection, (Chapters 5 & 6).

(ii) To compare the relative structural performance of trusses formed from noded gap joints and eccentric 100% overlap joints, (Chapter 6).

(iii) To define which parameters influence the behaviour of 100% overlap truss joints, (Chapters 5 and 6).

(iv) To assess whether the structural behaviour of 100% overlap joint trusses can be simulated by the use of elastic plane-frame analyses, (Chapter 7).

(v) To assess whether the design strength equations which have been proposed for 100% overlap joints are relevant in a truss environment, (Chapter 8).

(vi) To compare the relative structural performance of 100% overlap joints tested in isolation with corresponding truss joints, with respect to ultimate strength and modes of failure, (Chapter 8).

(vii) To establish a safe and reliable design method for structures fabricated from 100% overlap joints, (Chapter 9).

The research programme was essentially concerned with establishing an understanding of the behaviour of RHS lattice trusses formed from 100% overlap joints. It has been concluded from isolated joint tests that 100% overlap joints are stronger than equivalent gap joints. However, most structural engineers still favour centre-line noding because it is felt that a noded joint is structurally more efficient. Any eccentricity of the intersection of the branch members to the centre-line of the chord is normally considered to be a disadvantage, in that it produces primary bending moments in the chord in addition to the secondary moments associated with the member continuity at the joints, and is therefore undesirable.

Noding can however cause problems in the design of RHS lattice trusses with small economical branch members by ensuring large gaps at the joints with undesirable flexibility for slender chord walls. These problems have been described by Coutie et al[42] (see also Chapter 6). The 100% overlap joint overcomes this problem while still maintaining economic single cut bracing ends. It is hoped that the information contained

within this thesis will aid designers in furthering their understanding of eccentric joint connections. For this reason particular attention has been focused on the practical design implications arising from the research.

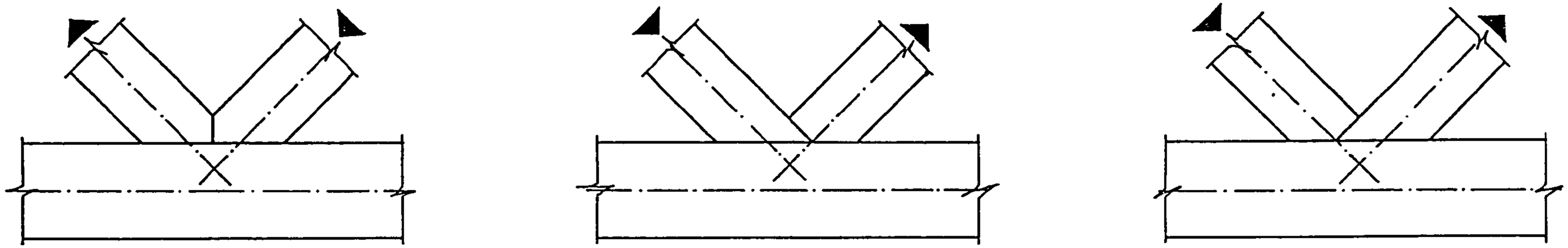

a) Both bracings double mitred

b) Tie double mitred

c) Strut double mitred

Fig 1.1 Methods of forming partial overlap joints.

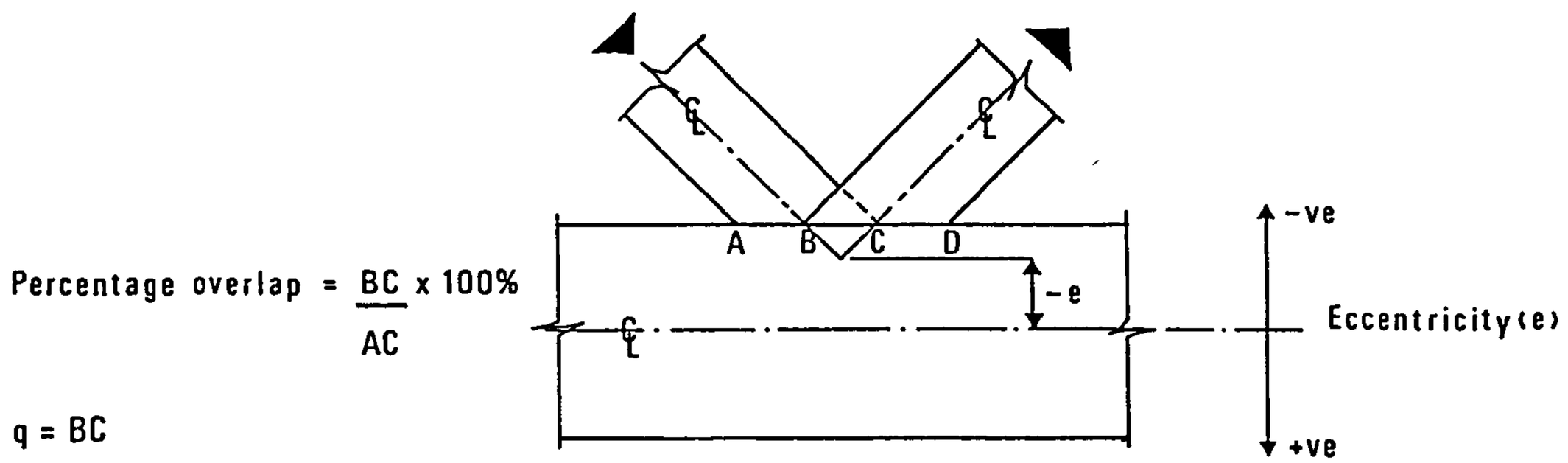

Fig 1.2 Definition of overlap.

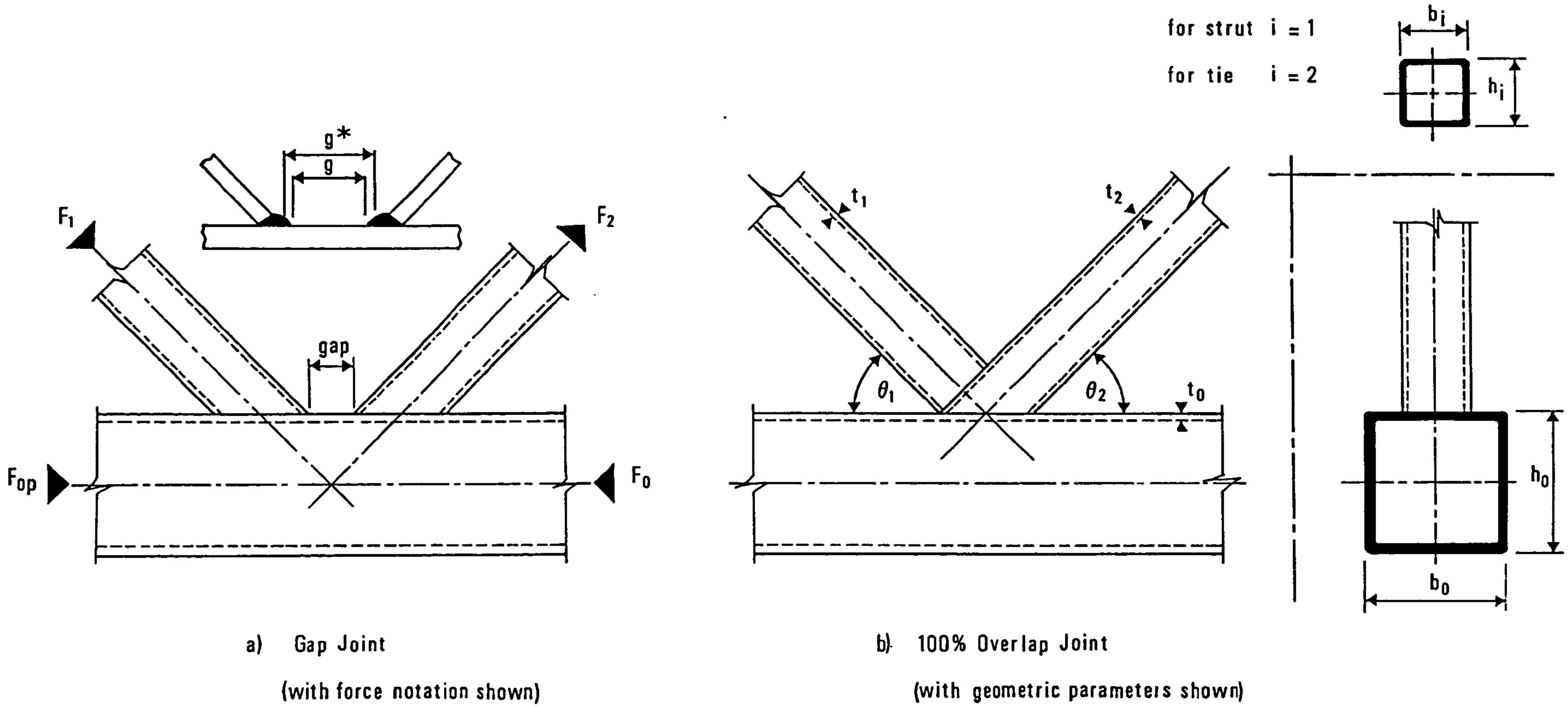

a) Gap Joint (with force notation shown)

b) 100% Overlap Joint (with geometric parameters shown)

Fig 1.3 Examples of gap and 100% overlap joints.

CHAPTER 2
LITERATURE REVIEW

2.1 Introduction

The CIDECT Monograph 6[43] on tubular connections was published in 1986. It is a 'state of the art' document containing SHS design guide-lines. The research programmes and developments leading up to its publication are reviewed extensively within the document itself.

A summary of the main development work with respect to RHS gap and overlap joint design is discussed in this chapter. Isolated 100% overlap joint tests and the static testing of RHS trusses have been reviewed in detail.

2.2 Summary of RHS isolated joint testing

2.2.1 Gap and partial overlap joints

For RHS gap and partial overlap joints the most significant early contribution was made by Eastwood and Wood[1]. They carried out a small number of tests on a narrow range of section sizes and developed several empirical design rules. Most of these tests were on isolated N type (Pratt) joints with CHS branch members and RHS chord members. At the conclusion of their test programme in 1970 they published a set of empirically derived joint strength equations.

An extensive programme carried out at the Mannesman Research Institute[2], examined the behaviour of Warren braced (gap and partial overlap) joints with RHS chords and square or rectangular branches. The programme comprised forty-one tests and examined the effect of different branch angles and different methods of dealing with the intersection of branches.

After Eastwood and Wood summarized their findings in 1970, a great deal of systematic experimental research was undertaken, principally in Europe, under the sponsorship of CIDECT. CIDECT programme 5EC[3] was conducted to supplement the Sheffield work and to extend the range of parameters. A total of five gap joints were tested. There was one 45^{o} Warren joint, but the rest were N-braced joints. Both circular and square branch members were examined and in two of the tests, rectangular rather than square chords were used.

At Delft University of Technology[4] a major systematic investigation of CHS-RHS and RHS-RHS welded joints was organized by Wardenier, with final results published in 1978. A total of thirty-two N-braced joints, (28-gap; 4-partial overlap) and two-hundred and forty-one Warren joints, (230-gap; 11-partial overlap) were tested. The major part of the test programme was carried out on 100mm x 100mm chord sections of various thickness, however the effect of rectangularity and size of the chord was also examined. Based upon the Delft results, Wardenier and Stark[4] proposed a series of equations estimating the ultimate gap joint strength for square or rectangular branch members. To supplement the test programme in Delft large CHS-RHS and RHS-RHS trusses were fabricated at Corby, England, and tested at the University of Pisa, Italy[5] (see section 2.4.2). A number of corresponding identical isolated joints were tested at Corby[6]. There were four N-braced joints, (2-gap; 2-partial overlap) and eight Warren joints (4-gap; 4-partial overlap).

Although the strength equations suggested by Wardenier and Stark[4] gave a good correlation between predicted and actual joint strengths for the Delft results, substantial discrepancies were found when applied to the results from Corby. In order to improve the correlation with the latter tests Coutie and Davies[7] suggested a number of modifications to the mean ultimate strength formula for an RHS-RHS gap joint.

After reviewing the comments and proposals from different research groups, Wardenier et al[8] then proposed another more comprehensive design method. The mean ultimate strength of an RHS or CHS-RHS gap joint was evaluated from the governing failure mode. Thus for RHS-RHS gap joints, the mean ultimate joint strength according to Wardenier and Davies[9] was given by the minimum of the values calculated from a series of equations, associated with particular failure modes. For gap joints the approach proposed by Wardenier et al[8] is the basis of CIDECT[43] design strength equations (see Table I1 in Appendix I).

Work on various aspects of joint behaviour has also been carried out at Karlsruhe, CIDECT Programmes 5M[10], 5R[11] and 5T[12]. In 5M tests were carried out on twelve Warren braced joints (3-gap; 9 partial overlap) of large size to supplement the information on size effect developed at Delft[4]. In the second phase of this work the effect of using high yield steel chords and mild steel branches was examined. Programme 5R was specifically concerned with the behaviour of different joint types made from steels of a very high yield stress (up to 820 N/mm^2). A total of four Warren gap joints were tested. The behaviour of a further four Warren gap joints was examined

in 5T.

The objective of CIDECT Programme 5S[13] was to establish a correlation between the results of tests obtained from the three main test rigs, namely those at the TNO in Delft, Karlsruhe University, and the British Steel Corporation in Corby. This involved testing similar specimens in each rig. Both gap and overlap joints were used.

2.2.2 100% overlap joints

Gap joints have received much more research attention than overlap joints, because the latter have been found experimentally to be stronger than their gap counterparts.

Two types of joint are possible, the strut overlapping the tie and the reverse of this namely, the tie overlapping the strut. The testing of 100% overlap joints has been incorporated into only four research programmes. Three of these were carried out in Sheffield and the results were presented by Blockley[27], Shinouda[28], and Mee[29]. The latest testing of 100% overlap joints has been by De Koning and Wardenier[30] in the Netherlands.

Giddings[14] developed a number of empirical equations for the ultimate strength of overlap joints. Wardenier and Davies [9] also gave recommendations for the calculation of the ultimate strength of overlap joints. As far as overlap joints are concerned the approach suggested by Giddings[14] and outlined as a design method by Wardenier and Davies[9] has been adopted by CIDECT[43]. The CIDECT design strength equations for overlap joints are presented in Table I2 of Appendix I.

For strut overlapping tie the majority of tests that have been carried out were for $\theta_1=\theta_2=45^o$ and $b_1=b_2$. Most failures occurred by yielding of the tie, and the failure was gradual and not abrupt. In some of the Sheffield tests[29], where tie yielding was observed, the recorded failure load was significantly above the calculated yield strength of the member, this was thought to be due to the effect of strain hardening. CIDECT[43] suggests that for nearly equal square branches with the tie wall strength greater than that of the strut, the strut and tie efficiencies do not fall below 0.82 and 0.70 respectively (branch efficiency = $N_i / A_i.\sigma_{ei}$). Only a few tests have been carried out with $b_1/b_2=0.8$, where strut local buckling (L6) was observed (see Table 2.1).

The only tests carried out on joints where the tie overlapped the strut have been by de Koning and Wardenier[30]. In this case all were Warren type joints where the tie was deliberately made smaller than the strut to examine the effect of values of b_2/b_1 less than unity. Local buckling of the strut wall (L6) was found to be the most common mode of failure. Where this did not occur failure was usually in the tie, by rupture of the tie from the strut. The investigators also found there was a significant difference between the measured axial load in the strut and that in the tie.

A detailed study of the results of the isolated 100% overlap joint tests with respect to the predicted strength equations is presented in Monograph 6[43]. Only the conclusions of this study are outlined below.

For the strut overlapping the tie the design strength equations (see Table I2) were found to generally safely predict the failure loads found in the tests[27, 28, 29]. However, for test results[30] of tie overlapping strut the reliability of the strength predictions was affected by the mode of failure. Where failure was in the tie the joint strength was found to be safely predicted. However, failures occurred below the predicted strut load in the case of local buckling of the strut (L6), nevertheless the corresponding load in the tie was found to be at or above the predicted value. The reason for premature failure has been suggested by Wardenier[30] to be due to the build up of bending moment in the branch member, and is thought to be a function of the method of testing. Since the chord was not restrained at all at one end the moments generated by the branch eccentricity were reacted to by only one end of the chord and the branches. A study[43] of the strut and tie efficiencies shows that for square branches with b_2 greater than $0.75b_1$, the tie efficiency was never less than 0.80, but that the efficiency of the strut fell to 0.50.

2.3 Development of current design procedures for RHS joints

The CIDECT design recommendations are more comprehensive than those presently used by North American engineers, who for the most part follow the the proposals of Eastwood and Wood[1] which are incorporated into a tube manufacturer's connection manual, Stelco[23]. While the Eastwood and Wood method has proved satisfactory in practice, Packer[22] has shown that it often provides considerably different results to the CIDECT design recommendations, which having a more extensive research background lead to an improved joint design with a more consistent margin of safety.

The Canadian implementation of CIDECT Monograph 6, (based on the 1982 draft copy) has been produced by Packer et al[24]. In the Canadian implementation, the CIDECT recommendations are explained and adapted to be compatible with the Canadian code of practice for steel structures CAN3-S16.1-M78.

To assist Canadian engineers a design method to aid in the selection of members has been developed and described in (24, 25 & 26). This procedure relies on six design charts to simplify the joint strength calculations[24]. The method applied to K and N type (gap and overlap) truss joints with RHS chord members and circular or square web members. It relates specifically to single chord, planar Warren and Pratt trusses subject to predominantly static loading.

2.4 Static load testing of RHS lattice trusses

The static testing of RHS trusses has been confined to four research programmes[5, 31, 32, & 33]. In each case the trusses were simply supported, and the compression chord was restrained against lateral instability. However, only the trusses in two of the projects[31 & 33] were perfectly symmetrical about the midspan. In the other two projects the trusses were asymmetric due to the fact that a different joint arrangement was used on either side of each of the trusses.

The method of loading varied between projects. Dasgupta[31] applied loads vertically upwards at the central and quarter span points, this method was also employed in the testing of the Pisa[5] trusses. In the Dutch[32] and Polish[33] programmes the loads were applied vertically downwards. In the former a single point load was used at midspan, and in the latter two joints were loaded one on either side of the centre point, because the Warren configuration used did not have a joint at midspan. Dasgupta used asymmetric loading to initiate failure in joints on one side which could be subsequently strengthened. In the other projects the loads were applied symmetrically, with respect to the centre point.

A detailed account of the projects is provided below with particular reference being made to the objectives and conclusions drawn in each case.

2.4.1 Truss testing at the University of Nottingham

The first tests carried out on complete trusses were by Dasgupta[31] at Nottingham University. The joint design was based on the results of isolated joint tests

conducted at Sheffield[1]. Eleven tests were conducted on a total of three 'Pratt' (N) trusses, all with CHS branches and RHS chords. Only seven of the eleven tests were carried out on the initial eight-bay trusses. For the subsequent tests each of the trusses were modified to six bays. The basic failure modes identified were, strut buckling, and tensile failure at the toe of the tie branch corresponding to G2[b],G2[w], and G2[c] (see Fig. 2.2). The G2[w] modes were thought to be caused by the failure of fabricators to provide the welds specified.

For each of the original trusses a different type of joint was chosen. Thus three types of joint were incorporated into the testing, and all were gap joints. From Dasgupta's work the following points were deduced:

(i) Gap joints produced flexible connections; the resulting joint deformations were responsible for a significant proportion of the bending moments, and overall deflection of the trusses.

(ii) Truss joint failure loads were up to 30% lower than the equivalent isolated joint failures in Sheffield[1], even though these were subject to larger deflections, than the equivalent truss joints.

(iii) The distribution and magnitude of bending moments in the truss joints differed significantly from the isolated joints[1].

Dasgupta also wrote a computer programme using the matrix equilibrium method to analyse trusses with joint eccentricity. This programme incorporated the joint flexibility and the effects of axial forces. The actual joint flexibility was deduced by a finite element analysis.

2.4.2 Truss testing at the University of Pisa

As a part of CIDECT programme 5F, eight Pratt trusses with RHS chords and spans of between fourteen and sixteen metres were fabricated in England (British Steel Corporation Headquarters, Corby), and then tested at Pisa University, Italy[5]. Five trusses had CHS branches and three had RHS branches, in all cases the diagonal branches were inclined at 45^{o}.

The trusses were designed to cover a range of parameters shown to be significant from isolated joint tests and to establish a correlation with isolated joint test results. The truss members were designed to the requirements of the relevant British Standard, and standard fabrication techniques were employed with respect to the welds and joints. However, the gap joints were deliberately chosen to be weaker than the

members to ensure that joint failures occurred under test.

The joint details were arranged to give centre-line noding on one side of the truss and a nominal gap on the other side. This meant that in the majority of cases, the branches on the noding side of the truss overlapped each other; the degree of overlap depending on the size of the members. In all cases, the compression member was double shaped to fit over the tension diagonal. As all the branches were tack welded in place during fabrication before completing the welds, the toes of the tension diagonals in the overlap joints were not welded (this is a similar detail to that shown in Fig. A12 - Appendix A).

In association with these truss tests, some of the joints which were investigated in the trusses were reproduced as isolated joint specimens for testing at Corby[6]. In the absence of any published documentation of the results of the Pisa trusses a comprehensive appraisal of the research programme is not possible. From draft documents studied[34], three basic facts have been established:

(i) With respect to the overlap arrangement of branches, truss joints were found to be stronger than equivalent isolated joints.

(ii) Many of the isolated joint tests failed by local buckling of the chord but this did not occur in any of the truss tests.

(iii) In the truss tests no appreciable difference was observed between the strength of the joints on the compression chord and similar joints on the tension chord.

2.4.3 Truss testing at Delft University of Technology

At Delft University of Technology in the Netherlands, four Warren braced trusses with square chords and branches were tested[32]. Although the majority of the joints were K type, there were in each truss two N type joints, one at each support end. The main objective of the investigation was to compare the behaviour of the truss joints with regard to strength and stiffness with that of the previously tested isolated joint specimens[4].

The joints were designed to give a 50% overlapped condition on one side and a nominal gap on the other side. Contrary to the Pisa trusses the gap joints in two of the trusses were configured to produce noding, and positive eccentricity in the other two trusses. In the case of the overlap joints all eccentricities were negative, and the compression branch overlapped the tension branch, so that no weld was laid along the

toe of the tension brace (similar to the detail shown in Fig. A12 - Appendix A).

The conclusions derived from this test programme were as follows :

(i) Considerable bending moments occurred in the chords especially in those parts of the trusses where the joints were overlapped. These moments were thought to be caused by the eccentricities in the joints and overall truss deflection.

(ii) The influence of bending moments in the members affected the axial load distribution, which deviated from that calculated for an equivalent pin jointed truss.

(iii) A considerable degree of bending was identified in the top chords of the trusses with large span - depth ratio. This was attributed to the imposed deflection of the truss, and the proximity of the applied load at the midspan.

(iv) The local deformation of the truss joints was similar to that observed for isolated joints tested previously[4].

(v) For the trusses with relatively low depths, the deflections were nearly the same as calculated under the assumptions of pin ended members.

(vi) The static strength of the truss joints was found to be in good agreement with that observed in the isolated joint tests[4]. Furthermore, the same modes of failure were observed. In general the influence of chord pre-stress in compression was found to be less severe than for isolated gap joints. For chord pre-stress in tension the influence was small as was observed in the isolated joint tests. In the case of the overlap joints the influence of chord pre-stress was found to be negligible.

(vii) Even with joints of high flexibility, as in the case of the gap joints, a reduction was observed in the effective in-plane buckling length of the struts.

2.4.4 IIW programme XV-562-84 (in Poland)

The objectives of the Polish test programme[33] were similar to the Dutch, namely to examine to what extent the joint behaviour in a truss environment is reflected in isolated joint testing. Furthermore, the structural behaviour of the test trusses was examined in relationship to deflections, secondary moments, and stability of branch members.

The twelve Warren test trusses were fabricated totally from square RHS, and each was 7.5 metres in length. The test specimens were manufactured from welded cold formed hollow sections of mild steel. For ten of the trusses the same section size was used for the tension and compression chords, while in the other two a thicker section

was used on the compression chord. With respect to the branch members the same section size was used for the tie and the strut in each truss.

Each truss was made up of one joint type (two in the case where the wall thickness of the chord was differentiated between top and bottom). There were thus fourteen different joint types, with seven trusses formed from gap joints and the remainder from overlap joints. Two branch angles used 45°, and 60°, with brace to chord width ratios ranging from 0.4 to 0.8.

With respect to the modes of failure the distinction was made between joint failures and member failures, however, the failure modes have not been classified according to the CIDECT definitions (Figs. 2.1 & 2.2). Joint failure was identified as chord face plastification, and member failure as instability (in-plane) of the branch member. Simultaneous failure of the joint and compression branch was also identified. Cracking of the weld at the toe of the tie branch was observed in the joints with small gap joints. The findings of the Polish test programme were as follows:

(i) The highest flexibility was in the gap joints with the lowest width ratio and the biggest gap size. In the other joints local deflections were lower, and in the case of the overlap joints, hardly visible. In general joint deformations were found to be 2-3 times smaller than those found in the equivalent isolated joint tests.

(ii) Experimental centre spandeflections proved to be 15% to 60% greater than those calculated from a simple pinned joint model. A second order model, taking into account joint flexibility was found to under-estimate by 20% the deflections of the overlapped trusses and give close estimates in the case of gap joint trusses.

(iii) The branch members in all lattice trusses were subject to a much larger degree of bending than predicted from corresponding rigid frame analyses. This bending was attributed to local joint deformation, which was thought to alter the original geometry of the joint, thus inducing additional eccentricity moments. It was found that the second order model gave good estimates of the distribution of bending within the trusses.

(iv) It was identified that branch members behaved as double curvature deflected beam columns. The effective length factors derived from non-linear interaction formulae taking into account the bending moments were found to be between 0.5 and 0.7. It was concluded in this respect that it is not safe to assume that branch members are axially compressed and that an arbitrary effective length factor can be used.

(v) The gap joints with the smallest width ratio proved unexpectedly weak, by about 40% than in the corresponding isolated joints. This was thought to be caused by a rapid reduction of overall structural rigidity affected by strongly increased 'post-yield' flexibility of a joint.

(vi) The strength of remaining joints was found to be greater than predicted theoretically, but less by 10% with respect to the isolated joints. Furthermore no correlation was apparent between joint strength and chord loading.

(v) It was found difficult to identify the failure mechanism in overlap joints, and failure of these joints appeared to interact with the instability of the strut. However, in general the truss joints failed less explicitly than those tested in isolation.

2.5 Current position of RHS truss testing

The conclusions derived from the Delft[32] programme conflict in many instances with those from the other projects[5, 31 & 33]. The two most significant differences are, firstly that the Delft results indicate a good correlation between the strength of truss joints and isolated joints, and secondly that good agreement is obtained with respect to the experimental truss midspan deflections and those calculated from a pin jointed frame analysis.

The structural behaviour of 100% overlap joints has not yet been clearly defined. For tests in isolation it is thought that the various test rig characteristics affect the joint strength obtained. Furthermore, this type of joint has never been tested in the context of a complete truss.

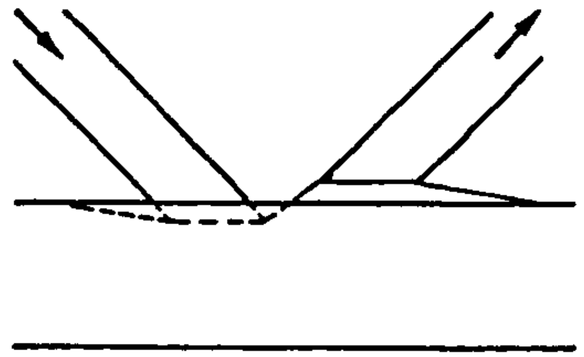

G1 :chord face failure

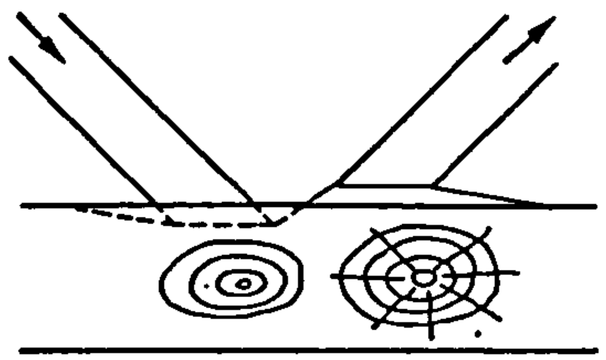

G2 b,w or c : chord face and wall failure with cracking

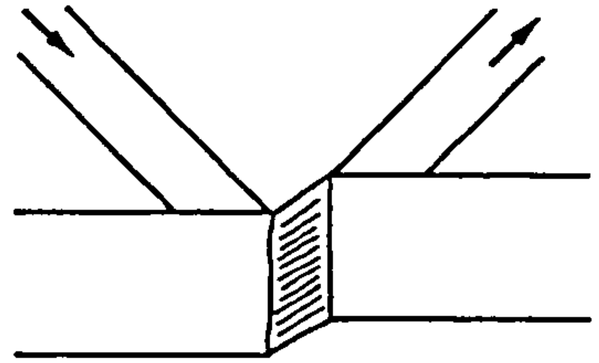

G3 : shear failure

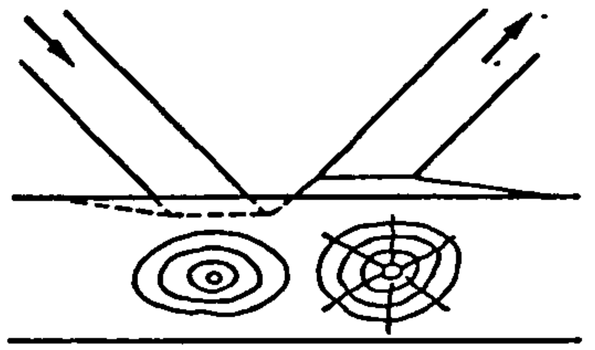

G4 : chord face and wall failure without cracking

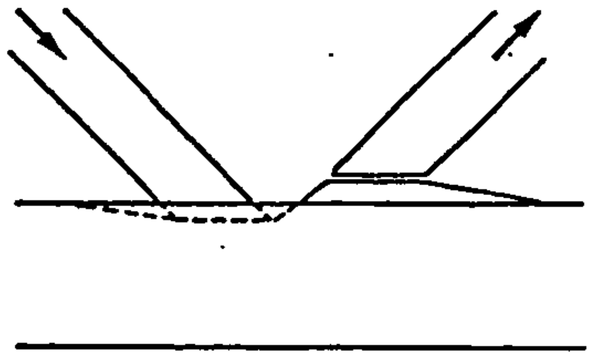

G5 b,w or c : diagonal failure

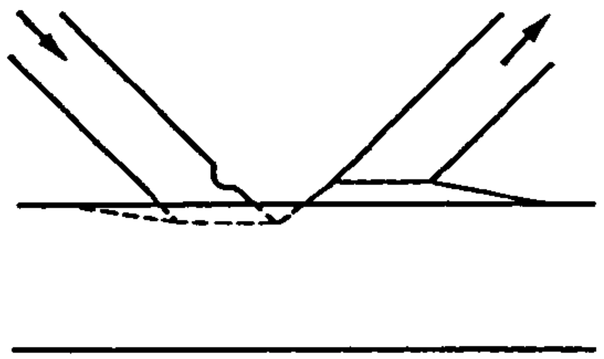

G6 : local buckling of compression brace

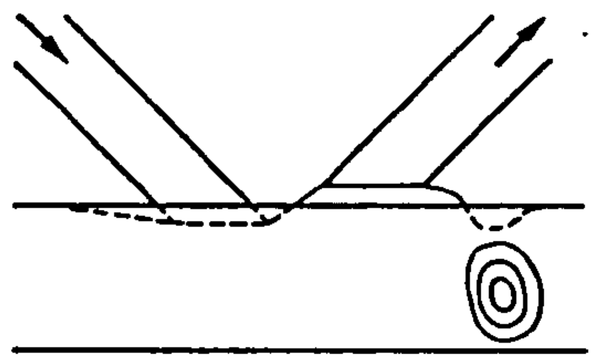

G7 : chord buckling

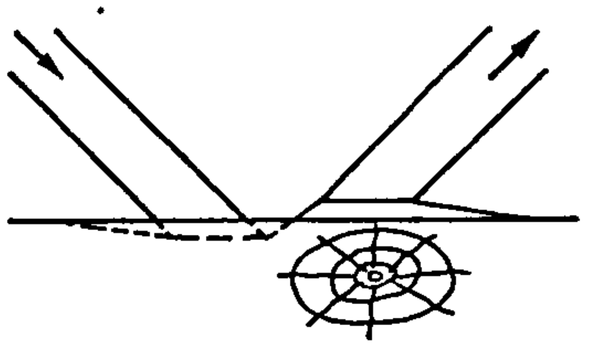

G8 : chord face and wall failure around tension brace

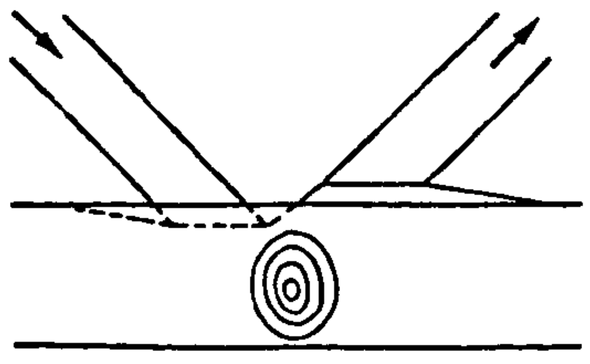

G9 : chord wall buckling

key

b - brace crack

w - weld "

c - chord "

outward deformation

inward "

Fig 2.1 CIDECT categories of gap joint failure modes.

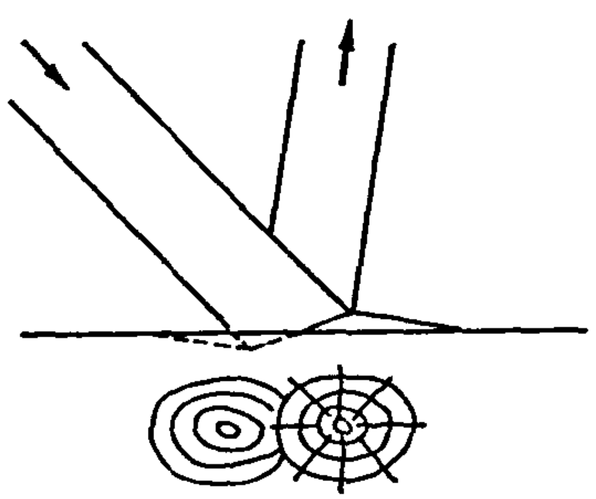

L4 : chord face and wall failure

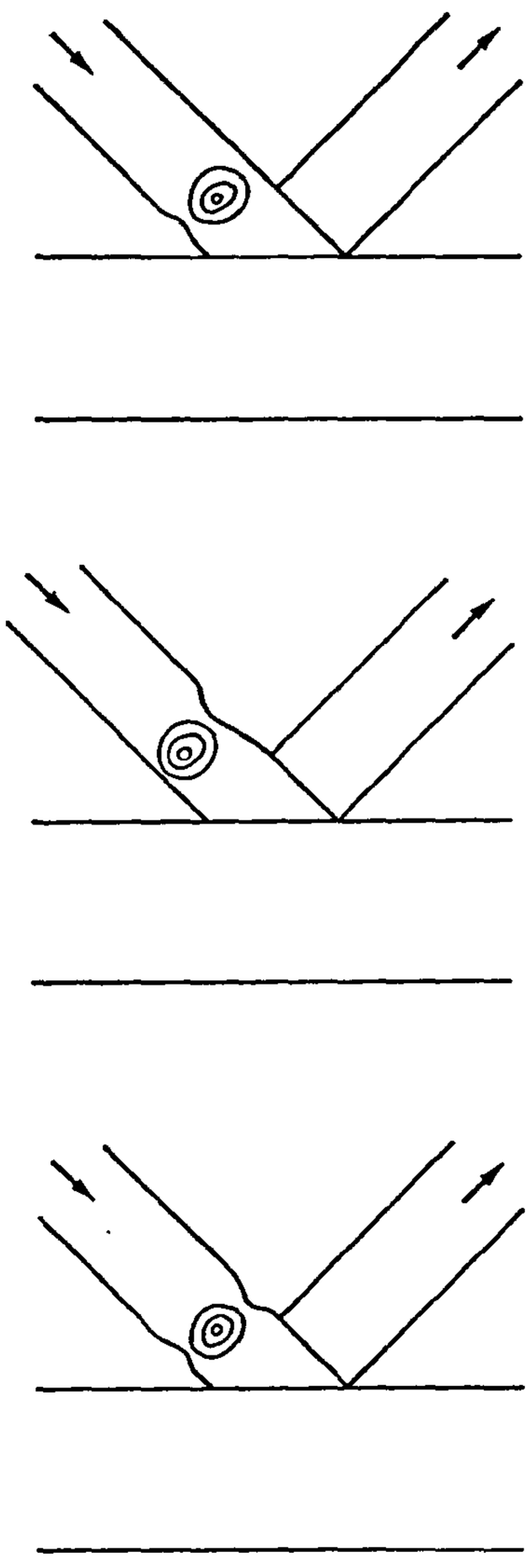

L6 : strut local buckling

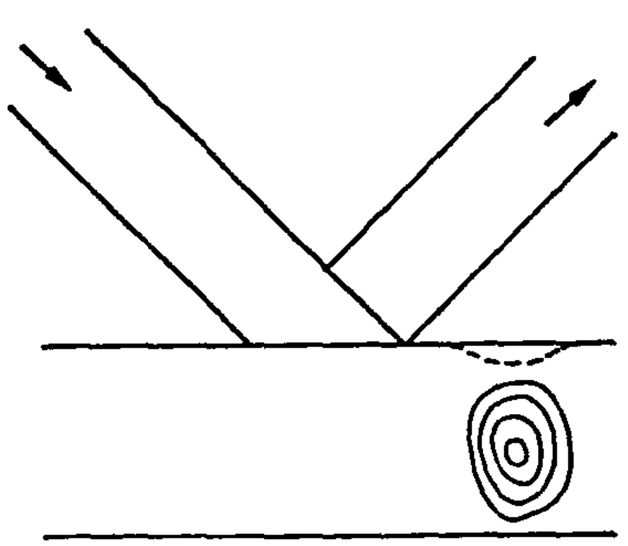

L7 : chord local buckling

key

outward deformation

inward "

Fig 2.2 CIDECT categories of overlap joint failure modes.

CHAPTER 3
DESIGN OF TEST TRUSSES

3.1 Scope of the experimental work

A total number of six trusses were fabricated. They were designed to cover a range of parameters which are commonly used in practice, and as such they were intended to be practical trusses in terms of their general member size and load carrying capacity.

The first truss (T1) to be tested was fabricated entirely with noded gap joints, while the five subsequent trusses (T2, T3, T4, T5, & T6) were formed using eccentric 100% overlap joints. Of the overlap joint trusses one was an N type truss (T5), while the remainder were Warren trusses.

The general layout and joint configurations of the trusses are summarized in Figs. 3.1 and 3.2, but presented in detail in Appendix A. The section sizes and parameter range are defined in Tables 3.1 and 3.2 respectively.

The test programme was conducted in two stages. Stage 1 was a direct comparison of two trusses, one fabricated from gap joints (T1) and the other from 100% overlap joints (T2), but where the corresponding members were identical. The aim was to assess the relative performance of the trusses with respect to ultimate strength and serviceability, and to determine whether the inherent joint eccentricity in the 100% overlap joint truss would be detrimental to its structural performance. Stage 2 was concerned solely with 100% overlap joints, and entailed the testing of the four remaining trusses. The objective in this case was to assess the performance of 100% overlap joints within a truss environment.

One aspect of the test programme was to compare the behaviour of all the trusses with that predicted from simple analytical models namely pin joint and rigid joint frame analyses, and hence define the most practical approach with respect to the modelling of the elastic force distribution and deformation of the trusses. Furthermore, the reliability of the CIDECT design equations (ie., those presented in Tables I1, & I2), was assessed by comparing the predicted and experimental failure loads. These design equations are based on the results of previous isolated joint tests.

In order to understand the mechanisms causing truss failure, it was necessary to

study the plastic behaviour. Of particular interest was the degree of ductility, and the capacity for plastic deformation. Sudden onset of failure in a structure is undesirable. With respect to the test trusses, it was thus important to assess both the elastic and plastic behaviour.

The basic objective however, was to assess what parameters influence the behaviour and ultimate strength characteristics of 100% overlap joint trusses, and hence define a design method for such structures.

3.2 Design parameters

The main geometric parameters which define the strength of an RHS joint are:

(i) Ratio of branch width to chord width, (β).

(ii) Ratio of chord width to chord thickness, (b_0/t_0).

(iii) Angles of branches relative to the chord, (θ).

(iv) Size of the gap (for gap joints).

(v) Percentage overlap (for overlap joints).

In selecting the range of parameters to be incorporated into the test programme particular attention was paid to producing the most practical combinations, rather than attempting a detailed investigation of a wide range.

There are several basic principles which were adhered to in the selection of the test trusses:

(i) All trusses were fabricated from square RHS.

(ii) For each particular truss the outside dimension of the tension and compression branches was the same, although the thickness was different in four cases (namely, trusses T1, T2, T3, & T5). In these trusses the strut always had the greater wall thickness.

(iii) With the exception of T1 and T2 the top and bottom chords were fabricated from the same section size. For these trusses the top and bottom chords had the same outside dimensions, but a different section thickness was used for the central and outer lengths.

(iv) For the overlap joint trusses the sense of overlapping was reversed on one side of the truss, so that both tie overlapping strut, and strut overlapping tie conditions could be studied.

3.2.1 Stage 1 - Trusses T1 & T2

For the gap joint truss (T1) the most critical value of branch to chord width was selected, namely β=0.4. This corresponds to the lower limit recommended by CIDECT, with respect to the proposed design strength equations. Chord splices on the top and bottom chord provided, in each case, two values of b_0/t_0, namely 25 and 20.

Truss T2 was fabricated to be similar to T1, with corresponding matched members from the same rolled section, but where the joints were 100% overlap. This was achieved by modifying the branch angle between the branch members and the chord. The design of the remaining trusses was not undertaken until T1 and T2 had both been tested. It was found in the case of T2 that to avoid chord member failures the truss had to be shortened, and the number of bays reduced. This was expected since T2 was designed on the basis of being matched to the gap joint truss T1, and as such the joint strength was not critical.

3.2.2 Stage 2 - Trusses T3, T4, T5, & T6

In Stage 2 of the test programme the same section size was used for the chord members in T3, T4, and T5 namely a 100x100x5 RHS. This size corresponds to the section used in the central chord span of T1 and T2. To prevent chord failures in these trusses a shorter span was used than that in Stage 1.

Truss T3 was formed using branch angles of 63^o while retaining the same section sizes for the chord and branch members as those in T2. The objective was to assess the significance of the branch angle θ by directly comparing the results of T2, and T3.

Truss T4 was identical in general layout to T3, however a larger section size was used for the tension and compression branch members, so that the ratio of branch to chord width (β) was increased to 0.6. The chord section used was the same as in T3, thus a comparison between these two trusses was intended to define the effect of altering the β ratio.

Truss T5 was an N type truss fabricated using the same section sizes as T2 and T3. The objective in this case was to compare the relative efficiency of the branch geometry, and to assess whether one is more efficient than the other. The branch angles chosen for T5 are those which are most common in design namely 45^o for the tie and

90° for the strut.

Truss T6 was formed using the same section size for the branch members as T4, namely a 60x60x3.2 RHS. The angle of the branch relative to the chord was also the same, however a larger section was used for the chord (150x150x6.3 RHS), thus giving a β ratio of 0.4, and a b_0/t_0 value of 23.8. This truss was designed primarily to investigate the incidence of local buckling of the chord face behind the tension branch, which has been identified in isolated joint testing and referred to as L7 (see Fig. 2.2). This particular mode of failure is associated with small β ratios and large values of b_0/t_0.

Thus several comparisons were set up between the test trusses incorporating a variation of the parameters thought to be significant. However, it was not intended to be simply a comparative study, but rather to help clarify the role the various parameters play in defining the structural behaviour and mode of joint failure.

3.3 Design of test trusses

The standard approach adhered to by designers was followed in most respects. As a first step basic engineering principles were applied to assess the joint strength, namely checking combined stresses, punching shear, and bearing stresses. However, the CIDECT recommendations[43] relating to joint capacity were also used.

3.3.1 Member design

The trusses were designed to BS 5950[45], Part 1, assuming Grade 43C steel. Initially the nominal dimensions were used in conjunction with an assumed yield stress of 275 Nmm^{-2}. Subsequent to the tensile testing and measurement of the section properties the design of each truss was re-assessed using the measured properties.

Member axial loads were calculated using a pin frame analysis, based on member centre-line noding, and using the member lengths and branch angles such a condition would produce (clause 4.10, BS 5950, Part 1). The compression branches were designed in accordance with BS 5950 Part 1, clause 4.7. The effective length factors of the compression members were taken as 1.0 for the chords (based on the distance between lateral supports), and 0.7 for the branches (based on the distance between the centre-lines of the chords).

Where centre-line noding did not occur, the bending stresses in the chords were evaluated. The moment generated by the joint eccentricity was assumed to be carried by the chord alone and to be distributed equally either side of each joint. The effect of the combined stresses was calculated for each panel according to BS 5950, Part 1, clause 4.2. The compression chord alone was considered, as this gave the worst case. For the branch members only the axial forces were considered to be effective.

3.3.2 Detailing and welding

All chord welds were full strength butt welds. Truss branch welds were either 5mm fillet welds or full strength butt welds. All details used are shown in Fig. 3.3. Particular attention was paid with respect to the welding to ensure that the CIDECT recommendations[43] were adhered to, and that standard practice was incorporated in both the detailing and the fabrication process. All welds were fabricated in accordance with BS 5135[46].

3.3.3 Shear strength of the branch members

The shear capacity of the connecting branch member to transfer horizontal forces to the connecting chord face was not used as a criterion for design (see Fig. 3.4). According to BS 5950 Part 1, clause 4.2.3 only the sidewalls of the member should be assumed as being effective in carrying shear (see Fig. 3.4 - section A-A).

Horizontal shear failure of a branch member has never been identified in any previous testing programme, so it was decided to ignore the recommendations of the code, and thus assess the validity of the assumptions made by BS 5950, clause 4.2.3.

3.3.4 Joint strength

The equations presented in Tables I1 & I2 were used to assess the mean ultimate joint strengths for the trusses. In the case of the gap joint truss T1, the joints were designed using the RHS gap joint formula (Eqn. 1, Table I1), which is based on the mean strength results for isolated joints. Truss T1 was designed such that failure would occur at the joints before yielding or buckling in any of the members.

For each of the overlap joint trusses there were two possible joint configurations per truss, namely strut overlapping tie and vice versa. The respective joint strengths were assessed using Eqns. 1-4 in Table I2. Unlike the other trusses T2 was not

designed to produce joint failures. It was fabricated purely to be similar to T1 and thus allow a comparative study.

3.4 Materials Testing

As soon as the material was delivered from the rolling mill, samples of full size tube were taken from each batch and used to measure the actual section properties to assess whether the rolling tolerances were within the specified limits. Before fabrication of the lattice trusses, samples from each batch were machined to produce tensile test coupons which were tested for strength by BSC staff. The results of the tensile coupon tests are presented in Figs. 3.5, 3.6 and 3.7. No stub column tests were carried out.

For the purpose of measuring the cross-sectional area of the RHS sections a length of tube was cut from each batch and machined to an exact length. This length was then cleaned and weighed, and the volume was calculated by assuming a density of 7860 kgm^{-3}. The volume was then divided by the length of the tube to derive the cross-sectional area. The thickness of each length of tube was measured around the cross section at each end of the cut length. Three measurements were taken on each wall with a micrometer screw gauge. For each tube length the mean section thickness was then calculated. The width and depth of each tube length were measured with vernier calipers at the midspan of the length.

The British Steel Corporation produce data tables giving the nominal section properties of Rectangular Hollow Sections. From these tables it was possible to establish a relationship between the second moment of area and the cross-sectional dimensions (b_i, t_i) such that :

$$I_i = \left(\frac{b_i t_i^3}{6}\right)\left(4\alpha^2 - 12.72\alpha + 11.946\right) \qquad \text{Eqn. 3.1}$$

where,

$$\alpha = \left(\frac{b_i}{t_i}\right)$$

The second moment of area for each specimen was calculated from this equation. The section modulus was then calculated from:

$$Z_i = \left(\frac{2I_i}{b_i}\right) \qquad \text{Eqn. 3.2}$$

It is commonly understood amongst engineers that there can be considerable variation of yield properties of steel as supplied even to the same grade specification. As long as the material used satisfies the minimum requirements, the designer is not normally worried by what is usually an excess of strength. This is not the case however for the researcher who is setting out to understand physical phenomena, and attempting to produce coherent design recommendations on the basis of the same material throughout. The interpretation of the results is made particularly difficult in such cases when failure can be in a range of members or joints and associated with different modes of failure. This has certainly been true in this investigation.

Although the tensile strength specification was generally satisfied, the specified minimum yield stress was not reached in two cases (see Fig. 3.5). The major cause for concern was, however, the considerable variation of yield strength recorded. Using the gap joint equation, the applied loads for the failure for each of the joints and the members had been calculated, and the estimated order of failure ascertained on the basis of a uniform yield strength of 275 Nmm^{-2}. The strength of the gap joints in truss T1 were thus re-estimated using the actual measured yield and ultimate stress values. In the case of the 100% overlap joints the strength estimates were also re-calculated using the measured section properties and tensile strength values.

The strength of the sections ordered to form the branch members in the trusses were generally higher than those of the chord sections. The member design was thus re-assessed to prevent the incidence of premature chord failures. The non-uniformity of the strength of the steelwork also meant that the specification of the welds had to be modified from Grade 43C to 50C to avoid the occurrence of weld failures.

The limits of validity for the strength equations in Tables I1 and I2 state that the yield stress of the chord section should never exceed 360 Nmm^{-2}. It was not possible under the circumstances to meet this requirement in all of the test trusses.

Table 3.1 Nominal section sizes used for test trusses.

Truss	Tension chord	Compression chord	Posts chord	Compression bracings	Tension bracings
T1	100x100x4.0 100x100x5.0	100x100x4.0 100x100x5.0	100x100x4.0	40x40x4.0	40x40x3.2
T2	100x100x4.0 100x100x5.0	100x100x4.0 100x100x5.0	100x100x4.0	40x40x4.0	40x40x3.2
T2/2	100x100x5.0	100x100x5.0	100x100x4.0	40x40x4.0	40x40x3.2
T3	100x100x5.0	100x100x5.0	100x100x5.0	40x40x4.0	40x40x3.0
T4	100x100x5.0	100x100x5.0	100x100x5.0	60x60x3.2	60x60x3.2
T5	100x100x5.0	100x100x5.0	100x100x5.0	40x40x4.0	40x40x3.0
T6	150x150x6.3	150x150x6.3	150x150x5.0	60x60x4.0	60x60x3.2

Notes :
1) To be read in conjunction with Appendix A.
2) All dimensions are in mm.
3) All sections are square RHS & Grade 43c.

Table 3.2 Parameter range for joints based on nominal dimensions.

Truss	Joint type	θ_1	θ_2	β	b_0/t_0	b_1/t_1	b_2/t_2	b_1/b_2
T1	gap	47.0	47.0	0.4	20.0 & 25.0	10.0	12.5	1.0
T2	100% overlap	42.9	42.9	0.4	20.0 & 25.0	10.0	12.5	1.0
T2/2	100% overlap	42.9	42.9	0.4	20.0	10.0	12.5	1.0
T3	100% overlap	63.3	63.3	0.4	20.0	10.0	13.3	1.0
T4	100% overlap	63.3	63.3	0.6	20.0	18.8	18.8	1.0
T5	100% overlap	90.0	45.0	0.4	20.0	10.0	13.3	1.0
T6	100% overlap	63.3	63.3	0.6	23.8	18.8	18.8	1.0

Notes :
1) To be read in conjunction with Appendix A.
2) All dimensions are in mm.
3) All sections are square RHS & Grade 43c.

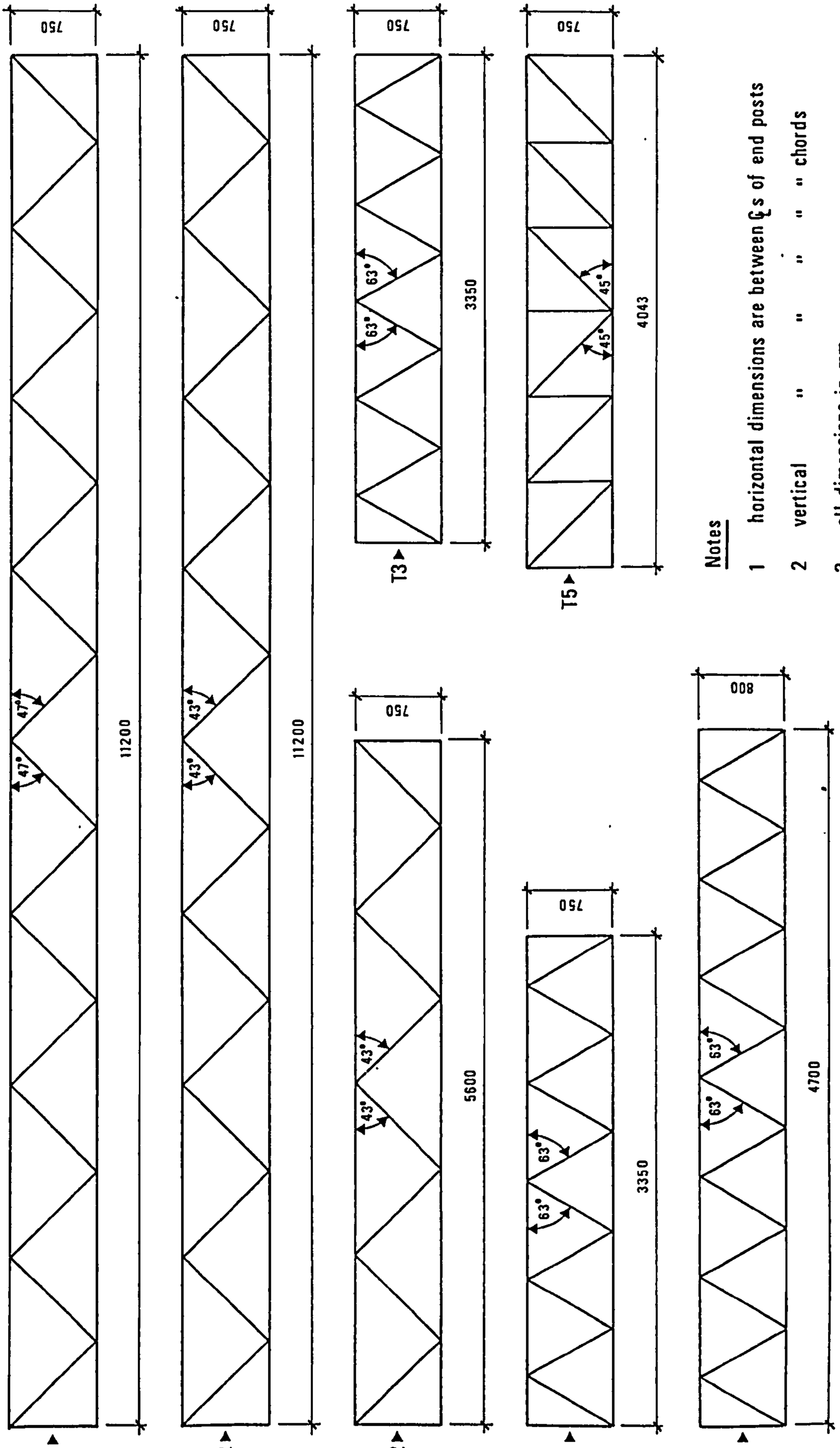

Notes

1 horizontal dimensions are between ℄s of end posts

2 vertical " " chords

3 all dimensions in mm

Fig 3.1 General arrangement of test trusses.

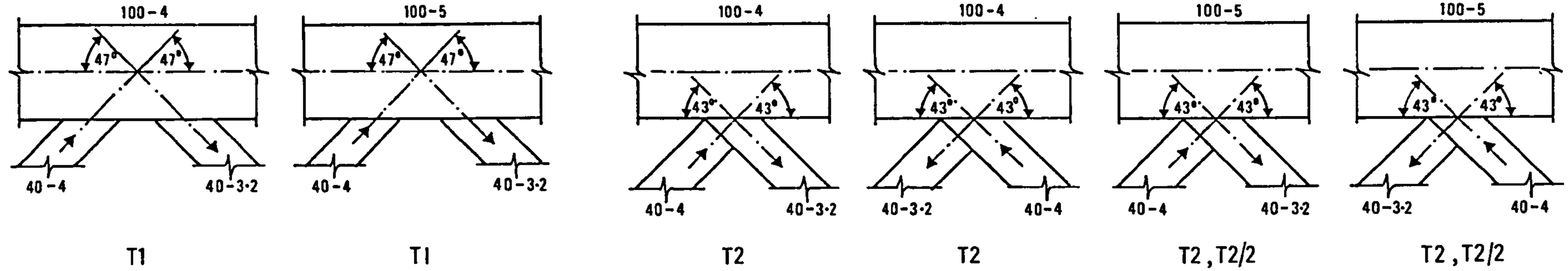

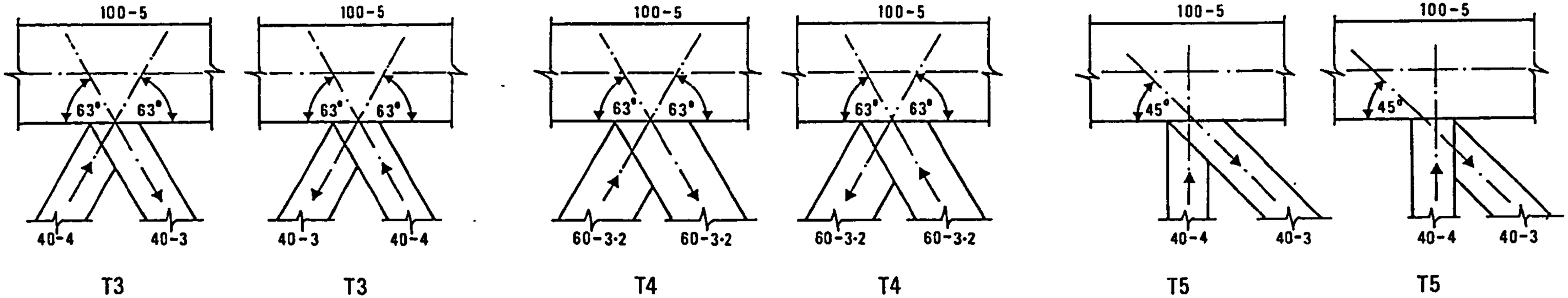

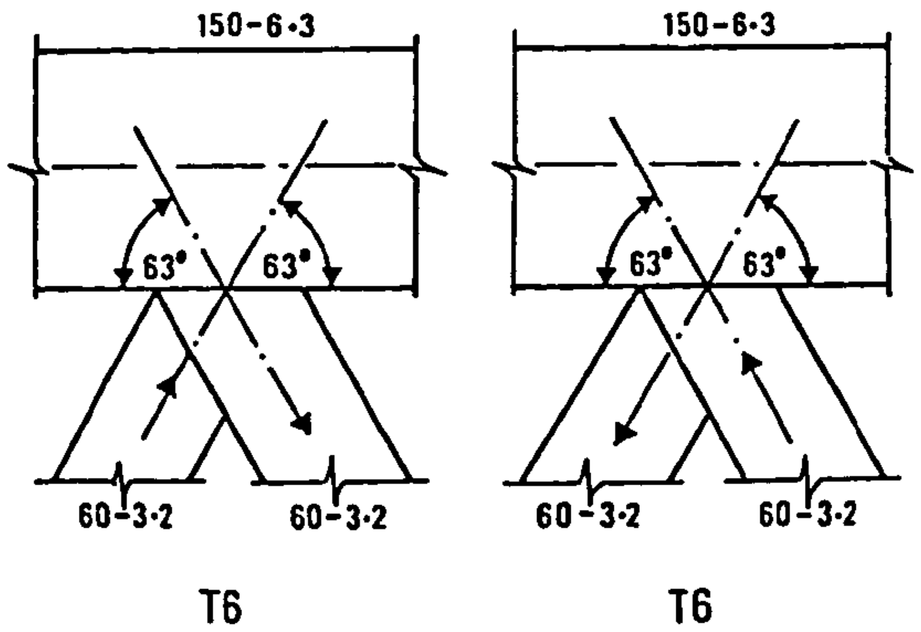

Notes

1 all sections are SQUARE RHS

2 section is defined by (outside dimension - wall thickness) in mm

Fig 3.2 Truss joint geometries.

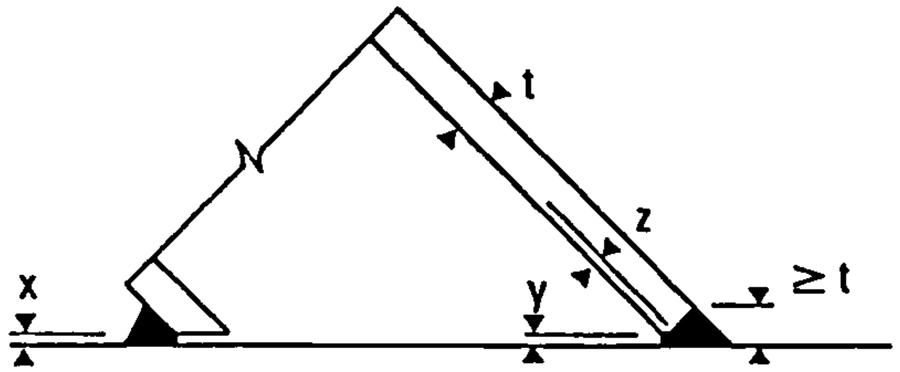

a) T1 gap

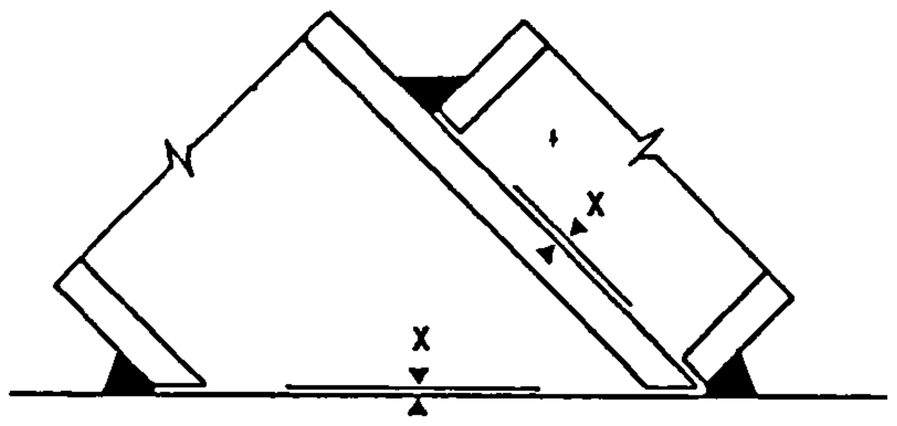

b) T2 , T3 , T4 , T6 100% overlap

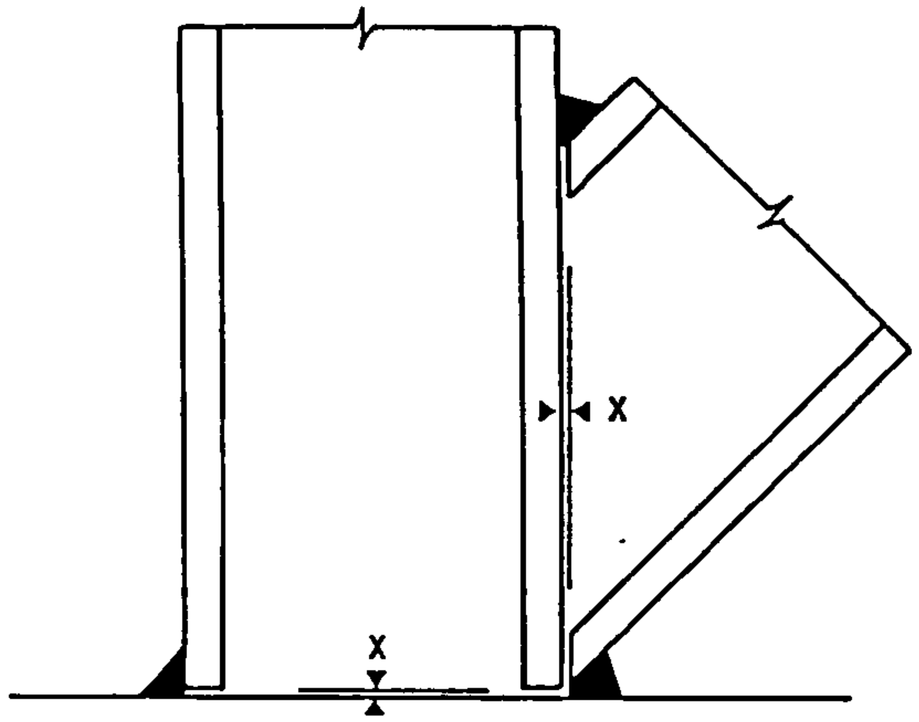

c) T5 100% overlap

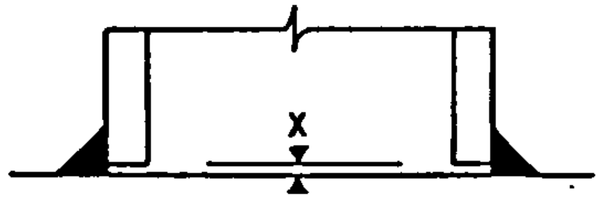

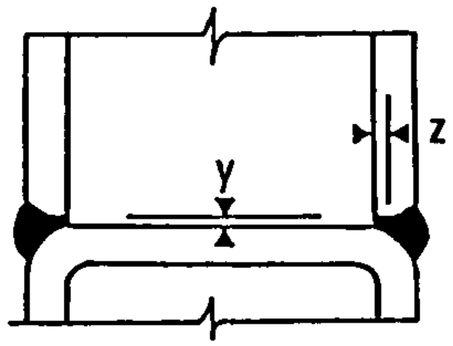

d) T1 , T6

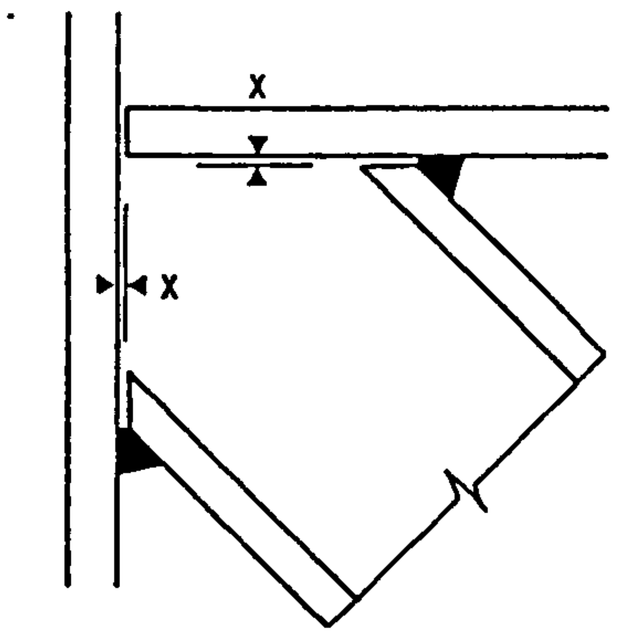

e) T1 , T3 , T4 , T5 , T6

Notes

1 a,b,c,e show connections along toe and heel of bracings

2 d shows " " sidewalls " "

3 all fillet welds are 5mm leg length

Tolerances

$x \leq 2mm$ $y = 2\text{-}3mm$ $z = 1\text{-}2{\cdot}5mm$

Fig 3.3 Weld details.

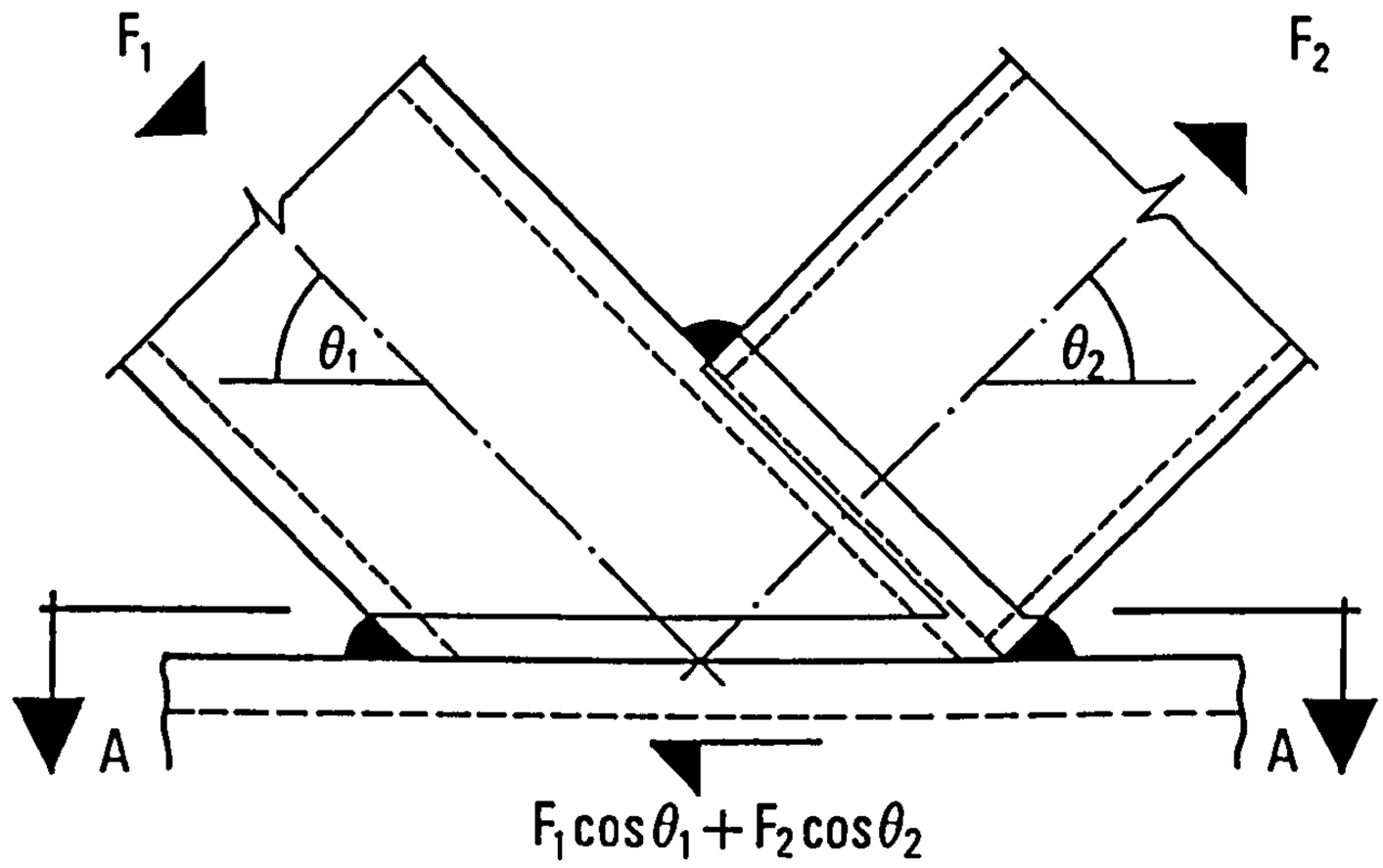

side elevation of 100% overlap joint

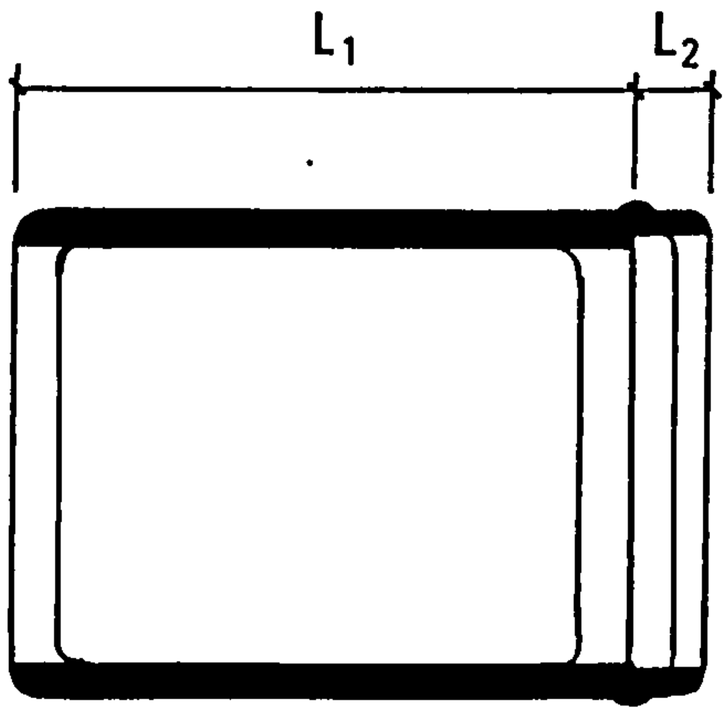

only sidewalls are assumed to be effective in transferring shear according to BS 5950 (clause 4·2·3)

A - A

Fig 3.4 The transfer of shear force from the branches to the connecting chord face.

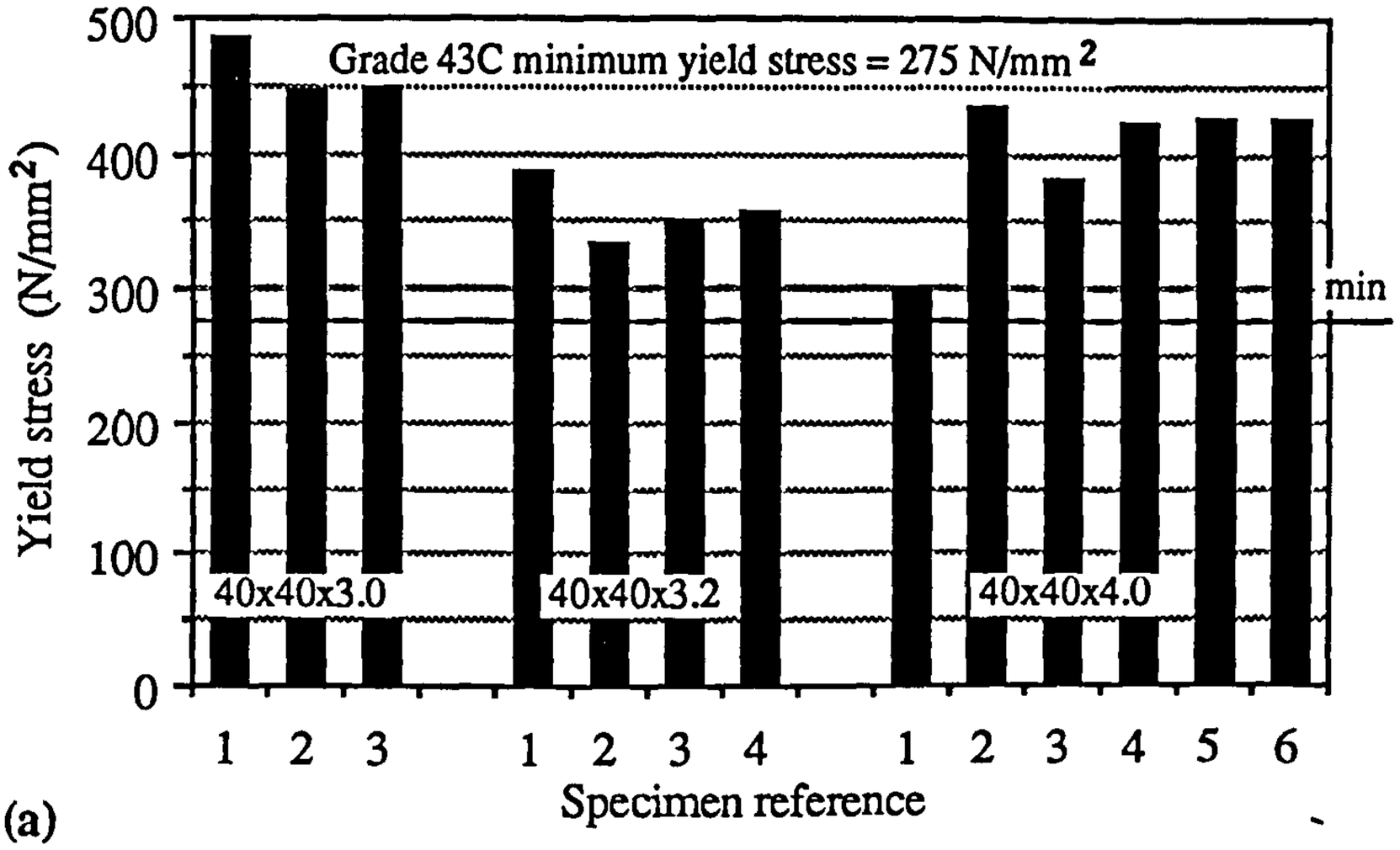

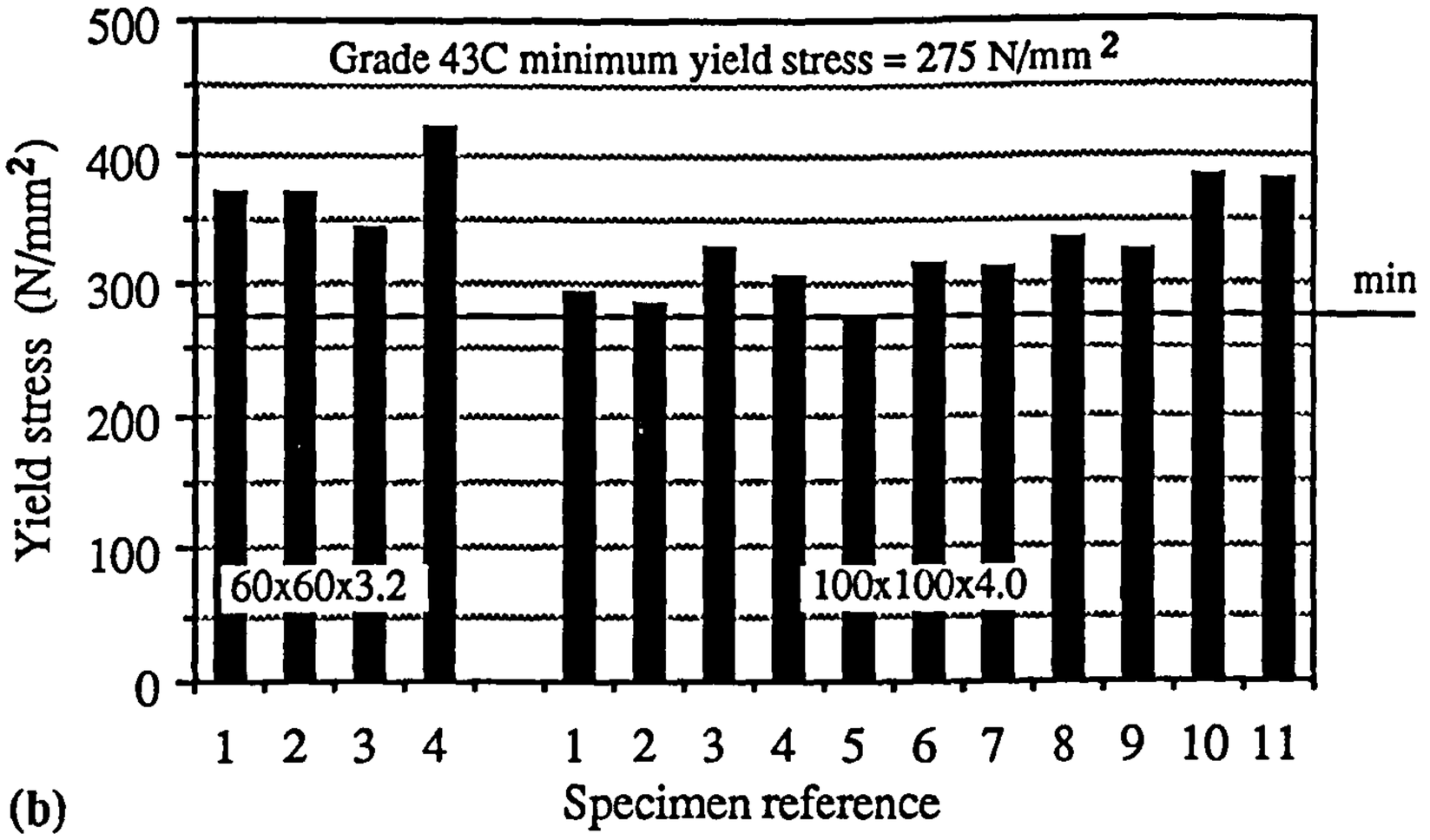

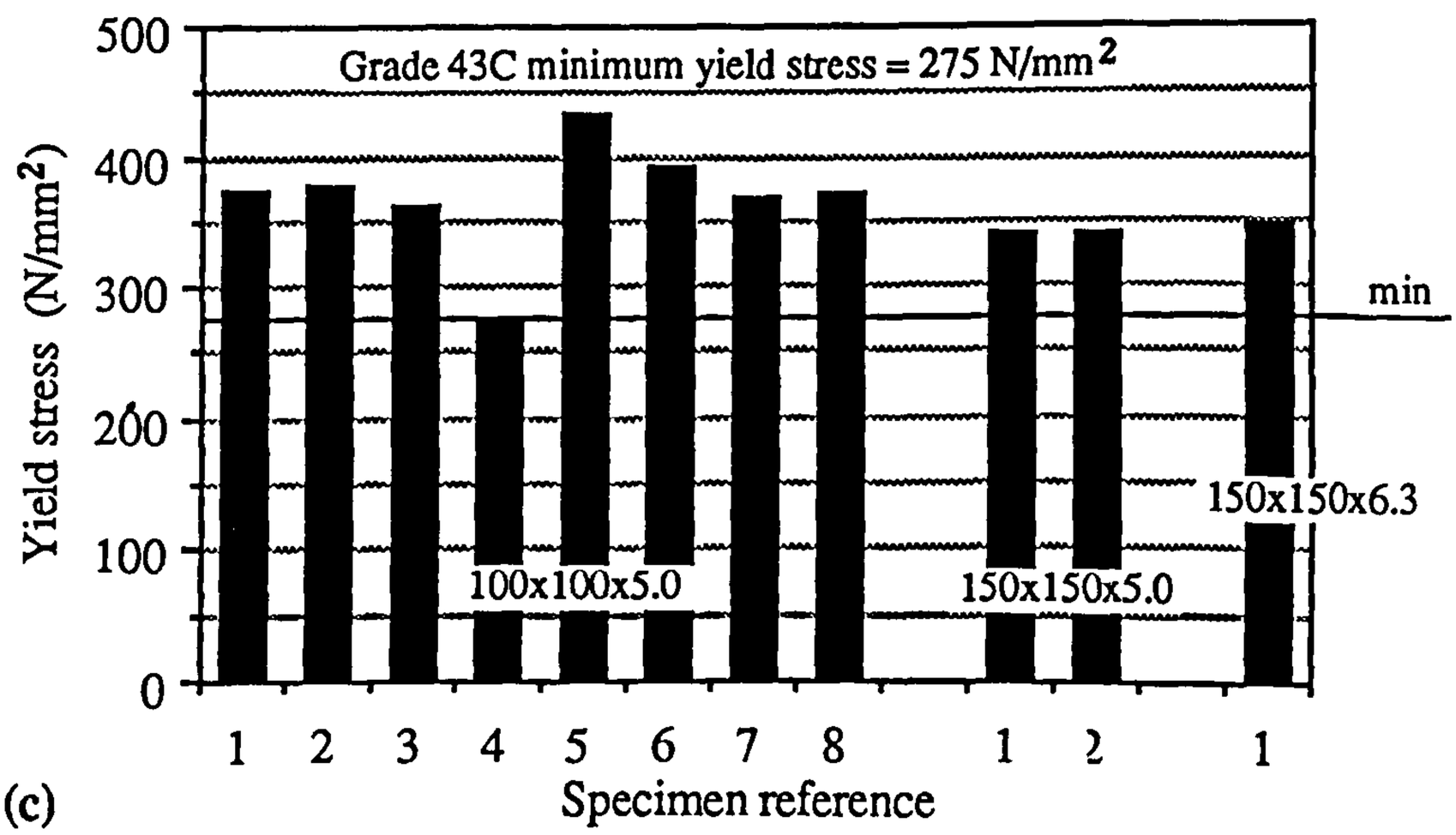

Fig 3.5 Measured yield stress values

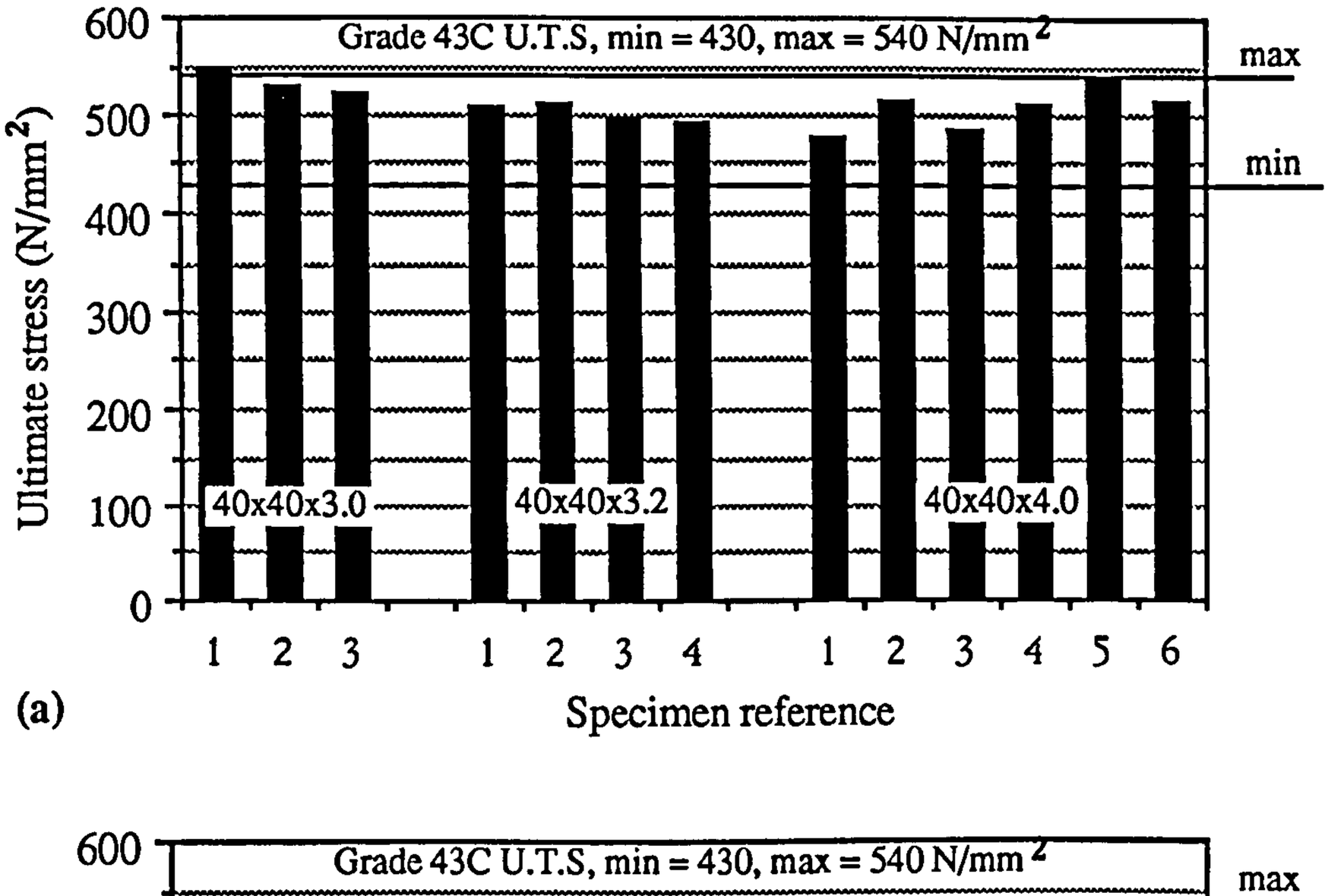

(a)

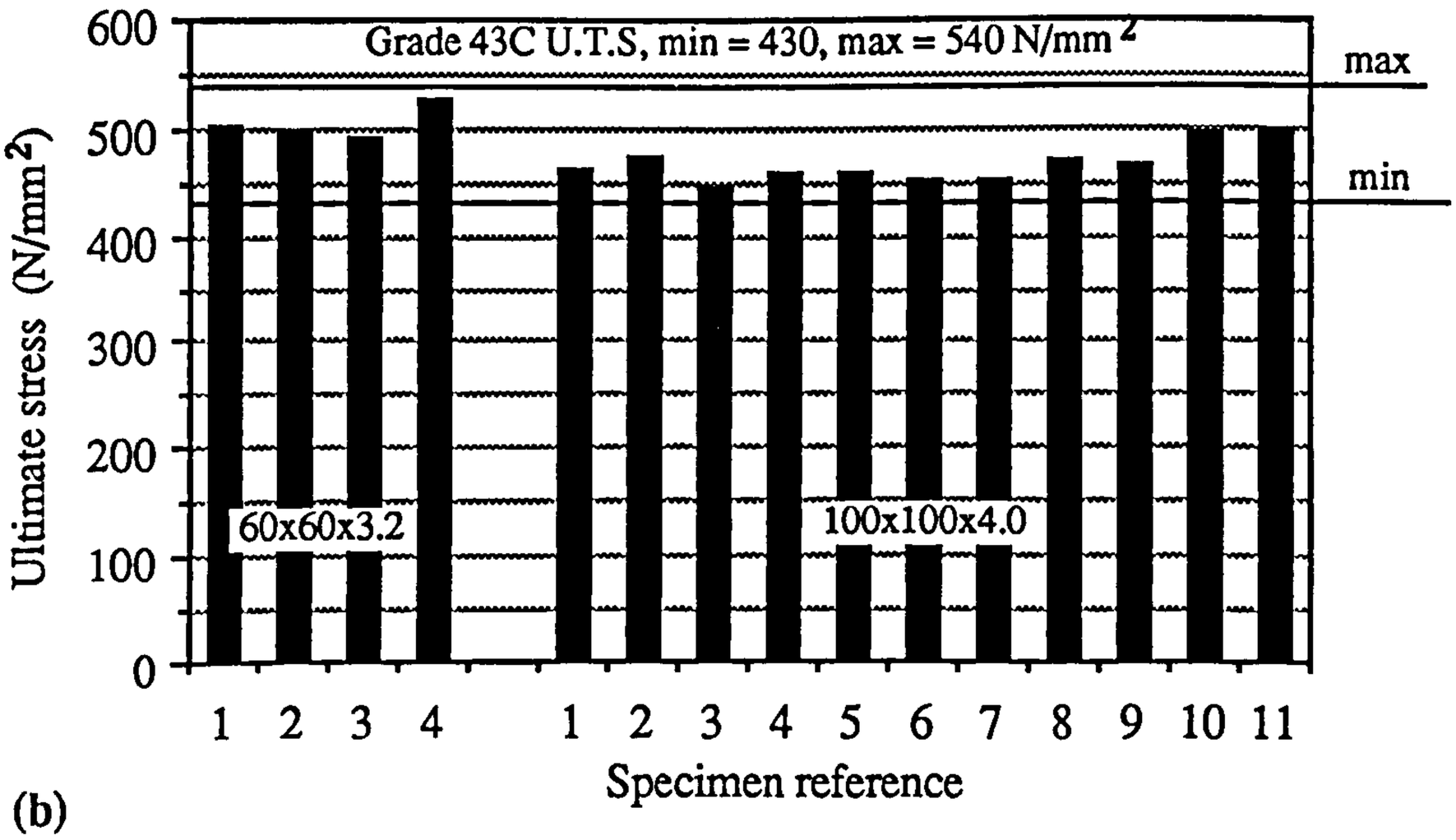

(b)

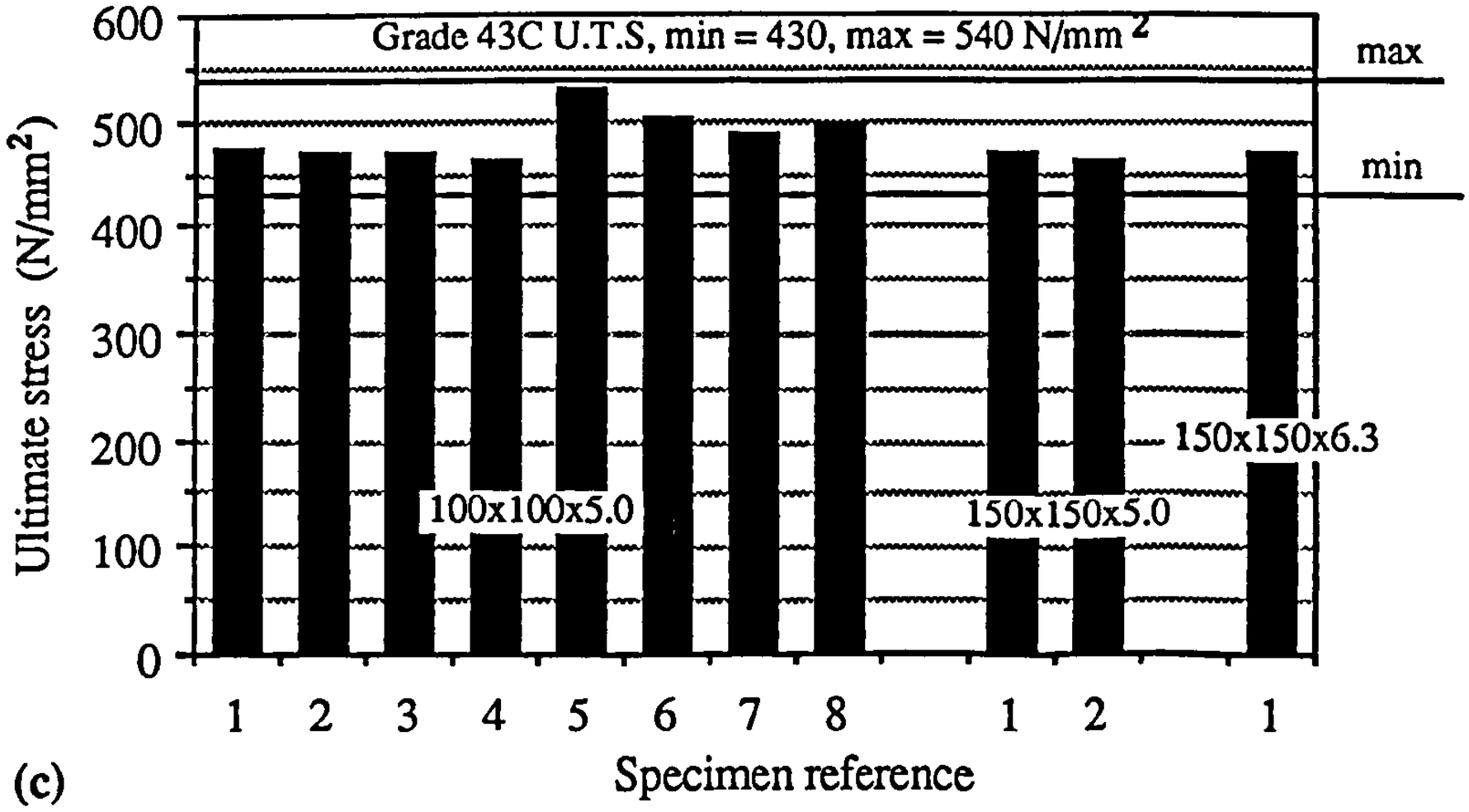

(c)

Fig 3.6 Measured ultimate tensile stress (U.T.S) values

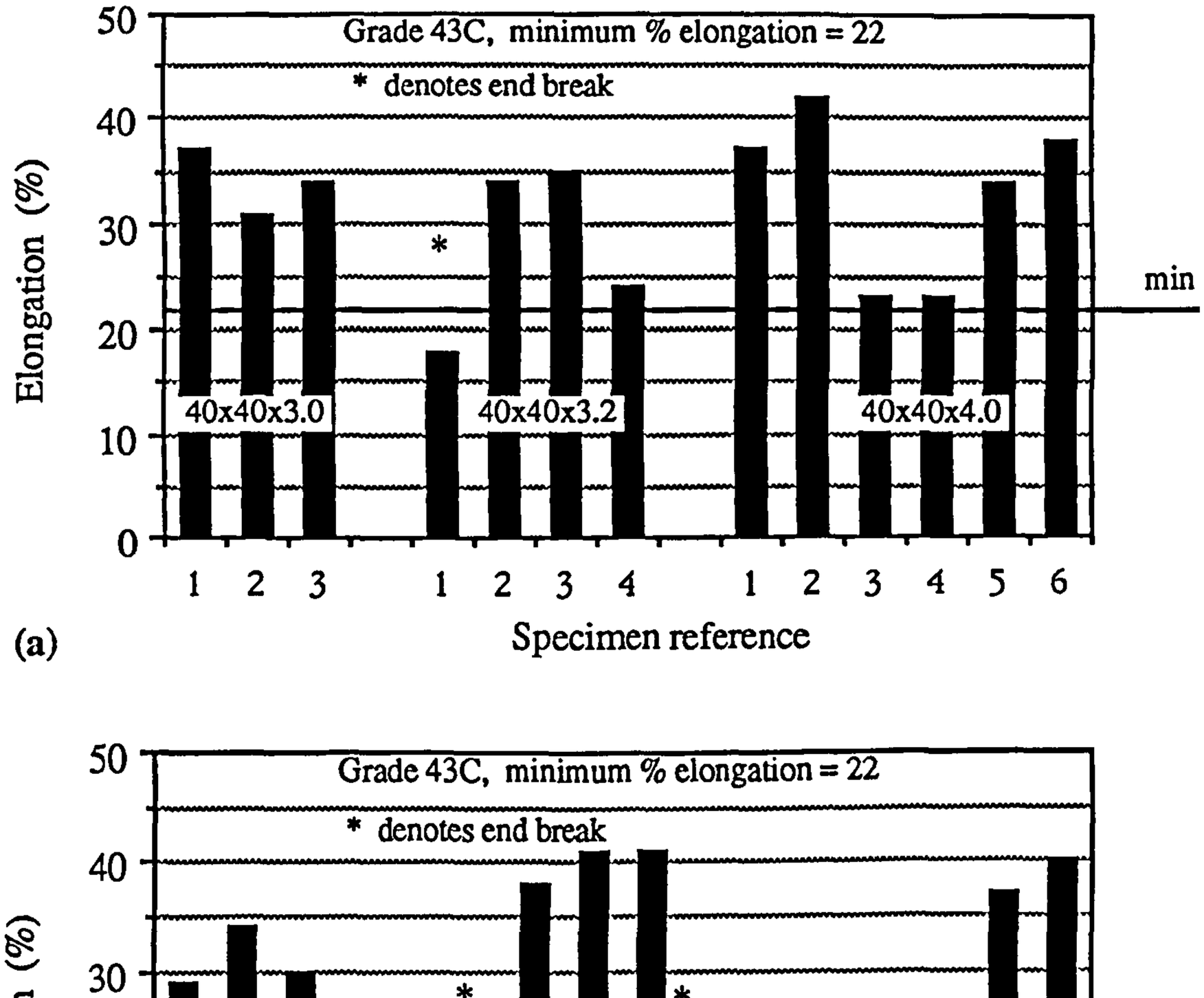

(a)

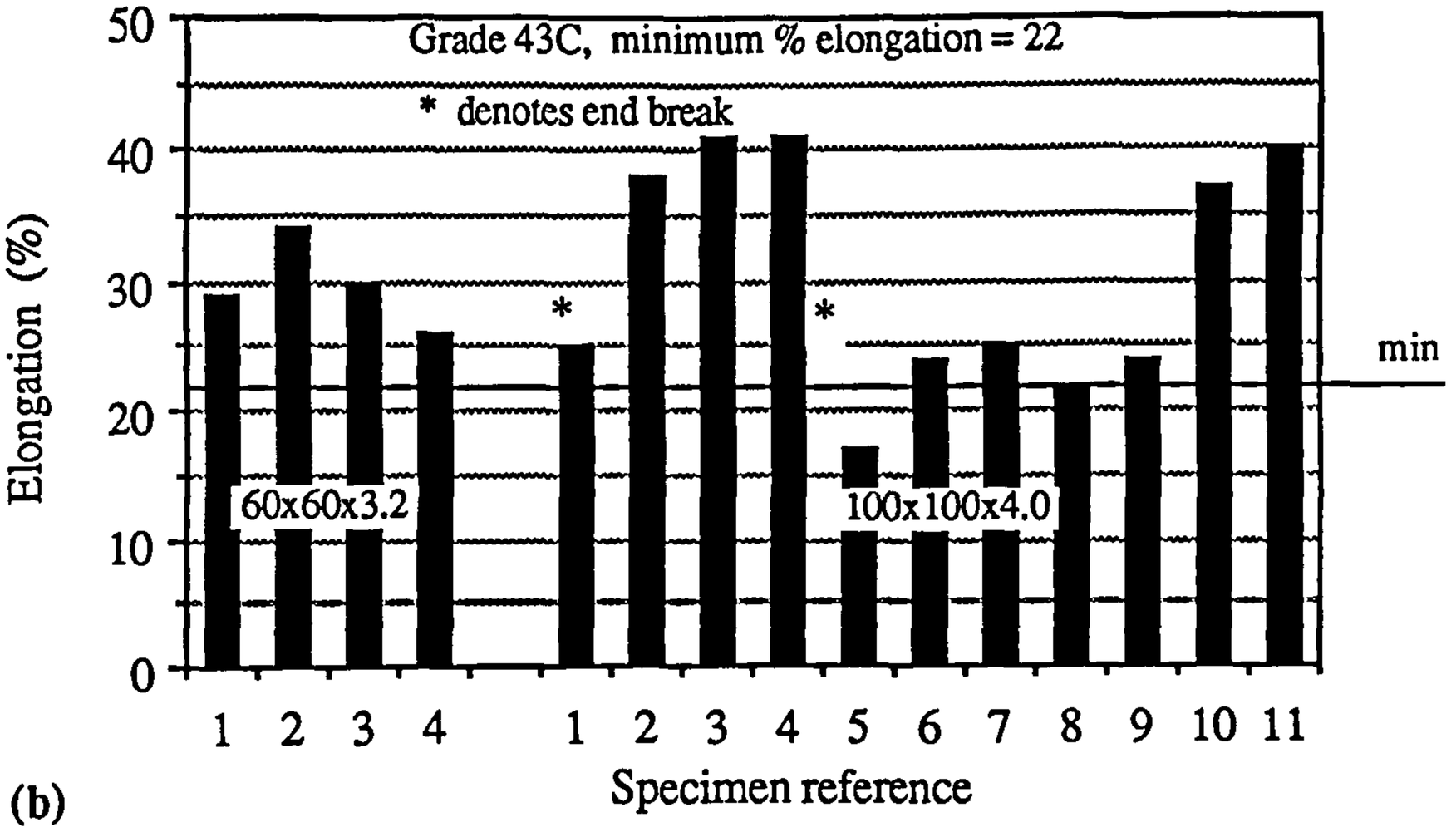

(b)

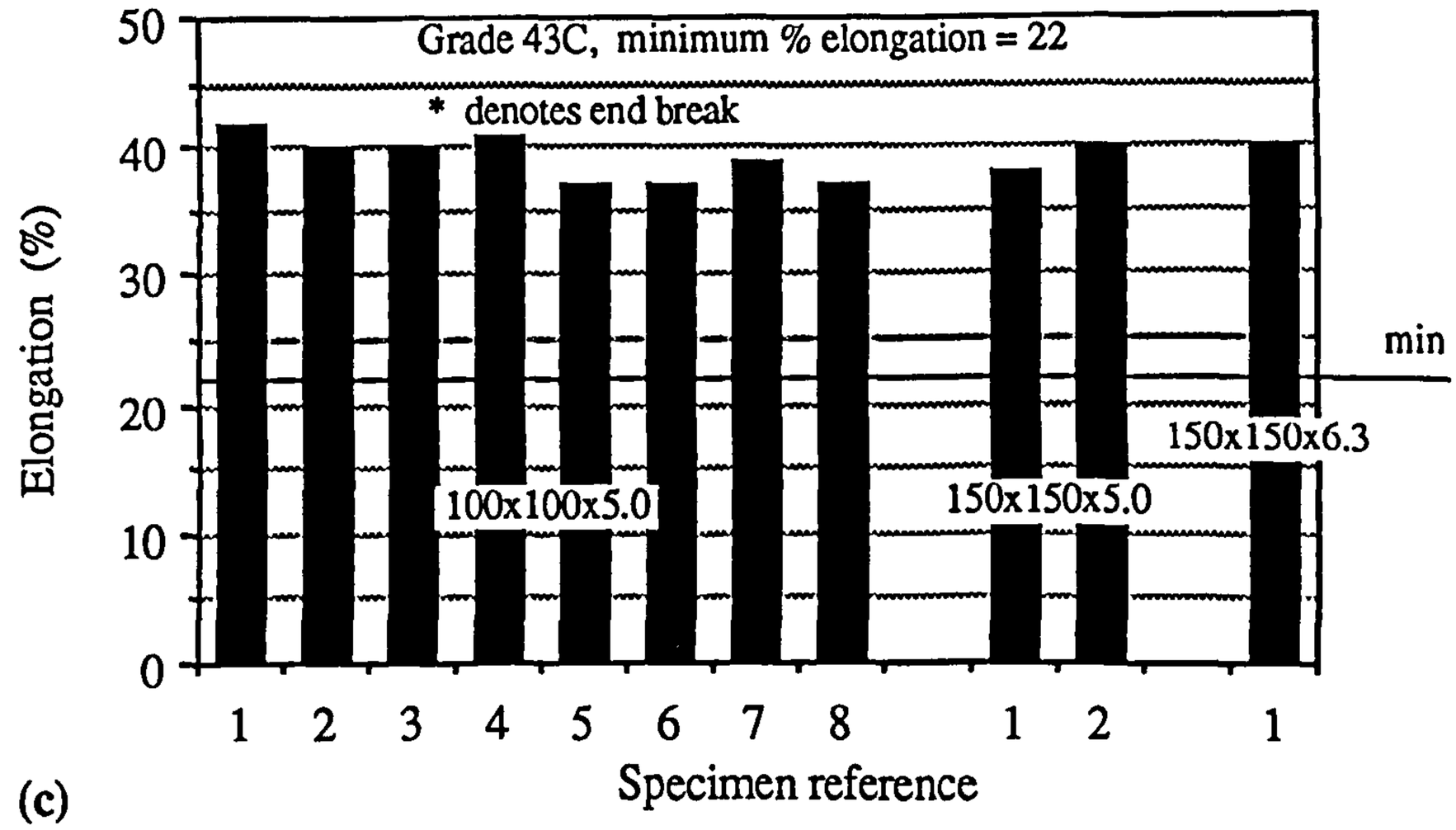

(c)

Fig 3.7 Measured percentage elongation values

CHAPTER 4
EXPERIMENTAL INVESTIGATION AND INTERPRETATION OF RESULTS

4.1 Test set up

The trusses were tested under simply supported end conditions, with a roller bearing at one support and a rocker at the other (see Fig. 4.1). Although such trusses would normally have purlin loads at each joint, it was decided to carry out all the tests with a central point load only, so that shear and hence the forces in the branches were constant throughout. The test rig is shown in Plate 4.1.

Special strengthening was applied at the loading point, where the ram was located on to the top chord by means of a machined plate (see Appendix A, Fig. A12). The load was applied vertically downwards by means of a hydraulic jack. For the testing of trusses T1, T2, and T2/2 a semi-automatic hydraulic system was used to control the jack, however the hydraulic system in this case only had a maximum capacity of 350 kN. For the remaining test specimens a hand pump was used to control the jack. The load was always applied under controlled deformation loading. The structural components of the test rig (see Plate 1) were as follows :

(i) A steel frame to which the hydraulic jack was attached. This was bolted together, and fixed to the laboratory strong floor by holding down bolts.

(ii) A rocker bearing under one end of the test truss and a roller bearing at the other.

(iii) A mechanism to prevent lateral instability of the compression chord (see Plate 4.2). This comprised of roller ball-races which were fixed on to steel frames bolted to the laboratory floor. The design of the lateral restraint system was in compliance with BS 5950[45], Part 1, clause 4.2.2, such that the sum total lateral capacity of the system was equivalent to 1.0% of the maximum expected axial force in the compression chord. Lateral restraint to the compression chord was provided near the end supports and at several intermediate points (see Plate 4.1).

All structural steelwork was designed to BS 5950[45] and the reinforced concrete strong floor was checked using CP110[47]. The most important consideration was safety. The rig was designed such that the serviceability limit state was never to be exceeded in any component. This also ensured that the deformation of the rig was kept to an acceptable level.

Allowance was made in the rig design to accommodate the large in-plane deformations of the test trusses. Therefore the positioning and fixing of the sensors was given careful consideration. It was important that the sensors were able to function reliably throughout the entire load range.

Although the self-weight of the test trusses acted in each case in the direction of the applied load, it was decided to neglect the effects caused by the weight of the trusses, instrumentation and cables. For the largest test specimens, namely T1 and T2 this was of the order of 0.6 kN.

Before testing, each joint of the respective test truss was whitewashed with hydrated lime, which when dry provided a brilliant white brittle surface. The dry hydrated lime allowed cracking and local deformations to be identified more easily. One important characteristic of this whitewash was that at loads close to the yield stress of the steel striation marks developed. These were caused by 'shear slip' between the crystals in the steel, thus defining the directions of the principal shear planes. Thus it was possible to identify the direction of the principal stresses in the vicinity of a joint. This proved to be useful in defining what force combinations had caused a particular failure mode.

4.2 Instrumentation and measurements

The instrumentation consisted of Electrical Resistance Strain Gauges (ERSG's), Linear Potentiometers (LP's), Linear Variable Differential Transformers (LVDT's), Load Cells (LC's), Dial Gauges(DG's), and a thermo-couple. Only the DGs were recorded manually, all other sensors were automatically scanned by a 3530-D Orion data logger[48] (see Fig. 4.1). By inputing the respective factors and calibrations for the various instruments into the logger, all outputs were in the form of direct values ie., micro-strain for the ERSG's, millimetres for the LP's and LVDT's, kilo-Newtons for the LC's, and degrees Celcius for the thermo-couple. The arrangement of sensors at a joint is shown in Plate 4.3, and consisted of four LP's and eight ERSG's.

All setting up and operation was achieved using the Orion front panel which contains control keys for the main functions. The built-in magnetic cartridge recorder was used to record and replay logged data, and to store and retrieve setting up programs. All analogue measurements were performed via the analogue to digital convertor (adc) which employs the pulse-width conversion technique[48], offering fast and accurate measurement.

Each measurement by adc is by continuous integration. A reading rate of 40 channels per second was chosen in preference to the other options available, namely 500/s, 150/s, and 10/s. The 40/s rate was chosen because of its increased sensitivity and better interference rejection with respect to the faster rates. The reading rates are applicable to DC voltage based measurements and are the effective rates at which the measurements are accepted by the memory.

A 1000 measurement buffer is used by the Orion for temporary storage of results; when this is filled the average scan rate is slower than that selected to accommodate any process or output device throughput. An auto-zero and calibration sequence is performed automatically which ensures that the highest possible accuracy of measurement is attained. 'Zeros' are measured for each range at appropriate resolutions and stored. These readings are used as corrections when the active channels are scanned. Thermo-offset correction is offered on resistance-type measurements. This is useful in cases where unavoidable thermal EMF's are produced, ie., in wiring, connectors and switches associated with the transducers being measured.

The adc has five measurement ranges. During the first scan, or as a result of any initializing scan (such as that used for the strain gauges) the range for each channel is automatically established and stored. On subsequent scans the same respective range for each channel is adopted. If an input is too high or too low for the adopted range, the adc automatically moves to a more appropriate range. When an overload is detected the measurement is stopped and the adc up ranges so that the input is re-measured.

The wiring from inputs are taken to screw terminals located within a plug-in input connector, thus each input in turn is connected to the measuring circuit by means of switches on a selector card. Each connector is totally enclosed and incorporates wiring clamps. The 3530-D Orion data logger has the advantage that nearly any type of sensor can be connected to any channel in any sequence. Thus instrumentation layout is the operator's choice and not the criterion of the data logger. In most other systems each different sensor requires a particular dedicated module. The system used thus allowed all the sensors for each joint (ERSG's and LP's) to be connected in the same logger connector.

4.2.1 Strain Gauge Installation

The cost was a prime consideration in the selection due to the large number of strain gauges being used. TML FLA-6 strain gauges[49] were used throughout. These were foil as opposed to wire strain gauges. The strain gauges were installed and positioned in accordance with the manufacturer's recommendations[49] and allowed accurate and reliable strain measurements to be made.

For each strain gauge the logger requires data to be input relating to the gauge factor, and resistance. Furthermore, the data logger includes a thermistor to reduce effects produced by fluctuation in temperature, by compensating for any apparent strain. The logger takes a reading of a strain gauge channel without energizing, and then takes a reading when energized - it then subtracts one reading from another to derive the recorded value. This value is thus free from 'electrical noise' and heating effects. The logger only takes a reading of one channel/sensor at a time, thus reducing the risks of one channel 'electrically interfering' with an other.

4.2.2 Member forces and bending moments

Member axial forces, in-plane bending moments and shears were calculated from the surface strains. For each member four strain gauges were mounted. These were placed in pairs at a known distance apart, and far enough from the member ends to avoid the effects of local deformation adjacent to a joint. From each pair of ERSG's an axial force and a bending moment were derived using the measured cross-section properties. A linear extrapolation was used to obtain the end moments of each member. The positioning of the ERSG's for each truss is presented in Appendix C.

4.2.3 Loads and reactions

Compression load cells were used under the hydraulic jack and at the support points to measure the applied load and the resulting end reactions. An initial calibration of the LC's in a standard calibrating rig did not yield good agreement with respect to equilibrium in the preliminary elastic testing. Therefore, all the load cells were re-calibrated 'in-situ' using exactly the same power supplies and lead wires as those used in the truss tests. This had the desired effect of removing the discrepancy between the LC's with respect to elastic equilibrium tests.

4.2.4 Joint deformations

At each joint linear potentiometers (LP's) were used to measure the in-plane joint deformations. Two LP's were mounted at each end of a branch member, one on each side of the member (see Plate 4.3). The reason for using two LP's in this way was to assess the component of the joint deformation caused by out of plane rotation, and eliminate it by taking the average of the two values. The object of using these sensors was to assess the chord face deformation at each joint.

The local deformation of the joint was measured relative to small indent marks on the chord. The rectangular frame (see Fig. 4.2 and Plate 4.3) was located at the correct position using the indent marks on the chord. The rectangular frame was designed so that the locating spindles would remain in the same position regardless of any deformation or buckling of the chord sidewalls. It was for this reason that the idea of fixing the spindles directly onto the chord faces was rejected.

Conductive plastic LP's were chosen due to their infinite resolution, compact size, and low cost. The LP's were powered by an external power unit designed specifically for the test, and calibration was undertaken 'in-situ' using the same electrical configuration as for the testing.

4.2.5 Truss deflection

LVDT's were used to measure the deformation of the bottom chord of the trusses relative to the laboratory strong floor. The deflection was measured at midspan (and at the quarter-points in the case of T1 and T2). As in the case of the LP's, the LVDT's were also powered by an external power unit and calibration was conducted 'in-situ'.

Two dial gauges were used at each support to monitor the vertical movement at the supports during the loading sequence. These dial gauges were placed on each side of the truss, so that the difference in reading between the two at a support would give an indication of vertical movement caused by out of plane rotation.

4.3 Test monitoring

The control desk is shown in Plate 4.4. An X-Y plotter was used throughout all testing sequences to automatically plot applied load against central deflection. However

for the most part 'live' graphical representation of the truss behaviour during testing was carried out using a BBC microcomputer. The computer was connected to the Orion data logger via an RS-232 interface. A program was written[50] to retrieve the data from the logger immediately on completion of a scan. The program had the facility of plotting graphically one selected channel against any other channels, and to display up to a maximum of six simultaneously.

While the data was displayed graphically on the screen it was simultaneously stored onto floppy disk. Facilities were also available within the program to design finished graphs of the stored data, and to print out all recorded data. For the most part the microcomputer was used to display the applied load against either the outputs from the strain gauges, linear potentiometers, LVDT's, or reaction load cells. For these tests the applied load channel was always chosen to be the ordinate. At each load increment the values of all the sensors were recorded by the data logger and stored on magnetic tape as well as on floppy disk by the BBC microcomputer.

At each load increment a visual examination of the truss was conducted, with particular reference being made to the joints, so that the initial signs of yielding, cracking or buckling were noted with respect to applied load. In this way a detailed account of the structural performance of the each truss was afforded.

4.4 Test procedure

Prior to loading a test truss to failure, a preliminary elastic test was conducted where the maximum ram load was limited to 30% of the expected failure load. The object in this case was to check that all the instrumentation was functioning correctly. Some degree of 'settling in' of the truss was always apparent, however bearing this in mind all the sensors were expected to behave linearly with respect to the applied load for the duration of the test and to return to the initial zero mark on removal of the load, with negligible hysteresis. Once this criterion had been checked and satisfied for all the sensors the test specimen was deemed ready for testing to failure.

During the load sequence leading to the failure of the truss, the load was initially incremented until approximately 50%-70% of the estimated maximum capacity was reached, the load was then decremented to zero. This was done to allow 'settling in' of the truss. Once the zero scan had been taken the load was once more incremented and the test continued until failure was achieved.

Ultimate truss load (ram failure load) was characterized in all cases by the truss unable to sustain further increases in load. At the point of failure the deformation was maintained at a constant value and a detailed visual investigation was undertaken, to assess yielding patterns, cracks and modes of failure. Once joint and/or member failure had occurred in a truss the applied load was removed in a controlled manner, and a number of scans were taken during the unloading sequence. A scan was also taken immediately on reaching the zero load. At zero applied load a scan of all the instruments was made and recorded on the datalogger. The truss was then allowed to settle for a one hour period after which a second scan was taken. Photographs were then taken of the members and joints that exhibited signs of distress.

Where possible failed members and joints were strengthened by plating. On completion of the repair work the truss was allowed to cool down for a period of twelve hours after which a scan of the strain gauge values was taken. The strain gauge values were then initialized (ie., set to zero) and the test repeated until a higher truss ultimate load (ram failure load) was achieved. This procedure allowed a history to be maintained with respect to the residual strains in the truss members. The repair process on completion of each load cycle was repeated until the maximum helpful information for each truss had been obtained. The loading sequence for each truss is shown in Figs. 4.3 to 4.9.

4.5 Test results

The test data obtained at each load increment and recorded on the Orion data-logger's magnetic tape was transferred on completion of each test to a Sinclair QL microcomputer where it was processed to provide output in a convenient graphical and tabular form.

In order to allow comparisons between trusses and analytical models only the first load cycle leading to failure has been considered. Subsequent failure cycles proved to be unreliable for this purpose because the trusses had already undergone yielding and repairs.

4.5.1 Graphical presentation of results

For each truss five types of graph were used to assess the behaviour up to ram failure load (typical examples are shown in Fig. 4.10). The ordinate in each case represents the applied ram load, and the values plotted as the abscissa are:

(i) Strains at the gauge positions .
(ii) Chord face local deformation.
(iii) Member axial force.
(iv) Member bending moments.
(v) Midspan truss deflection.

For the sake of clarity only the values on the increasing part of the load cycle have been plotted.The first two types of graph relate to the joints, while (iii) and (iv) have been plotted with respect to each member. For the axial force and bending moment plots two values are presented per graph, one for each end of the member.

It is impractical to present all the graphical information in this thesis. However, relevant examples have been provided in the main body of the text. For each truss a full set of the graphs is provided in independent reports[51, 52, 53, 54, 55, 56, 57].

4.5.2 Joint strength tables

For each truss an assessment of the joint forces at ram failure load has been made. This information is provided in a tabulated form and referenced against the respective modes of failure. All tabulated information relating to joint behaviour at ram failure load is presented in Appendix D. Appendices J, K, L and M are referred to in Chapter 8. The tables in these appendices have been used to compare experimental joint and member strengths with those predicted from various equations and design methods.

4.5.3 Stress distribution diagrams

For each of the truss joints the stress distribution has been plotted in the sidewalls at the gauge positions (see Fig. 4.11). There are two stresses, one relating to an applied load in the elastic range and the other to the distribution at the ultimate load (ram failure load). The stress distribution diagrams for each truss are presented in Appendix E.

4.5.4 Distribution of axial forces and bending moments

The measured elastic axial forces and bending moments are tabulated for each test truss in Appendix F, where the experimental results are compared to those derived from various theoretical elastic frame analyses. The distribution of axial forces and

bending moments at ram failure load are also presented in Appendix F. For each of the trusses the measured and theoretical elastic bending moment diagrams are presented in Appendix G. The distribution of bending moments at ram failure load is presented in Appendix H.

4.6 The derivation of forces and deflections

4.6.1 Truss deflection

All graphs of truss deflection relate to the deflection of the tension chord at midspan relative to the supports. All LVDT's measured the deflection of the truss relative to the laboratory floor. To define the actual truss deflection relative to the supports, the settlement at the supports has also been considered (see Fig. 4.12).

4.6.2 Joint deformation

In the case of graphs displaying joint deformation, the deflection normal to the chord face has been plotted. In the case of the gap joint truss two values exist per joint, one relating to the tie and the other, to the strut (see Fig. 4.13[a]). For 100% overlap joints there is only one value (see Fig. 4.13[b]).

For truss T1 (gap joint truss) the displacements were measured along the centre-line of the branches, from the clamp position to the intersection point of the branch member centre-lines. The locating spindles were thus positioned on the chord centre-line. The joint deformation has been calculated in a direction perpendicular to the chord face (see Fig. 4.14[a]). For the overlap joint trusses where the branch member centre-lines intersected on or above the chord face, the locating spindles were positioned at a depth of 5mm from the connecting chord face (see Fig. 4.14[b]). In all cases the clamps holding the LP's were placed at a distance of 150mm from the chord face, as measured along the centre-line of the branch member.

The elastic elongation of each branch was accounted for in the calculation of joint deformation, however with the onset of branch yielding this component could not be determined accurately. Consequently, it was not possible to define what component of the non-linearity prior to the attainment of ram failure load was due to member yielding.

4.6.3 Axial forces and bending moments

Since strain gauges were placed to assess only in-plane stresses, out of plane bending was ignored and the stress distribution in the sidewalls was interpolated (see Fig. 4.15[a]). The axial force and bending moment at a strain gauged section were calculated in the elastic range assuming the stress distribution in the sidewalls was as shown in Fig. 4.15[b]. Where extreme fibre yielding occurred at the strain gauges a number of yield patterns were possible, as shown in Figs. 4.15[c], [d] & [e]. The axial force and bending moment were calculated according to the relevant stress distribution.

In the graphical representation of member forces with respect to applied load (see Fig. 4.10[e]), the axial forces calculated at the gauge positions were plotted. However, in the case of bending moments, although the values were first evaluated at the gauge locations, the distribution was extrapolated to the ends of each member (see Figs. 4.16 & 4.17).

Two values of axial force were calculated per member. However for the tabulated results only one value of axial force has been quoted for any given member. This value was derived either by taking the mean of the two sets of gauges or using the most reliable value.

Within the elastic limit of a member the difference in the two values of axial force expressed as a percentage of the lower value was generally found to be lower than 3%. Outside the elastic range this difference was higher, but in most cases still lower than 10%. Where the discrepancy was greater than 10% it is likely that the assumed stress distribution from which the axial force was calculated (see Fig. 4.15) does not apply (for overlapped branch members the possible reasons for this are discussed in section 5.5.2).

Where the calculated difference was less than 10% then the mean of the two values was used. For errors greater than 10% the strain paths were studied to assess which of the two sets of gauge values was more reliable. At ram failure load, however, there are examples where the extreme fibre yielding occurred in all four strain gauges. In such cases the axial force in the member was assumed to be equivalent to the squash load (see Fig. 4.18). However, for 'overlapped' branch members where extreme fibre yielding occurred at all four strain gauges, there is evidence to suggest that the true axial force was in fact less than the squash load (see section 5.5.2).

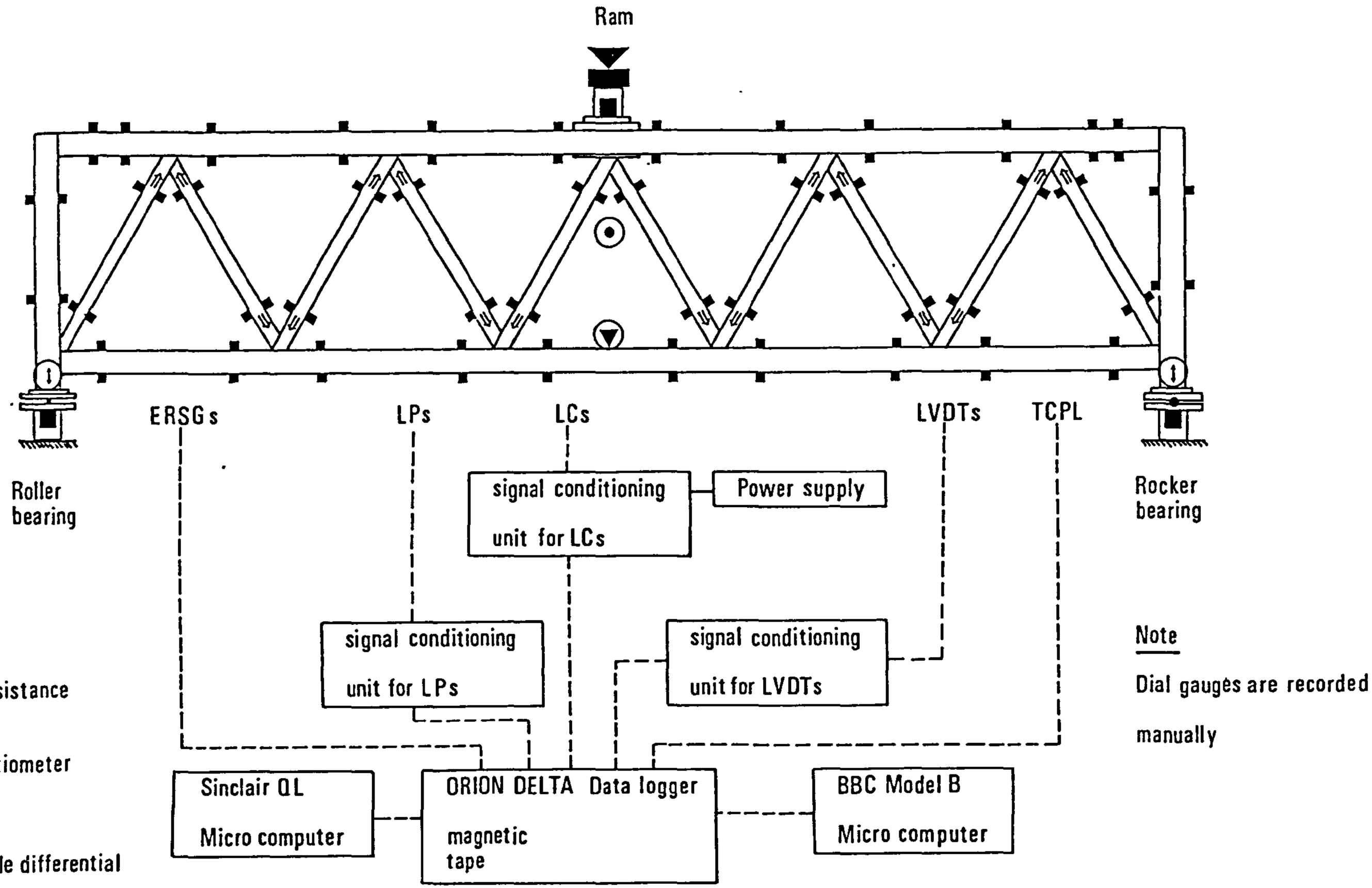

Fig 4.1 Diagram of instrumentation set up.

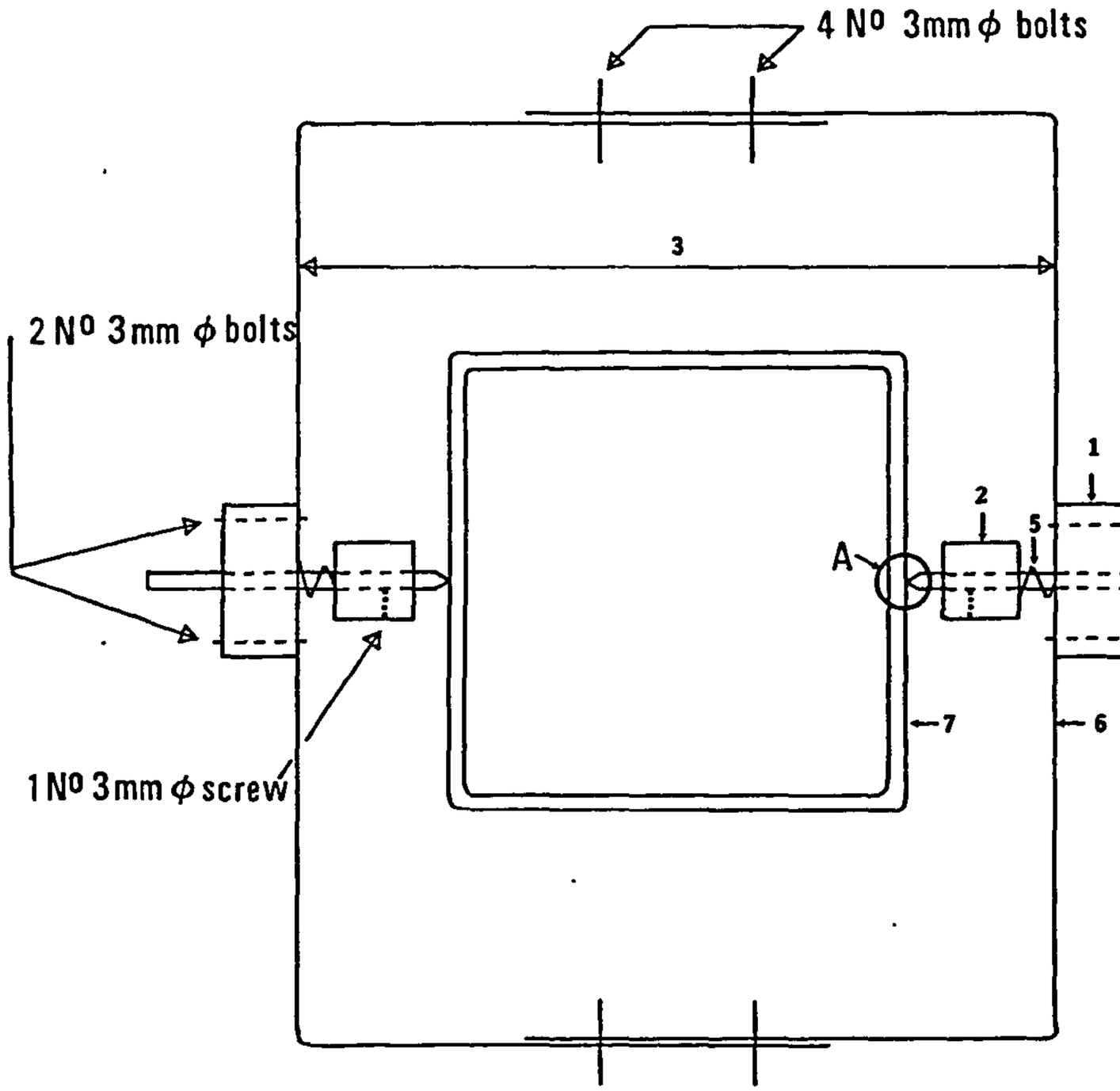

Note

Linear potentiometers bear on the cylindrical brass barrel

Key

1 stabilizing block : bored to suite spindle

2 cylindrical brass barrel : " " " "

3 adjustable dimension

4 8mm ϕ steel spindle

5 spring

6 rectangular steel frame

7 chord section

Fig 4.2 Diagram of rectangular frame used, in conjunction with the linear potentiometers, to measure the local chord face deformation.

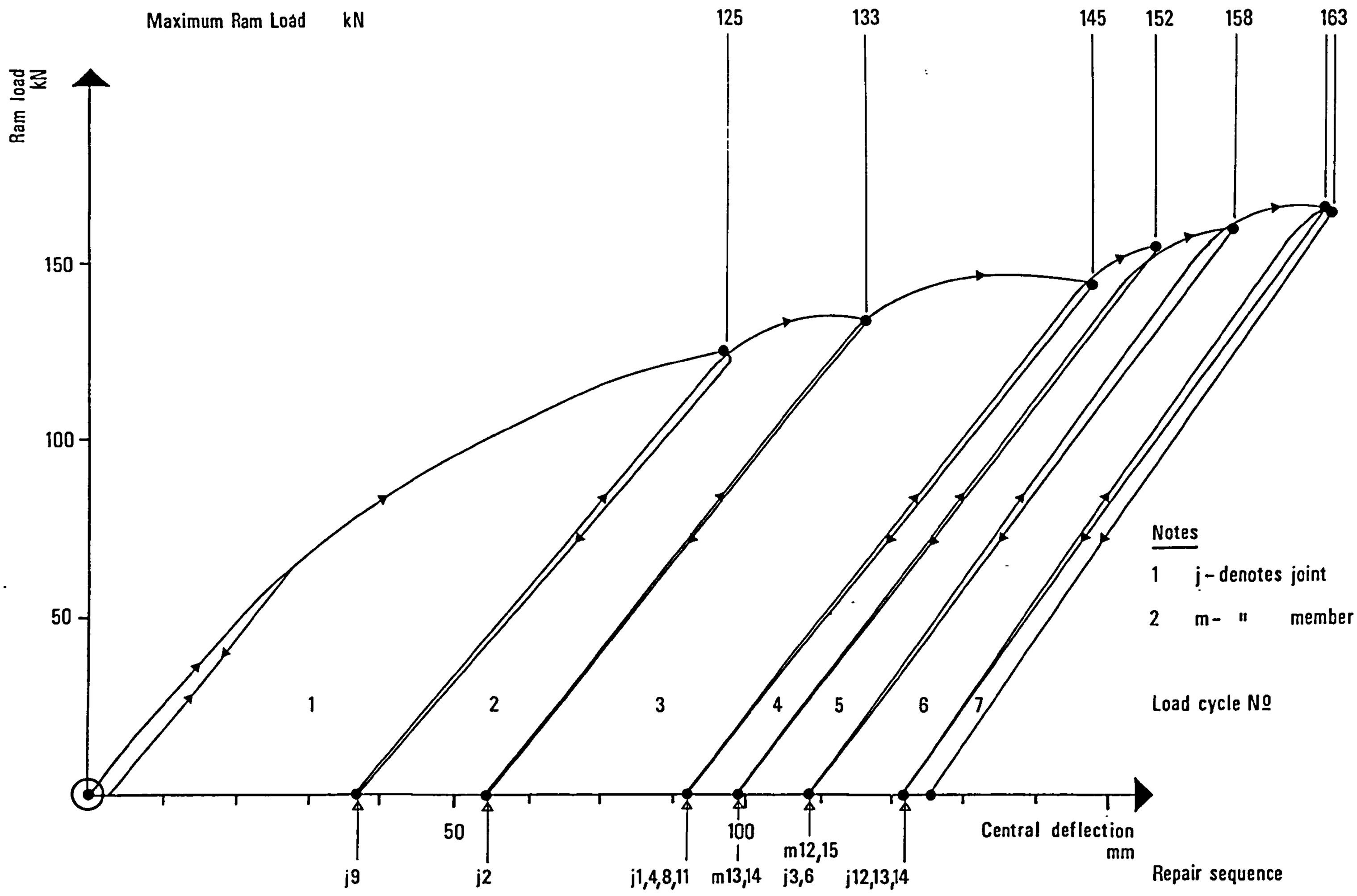

Fig 4.3 Truss T1: Loading Sequence.

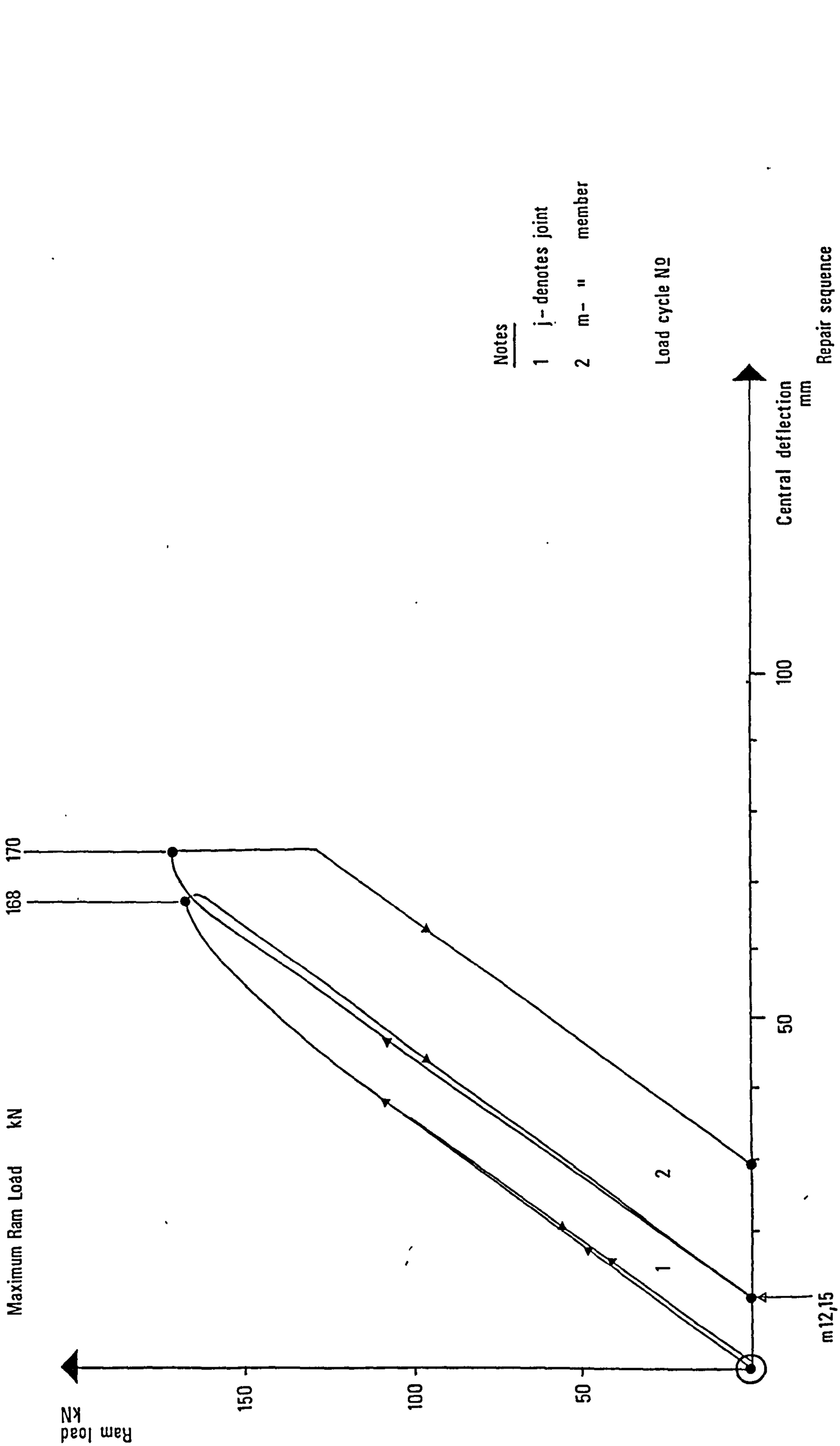

Fig 4.4 Truss T2 : Loading sequence.

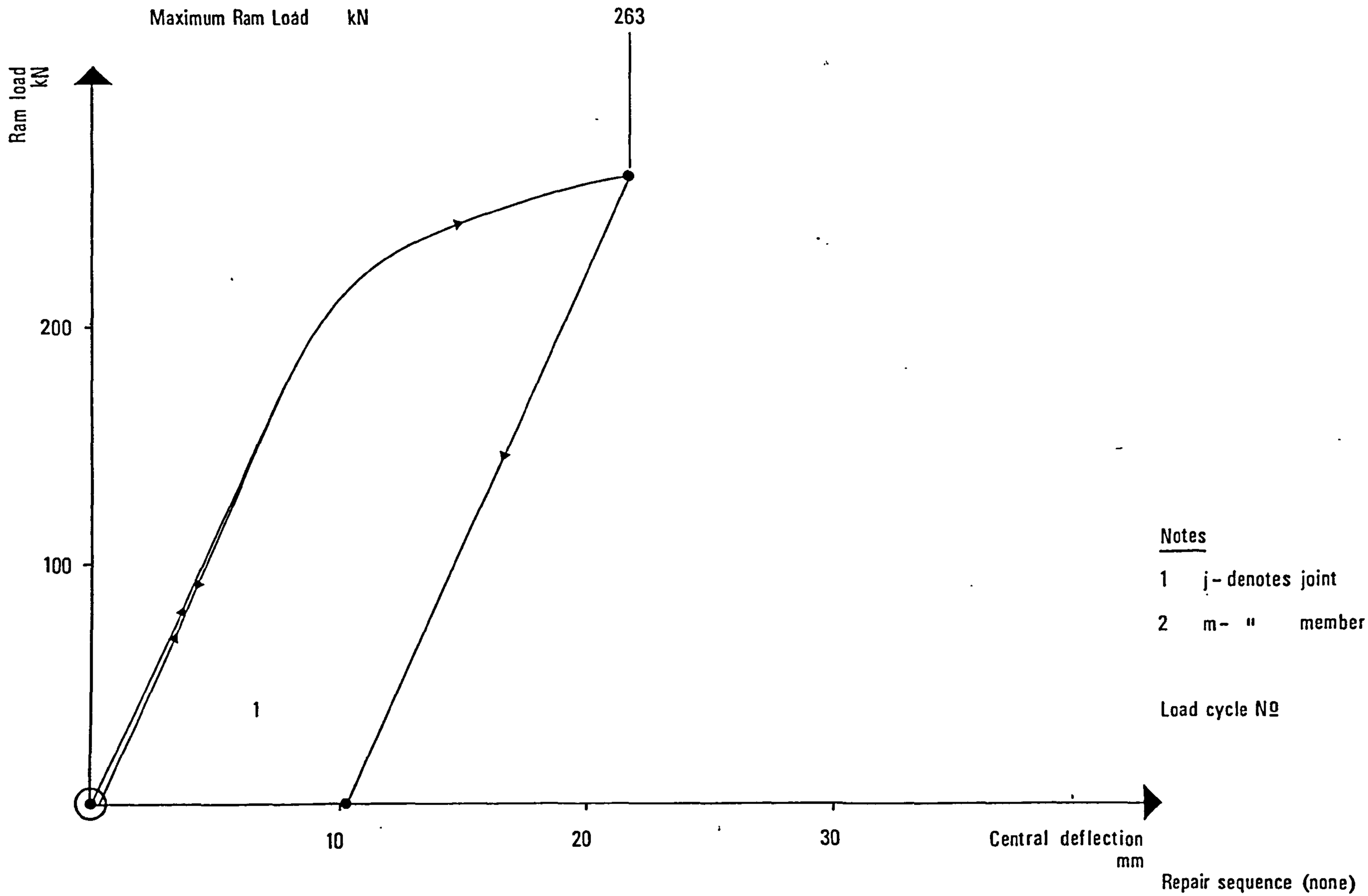

Fig 4.5 Truss T2/2 : Loading sequence.

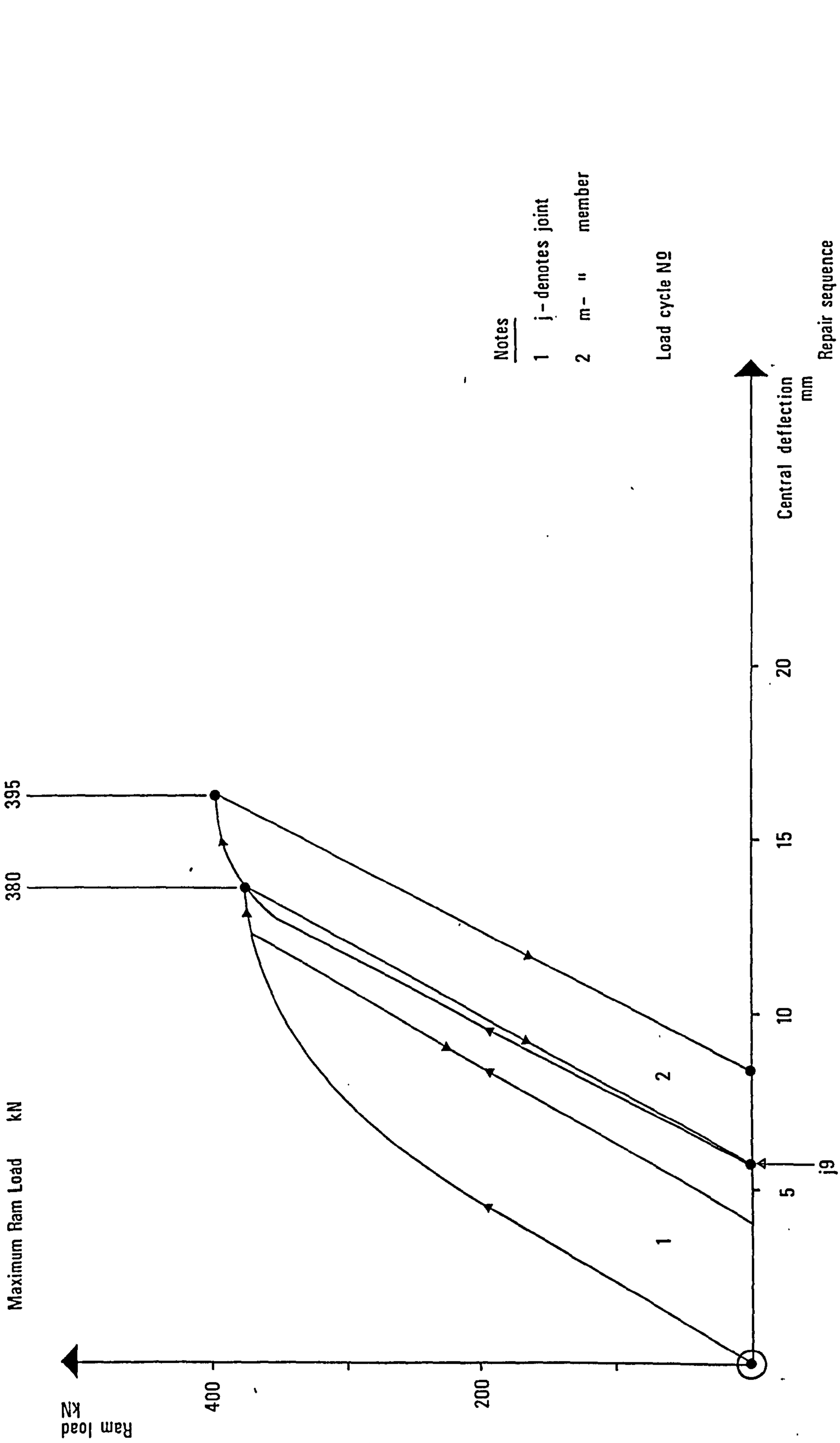

Fig 4.6 Truss T3 : Loading sequence.

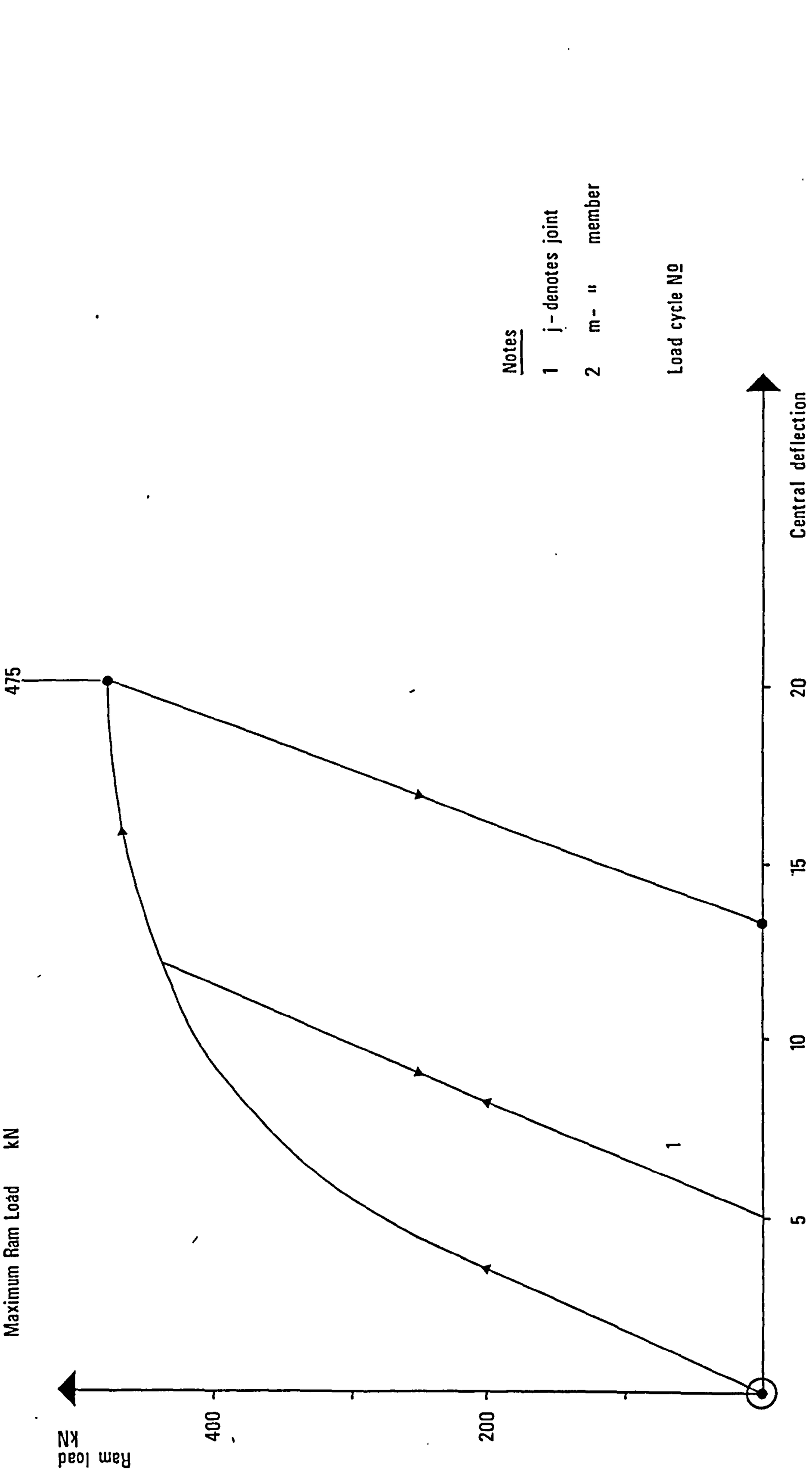

Fig 4.7 Truss T4 : Loading sequence.

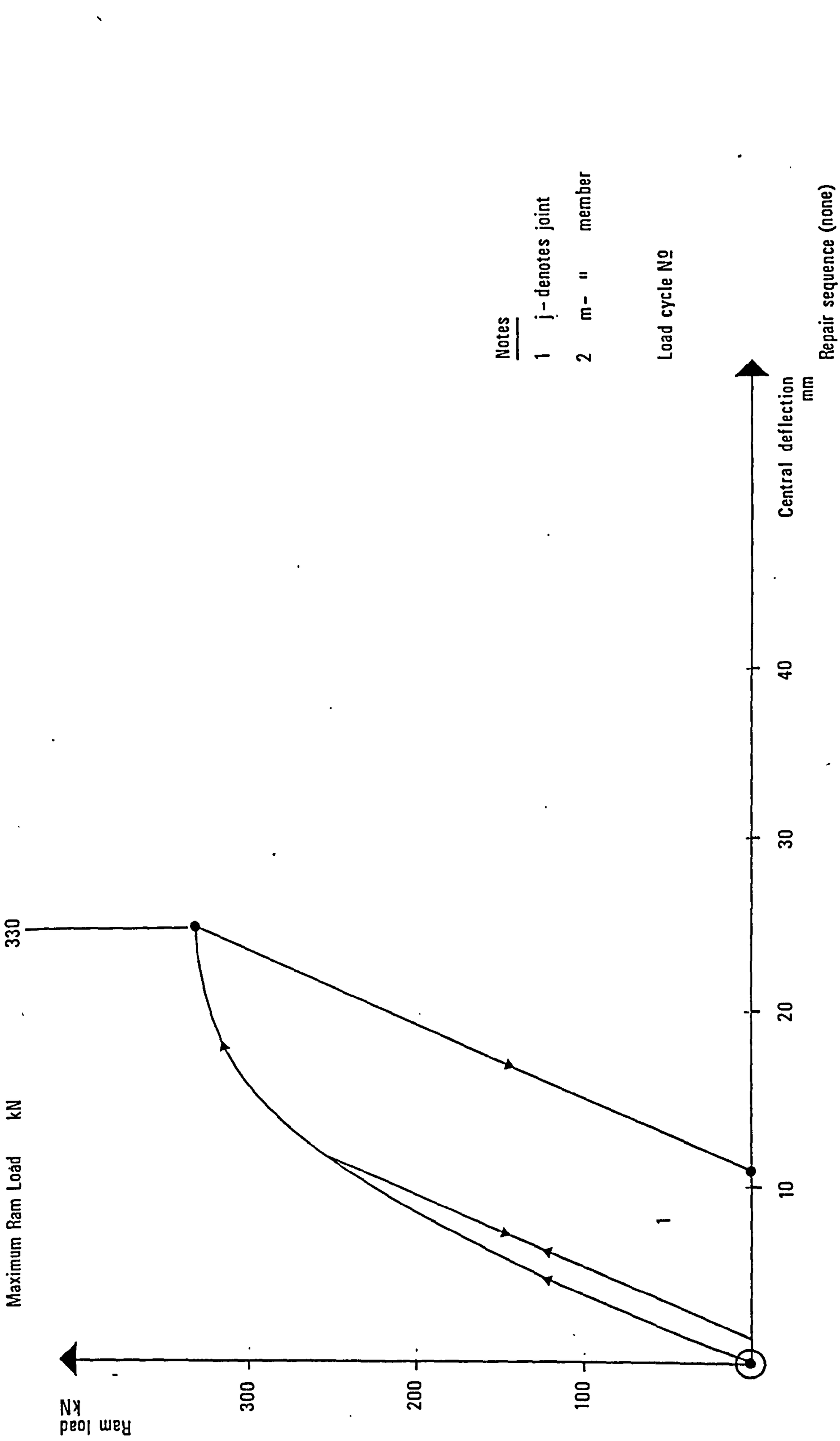

Fig 4.8 Truss T5 : Loading sequence.

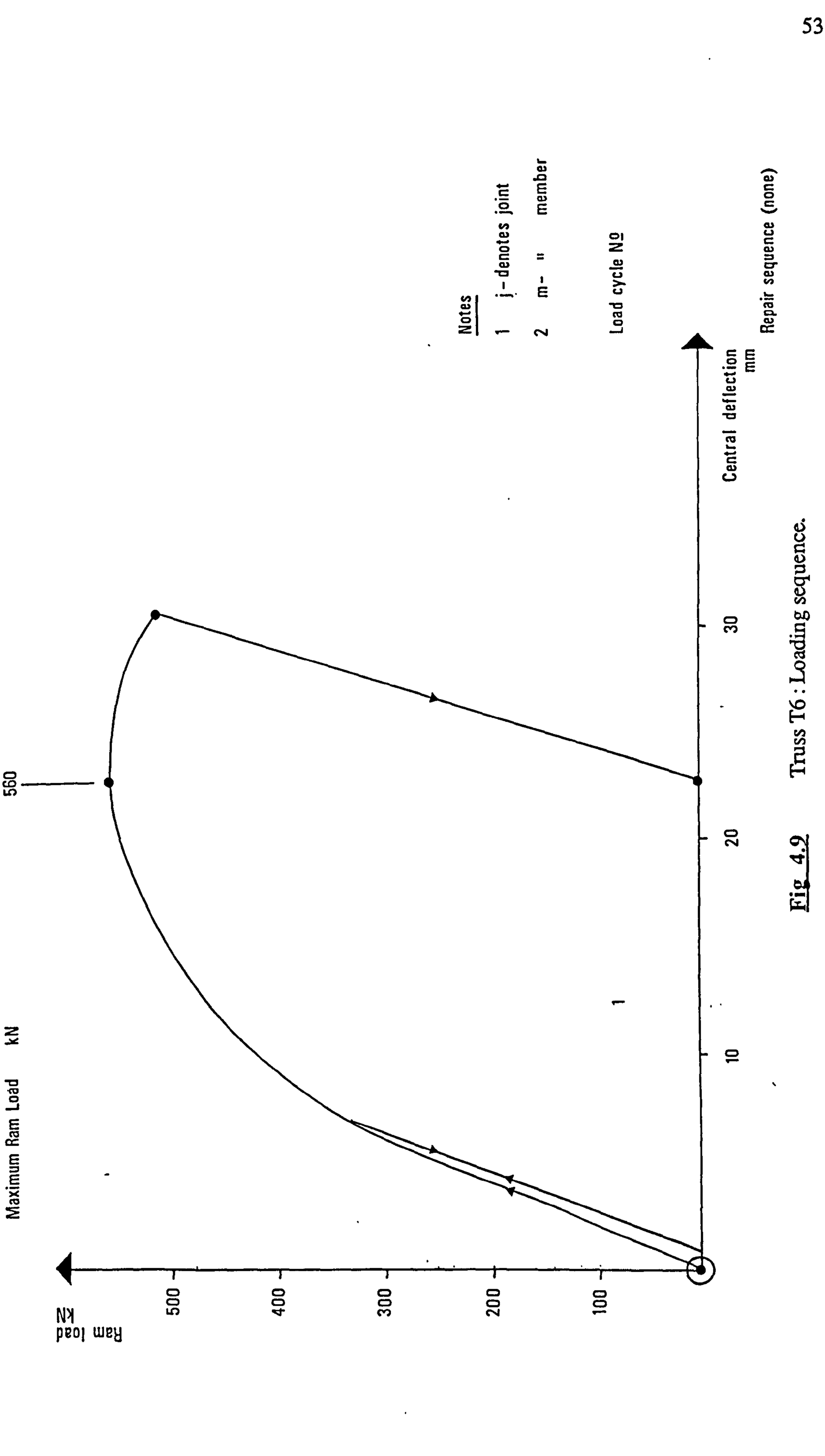

Fig 4.9 Truss T6 : Loading sequence.

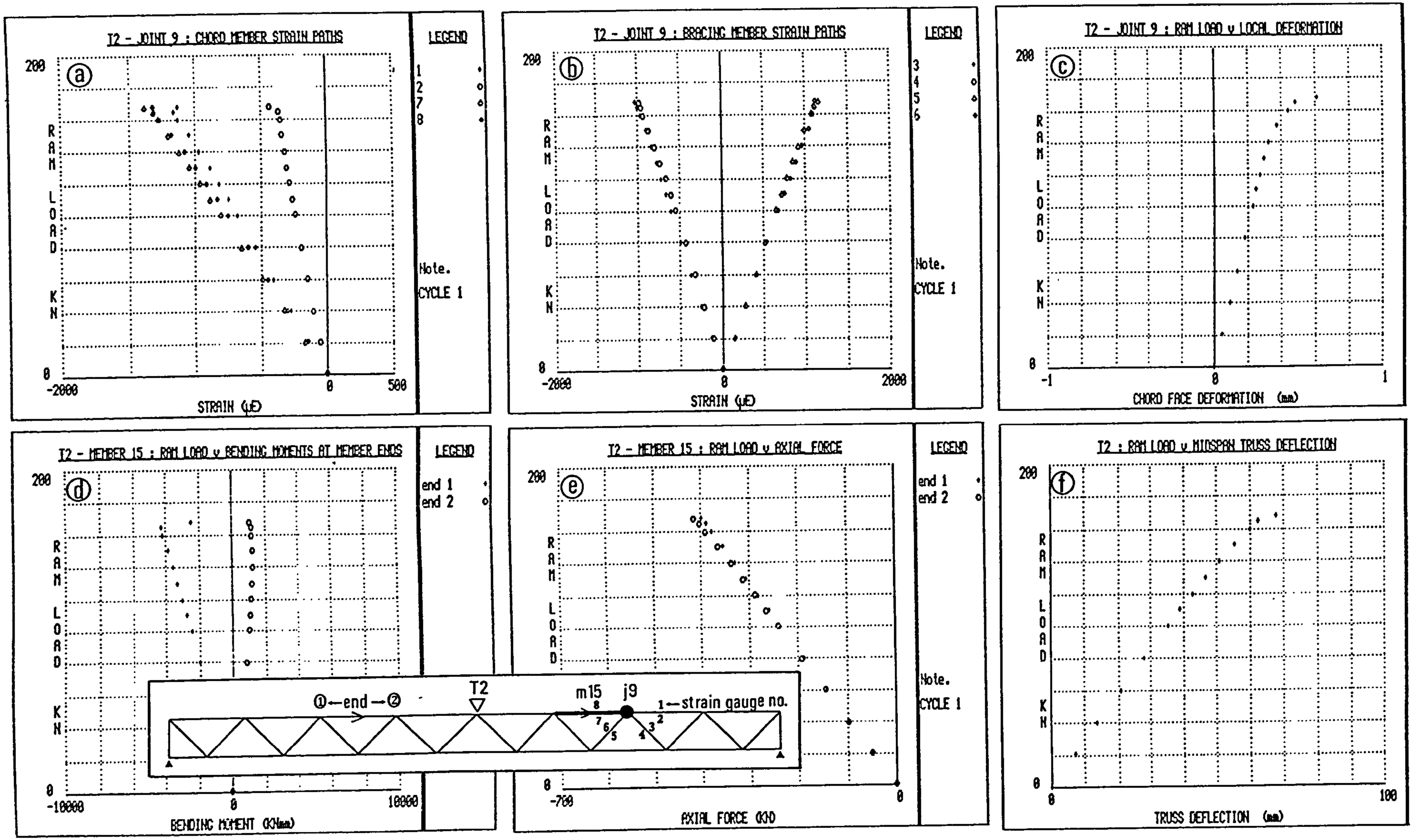

Fig 4.10 Examples of graphical results.

Key

● strain gauge position (see Appendix C)

——— stress at ultimate truss load

–·–·– stress in the elastic range

▶ direction of member force

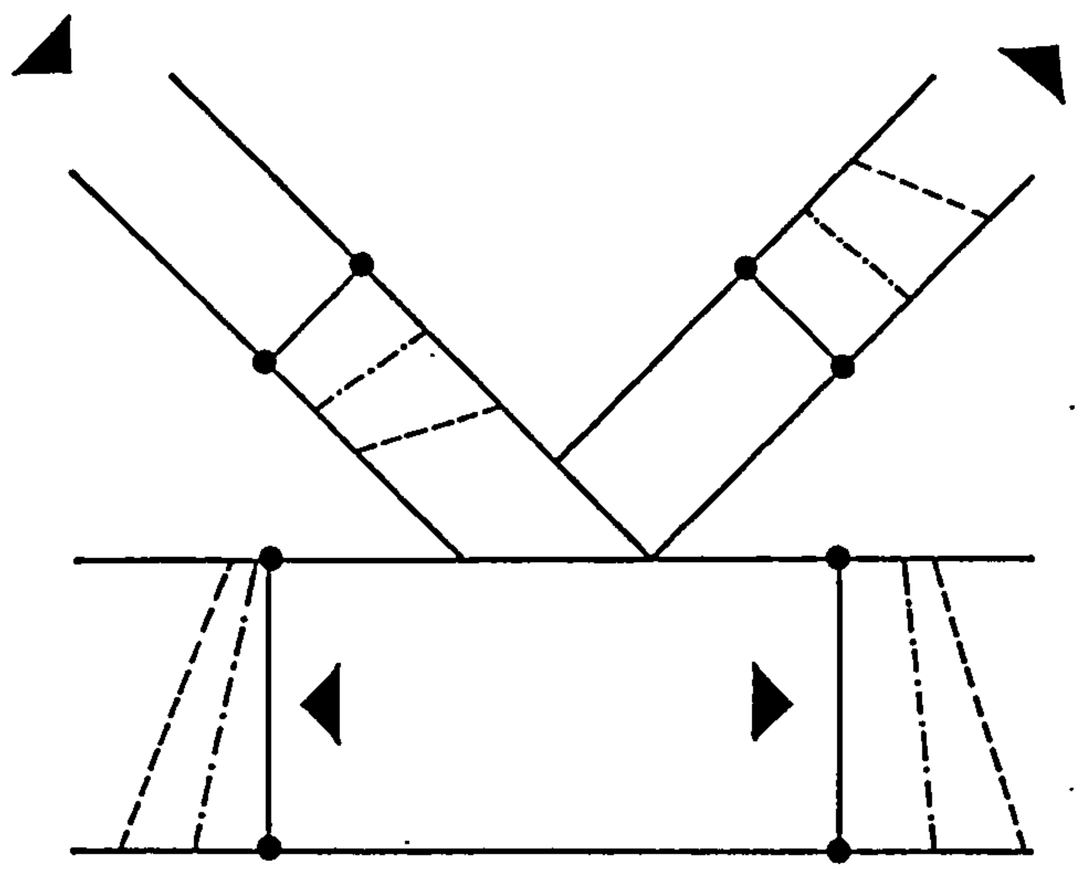

Note

see Appendix E for stress distribution diagrams

Fig 4.11 Typical example of joint stress distribution diagram.

Key

Δ_1 support settlement

Δ_2 " "

Δ_C central deflection relative to the supports

Δ_C' central deflection relative to the ground

– – – – deflection of tension chord

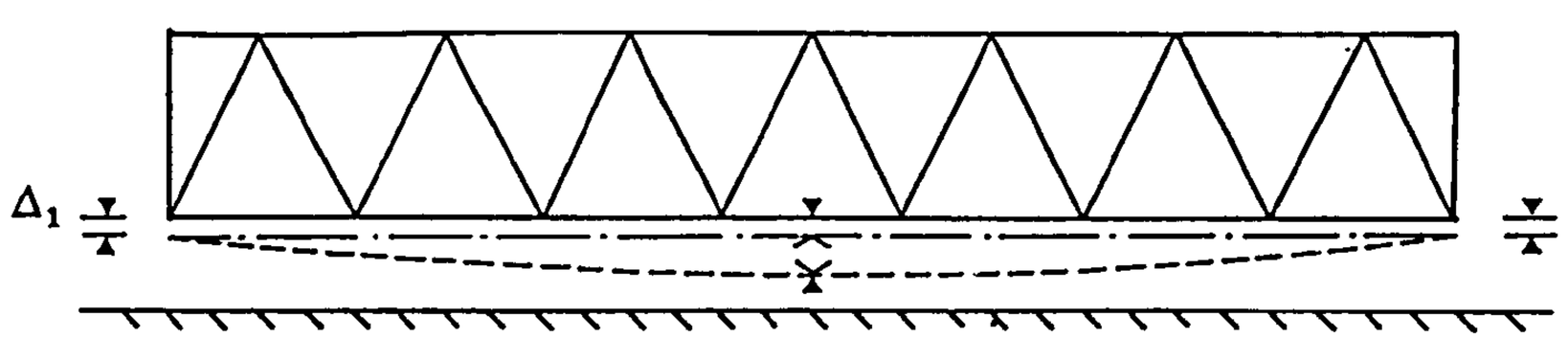

$$\Delta_C = \Delta_C' - \left(\frac{\Delta_1+\Delta_2}{2}\right)$$

Fig 4.12 Definition of truss central deflection.

a

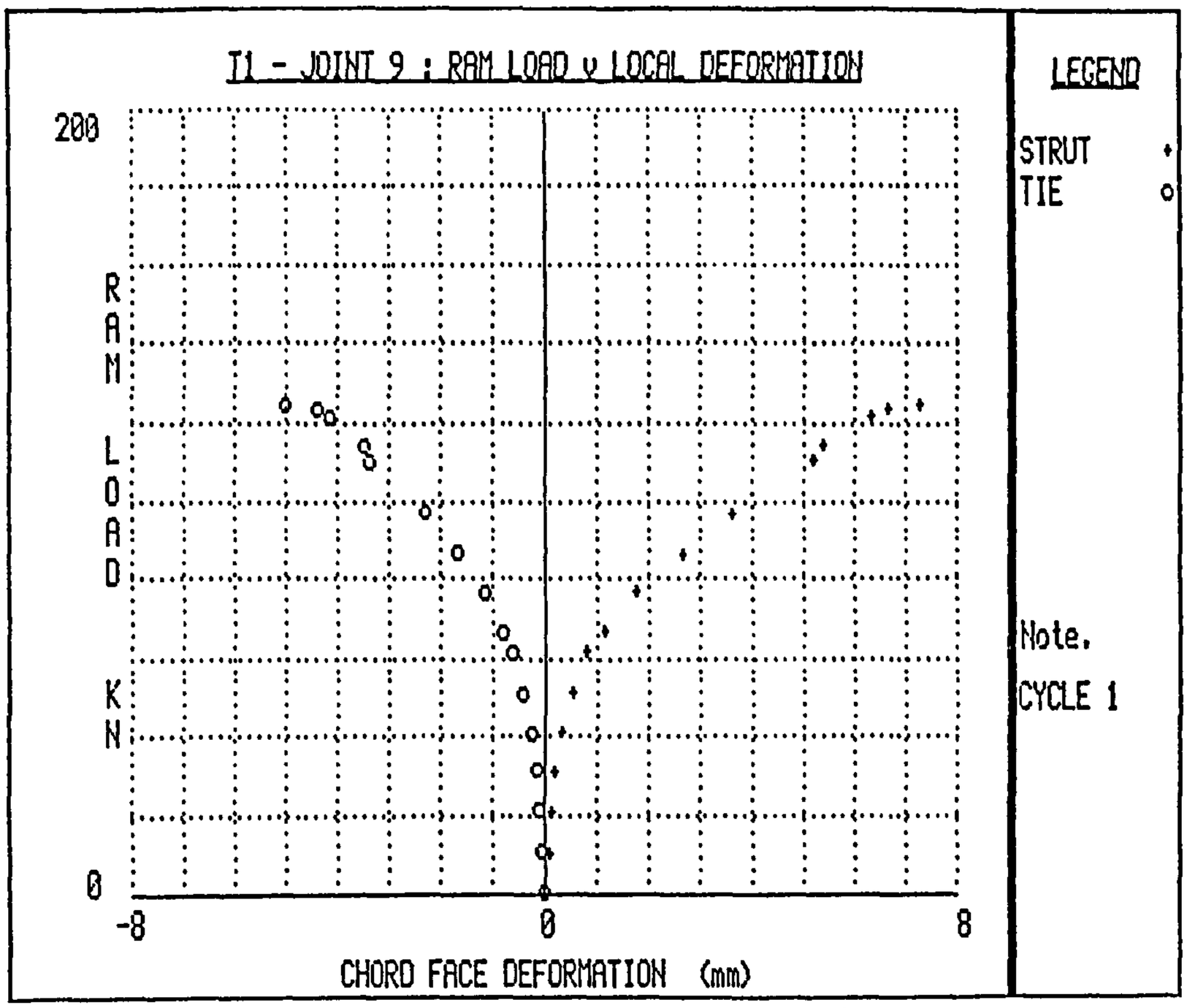

b

Fig 4.13 Typical graphical representation of chord face local deformation.

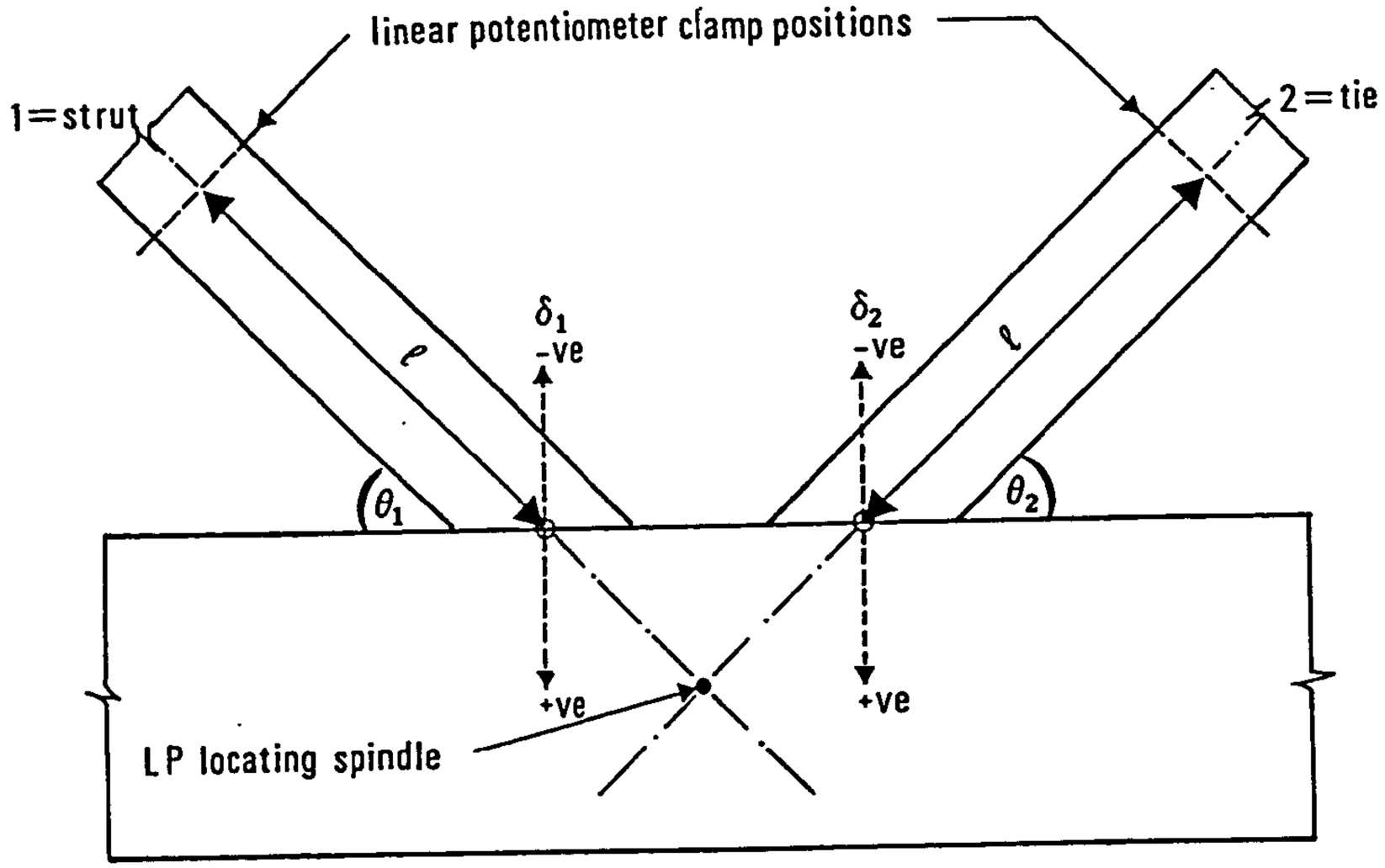

$$\delta_i = \left(R_i^{mean} + \left(\varepsilon_i^{mean} \cdot \ell\right)\right) \Big/ \text{Sin}\,\theta_i \qquad \text{for } i = 1, 2$$

a) Gap joint

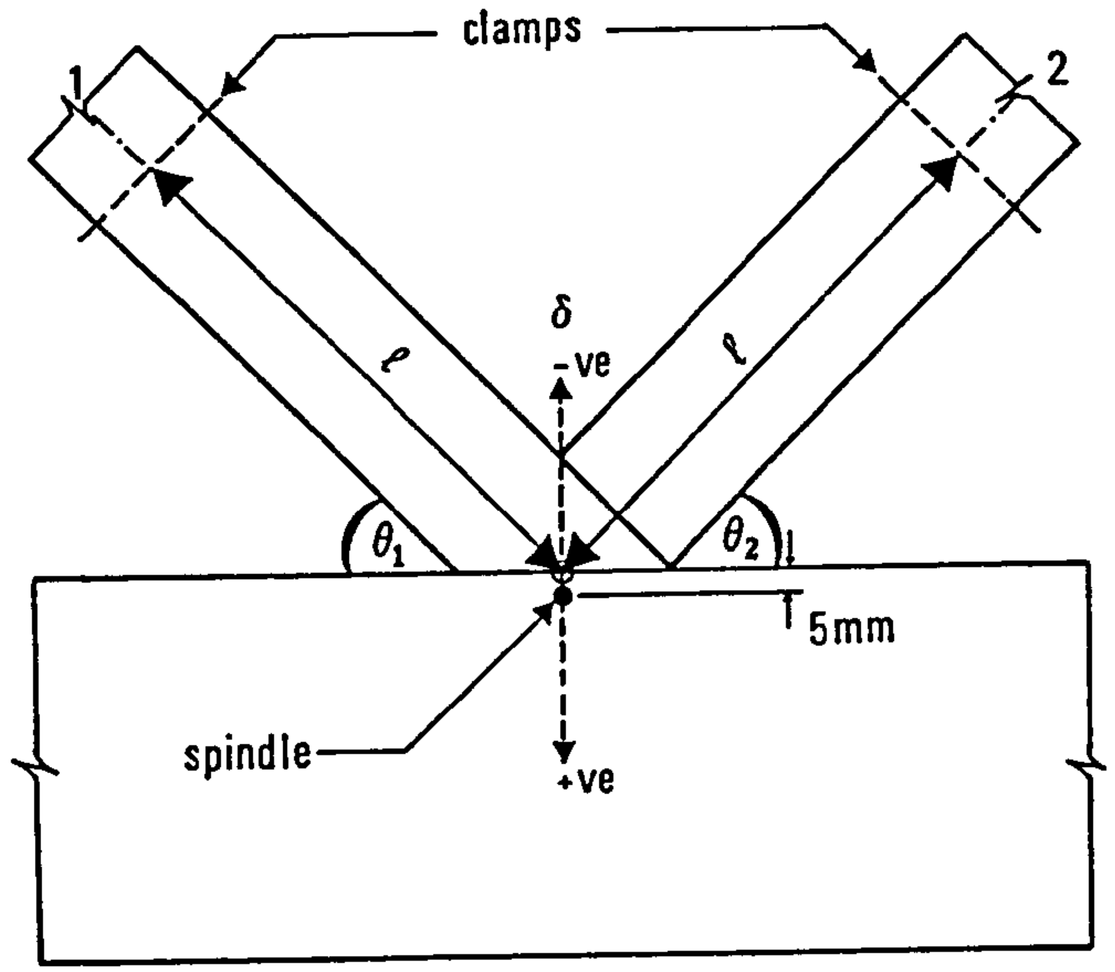

$$\delta = \left[\left(R_1^{mean} + \left(\varepsilon_1^{mean} \cdot \ell\right)\right) \Big/ \text{Sin}\,\theta_1 - \left(R_2^{mean} + \left(\varepsilon_2^{mean} \cdot \ell\right) \Big/ \text{Sin}\,\theta_2\right)\right]$$

b) 100% Overlap joint

key

ℓ = 150 mm (length from Linear potentiometer clamp position to the chord face)

R_i^{mean} mean value of two LP readings for i^{th} member

ε_i^{mean} " " " " strain gauges " " "

Notes

1 LP measures change in length between clamp and spindle

+ve reading = reduction in length

2 For strains +ve = tension

Fig 4.14 Measurement of chord face local deformation, δ.

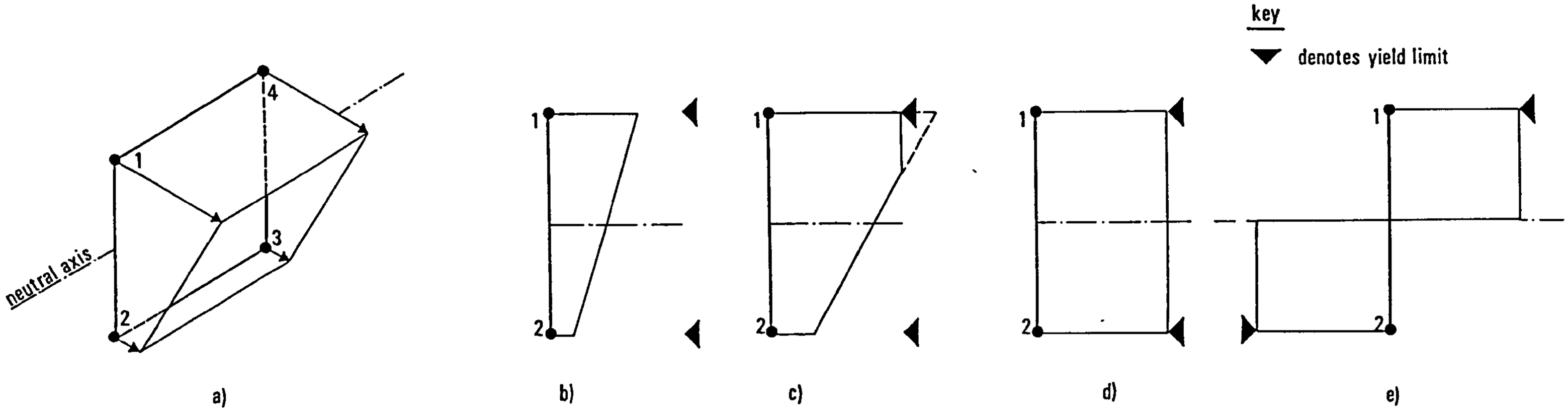

Fig 4.15 Assumed stress distributions for calculation of axial forces and bending moments.

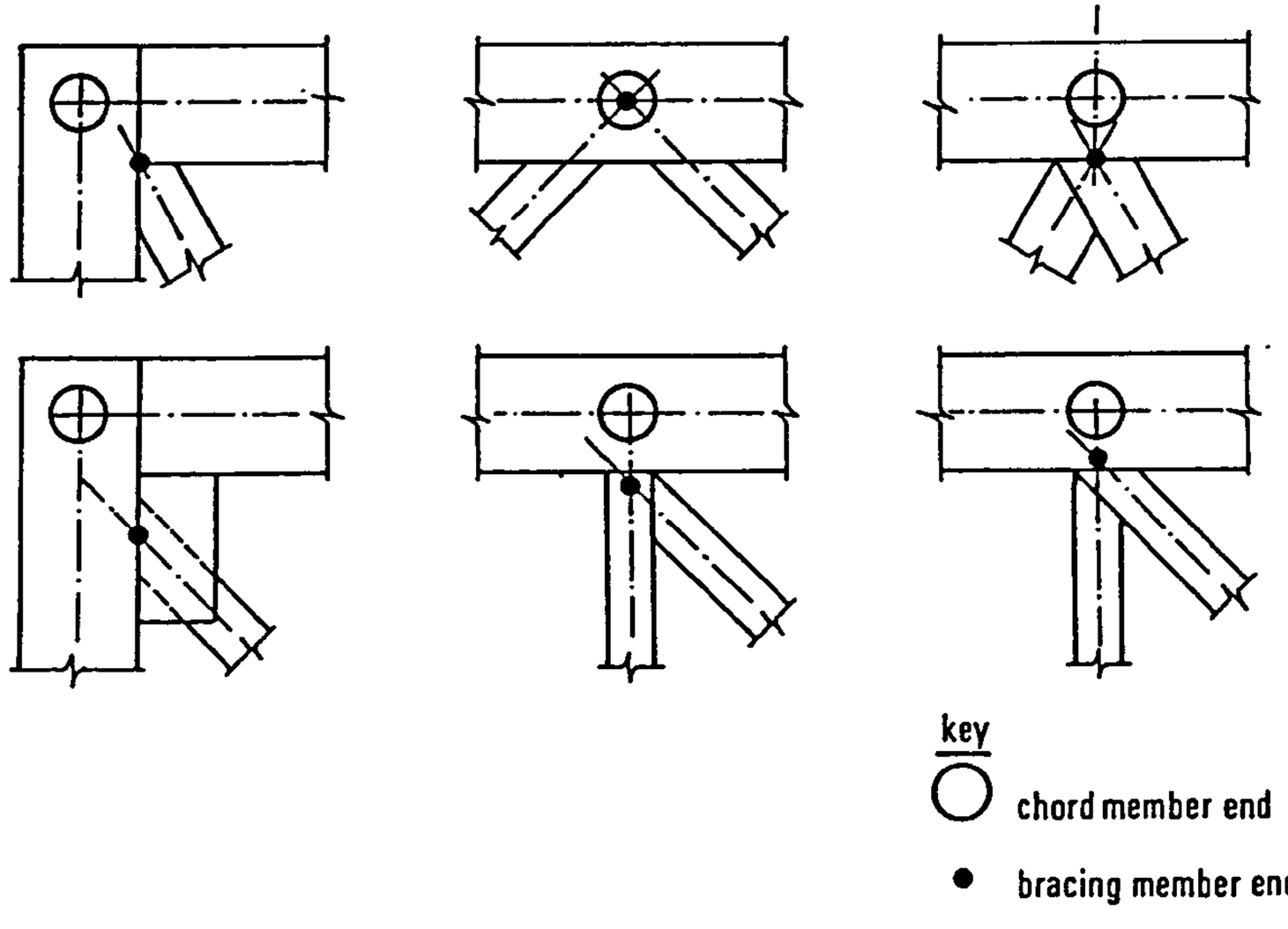

Fig 4.16 Member end definition for bending moment distribution diagrams.

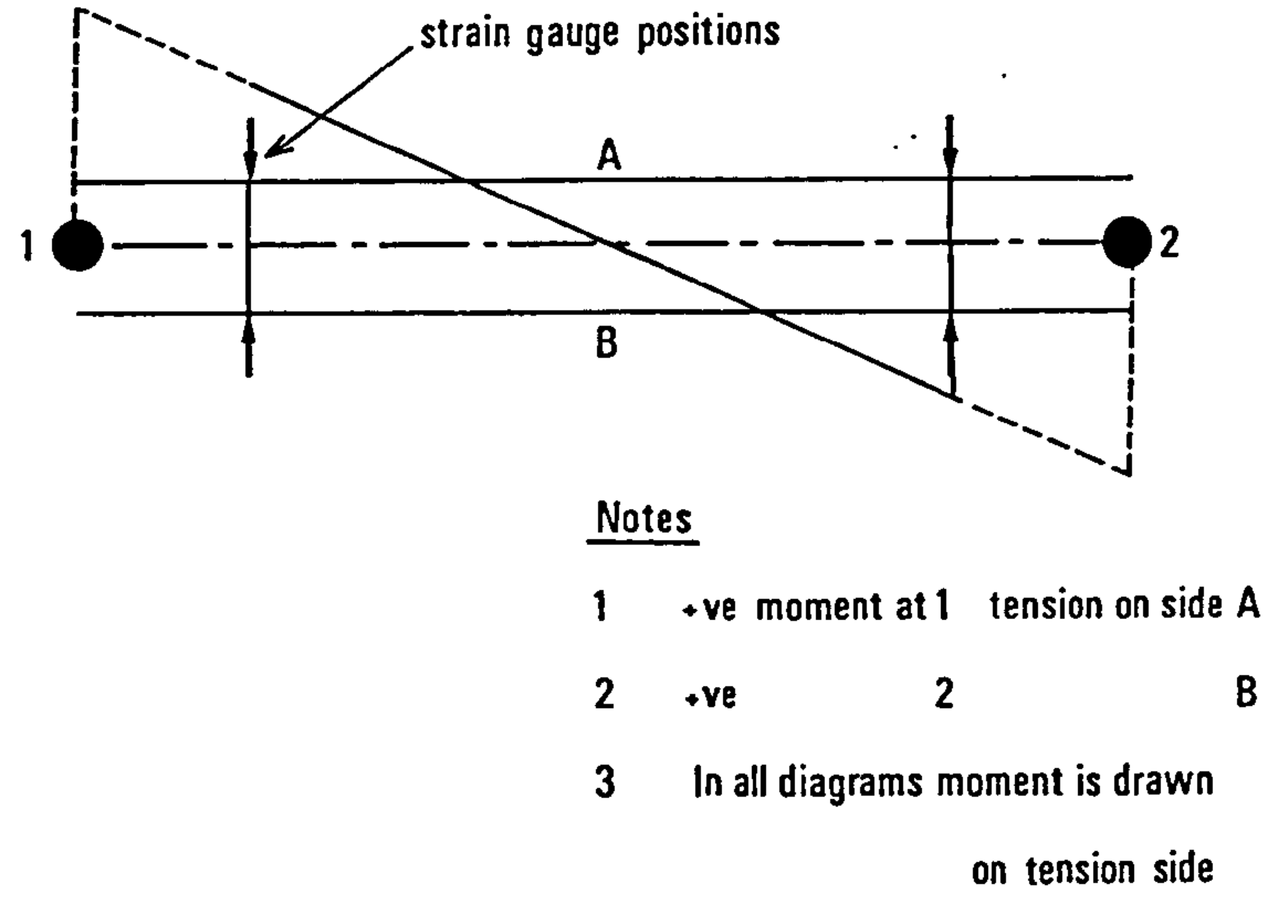

Fig 4.17 Extrapolation and sign of bending moments.

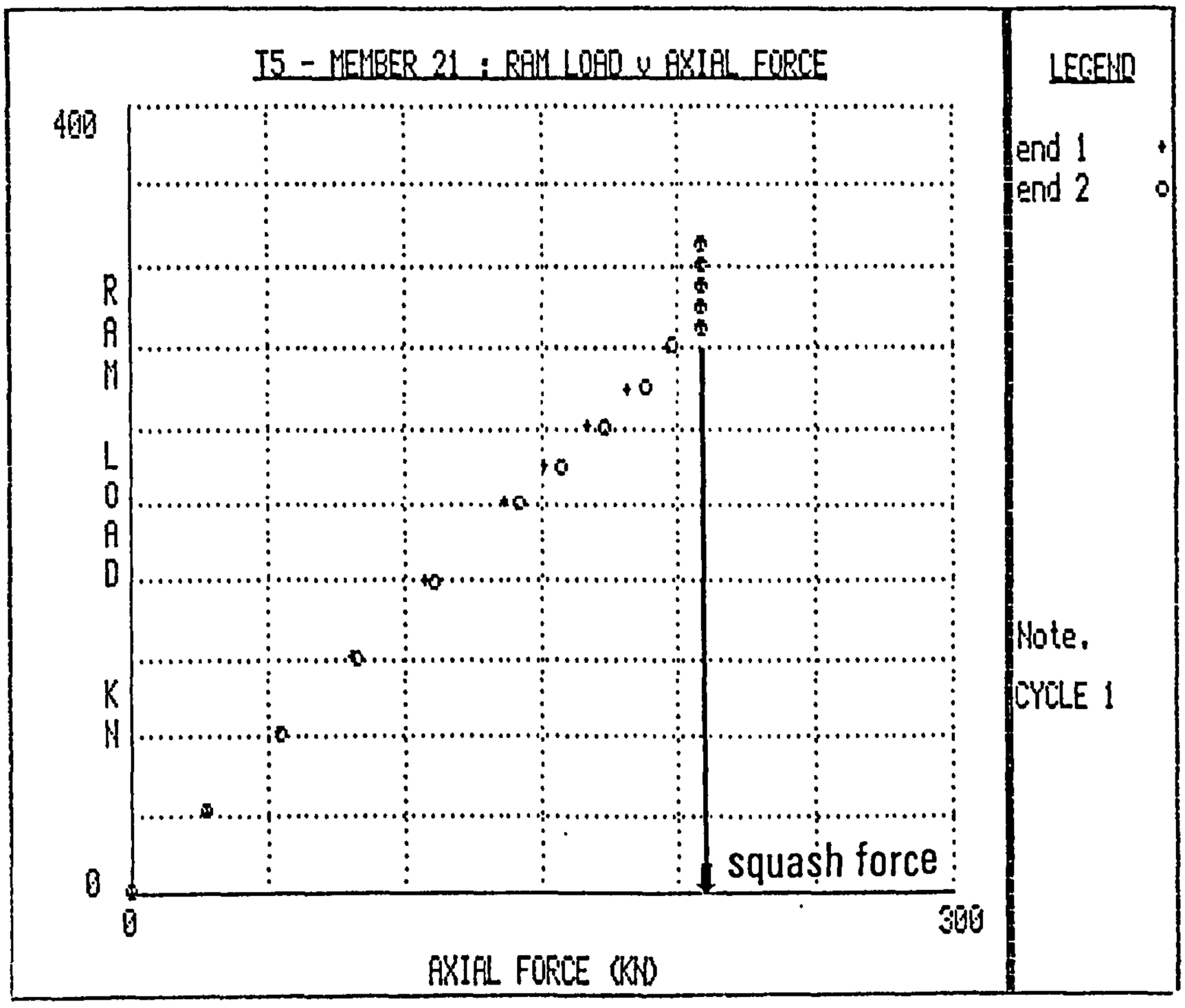

Fig 4.18 Example of overall member yielding of a tension bracing.

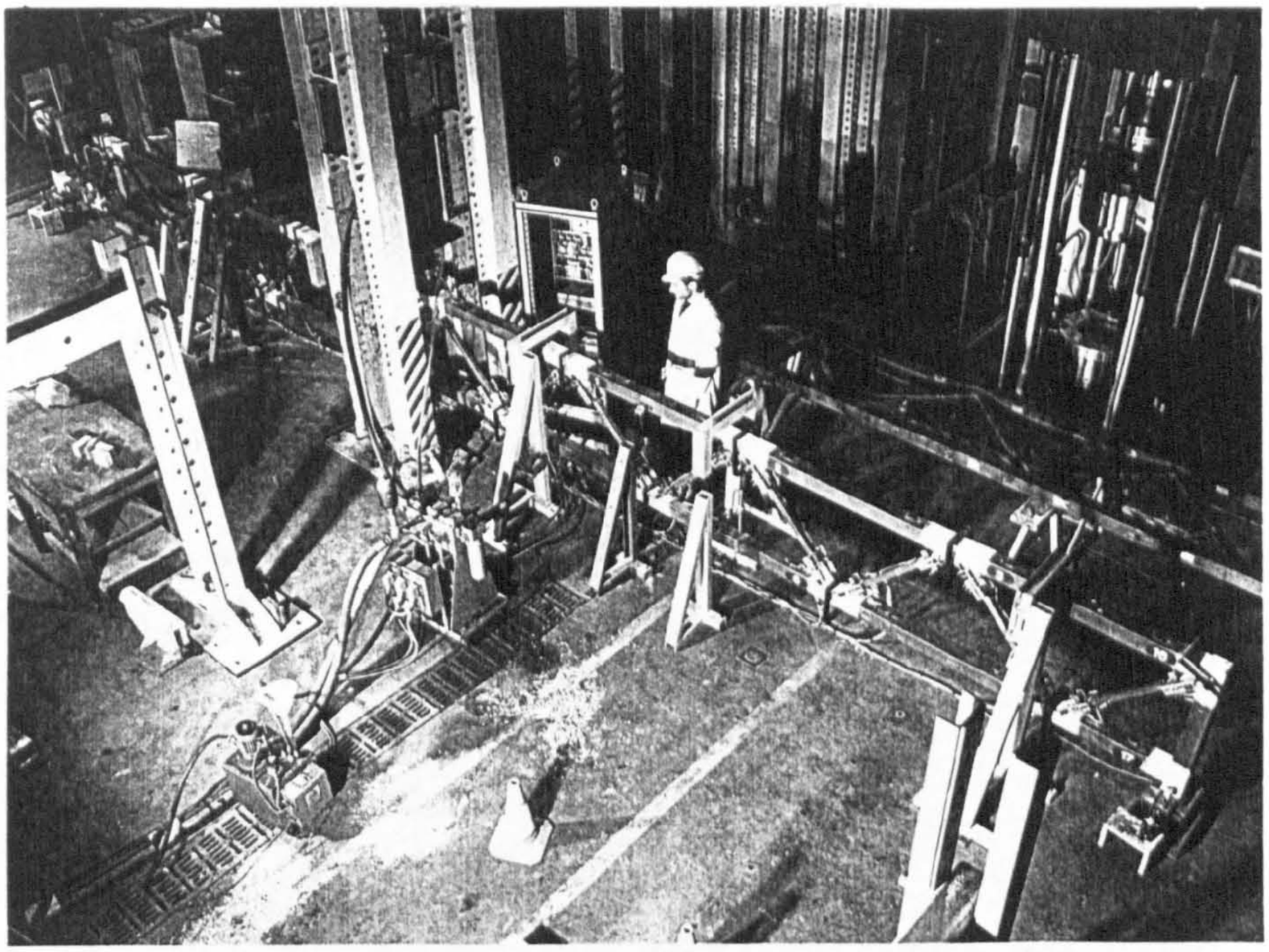

Plate 4.1 The test rig.

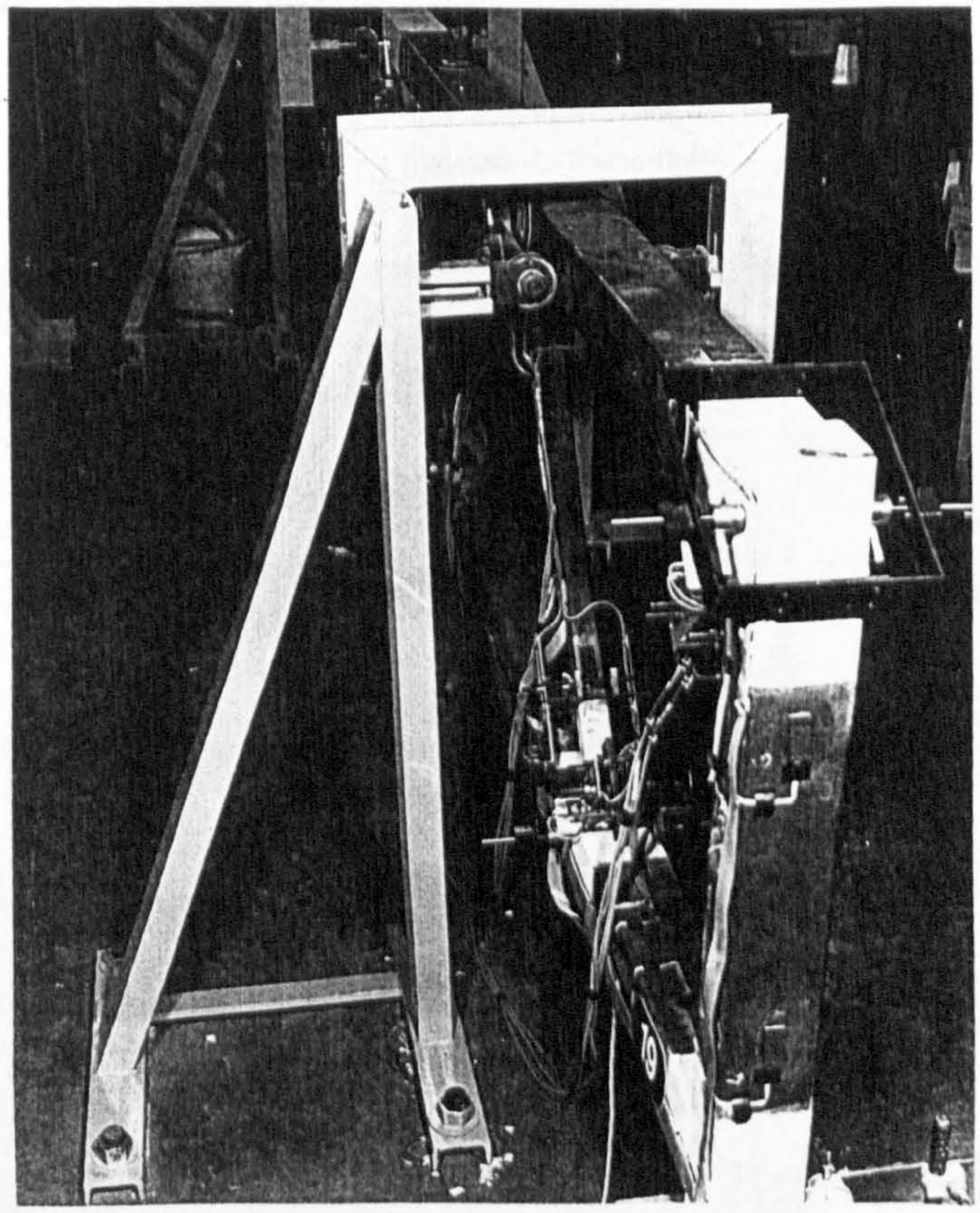

Plate 4.2 Lateral bracing of the compression chord.

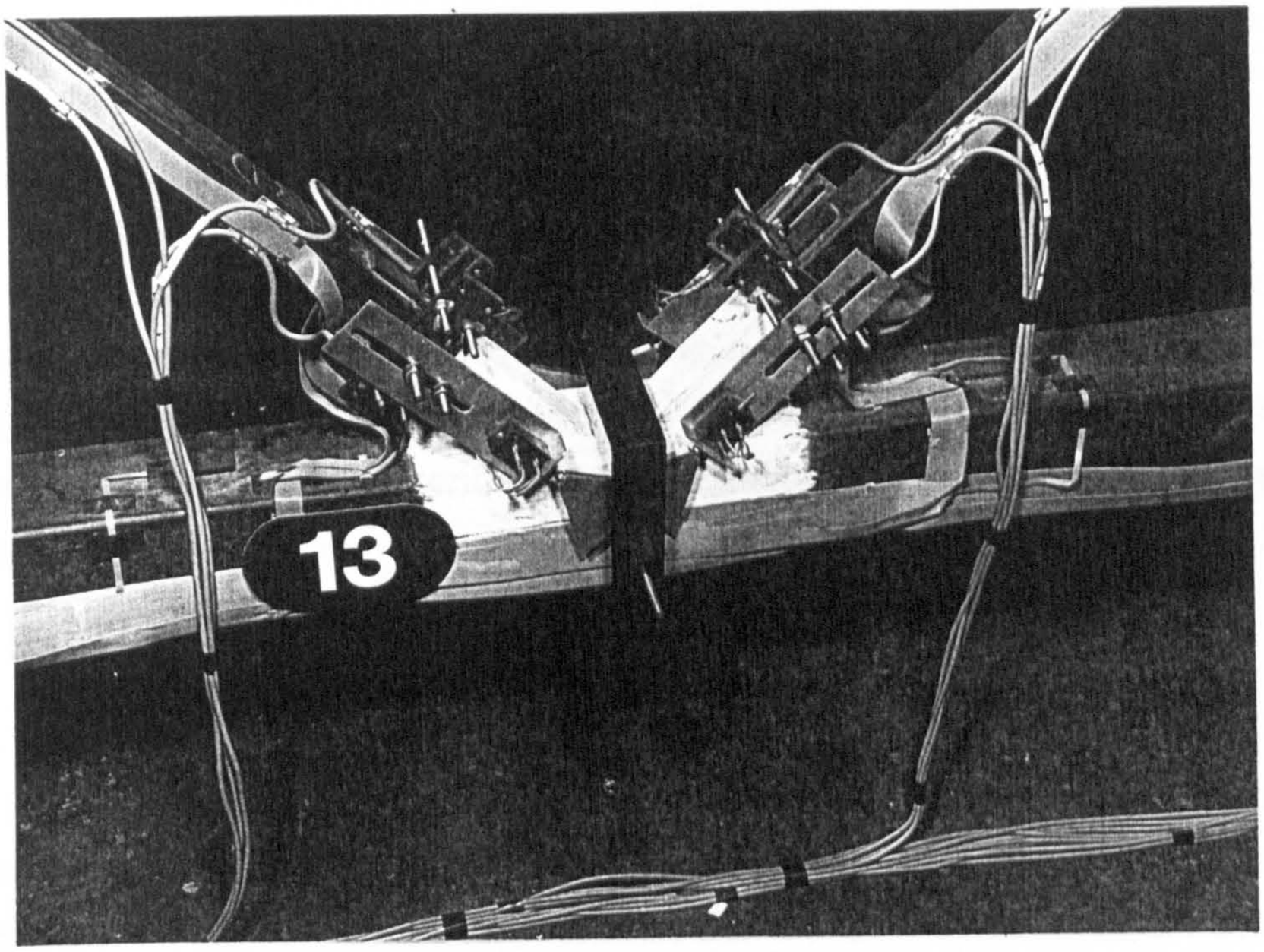

Plate 4.3 Typical arrangement of joint instrumentation.

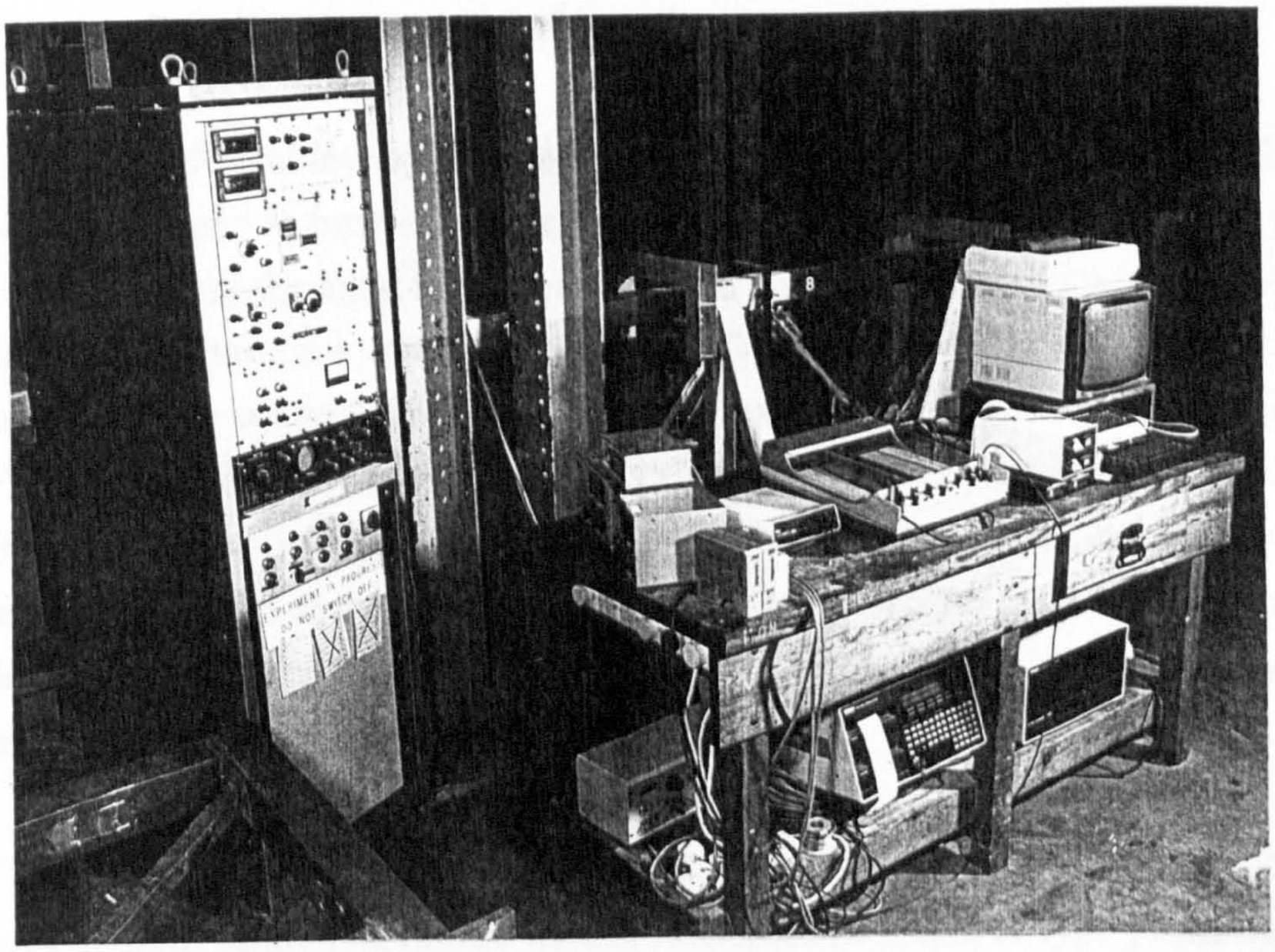

Plate 4.4 The control bench.

CHAPTER 5
FAILURE MECHANISMS AND CHARACTERISTICS RELATED TO FAILURE

5.1 Introduction

In this chapter the modes of failure which were observed in the test trusses are discussed. This chapter should be read in conjunction with Appendix D. The ultimate strength of the joints in the test trusses is discussed in Chapter 8 where detailed comparisons are made with various design formulae and the results of isolated joint testing.

5.2 Definition of failure and failure modes

In joint testing the ultimate strength is normally defined as the maximum resistance to applied load - ie., a joint is deemed to have failed when it is no longer capable of resisting further increases in load. For the test trusses ultimate strength has been defined in a similar manner - ie., the ultimate load is the ram load at which the structure was unable to sustain further increases in applied load.(see Fig. 5.1[a]). Other researchers have chosen to define joint failure by different criteria. For example Mang[58] proposed a method in which joint failure is deemed to occur when the rate of change of slope of the load/deformation graph is greatest. However, application of this criterion to the truss joints would generally give values for the joint failure loads which are lower than the ultimate strengths of the joints.

In isolated joint testing the loads in the branch members are normally measured by load cells placed in between the member and the hydraulic jacks. As a result it is possible to measure the axial forces in the branch members directly without relying on calculations involving the strain gauge values. Therefore, for isolated joints, the local deformation of the connecting chord face is normally plotted against branch axial force (see Figs. 5.1[b] & [d]). For the joints in the test trusses the branch axial forces calculated from the strain gauge values were found to be unreliable once extreme fibre yielding had occurred at the strain gauge positions (see section 5.4.2). Consequently, it was decided to plot the local deformation of the connecting chord face against the measured ram load (see Figs. 5.1[c] & [e]).

Experimental research[43] has shown that many different failure modes may occur for an SHS joint. The failure modes identified in K and N type joints have been

summarized in Figs. 5.2 and 5.3. The notation used is that suggested by CIDECT[43], whereby the letter defines the type of joint and the number refers to the failure type, ie., G4 is equivalent to a type 4 failure mode in a gap joint configuration, L4 would refer to the same failure mode but in an overlapped joint. The failure mode depends on the type of joint, loading conditions, and various geometrical parameters. Failure in test specimens has also been observed to be a combination of more than one mode.

5.3 Identification of failure modes

Truss failure characterized by an increasing central deflection under constant applied load, was determined from the plots of applied ram load against overall truss deflection. In order to assess individual joint failure mechanisms it was necessary to study the processed data obtained from the instrumentation in conjunction with qualitative information derived from visual examinations. Yielding at a joint was identified by the development of 'shear-slip' lines in the hydrated lime whitewash (see section 4.1). The onset of localized joint yielding did not usually correspond to the yield strain being exceeded at the gauge positions. At truss ultimate load two possibilities were found to exist:

(i) Local yielding at a member end (ie., a joint) identified from the existence of 'shear-slip' lines, occurred in conjunction with extreme fibre yielding at one or both of the corresponding strain gauges (at that end of the member).

(ii) Local yielding at the member end did not occur in conjunction with extreme fibre yielding at either of the two corresponding strain gauges.

For the purpose of this research project 'member' yielding relates to case (i), and 'local' yielding to case (ii). Local yielding was observed in all joints at ultimate truss load, whether gap or 100% overlap. For this reason local yielding has not necessarily been identified as mode of failure. At truss ultimate load only the following characteristics were considered to be significant:

(i) 'Member' yielding.

(ii) 'Member' buckling.

(iii) 'Local' buckling.

(iv) Rupture of a weld or, fracture of the parent metal.

The failure modes identified in the gap joint truss, T1 generally differed from those of the 100% overlap joint trusses. The failure characteristics of each truss type have therefore been considered separately.

5.4 Failure modes in the gap joint truss T1

Truss T1 was subject to seven failure cycles. Each time a failure was achieved the load was removed in a controlled manner, and the joint or member which had failed was strengthened by plating. The joint failure modes which were identified in this truss are presented in Appendix D (see Tables D1 & D2).

A visual examination of the joints revealed several common features. From the 'shear-slip' patterns three main areas of stress concentration were identified, (see Plate 5.1):

(i) On the connecting chord face, adjacent to the heel of the compression branch.

(ii) On the connecting chord face, at the junction with the weld connecting the compression branch.

(iii) In the branch members, on the toe crosswall directly above the weld.

5.4.1 Joint failure

Joint failure caused by plastification of the connecting chord face was identified by studying the graphs of ram load v. local joint deformation, where at failure the slope tended towards zero (for example see Fig. 4.13[a]). Where joint failure occurred it always involved deformation of the connecting chord face. The joint failure modes which were identified in truss T1 can be defined according to the CIDECT categories:

(i) G4 chord face and wall local buckling without any fracture, (see Plate 5.2).

(ii) G2[b] chord face and wall local buckling with fracture in the tension branch, (see Plate 5.3).

(iii) G8 chord face and wall local buckling around the tension branch, (see Plate 5.4).

(iv) G1 chord face failure only, (see Plate 5.5).

The first three modes occurred only in compression chord joints. The G1 type failure was observed only in tension chord joints, where local buckling of the sidewalls did not occur. Overall yielding of branch members did not occur in any of these failure modes (N.B - the gap joint truss was designed to fail at the joints and not in the branch members). On the 1st load cycle, mode G4 at joint 9 occurred when the axial force in the tie (N_1) was 51% of the squash force (squash force = $A_1.\sigma_{e1}$). However, even for those joint failures which occurred during the the final load cycle the maximum member efficiency (member efficiency = $N_1/A_1.\sigma_{e1}$) sustained by the tie was only 0.74. This demonstrates that joint strength can be significantly less than the branch member

strength, a characteristic which is not always appreciated by structural engineers.

In conjunction with deformation of the chord connecting face, rupture did occur at joint 3 in the tension branch. This was on the toe crosswall directly above the weld in the 'heat affected zone' (see Plate 5.3), and occurred at a member efficiency of 0.71.

It was not possible to identify the onset of yielding in the connecting chord face with reference to the strain paths. However, the development of 'shear-slip' lines on the chord face did correspond to the onset of non-linearity in the graphs of local joint deformation. The maximum chord axial force that was developed at the joints at the instance of failure differed in the case of the tension and compression chords, (see Appendix D, Table D2). In the former the maximum member efficiency was 0.69 (joints 1 & 8), while in the latter this was 0.80 (joints 4 & 11). The strength of the compression chord joints was thus less than the corresponding tension chord joints. This demonstrates that a compressive axial force can have a detrimental effect on the local stability of the chord. This is discussed in greater detail in section 8.6.

5.4.2 Member failure

Member failures occurred only in the 4th, 5th and 6th load cycles, and were observed only in the chord sections. There were two types of member failure:

(i) In-plane buckling of the compression chord. This occurred during both the 4th and 5th load cycles. In load cycle 4 both of the chord members either side of the ram failed (members 13 & 14). In the 5th load cycle local yielding occurred at both of the chord splice positions on the compression chord (members 12 & 15).

(ii) Yielding of the tension chord. This mode of failure occurred in the 6th load cycle along the midspan section, (member 5).

In-plane buckling of the compression chord was always preceded by the development of 'shear-slip' lines along the face where the bending strain was compressive. With the progression of instability the 'shear-slip' lines were observed to extend onto the sidewalls. On the tension chord, at joints 4 and 11, 'shear-slip' lines were observed on the tie branch side of the joints, on the sidewalls and on the connecting chord face.

5.5 Failure modes in the 100% overlap joint trusses

Chord face deformation was negligible in the case of the 100% overlap joints. As such there was little interaction between the branch members and the chord section at a joint. The modes of failure that were identified in the test programme, can be divided into two groups. Firstly, those related to the chord section, and secondly those which involved the branch members. In the chord the following modes were observed.

(i) Local buckling of the compression chord behind the tension branch, L7, (see Plate 5.6).
(ii) General instability of a compression chord member (see Fig. 5.4[a]).
(iii) Yielding followed by local buckling at the ram position.
(iv) General yielding of the tension chord.
(v) General yielding of the compression chord.

In the branch members there were five modes of failure which occurred, namely:

(i) Member yielding of the tension branch.
(ii) Member yielding of the compression branch.
(iii) Rupture of the tension branch in the heel crosswall directly above the weld with the chord, (see Plates 5.7 & 5.8).
(iv) Local yielding and/or buckling of the compression branch, (see Plate 5.9).
(v) In-plane member buckling of the compression branch.

In T2 instability of the compression chord occurred without failure in any branch members, however the strain paths of the tie branches at joints 12 and 14, indicate that the yield strain was exceeded at the ram failure load. It is thought that this was caused by the development of the 'shear-plane' in the sidewalls of the overlapped branch, and is discussed in section 5.5.2.

The ultimate capacity of the modified T2 truss (T2/2) was defined by member yielding of the tension branches, although member yielding was also identified in some of the compression branches. In T3, at ultimate load, member yielding was observed in the tie members closest to the midspan (members 15 & 18). However, since local buckling also occurred in the compression chord either side of the ram, it is not clear which of these was the critical mechanism. The compression chord was strengthened and the load re-applied, however only a 4% increase in the strength was obtained, indicating that member yielding of the ties was in fact critical.

In T4, member yielding was observed in the compression chord and also in the majority of the branches in conjunction with overall buckling of the central struts (members 16 & 17). In T6 yielding of the tension and compression chords at midspan, member yielding of both tension and compression branches, and local buckling of the compression branches occurred.

In T5 yielding was observed at midspan on the tension and compression chords, and occurred in conjunction with member yielding of all the tie branches. Instability of the chord section and subsequent failure of the truss occurred only in T2. Although yielding and the onset of local buckling of the compression chord (at the ram position) was observed in T3, T4, T5 and T6 it did not lead to instability. The critical mechanism in these trusses appeared to be failure of the branches.

5.5.1 Chord failure

In general it was not possible to relate member failure in the chord directly to the measured strain values at the corresponding gauge positions. However, when the bending moments at the member ends were evaluated by extrapolation, and the combined stress due to axial and bending forces was calculated, it was found that the onset of yielding did correspond with the extrapolated stresses exceeding the yield limit.

On the first load cycle of T2 in plane buckling of the compression chord occurred (see Fig. 5.4[a]). Initially this involved local yielding in the 4mm thick section adjacent to the splice. The member was subsequently repaired, as was the corresponding section on the opposite side of the truss. On re-loading the same member failed but this time in the L7 mode (see Fig. 5.4[b]) which has been identified in isolated joint testing.

It is likely that the L7 failure mode was related to the stiffening that was afforded to the adjacent chord section. This appeared to prevent the redistribution of moments away from the area of stress concentration. In isolated joint testing redistribution of stresses in the chord section cannot occur to the same extent as in the continuous chord of a truss joint. The L7 mode is probably a characteristic of the test installation, and is unlikely to occur in homogeneous chord sections which form part of a complete structure. The influence of chord bending moments, generated in a truss environment, on the L7 mode is discussed in greater detail in Chapter 8.

The local buckling of the compression chord at the ram position was observed

in T3, T4, T5, and T6 irrespective of the fact that the section at this location had been strengthened by stiffening plates. This feature was related to the high bending stresses induced by the proximity of the ram.

5.5.2 Influence of shear stress in the branch member sidewalls

The most highly stressed regions of the 100% overlap joints appeared to be the sidewalls of the branch member connected to the chord face. Local yielding in the sidewalls above the weld to the chord face was a feature observed in all joints at truss ultimate load. Consequently, the development of 'shear-slip' lines was well advanced in this location. Two shear transfer mechanisms were identified, (see Fig. 5.5):

(i) Transfer of horizontal shear to the chord face in the direction A-A.

(ii) Transfer of axial force between adjacent branch members in the direction B-B.

A visual inspection of the joints revealed the existence of a shear plane in the sidewalls of the branch connected to the chord face, (see Plate 5.6). It was observed that this plane spanned between the heel and the toe above the line of the weld. With the onset of member yielding 'shear-slip' lines were observed to develop initially on the crosswalls of the 'overlapped' branch.

In joints 12 and 14 of truss T2, the shear plane was observed prior to failure of any branches, and corresponded to non-linearity in the strain paths of the ties, (see Fig. 5.6). When the truss was shortened and re-loaded, shear failure was expected to occur, however no rupturing was observed. In the remaining trusses the 'shear plane' was observed at each joint, however as in the case of T2 shear failure of the sidewalls did not occur.

There is, necessarily, an upper bound to the shear stress which the sidewalls of the overlapped branch member can sustain along section S-S (see Fig. 5.7). When this limit is reached it is likely that the sidewalls are no longer able to transmit direct stresses efficiently across the shear plane S-S, in the direction A-A. At the strain gauge position (section WXYZ) there would be a tendency for the stress relief in the sidewalls (W-X and Y-Z) to be balanced by an increase in stress in the crosswalls (W-Z and X-Y) in order to maintain the axial force. There are many examples where there was a significant difference (>10%) in the 'calculated' axial force between the two ends of an 'overlapped' branch member at the ram failure load (Fig. 5.8 is typical). However, the axial force must, necessarily, be the same at both ends of a branch member, irrespective of whether yielding has occurred at the strain gauge positions. This indicates that strains

in the sidewalls of 'overlapped' branch members cannot be interpolated from the measured strains on the crosswalls, once extreme fibre yielding has occurred at the strain gauge position. Hence the assumptions made in the calculation of axial force and bending moment (which have been described in section 4.5) are violated.

For the 'overlapped' branches yield patterns ('shear-slip' lines) were usually observed initially on the crosswalls (see Plate 5.10). With subsequent increases in load the 'shear-slip' lines developed on the sidewalls. Therefore, the horizontal shear plane S-S did appear to influence the pattern of branch member yielding even though shear failure itself did not occur. In the case of the 'overlapping' branches the yield patterns were usually first observed in the sidewalls or corners (see Plate 5.11). This indicates that the flexibility of the toe and heel connections reduces the axial stiffness of the crosswalls relative to the sidewalls, this causes the stress in the sidewalls to be higher relative to that in the crosswalls.

Considering the transfer of forces in the direction normal to the chord face (see Fig. 5.5, direction B-B) , this component is likely be transferred mainly by shear in the branch member sidewalls. This would explain the 'shear-slip' lines which were visible on the branch sidewalls in the direction perpendicular to the chord face (see Plate 5.12).

5.5.3 Failure of branch members

For all branch members local yielding was always initially apparent at the member ends (ie., at the joints). However at truss ultimate load yielding in many members extended over the entire length. The visual discrimination of member yielding correlated in all instances with the yield strain being exceeded at one or more of the gauge positions. For each truss the modes of failure and measured joint forces at truss ultimate load are presented in Appendix D.

Member yielding of the tie member was the most common failure mode. In addition to tie yielding there were two occurrences of fracture in the heel crosswall of the tie branches, namely in trusses T5 and T6 (see Plates 5.7 & 5.8, respectively). In both of these joints the tie overlapped the strut. This rupture was always in the region corresponding to the 'heat affected zone' adjacent to the weld, and on the most highly stressed face. It is significant that fracture was always in the parent metal and not in the weld, indicating that the welds were not defective. It is common knowledge among structural engineers that welding reduces the yield stress in high yield members directly adjacent to welds. Where fracture did occur it was in conjunction with member yielding

of the branch. It appears, therefore, that the welding did not have a detrimental effect on the ultimate load carrying capacity of the tension branches.

However, fracture of the weld or parent metal in the direct vicinity of a joint is classified by CIDECT[43] as a joint failure. In general, for the 100% overlap joint test trusses, member yielding occurred before joint failure. It is possible that fracture in the tension branch could be the critical failure mode in a 100% overlap joint truss where the joints are weaker than the member.

Member yielding of the tension branches was identified in all trusses except T2 where failure was by in-plane buckling of the compression chord. Comparing the forces sustained in those ties which were subject to member yielding (- extreme fibre yielding at one or more of the strain gauges) in T2/2, T3, and T5, a member efficiency of at least 0.86 was reached in each case. In T4 and T6 tie yielding occurred at member efficiencies of 0.76 and 0.71, respectively. It is likely that member efficiency for those tie branches which were subject to extreme fibre yielding at the strain gauges was influenced by the bending stiffness of the joint, and the bending stiffness of branch member. In this sense three joint parameters appear to be significant:

(i) β

(ii) b_1/t_1 & b_2/t_2

(ii) b_0/t_0

These parameters combined in trusses T2/2, T3, and T5 to produce a low joint stiffness, relative to the joint stiffness of T4 and T6. The increased component of bending stresses induced in the branch members of trusses T4 and T6 thus had a detrimental effect on the maximum axial force which those members were able to sustain, prior to the onset of extreme fibre yielding at the strain gauges. The member efficiency was also influenced by the sense of overlapping. The bending moments in the branch members were greater where the tie overlapped the strut (see also section 6.3.8). Comparing the member efficiencies on opposite sides of each truss, it can be seen that the values are higher where the strut overlapped the tie.

Member yielding of the strut occurred in T2/2, T4, and T6. The relationship that has been proposed between member yielding of the tie and the joint parameters also holds for the case of member yielding of the compression branches. Two buckling modes were identified in the compression branches:

(i) In truss T4 in-plane, single curvature member buckling occurred in two of the compression branches (see Fig. 5.9). However, in each case member

yielding of the branches occurred prior to the development of buckling.

(ii) Strut local buckling (L6) occurred only in truss T6. For the joints where the tie overlapped the strut local buckling was observed in both the toe and heel crosswalls. For those joints where the strut overlapped the tie local buckling occurred only on the heel crosswall.

For all the joints in truss T6 the L6 failure mode was normally preceded by yielding at one or both of the corresponding gauges. The heel face was always subject to more local deformation even though the toe face was more highly stressed in some cases. It is therefore likely that the heel connection to the chord face affords less restraint to local buckling than the toe interface.

Strut local buckling was not observed in T4 even though the same section size was used for the branches as in T6. The only difference between T4 and T6 was the size of the chord. In T6 the branch to chord width ratio was smaller (T4:β=0.6; T6:β=0.4), even though the slenderness of the chord section was only marginally greater (T4:b_0/t_0 = 20; T6:b_0/t_0 = 23.8). It is difficult to conclude from this limited information, which of these two parameters (β or b_0/t_0) is more significant in determining the occurrence of strut local buckling L6.

Overall strut buckling was observed only in truss T4. With the exception of trusses T4 and T6 the section used for the strut was stronger than the corresponding tie. Trusses T4 and T6 were fabricated using the same section for both compression and tension branches. Furthermore the branch members in these two trusses were identical with respect to length, inclination and section size. In T6 the lowest member efficiency ($N_1/A_1.\sigma_{e1}$) at which local buckling (L6) of the compression branch occurred is 0.69 (joints 7 & 9), while overall member buckling in T4 occurred at a member efficiency greater than 0.76 (joint 3). It was anticipated that overall member buckling would occur in T6, however strut local buckling proved to be more critical.

5.6 Difference between gap and 100% overlap joint failure modes

In the case of the gap joint truss the joint failures which occurred involved local deformation of the chord connecting face. In the case of the failure modes observed in the 100% overlap joint trusses, none involved deformation of the chord connecting face. Member yielding of the branches, which was the most common mode of failure in the 100% overlap joint trusses, did not occur in the gap joint truss.

However, similar types of member failure occurred in the chord section of both gap and 100% overlap joint trusses. In-plane member buckling of the compression chord, and yielding of the tension chord were observed in both types of truss.

5.7 Definition of ultimate joint strength

There were only two trusses where it was possible to relate truss ultimate load to failure in individual elements, and both involved failure of the compression chord. In T1 there was local buckling at joint 9 in the first load cycle, and in the second load cycle the corresponding joint on the opposite side of the truss failed by the same mode. In T2 in-plane chord member buckling was observed between joints 8 and 9. In all other cases the ultimate load of the structure was related to several modes of failure occurring simultaneously.

In the cases where overall buckling, local buckling or fracture were visible in a member it is likely that the element in question had attained its ultimate load, however when only local yielding or member yielding occurred it is possible that there was capacity in that member to carry further load. Therefore, in the testing of complete trusses the ultimate load capacity of individual joints and members can be difficult to define exactly.

In isolated joint testing the axial forces in the branch members are normally assessed using load cells. In the test trusses the axial forces were calculated from the strain gauge values. It has already been indicated that where extreme fibre yielding was observed in 'overlapped' branch members at the strain gauges the calculation of axial force proved to be unreliable (see section 5.5.2). However the unreliability of the measured strains at sections where one or both crosswalls had yielded was not restricted to 'overlapped' branch members. This is reflected in the discrepancy in the calculated axial force between each pair of strain gauges. Prior to extreme fibre yielding at any of the strain gauges on a member the error in the calculated axial force between each end was always less than 5%. Once yielding had occurred this error was observed to increase. Care was taken to select the most reliable axial force value for each member (see section 4.6.3).

Even with the high level and extent of instrumentation that was used during testing an understanding and definition of the modes of failure was only made possible by detailed visual examinations of the joints and members. The main problem proved to be the determination of the distribution of forces at those positions in the trusses where

yielding had occurred.

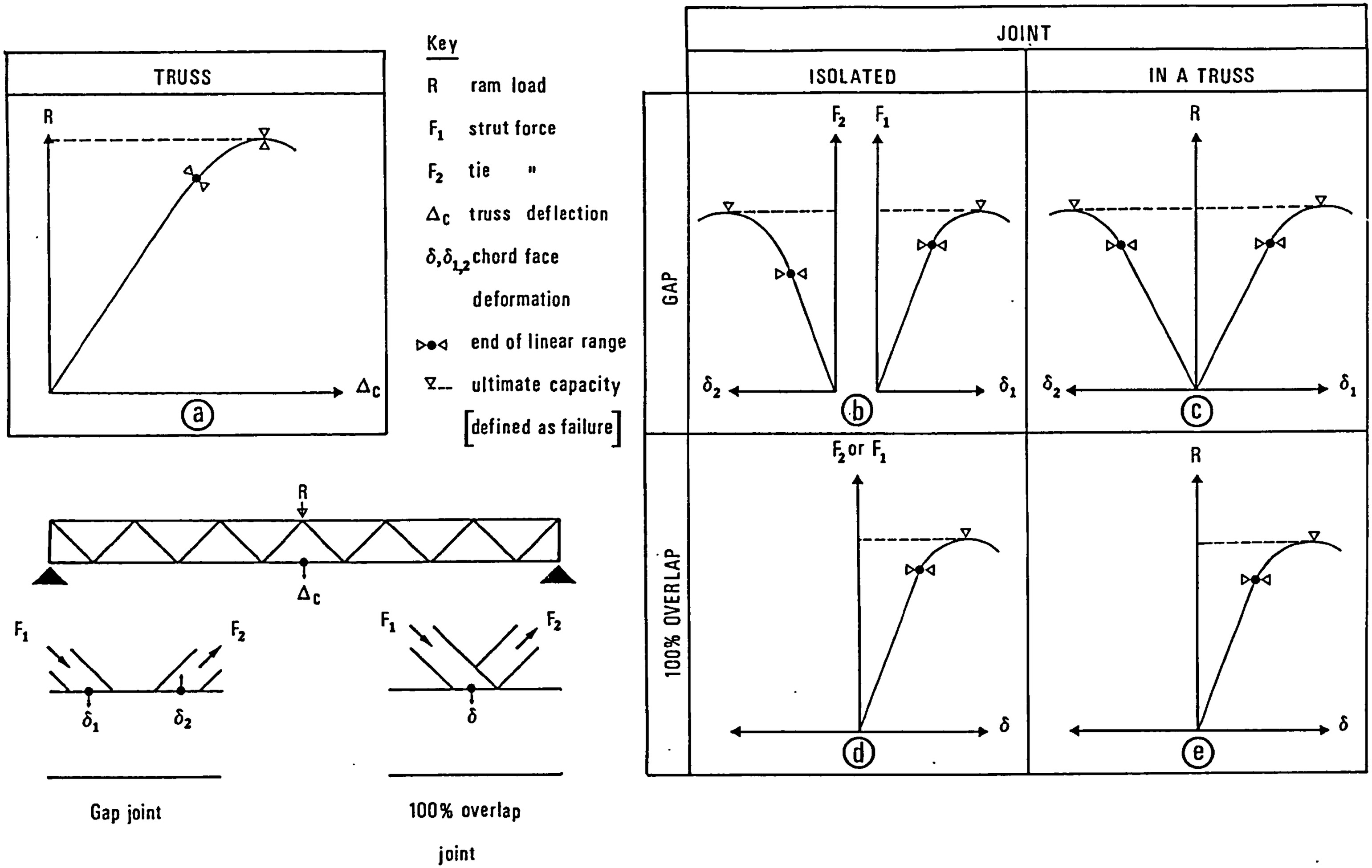

Fig 5.1 Definition of truss and joint ultimate capacity (failure load).

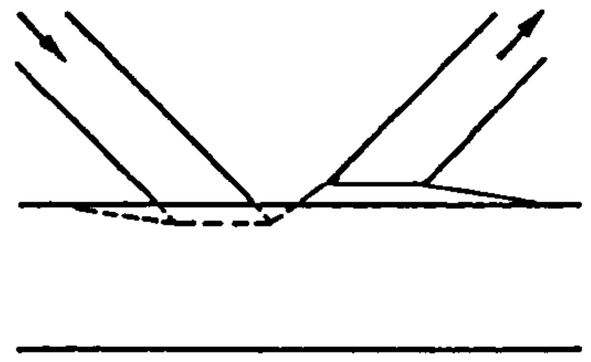

G1 : chord face failure

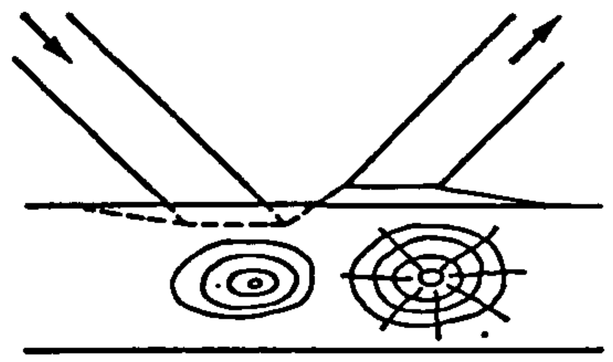

G2 b,w or c : chord face and wall failure with cracking

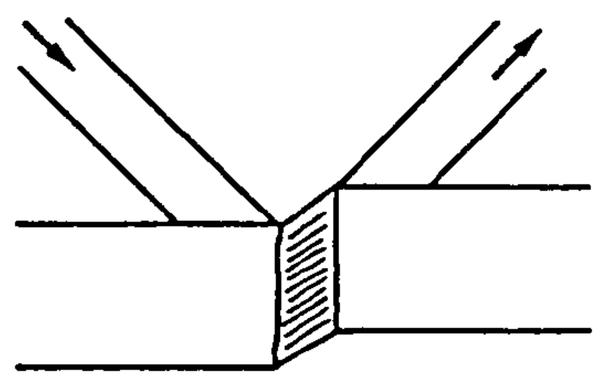

G3 : shear failure

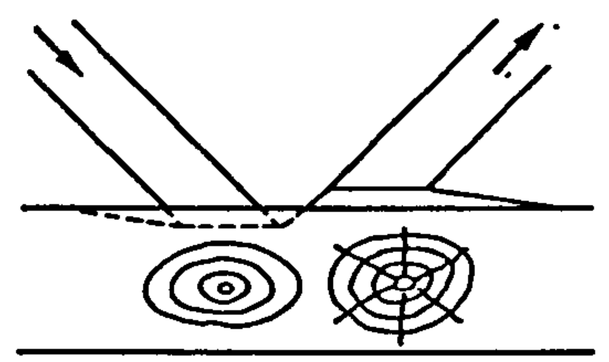

G4 : chord face and wall failure without cracking

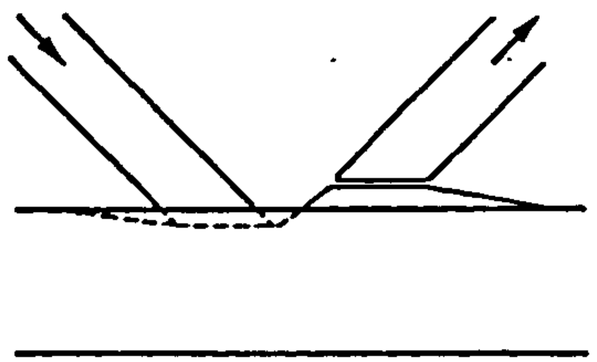

G5 b,w or c : diagonal failure

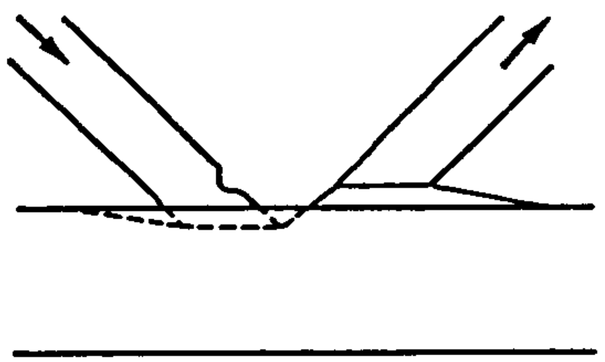

G6 : local buckling of compression brace

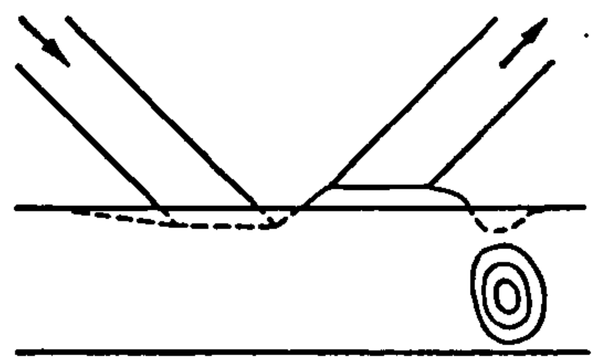

G7 : chord buckling

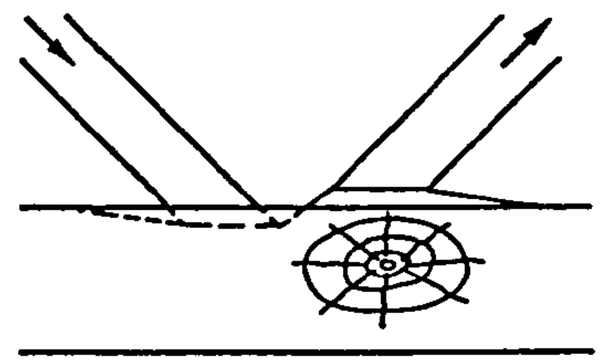

G8 : chord face and wall failure around tension brace

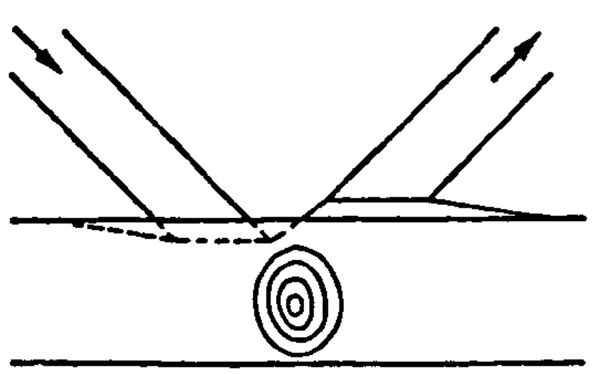

G9 : chord wall buckling

key

b - brace crack

w - weld "

c - chord "

outward deformation

inward "

Fig 5.2 CIDECT categories of gap joint failure modes.

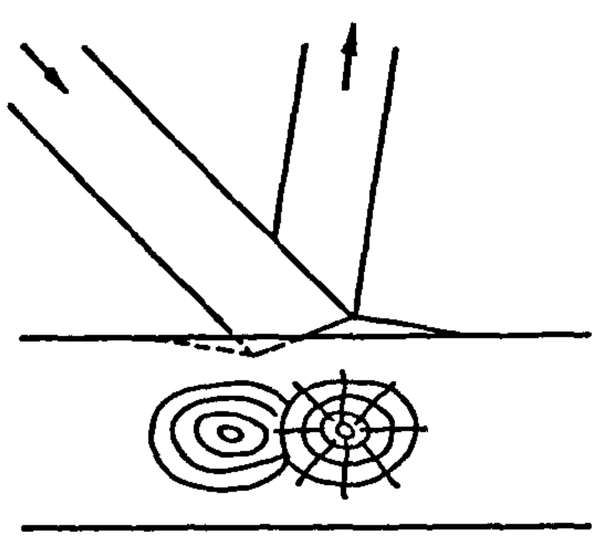

L4 : chord face and wall failure

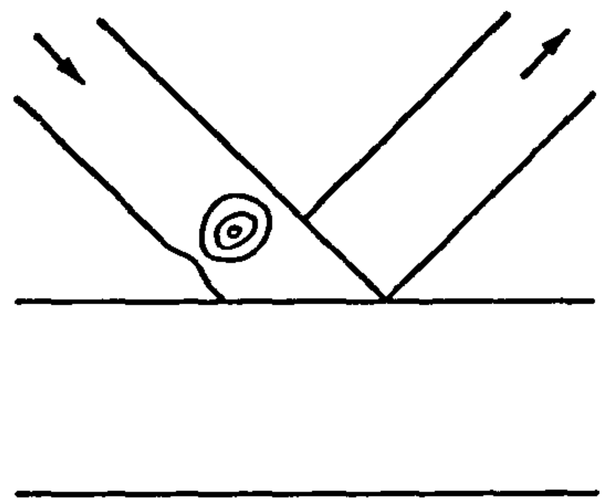

L6 : strut local buckling

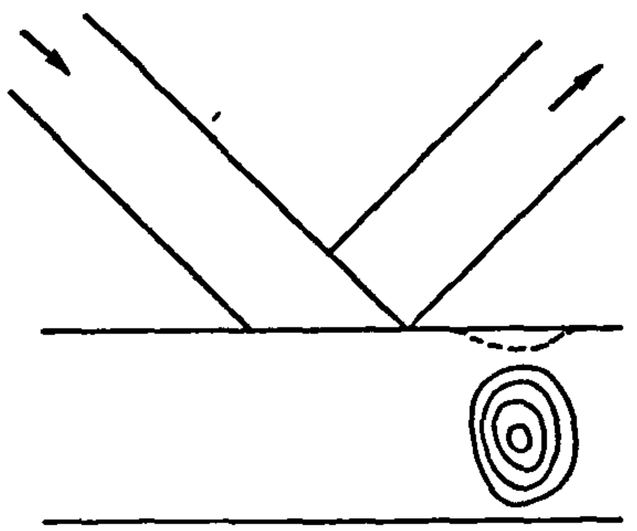

L7 : chord local buckling

key

outward deformation

inward "

Fig 5.3 CIDECT categories of overlap joint failure modes.

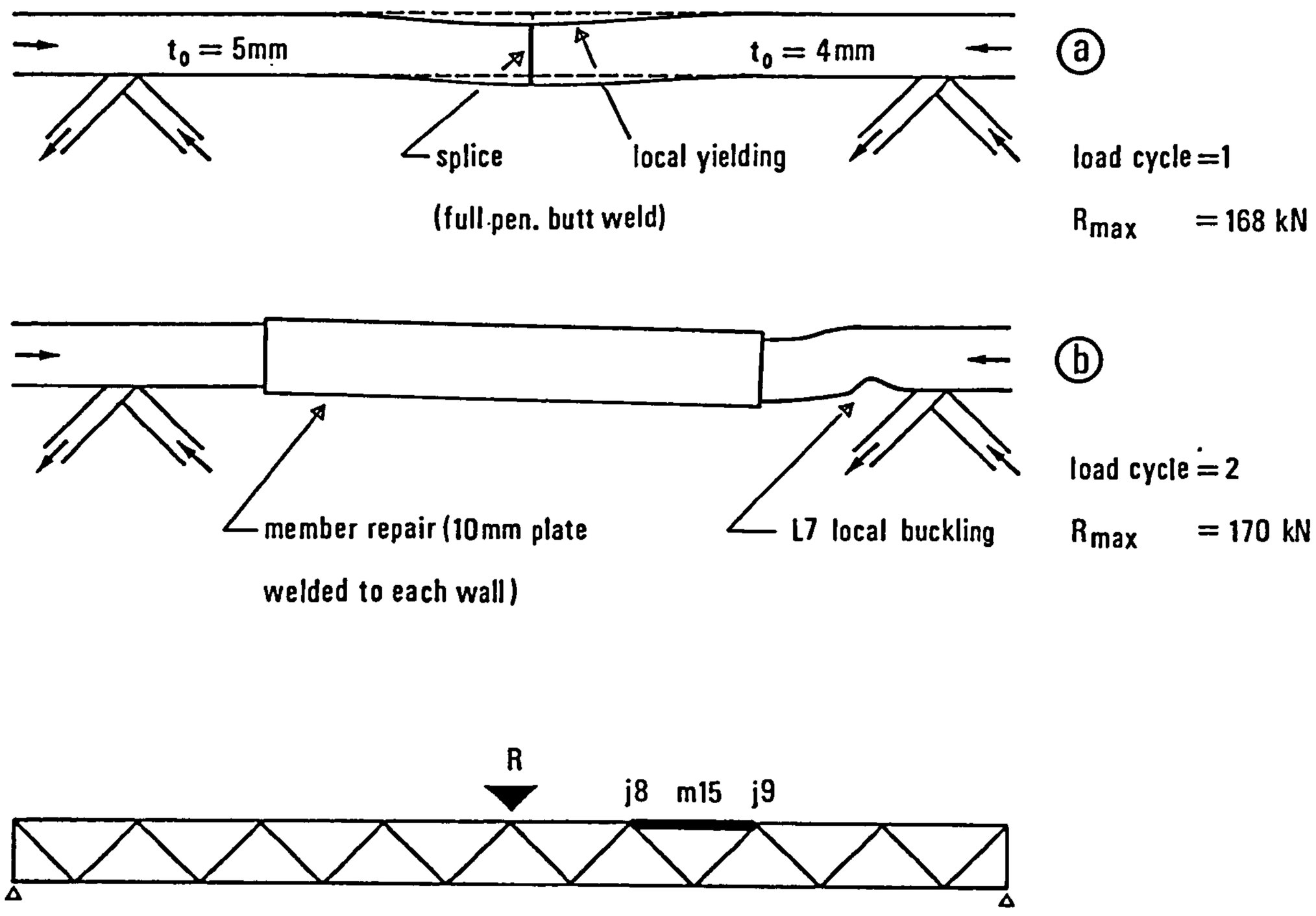

Fig 5.4 Failure of the compression chord in truss T2.

Force transfer in X direction

A – A

$$F_1 \cos\theta_1 + F_2 \cos\theta_2 = F_0 - F_{op}$$

Force transfer in Y direction

B – B

$$F_1 \sin\theta_1 = F_2 \sin\theta_2$$

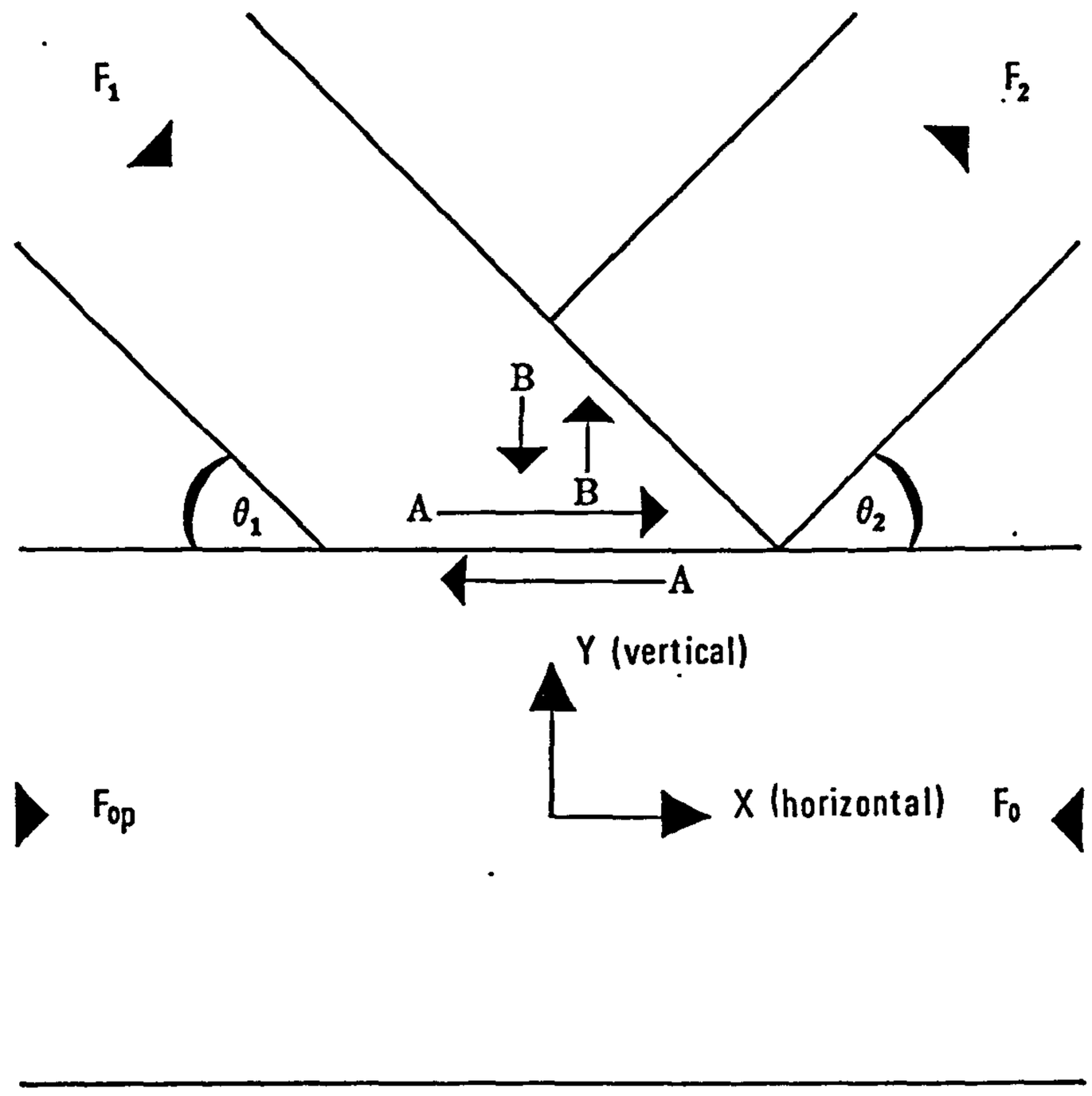

Fig 5.5 Observed force transfer mechanisms for the 100% overlap truss joints.

a)

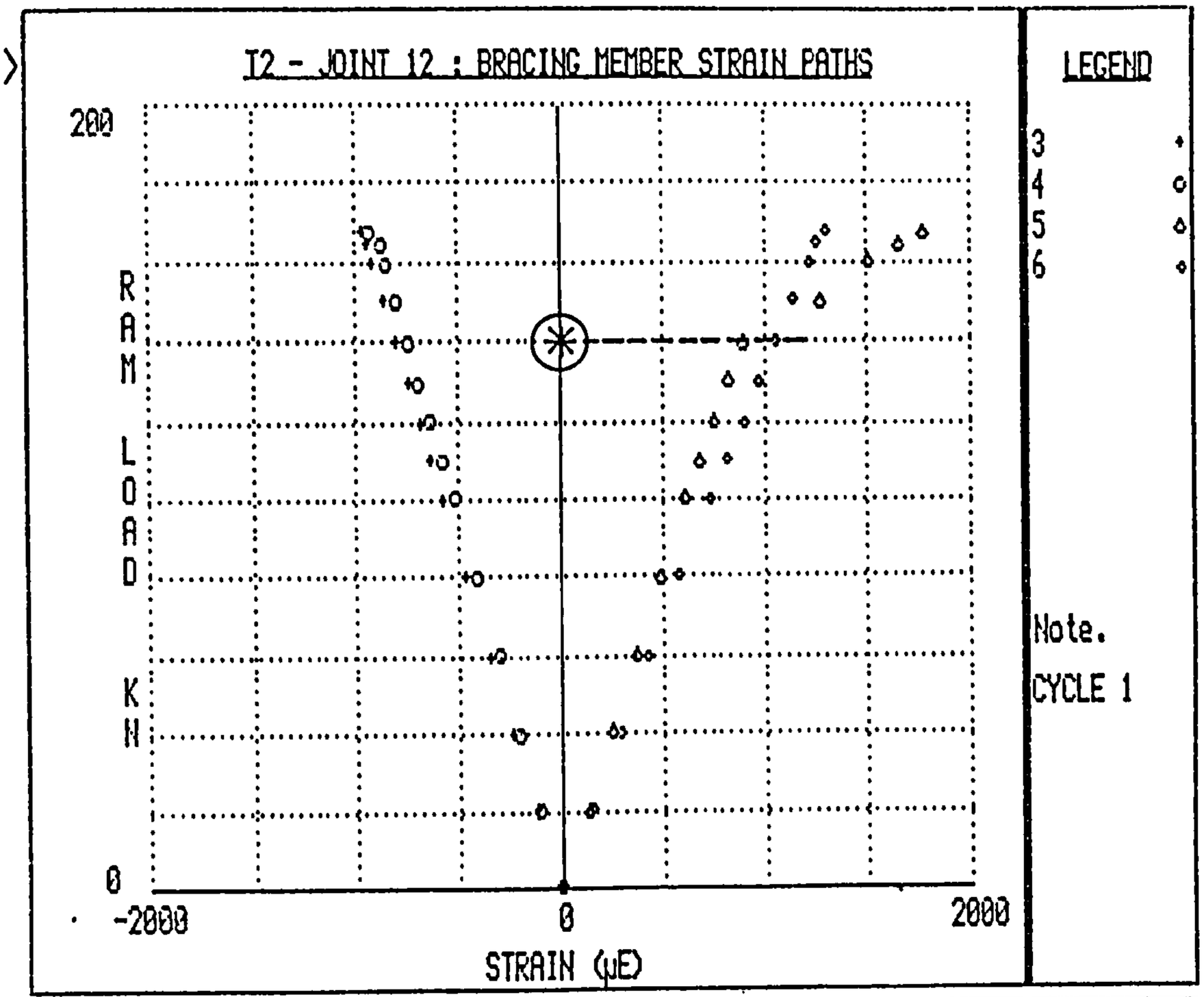

b)

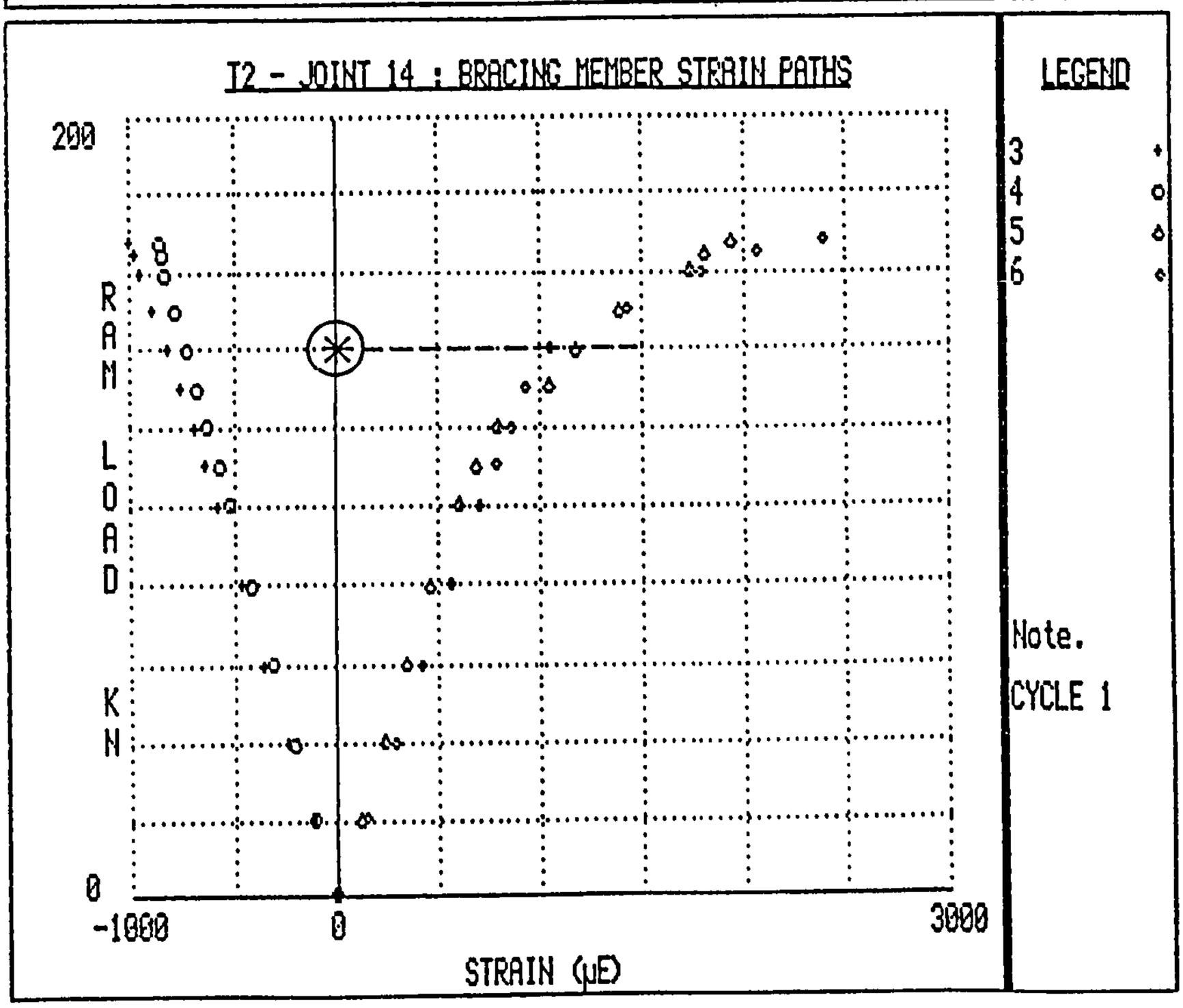

Key ⊛ load at which shear plane was observed in sidewalls of tie

Fig 5.6 Branch member strain paths for joints 12 and 14 in truss T2.

Key

---- Actual stress distribution

-·-·- Assumed stress distribution for calculation of member forces

NB : Stresses shown at strain gauge positions

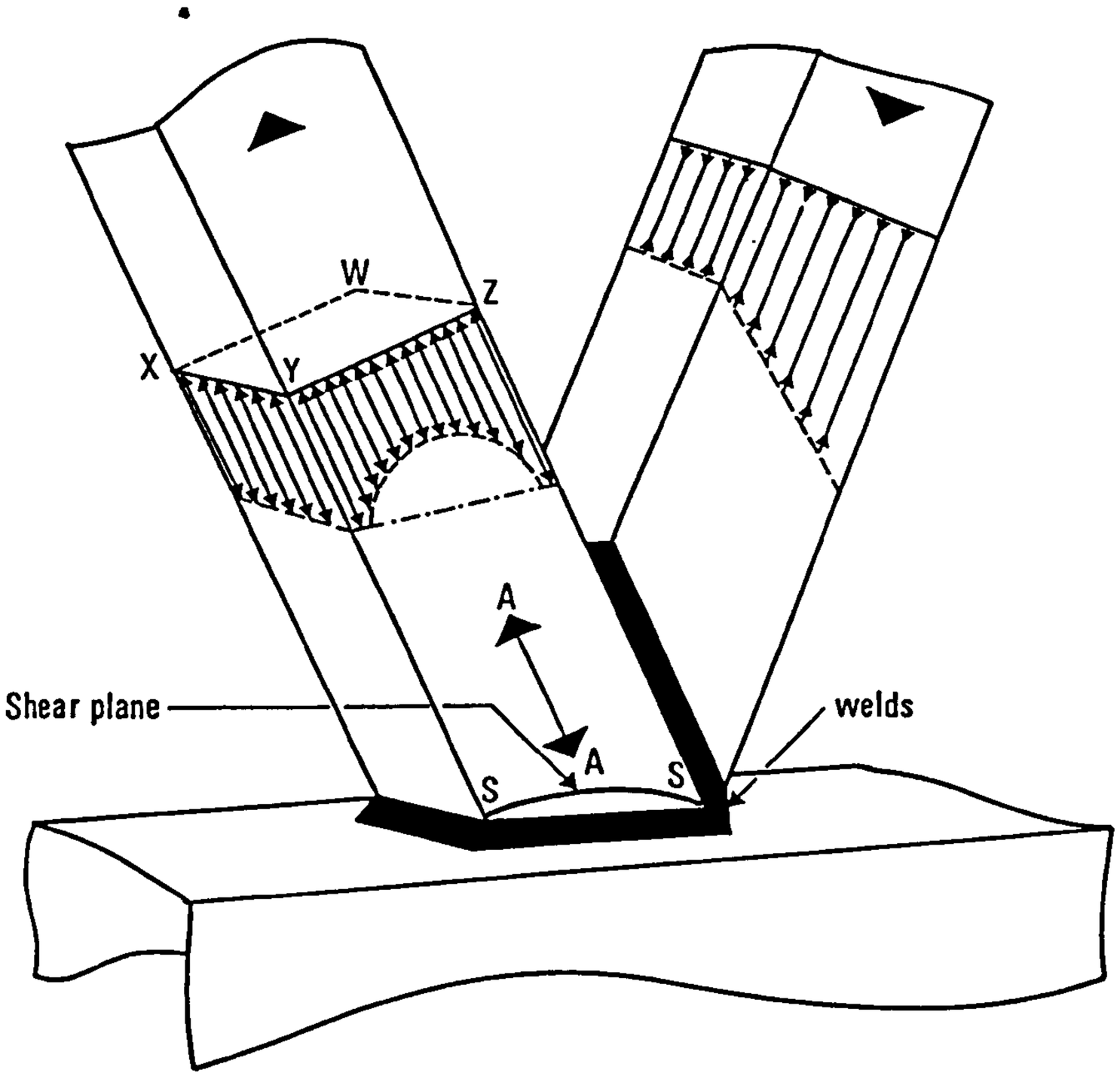

Note

Shear plane prevents efficient transfer of direct stress in direction AA thus reducing the stress in the sidewalls W-X, Y-Z

Fig 5.7 Interaction of the stress distribution in the 'overlapped' branch member with the observed shear plane in the sidewalls.

a)

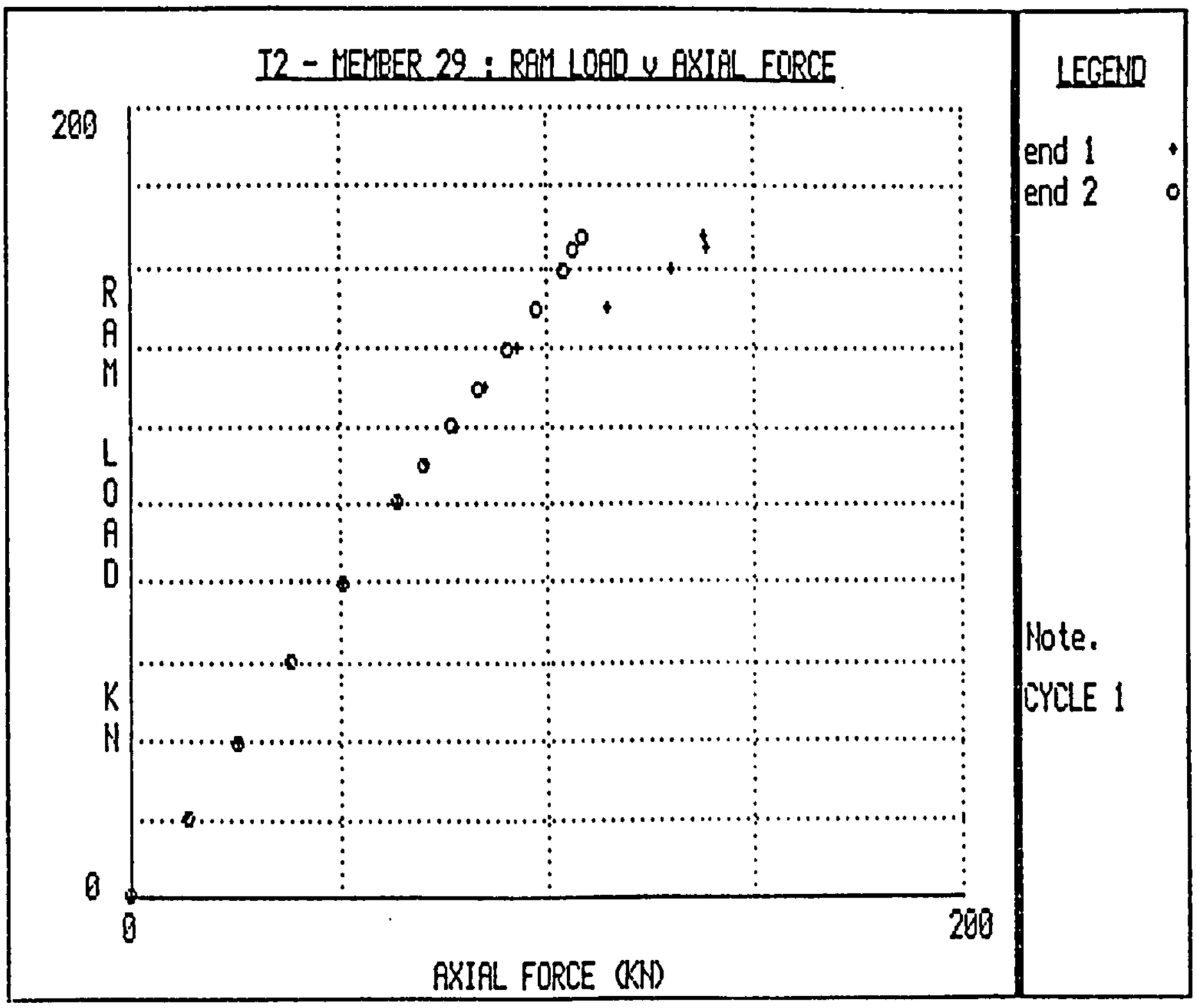

b)

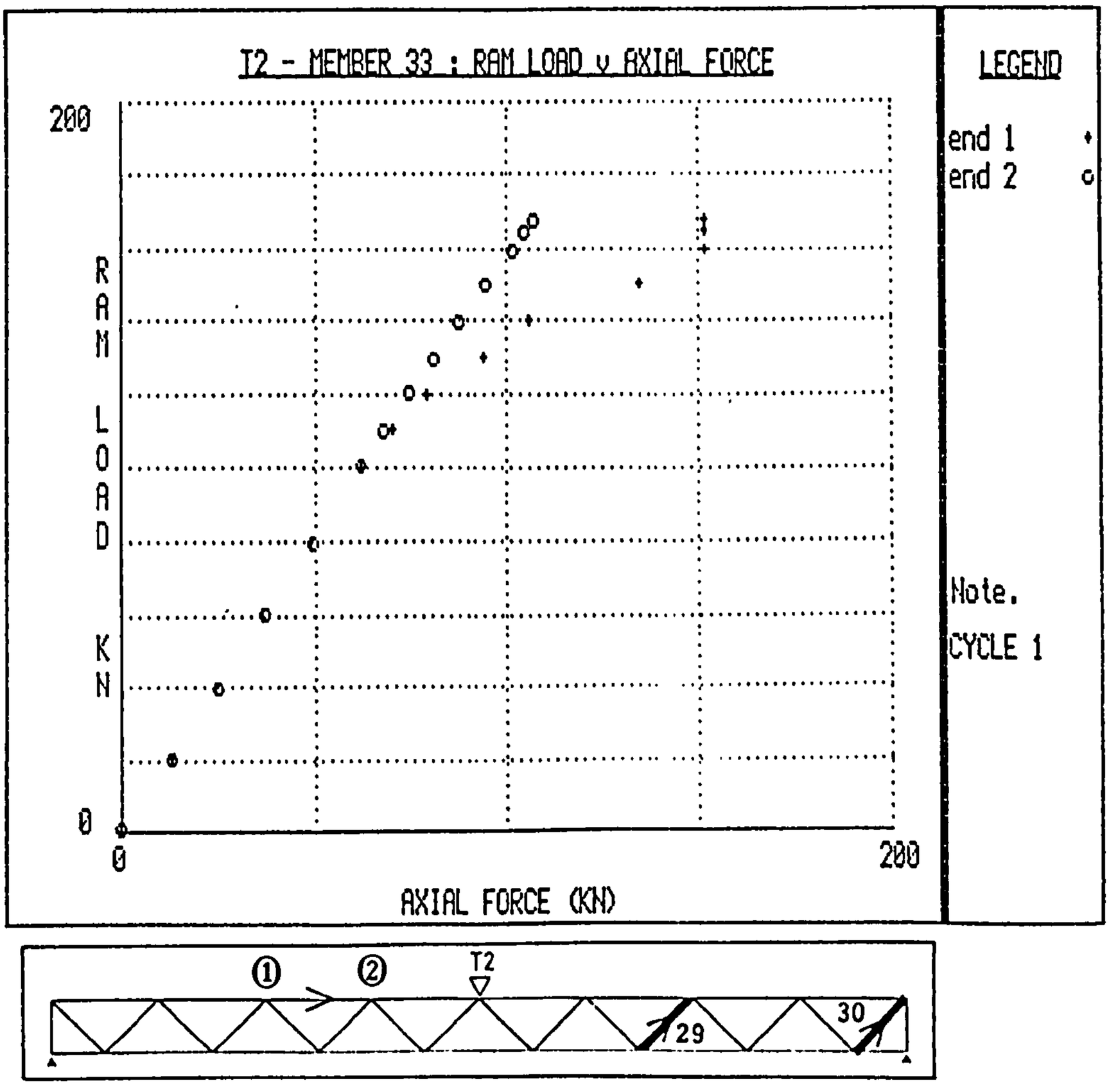

Fig 5.8 Typical examples of ram load v. axial force for the 'overlapped' branch members.

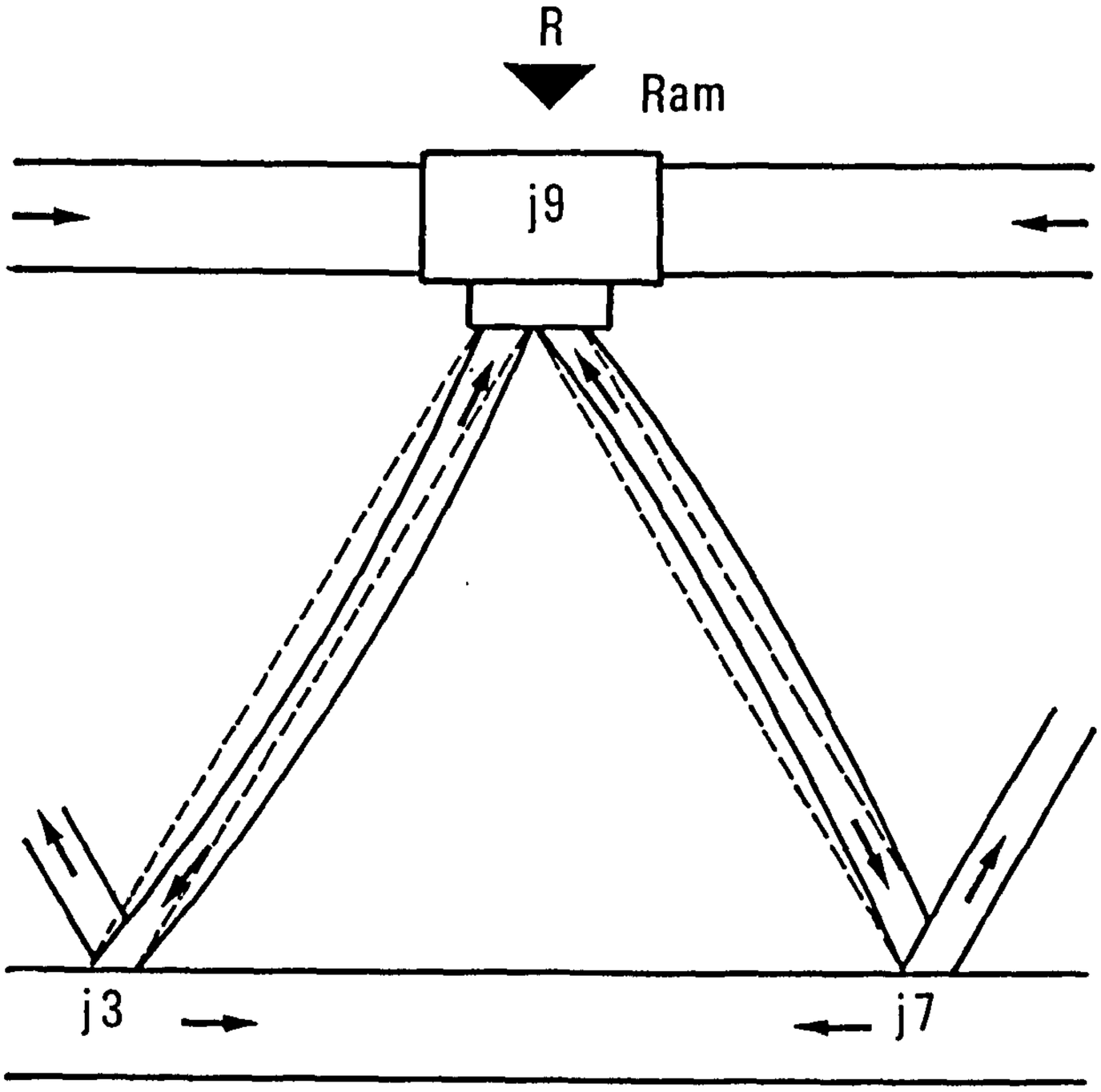

load cycle = 1

R_{max} = 475 kN

Fig 5.9 Overall in-plane single curvature buckling of the midspan compression branches in truss T4.

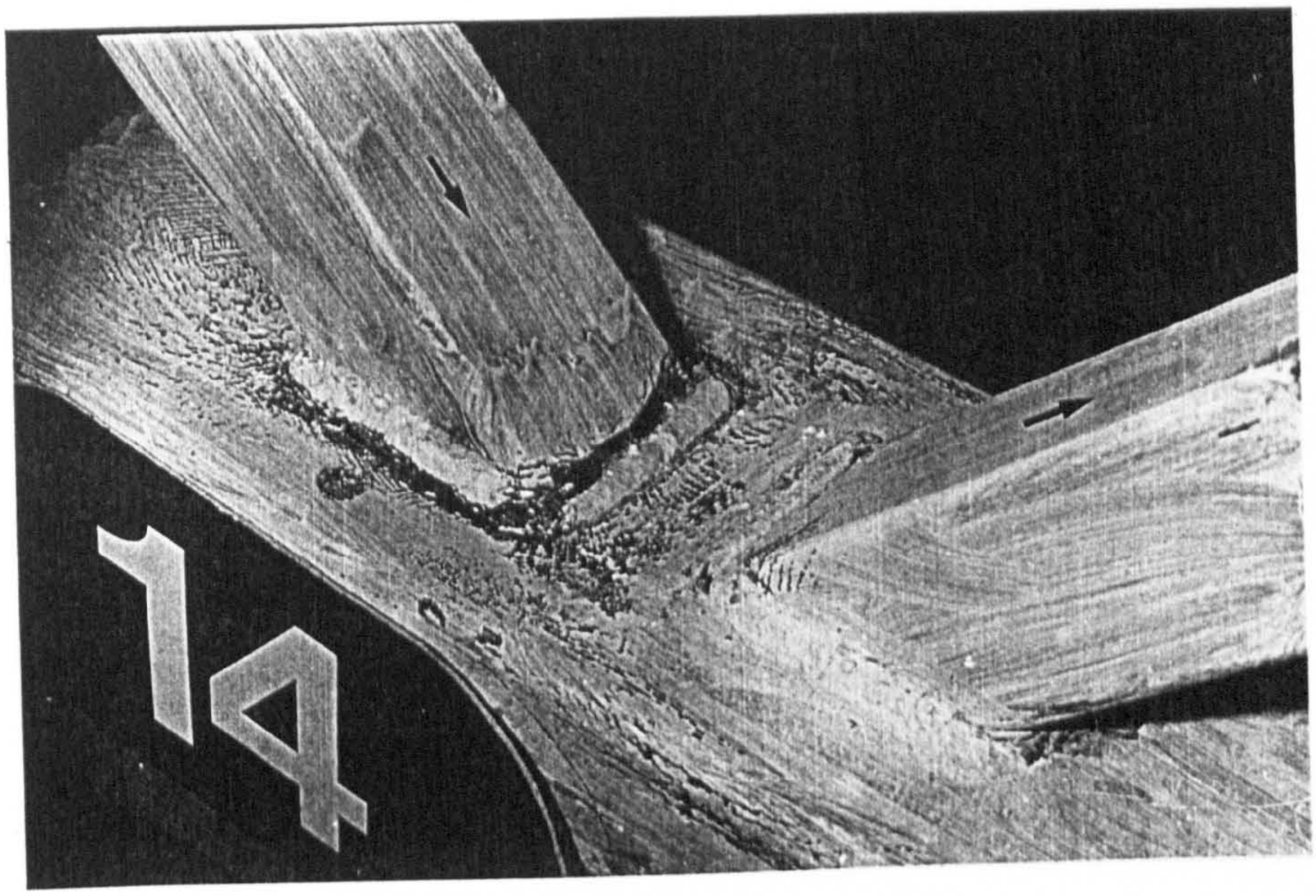

Truss T1 - joint 14 after unloading ; Ram failure load = 163 kN ; load cycle = 6.
(For description of the joint failure mode see Table D2 in Appendix D)

Plate 5.1 Typical stress pattern on the connecting chord face of the gap joints in truss T1.

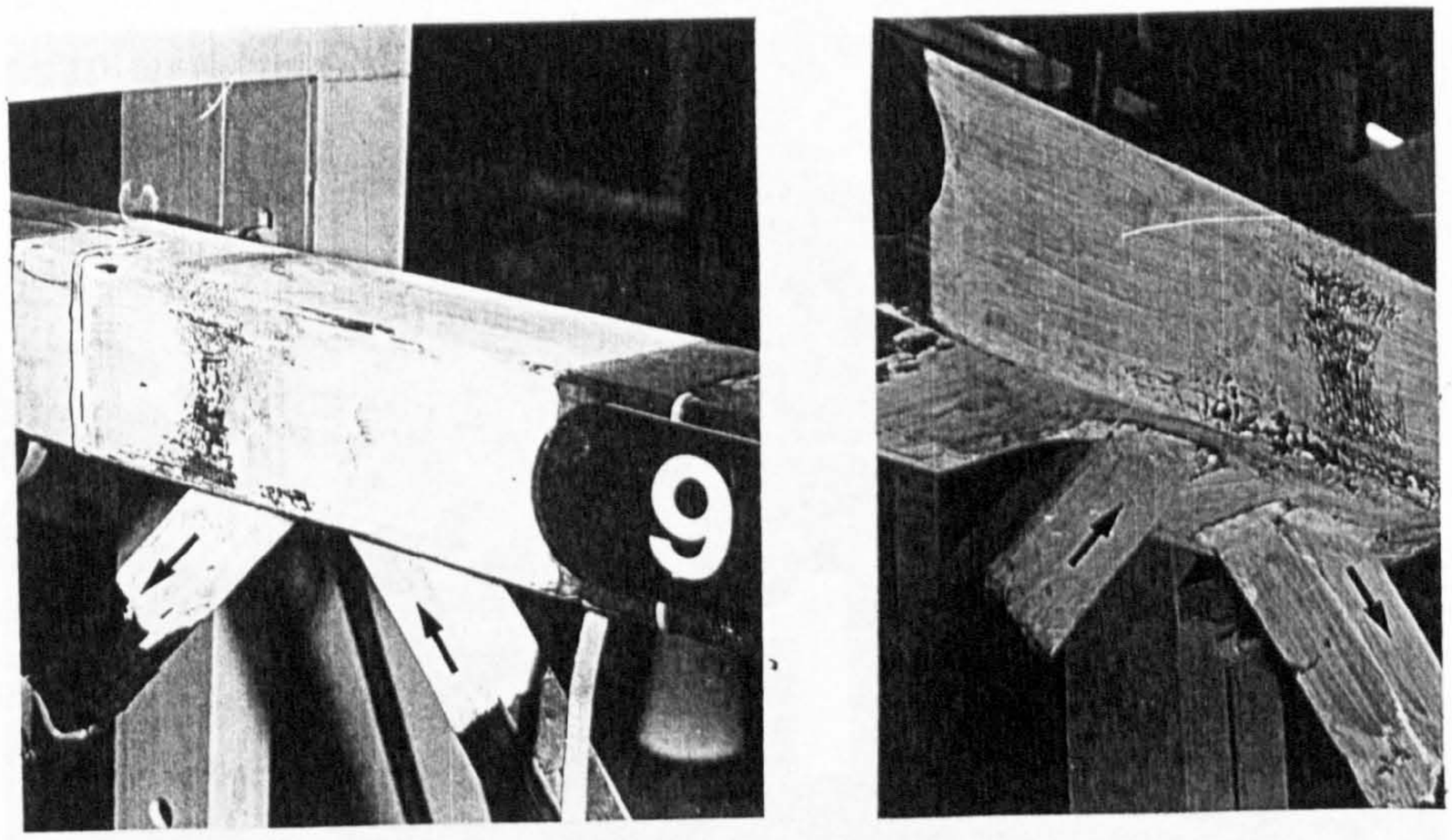

Truss T1 - joint 9 after unloading ; Ram failure load = 125 kN ; load cycle = 1.
(See also Tables D1 and D2 in Appendix D)

Plate 5.2 Failure mode G4 in a compression chord gap joint.

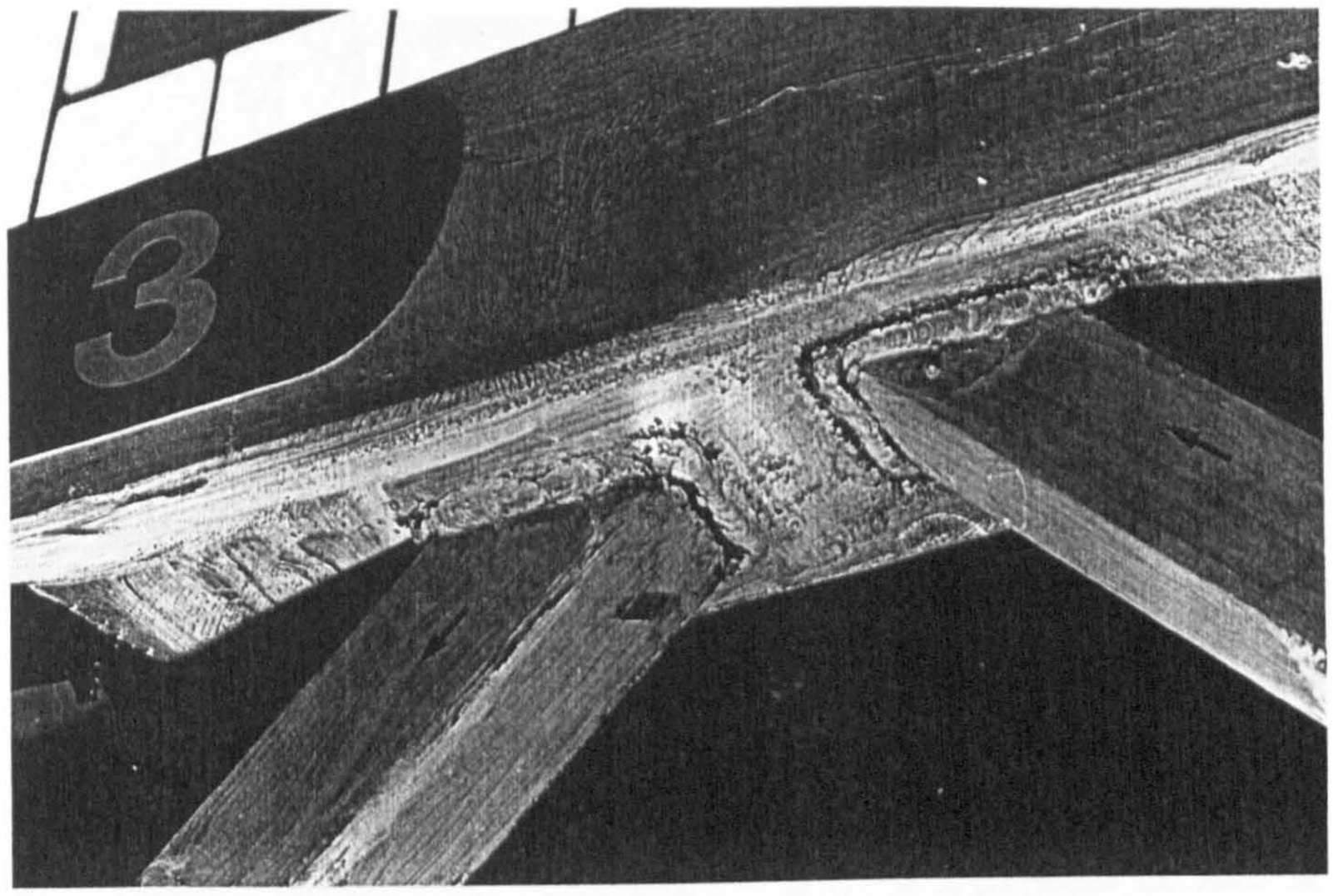

Truss T1 - joint 3 after unloading ; Ram failure load = 158 kN ; load cycle = 5.
(See also Table D2 in Appendix D)

Plate 5.3 Failure mode G2(b) in a compression chord gap joint.

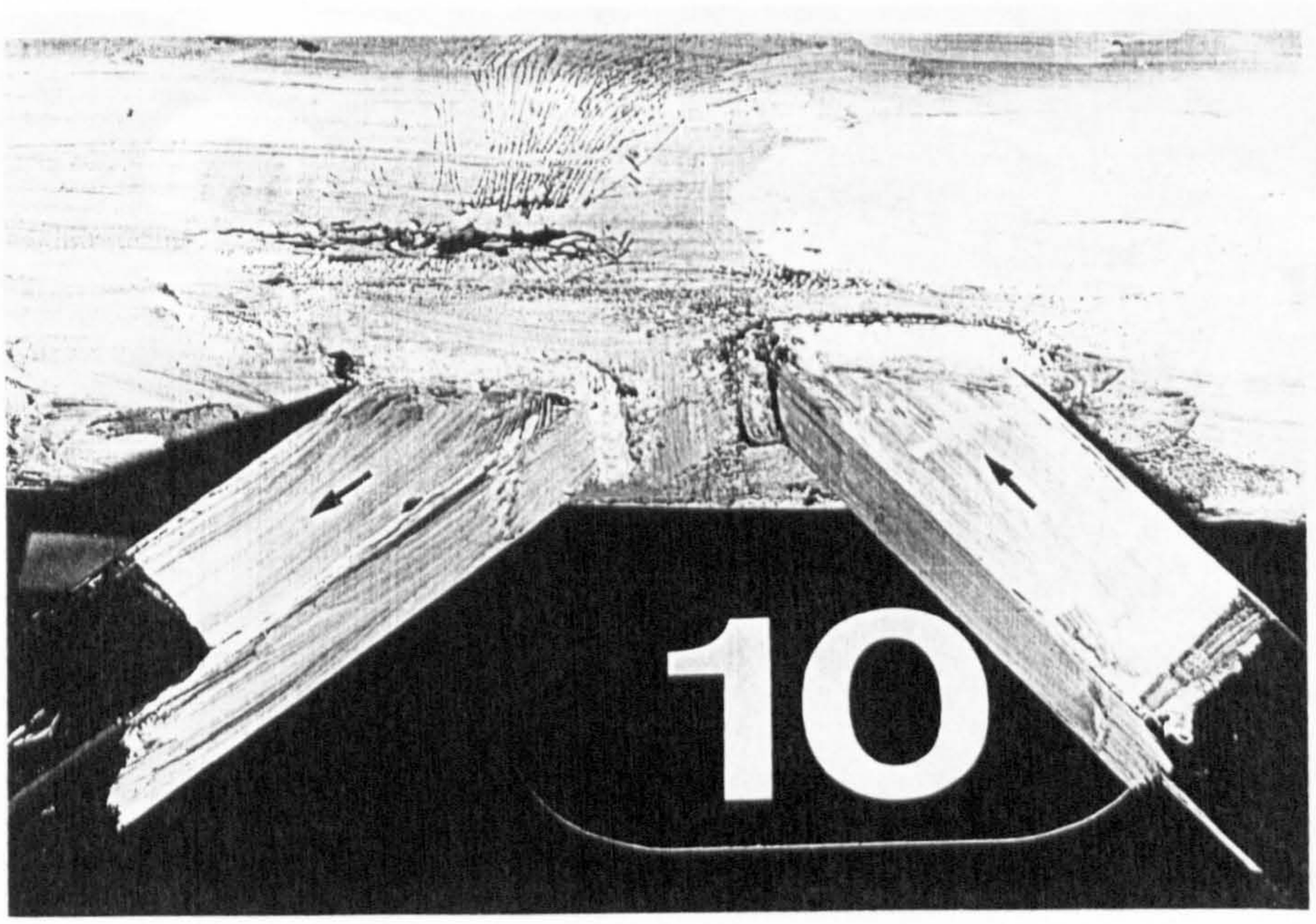

Truss T1 - joint 10 after unloading ; Ram failure load = 163 kN ; load cycle = 6.
(See also Table D2 in Appendix D)

Plate 5.4 Failure mode G8 in a compression chord gap joint.

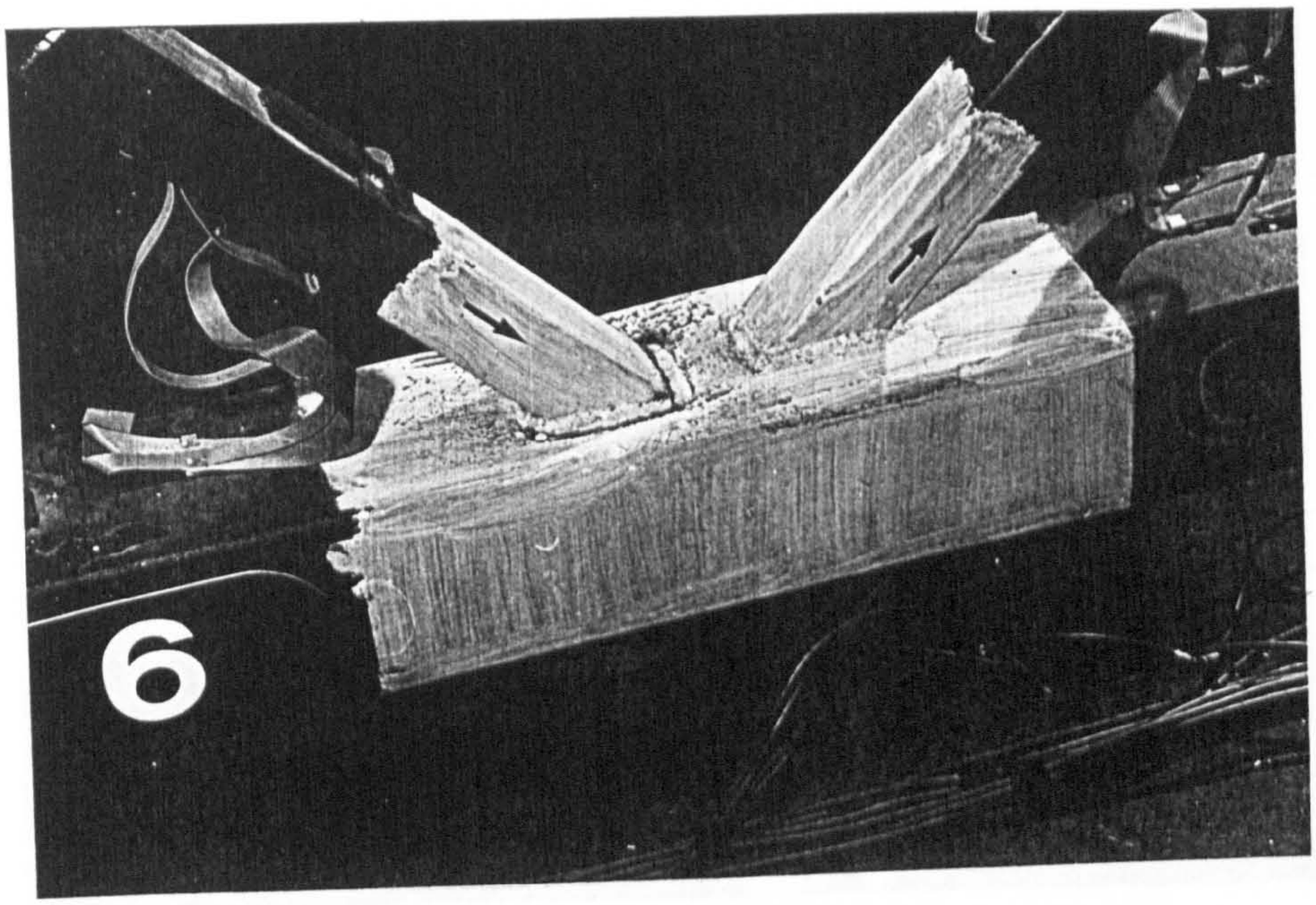

Truss T1 - joint 6 after unloading ; Ram failure load = 158 kN ; load cycle = 5.
(See also Table D2 in Appendix D)

Plate 5.5 Failure mode G1 in a tension chord gap joint.

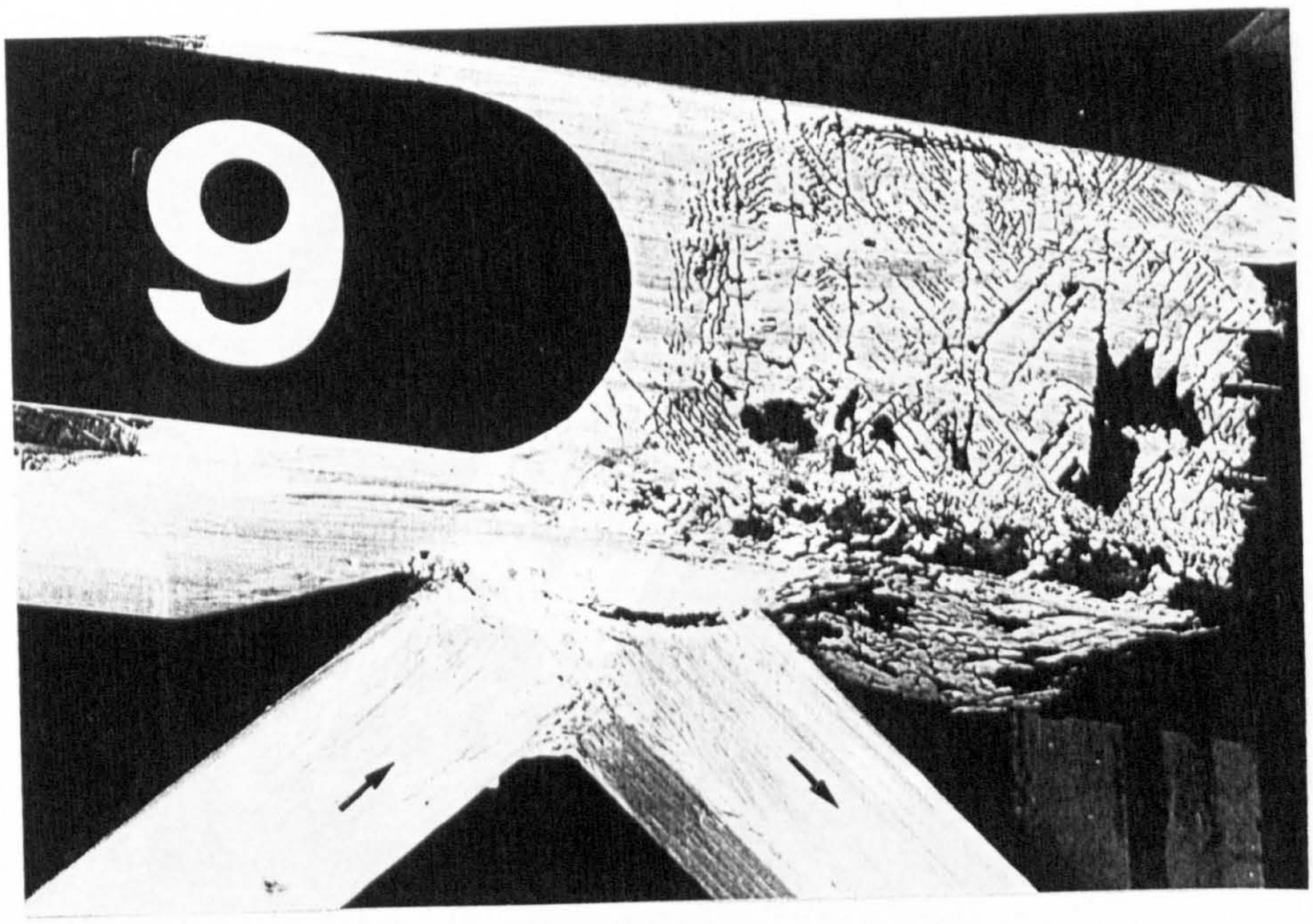

Truss T2 - joint 9 after unloading ; Ram failure load = 170 kN ; load cycle = 2.

Plate 5.6 The only occurrence of local buckling (L7) of the compression chord in the 100% overlap joint test trusses.

Truss T5 - joint 2 after unloading ; Ram failure load = 330 kN ; load cycle = 1.
(For description of the joint failure mode see Table D7 in Appendix D)

Plate 5.7 Rupture of the tension branch along the heel crosswall in a 100% overlap joint truss.

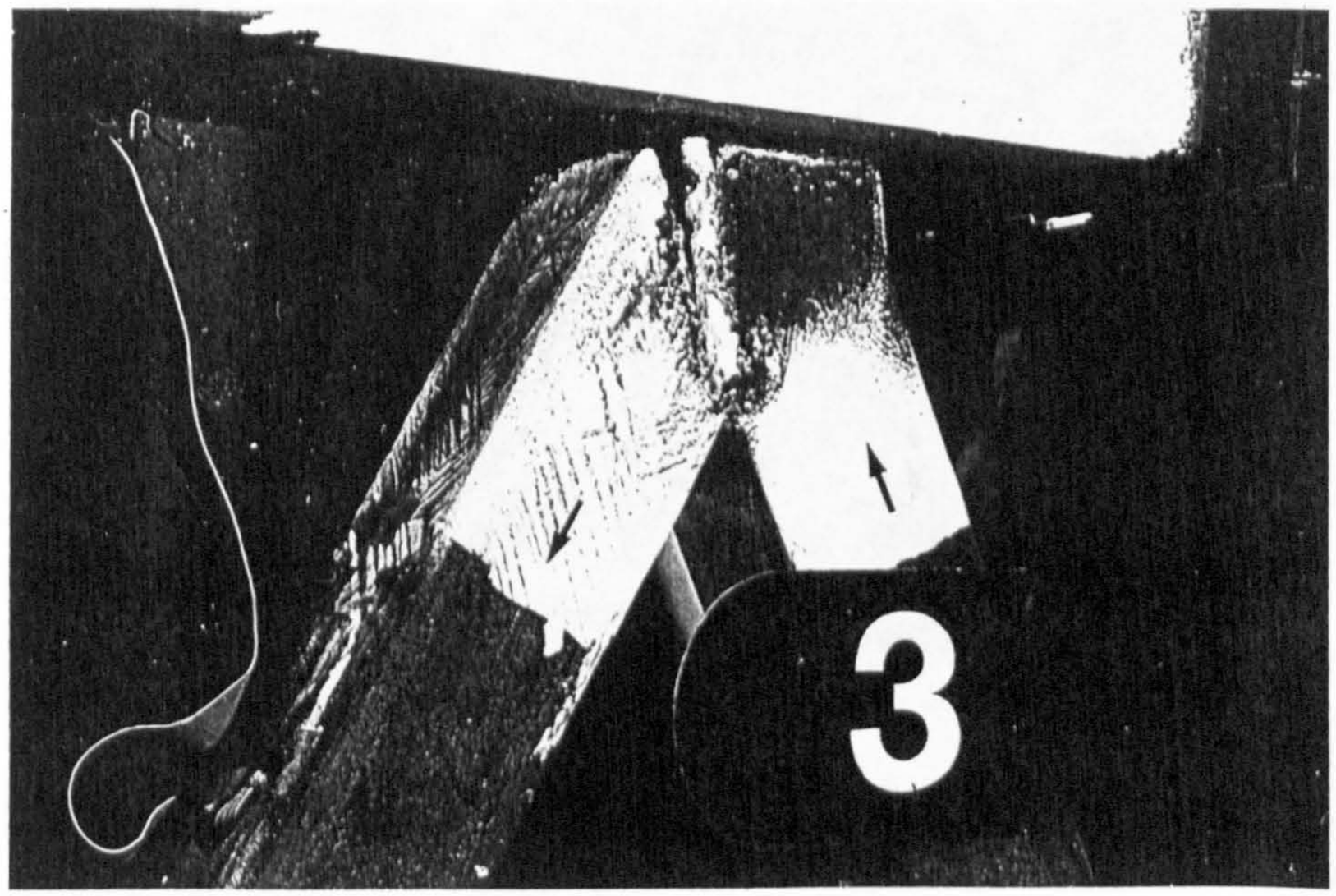

Truss T6 - joint 3 after unloading ; Ram failure load = 560 kN ; load cycle = 1.
(For description of the joint failure mode see Table D8 in Appendix D)

Plate 5.8 Rupture of the tension branch along the heel crosswall and the sidewalls in a 100% overlap joint truss.

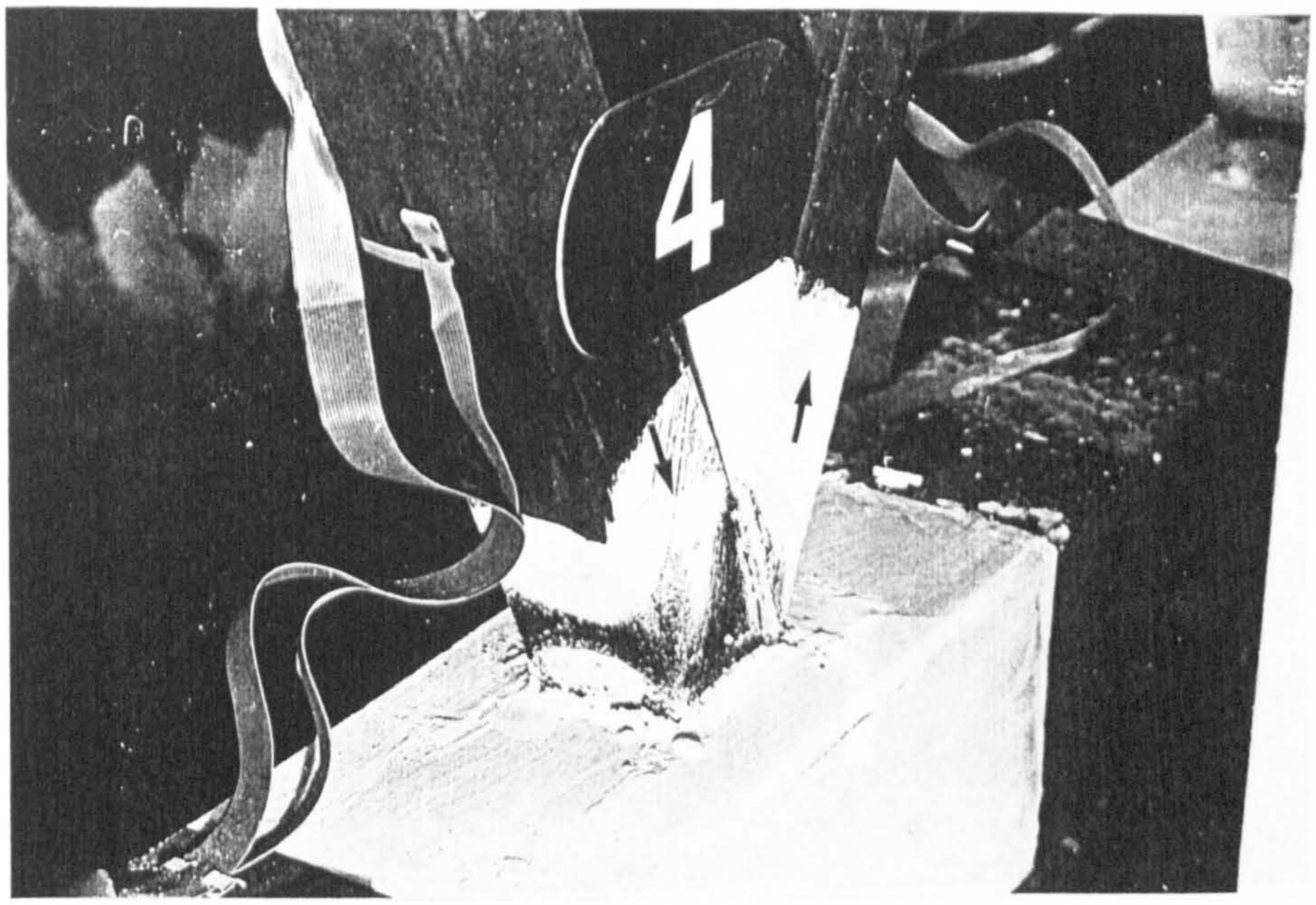

Truss T6 - joint 4 after unloading ; Ram failure load = 560 kN ; load cycle = 1.
(For description of the joint failure mode see Table D8 in Appendix D)

Plate 5.9 Local buckling (L6) of the compression branch in a 100% overlap joint truss.

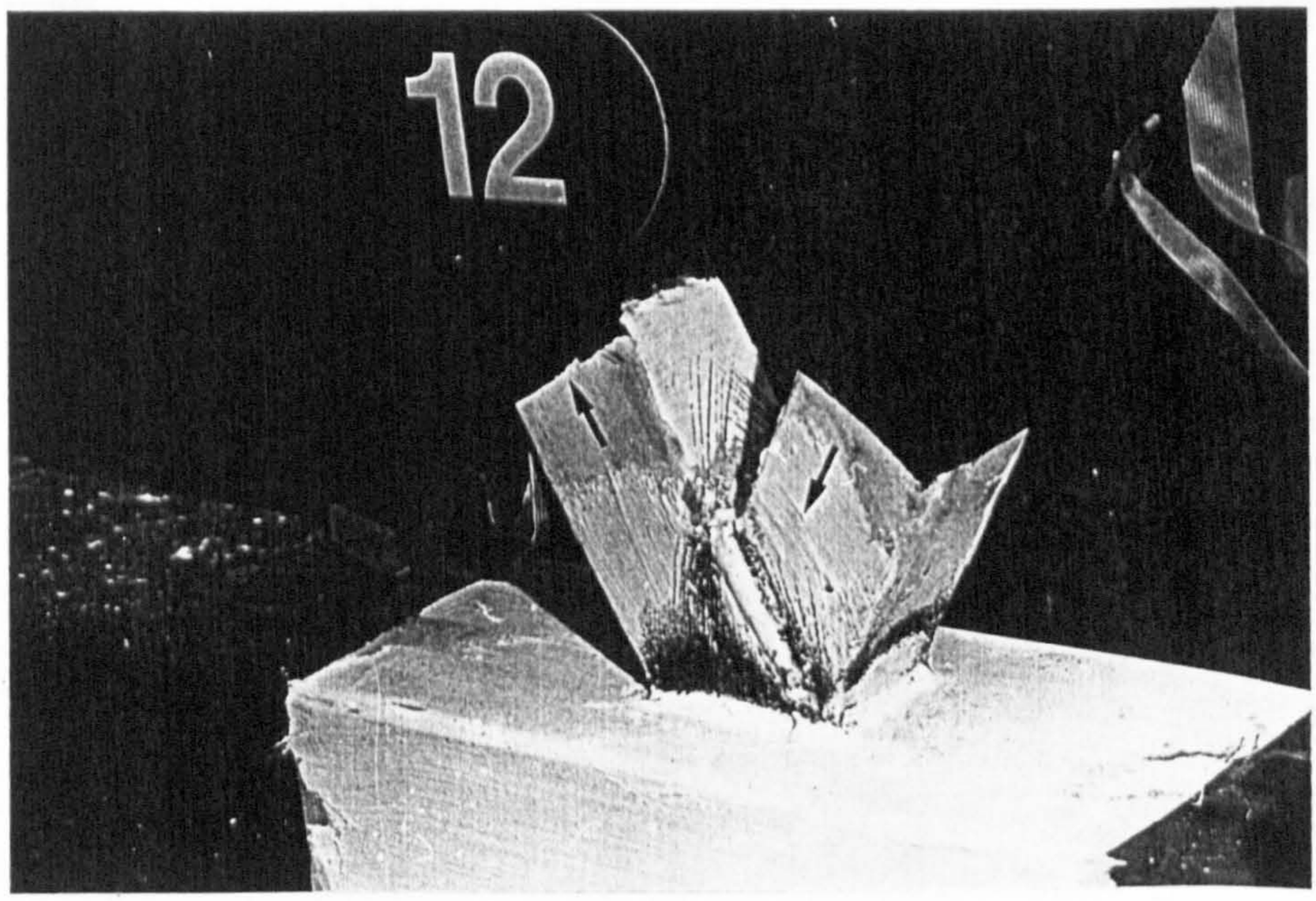

Truss T6 - joint 12 at a ram load of 530 kN.
Ram failure load = 560 kN ; load cycle = 1.
(For description of the joint failure mode see Table D8 in Appendix D)

Plate 5.10 The onset of member yielding in the toe crosswall of an 'overlapped' tension branch member.

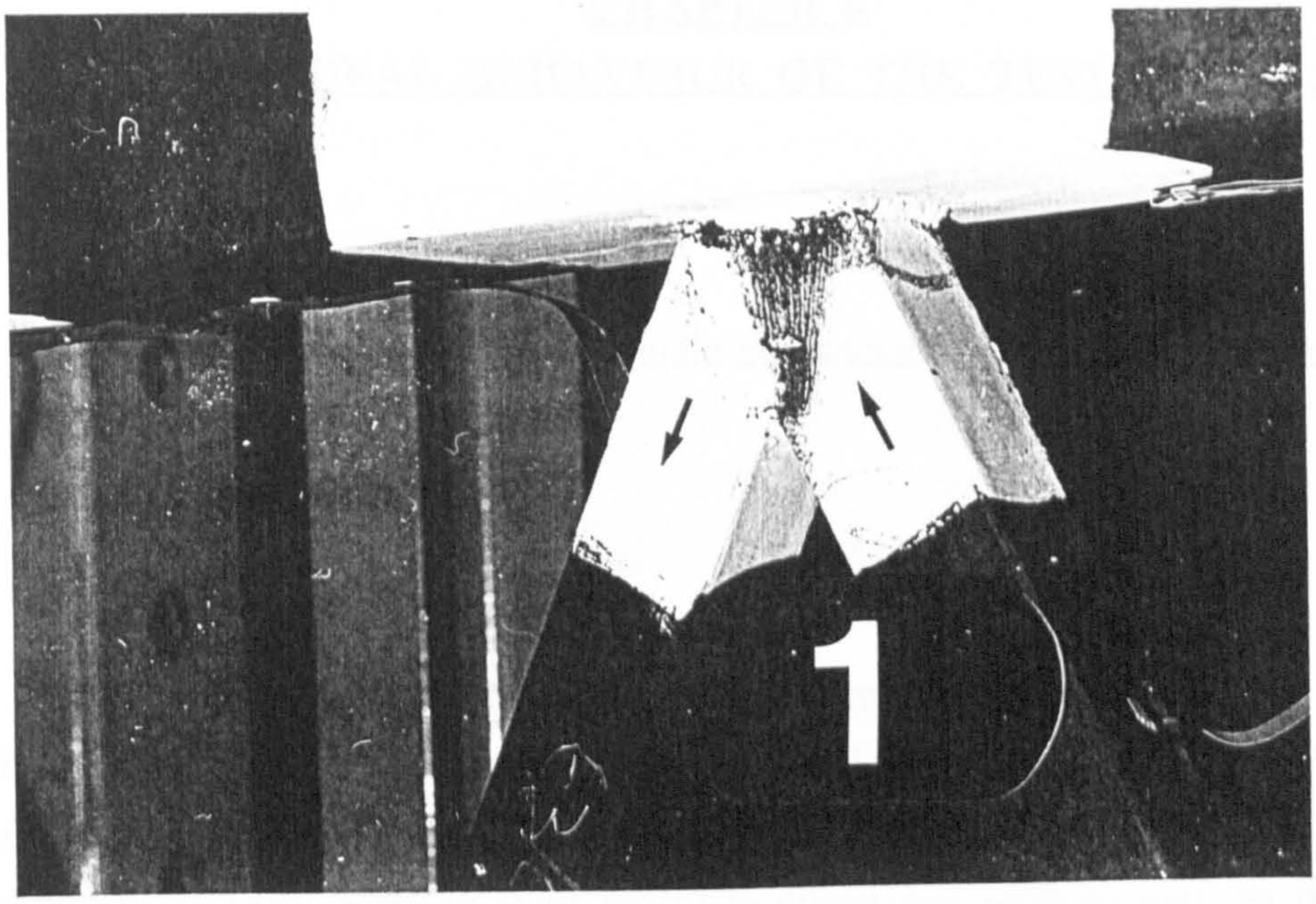

Truss T6 - joint 1 after unloading.; Ram failure load = 560 kN ; load cycle = 1.
(For description of the joint failure mode see Table D8 in Appendix D)

Plate 5.11 Typical stress pattern in the sidewall of an 'overlapped' branch member.

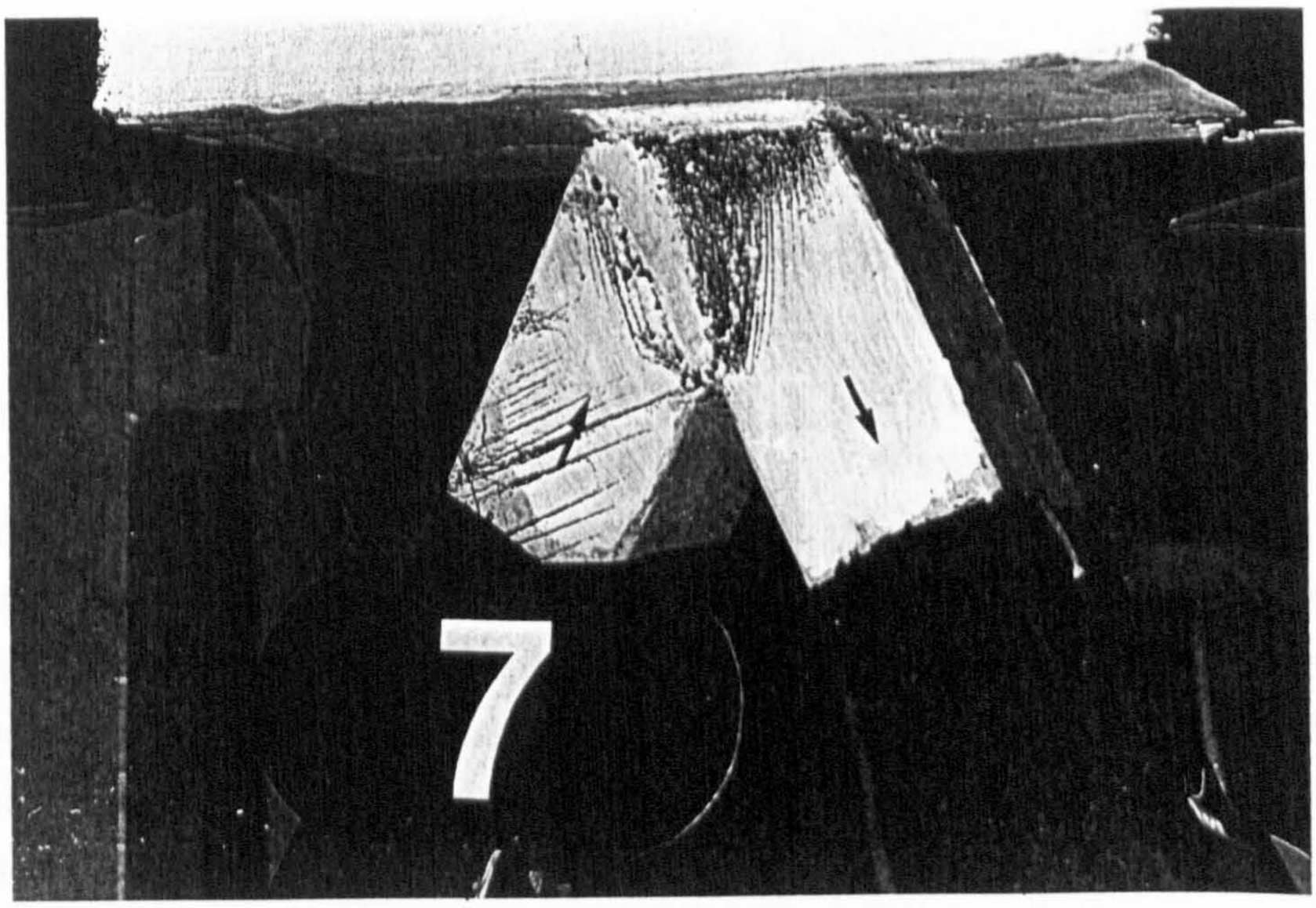

Truss T6 - joint 7 at a ram load of 530 kN.
Ram failure load = 560 kN ; load cycle = 1.
(For description of the joint failure mode see Table D8 in Appendix D)

Plate 5.12 The onset of member yielding in the sidewalls of an 'overlapping' branch member.

CHAPTER 6
STRUCTURAL BEHAVIOUR OF THE TEST TRUSSES

6.1 Introduction

In this chapter the elastic and plastic behaviour of the trusses is discussed, with reference to :

(i) Overall deflection.
(ii) Joint deformation.
(iii) Stress distribution at the joints.
(iv) Distribution of axial forces and bending moments.

The inter-relationship between the structural behaviour and the modes of failure is also considered. In addition, the structural performance of T1 (gap joint truss) and T2 (the corresponding 100% overlap joint truss) is compared with respect to the relative structural efficiency.

For the main part the structural performance has been assessed by studying the graph plots described in section 4.5.1. However, use has also been made of stress distribution diagrams (Appendix E), tabulated member forces (Appendix F) and bending moment diagrams (Appendices G and H).

6.2 Behaviour of gap joint truss, T1

6.2.1 Central Deflection

The midspan deflection over the first load cycle was approximately linear up to a ram load of 60 kN, and was thereafter non-linear (see Fig. 6.1). Thus the limit of the linear range corresponds approximately with the total imposed ram load at which the serviceability limit of span/360 was attained namely, 70 kN. However, in a normal situation a truss would be carrying both dead and imposed loading. For ram loads higher than 60 kN the slope of the load/deflection graph decreases with increasing load. Applying the span/360 criterion to the imposed load only, the proportion of imposed load that can be sustained would therefore dependent on the amount of dead load. The higher the dead load the less would be the permissible imposed load.

6.2.2 Joint deformation

A study of the plots of local joint deformation (see Fig. 6.2) indicates that there

were four basic features:

(i) The deformations on the 4mm chord section were larger than those on the 5mm section for both the tension and compression chord. For example in the case of the compression chord the relationship between chord thickness and joint deformation is indicated by comparing Figs 6.2[a] and 6.2[b]. The influence of chord thickness was less significant in the case of the tension chord.

(ii) The relationship between applied load and local deformation was approximately linear up to an applied load of 60 kN and thereafter became non-linear.

(iii) For the same chord section thickness the deformations on the compression chord were greater than those on the tension chord (compare Figs. 6.2[b] & 6.2[d]).

(iv) The axial force in the compression chord section appeared to affect the local deformation and hence influenced the mode of failure. This confirms the observations of previous investigations on isolated joint tests[43]. For the same chord thickness the deformation was greatest at the joints where the axial force was highest (compare Figs. 6.2[b] & 6.2[c]). In the G7 failure mode at joint 9 instability occurred in all four sides of the chord section. For the tension chord the effect of axial force on the deformation was negligible.

(v) For all the gap joints the deflection of the strut was always greater than that of tie (see Figs. 6.2[a]-[d]).

Gap joints are normally designed on the basis of strength, service behaviour being normally considered acceptable if the local deflection is less than 1% of the chord width (Wardenier[34]). With respect to truss T1, joint 9 was critical and the service limit was reached at an applied ram load of 65 kN (see Fig. 6.2[b]). The serviceability limit imposed for the chord face deformation at joint 9 corresponds approximately to the span/360 service limit for the overall deflection.

6.2.3 Joint stress distribution at the strain gauge positions
(see Appendix E)

The distribution of stresses in the branches and chord members followed a simple pattern (see Fig. 6.3). This pattern was usually the same in the elastic range and at the ram failure load. For the branches the more highly stressed face was always the toe face. This holds for both the strut and the tie. In the case of joint 9 the incidence of chord instability did not affect this distribution. For both the compression and tension chords the stress on the connecting chord face was at most joints less than that on the opposing face. This distribution was directly related to the secondary continuity

moment. Theoretically there should be no bending stresses in a noded gap joint, however the experimental results indicate that the level of secondary stresses was high even in the elastic region.

6.2.4 Chord axial forces and bending moments

The relationship between applied ram load and axial force was linear for all the chord members up to the point of failure (for example see Fig. 6.4[a]). This demonstrates that the distribution of axial forces was not significantly influenced by the overall truss deflection, or the joint deformation. At the failure of joint 9 there did not appear to be a redistribution of axial forces in the chord section (ie., the relationship between ram load and axial force for member 16 was linear up to and including the failure load - see Fig. 6.4[a])

Bending in the chords was predominantly single curvature, with double curvature evident only in the end bays (see Fig. 6.5). The bending moments in all the chord members behaved linearly with respect to applied load up to approximately a ram load of 60 kN (Fig. 6.4[b] is typical), however from this point on the behaviour was non-linear. Non-linearity appeared to be caused by local yielding of the connecting chord face at the joints.

There appeared to be two components to the bending moment distribution in the chord, both of which were secondary since the joints were noded :

(i) The deformation of the chord face at a joint induced an 'eccentric' moment.(ie., once chord face deformation occurred the joint was no longer geometrically noded). The resulting 'eccentric' moment produced a discontinuity in the chord bending moment at each joint (see Fig. 6.5).

(ii) The overall deflection of the truss induced a continuity moment in both the tension and compression chords.

The shear forces were higher in the 4mm thick compression chord section where the joint deformations were largest. However the most significant shear force was along the chord at the loading point, and is related to the large moment. This is typical of such trusses under symmetric loading, which produces zero slope at the loading point. In the tension chord the highest shear forces occurred in the end bays. Otherwise there was little variation in shear along the tension chord.

Thus in the case of the compression chord the magnitude of the shear forces

was related to the chord section thickness and was less in the case of the thicker section. The fact that this correlation does not hold in the case of the tension chord is an indication that the joint deformation had a significant effect on the distribution of chord shear forces.

The distribution and magnitude of moments were approximately symmetrical about the midspan of the truss, and remained so throughout the entire load cycle. Imbalances between corresponding members at, and prior to ultimate load were less than 10%.

6.2.5 Branch member axial forces and bending moments

The variation of axial force (with respect to applied ram load) in all the tie branches, was linear right up to the ultimate load. However, non-linearity occurred in those struts connected to the thinner compression chord where the deformations were greatest (Fig. 6.6[a] is typical). This takes the form of a change in slope at a ram load of approximately 60 kN. Above this load level the slope of the graph increases. This behaviour is related to the onset of non-linearity in the local joint deformation, and not to a loss of stiffness of the strut. The corresponding tie members were not affected (see Fig. 6.6[b]). To maintain equilibrium at these joints between the tie and strut axial forces, the imbalance between the two forces was, necessarily, reacted against by shear in the chord section.

The variation of bending moments with respect to applied ram load in the branches was non-linear. Three types of behaviour were identified:

(i) The bending moment increased with respect to applied load throughout the whole load cycle, and changes in slope were small (Fig. 6.7[a] is typical).

(ii) The relationship between bending and applied load had three components (Fig. 6.7[b] is typical). In the first part of the load cycle (0 to 40 kN ram load) the moment increased with respect to applied load. The moment then remained constant or decreased (40 to 80 kN), and finally the slope changed once more so that further increases in bending took place (80 to 125 kN).

(iii) The bending moment increased for the first part of the load cycle, then remained constant or decreased for the latter part (Fig. 6.7[c] is typical).

Type (i) relates to the end branches, (members 18 & 33) where the joint deformations were small. Type (ii) occurred in the branch members which spanned between the two thinner chord sections (members 19, 20, 21, 30, 31, & 32). There

was no difference in behaviour between the tension and compression branches. Finally, type (iii) occurred in both struts and ties which spanned between the two thicker chord sections (members 23, 24, 27 & 28).

The two members (22 & 29) which spanned between the 4mm compression chord and the 5mm tension chord, exhibited different types of behaviour at either end. Type (i) behaviour occurred at the end which was connected to the thicker section, and type (iii) at the opposite end (Fig. 6.7[d] is typical).

Nevertheless up to the service load (ram load = 70 kN) the relationship between bending moment and applied load was linear for all branches. It appears to be significant that the onset of non-linearity for ram load v. branch member bending moment occurred at the same ram load that the local joint deformations became non-linear. This suggests that the different types of non-linear behaviour that have been identified could be related to local yielding of the connecting chord face at the joints (ie., once local yielding occurred the variation of bending moment was related to the degree of local deformation of the connecting chord face).

The mode of bending was double curvature in all branches except the central struts where single curvature was observed. However, in one of these struts (member 26) double curvature developed prior to truss failure (see Fig. 6.8[a]). In member 28 (see Fig. 6.8[b]) there was a change from double to single curvature.

6.3 Structural behaviour of the 100% overlap joint trusses

6.3.1 Central deflection

The relationship between applied load and central deflection was linear almost up to the point of failure for T2 and linear over at least 80% of the load cycle for the remaining trusses (see Fig. 6.9). The failure mechanism in T2 differed from the remaining trusses in that only chord yielding was observed prior to failure. With the exception of T2/2, yielding of the chord and branches usually occurred simultaneously in the remaining overlap joint trusses. T2/2 was the only truss where chord local yielding did not occur, however an extended non-linear region was observed in the load/deflection relationship (see Fig. 6.9[b]).

6.3.2 Joint deformation

(for definition see Fig. 4.13[b])

The deformation of the chord face (see Fig. 4.14[b]) never exceeded 1% of the chord width prior to the onset of member yielding in the branch members (see Fig. 6.10). The sense of the deformation was always inwards (ie., positive - see Fig. 4.14) and not related to the direction of the resultant force perpendicular to the connecting chord face. This resultant force at a joint was caused by the difference in adjacent strut and tie forces.

The joint deformation was always positive because under the applied load the centre-lines of the tension and compression chords move closer together. Even in the case of the gap joint truss T1 the chord face deformation under the strut was greater than that under the corresponding tie (see Fig. 6.2). This indicates that the depth between the centre-lines of the tension and compression chords was reduced under the action of the applied load.

Once member yielding of the branches occurred the relationship between joint deformation and applied load tended to become non-linear (see also section 4.6.2). Nevertheless at ultimate load the deformation of the connecting chord face never exceeded 3% of the chord width in any of the trusses.

For the corner joints the local deformation was only measured in T5 and once more non-linearity was associated with member yielding of the tie. In this type of joint the deformations were negligible and always directed away from the chord face.

6.3.3 Stress distribution at the strain gauge positions

(see Appendix E)

The stress distribution in the branch members appears to be related to the sense of overlapping (ie., whether the strut overlapped the tie and vice-versa). Of particular significance is the fact that there was no weld along the toe face of the overlapped member (see Fig. 3.3).

For the tie overlapping the strut there were three possibilities with respect to the transfer of force to the chord via unwelded toe face of the strut :

(i) The toe was proud of the chord face and there was no force transfer between the toe and the chord face.

(ii) The toe was perfectly settled and able to transfer forces by means of bearing to the chord face.

(iii) The toe was partially settled on the chord face allowing some force to be transferred via the interface.

Type (i) would have relieved the stress on the toe face, thus causing it to be less than that on the heel face. Conversely, type (ii) would have attracted stress to the toe face and is probably associated with those stress distributions where the toe face of the overlapped strut was more stressed than the heel face - this was the most common stress distribution for both 45° and 60° Warren joints at the ram failure load (see Fig. 6.11[a]). The stress distribution for the overlapping tie member did not appear to be related to that of the strut, and the more highly stressed face was usually the one connected to the chord (ie., the heel face).

In those joints where the strut overlapped the tie the stress on the toe face of the tie was, for the majority of joints, higher than on the heel face (see Fig. 6.11[b]). This suggests that there was little or no bond to the chord along the toe face, thus relieving the stress. For the overlapping strut, as in the case of the overlapping tie, the stress was for the majority of joints greater on the heel face which was connected to chord.

For the 100% overlap Warren joints it is possible that weld did penetrate beneath the heel of the overlapping member and further aided the transfer of force via the toe of the overlapped branch and the chord.

In the N-type truss the general distribution of stresses differed from that of both the 45° and 60° Warren joints. For the joints where the strut was connected to the chord face, the heel faces of both the strut and the tie developed the highest stresses (see Fig. 6.11[c]). Where the overlapping was reversed the stresses on opposing faces of the tie member were approximately equal, but the overlapping strut was always more highly stressed on the toe face (see Fig. 6.11[d]). As in the case of the Warren joints no weld was specified along the toe of the overlapped branch. However a visual inspection of the N-truss indicated, for all joints, that the weld had penetrated beneath the heel of the overlapping member, thus forming a connection between the toe of the overlapped branch and the chord face. In the case of the Warren joint trusses this was not observed visually, although it is possible that it did occur in some joints.

The magnitude and sense of the bending moments in the branch members was influenced by the rotational stiffness of the joints. The absence of a weld between the

toe of the overlapped branch and the chord face appeared to reduce the rotational stiffness of the joint if no force could be transferred across the interface. For this reason the rotational stiffness of the joints at which the strut overlapped the tie was less than at those joints where the sense of overlapping was reversed. Transfer of force between the toe of an overlapped compression branch and the chord is possible via bearing, although the efficiency of the transfer would be determined by how settled the toe is on the chord after fabrication. Therefore, the rotational stiffness of the 100% joints in the test trusses (both strut/tie and tie/strut) varied according to how efficiently the overlapped branch member transferred forces into the chord via the toe face.

6.3.4 Distribution of axial forces

The relationship between applied load and axial force was linear up to the point where member yielding occurred. This is true for both branch and chord members (for example see Fig. 6.12[a] & [b]), but not the end posts (for example see Fig. 6.12[c]). In those corner joints on the top chord where there was no branch connection (trusses T3, T4, and T6) the axial force in the end post was equivalent to the shear force in the adjoining compression chord member. Local yielding of the compression chord at the midspan joint caused moment redistribution along the chord, which reduced the shear force in the end bays. For the end posts, therefore non-linearity in the relationship between applied ram load and axial force coincided with local yielding of the compression chord at midspan. At the load level where chord local yielding began the posts attained a maximum axial force, and further increases in load caused a reduction in axial force.

Although, for each truss, the elastic axial force distribution was symmetrical about the centre-line (for example see Table 6.1), the forces in the branches were not constant. For the test trusses the shear force in a member was equivalent to the slope of the bending moment distribution along the length of the member. In the 100% overlap joint trusses the slope of the bending moment diagram for both the tension and compression chords varied (Fig. 6.13is typical). Therefore the shear force in the chord was different for each member. Consequently there was a resultant force at a joint caused by the difference in the chord shear forces either side of the joint. In order to maintain equilibrium of the in-plane forces perpendicular to the chord, the resolved components of the axial forces in the branch members were caused to differ in magnitude. This difference was equivalent to the shear force in the chord at the joint. The largest differences between the axial forces of the tie and strut at a joint occurred where the change in the chord shear force across a joint was greatest, namely where the

change in slope of the chord bending moment diagram was most pronounced. For the compression chord joints this was either side of the midspan, and for the tension chord in the joints adjacent to the end posts (Fig. 6.I3is typical).

The imbalance at the joints between the measured axial forces in the strut and tie was observed in all 100% qverlap joint trusses, and to a lesser degree in the gap joint truss (see Table 6.1). The difference in the measured axial forces was observed both in the elastic and plastic region. The difference was in some cases as much as 25%. The strut force normally exceeded the tie force at a joint, however there were also joints where the tie force was greater than the strut.

The shear forces in the branch members were negligible compared to the axial forces in the chord (of the order of 1%), and thus although there was interaction between the two it was insignificant.

6.3.5 Elastic bending moment distribution

Over the range where the relationship between applied load and bending was linear, bending in the chord was usually double curvature, with a point of inflection occurring between two adjacent joints (for example see Fig. 6.13). However for both the tension and compression chords there was a continuity component to the distribution, and therefore the point of inflection was never at the midspan of the member. The continuity moment was a secondary effect caused by the overall deflected shape of the truss. The distributions were symmetrical about the centre-line.

The discontinuity in the experimental bending moment distribution at the position of the applied ram load (Fig. 6.13 is typical) was probably caused by the imbalance of axial force in the branch members connected to the central joint. The large central moment associated with the loading position occurred in all the 100% overlap joint trusses. It is associated as in the case of the gap joint truss with symmetry and zero slope at the centre-line.

6.3.6 Moment redistribution

Non-linearity in the relationship between applied load and bending moment for the chord members indicates a redistribution of moments away from the sections where yielding occurred. This is demonstrated in Fig. 6.14 where the experimental distribution of bending at ultimate load in truss T6 is plotted against that extrapolated

from the elastic range. The behaviour in the remaining trusses was similar (see Appendix H).

The difference between the two distributions indicates the amount of redistribution which took place prior to the attainment of ultimate load. In each truss yielding occurred at one or more points in the chord sections. The most critical position was at the midspan of the compression chord where the load was applied. Yielding at this location was the primary factor influencing the redistribution of bending moments.

Chord section yielding defined an upper limit to the bending capacity of the section. Once yielding had occurred the bending moment at that section either remained constant at further increases in load (ie., end 1 of the member in Fig. 6.15[a] is typical) or decreased (ie., end 2 of the member shown Fig. 6.15[b] is typical). To maintain equilibrium the moment that was shed was distributed along the chord. The loss in stiffness associated with the yielding of the compression chord was reflected in the response of the tension chord. Along the tension chord there was an increase in the continuity component of the moment distribution. The redistribution of moments also caused a change from double to single curvature bending in some members. This however, did not occur in all trusses.

6.3.7 Interaction between chord and branches

Apart from the case of T2 where only chord failure was observed, all the other 100% overlap joint trusses were subject to the simultaneous occurrence of chord and branch member yielding. Since member yielding of a branch affected the axial force in that member it also influenced the distribution of bending in the chord. Loss of branch force at constant applied load led to an increase in chord shear force at that joint.

6.3.8 Bending moment distribution in the branches

For all trusses the relationship between bending moment and applied load in the branch members was non-linear (Fig. 6.16 is typical). Furthermore the distribution was not symmetric with respect to the truss centre-line (see Fig. 6.13). On the side where the tie overlapped the strut the moments were larger than those of the corresponding members on the opposite side. The joints where the strut overlapped the tie had a lower rotational stiffness than the joints where the sense of overlapping was reversed - this is described in detail in section 6.3.3. Even considering just one side of a truss there was variation in the magnitude and sense of the branch bending moments. This is possibly

an indication of how sensitive the rotational stiffness of the joints was to the weld detailing.

When a branch member began to yield there was a corresponding decrease in the bending moment which it was able to sustain (see Fig. 6.16[a]). There are also branch members where the moment was shed completely at either one or both ends (for example see Fig. 6.16). This moment was redistributed into the chord section and not the adjacent branch. However, due to the relative stiffness, moments in the branches were negligible in magnitude compared to those of the chord. Therefore the effect of this redistribution was negligible.

In the elastic range bending in the branches was normally double curvature, however changes in curvature over the load cycle did occur (for example see Fig. 6.17). The most common change was from double to single curvature. Complete reversal of curvature was only identified in the cases where the branch member was connected to the chord face (ie., the overlapped member).

6.4 Comparison of structural performance for trusses T1 and T2

6.4.1 Central deflection

The measured deflections of the trusses at the centre of the tension chord are shown in Figs 6.1[a] and 6.1[b]. By comparing the deformation behaviour of T1 and T2 it is apparent that the latter represents the stiffer system. At the failure load of T1, the deflection of truss T2 (which was still unfailed) was only 50% of the deformation of the former.

6.4.2 Joint deformations

The local joint deformation for joint 9 in trusses T1 and T2 is compared in Fig. 6.18 which is typical. For T1 the local joint deformations became non-linear at an applied ram load of approximately 60 kN. In the case of T2 the local joint deformations were linear up to a ram load of 140 kN. Unlike T1, the joint deformations on the tension and compression chords were approximately the same. Furthermore, the magnitude of the joint deformations are largely independent of the chord thickness and chord axial force. A comparison between the two trusses indicates that the joint deformations in T1 were ten times greater than those of T2. While the maximum joint deflection in T2 was less than 0.7 mm, that of T1 was greater than 7.0 mm

6.4.3 Axial forces and bending moments

For each truss a comparison of the graphs of applied load v. measured member axial force indicates that the relationship was linear in both cases. Non-linearity was only observed in the critical elements with the onset of yielding. A study of the forces in corresponding members for the two trusses indicates that the axial forces were approximately equivalent (see Table 6.1).

From a comparison of the bending moment distribution with respect to applied load two points emerge:

(i) The moments in the chord and post members were linear for T2 prior to the onset of the chord yielding. However, the chord moments in T1 were non-linear over the whole load cycle.

(ii) For the branch members non-linearity in the bending moments was observed in both T1 and T2, but was more pronounced in T1.

At the 50 kN ram load the bending moments in the chord members were generally greater in the case of T2, (see Fig. 6.19). However at 100 kN, the moments in T1 exceeded those in T2 at several joints, (see Fig. 6.20). At this load therefore the secondary moments in truss T1 exceeded the primary moments generated by the joint eccentricity of T2. This indicates that in the design of the chord members of gap joint trusses with slender chord sections and small β ratios the secondary bending moments in the chord should not be ignored. The bending moments in the branch members at both load levels were significantly larger in T1. The moments were in most branch members at least three times larger in T1 at the higher load level.

6.4.4 Ultimate load carrying capacity

Truss T1 attained its maximum load carrying capacity at an applied ram load of 125 kN, when joint 9 failed by mode G7 - chord face plastification with sidewall buckling. The ultimate strength of truss T2 was reached at a ram load of 168 kN, indicating a 35% increase in strength over T1. Failure in T2 was due to in-plane single curvature buckling of member 15 between joints 8 and 9. This was ascribed to the combined axial and bending stresses induced by the joint eccentricity. Thus T1 was joint critical while T2 was member critical.

6.4.5 Structure serviceability limits

Assuming an upper limit on chord face deformation of 1% of the chord width, the service load of T1 corresponds to a ram load of 70 kN (joint 9 was critical). For T2 no joint reached the limit, and even at failure the maximum joint deformation was only 0.7% of the chord width.

Assuming a serviceability limit of 1/360 of the span for imposed loading, the central deflection is set at 31 mm. For T1 this limit was attained at a total applied load of 70 kN, and for T2 at 90 kN. The acceptable service load was 29% greater in T2 - on the basis of overall deflection limits. On removal of the load truss T1 only recovered 57% of the maximum deflection, and there was a 37mm permanent set. In the case of T2 the recovery was 85% and the permanent set was only 10mm.

6.4.6 Effect of chord face deformation

Since in all other respects T1 and T2 were identical, the joint geometry and force transfer mechanism at the joints are the factors responsible for the difference in the structural behaviour of the two trusses. Essentially the joint geometry dictates the mechanism by which the forces are transferred between the respective members. In the case of a gap joint the forces in the branch members must interact via the chord face. However in the case of a 100% overlap joint the forces perpendicular to the chord face are transferred directly from one branch to the other, leaving only a horizontal shear force to be transmitted to the chord. This explains why the deformation of the connecting chord face was negligible in the case of the 100% overlap test joints.

6.4.7 Relative strength

Truss T2 proved to have a superior load carrying capacity as well as being a stiffer structure. In T1 the joint flexibility coupled with the force transfer mechanism, combined to produce large local joint deformations. The chord face deformation at a joint allowed large translations and rotations, thus producing a flexible joint which, necessarily, affected the overall truss deflection and led to the development of significant secondary bending moments in the structure. The joint deformation thus appeared to have a detrimental effect on the structural efficiency. For the gap joints on the compression chord the deformation of the chord face caused a loss in strength of the chord - by increasing the tendency to buckle locally.

In trusses composed of gap joints with low β ratios and high b_0/t_0 values the bending moments induced by joint deformations are likely to be significant and should not be ignored in design. The 100% overlap joint truss thus represents the more efficient structural system, in spite of the joint eccentricity.

The gap in T1 was large (43mm), and the chord slender. In gap joint trusses with smaller gaps and less slender chords the local joint deformations and the resulting secondary bending moments are likely to be less. However, irrespective of the chord slenderness, or size of gap it is 'unlikely' that, for small β ratios (< 0.6), a gap joint truss will be more efficient in strength and serviceability than an equivalent 100% overlap joint truss. This however needs to be verified experimentally.

Table 6.1 Elastic axial force co-efficients for trusses T1 and T2.

Member type	Member No	Axial force co-efficients truss T1 kN	truss T2 kN
Tension chord	1	-0.02	0.02
Tension chord	2	0.96	0.95
Tension chord	3	1.91	1.92
Tension chord	4	2.98	2.86
Tension chord	5	3.93	3.80
Tension chord	6	2.86	2.88
Tension chord	7	1.93	1.92
Tension chord	8	0.93	0.96
Tension chord	9	-0.03	0.03
Comp. chord	10	-0.48	-0.47
Comp. chord	11	-1.43	-1.43
Comp. chord	12	-2.36	-2.36
Comp. chord	13	-3.21	-3.26
Comp. chord	14	-3.27	-3.22
Comp. chord	15	-2.36	-2.40
Comp. chord	16	-1.44	-1.44
Comp. chord	17	-0.48	-0.47
Tie	18	0.64	0.61
Strut	19	-0.67	-0.64
Tie	20	0.69	0.64
Strut	21	-0.69	-0.64
Tie	22	0.68	0.65
Strut	23	-0.70	-0.63
Tie	24	0.64	0.60
Strut	25	-0.69	-0.68
Strut	26	-0.69	-0.71
Tie	27	0.65	0.60
Strut	28	-0.71	-0.63
Tie	29	0.69	0.63
Strut	30	-0.68	-0.66
Tie	31	0.68	0.64
Strut	32	-0.72	-0.67
Tie	33	0.64	0.61
Vertical post	34	-0.51	-0.52
Vertical post	35	-0.51	-0.51

Notes :
1) To be read in conjunction with Fig S1.
2) Co-efficients for each truss have been derived at a ram load of 50 kN.
3) Values are in kN per 1 kN of applied ram load.

a)

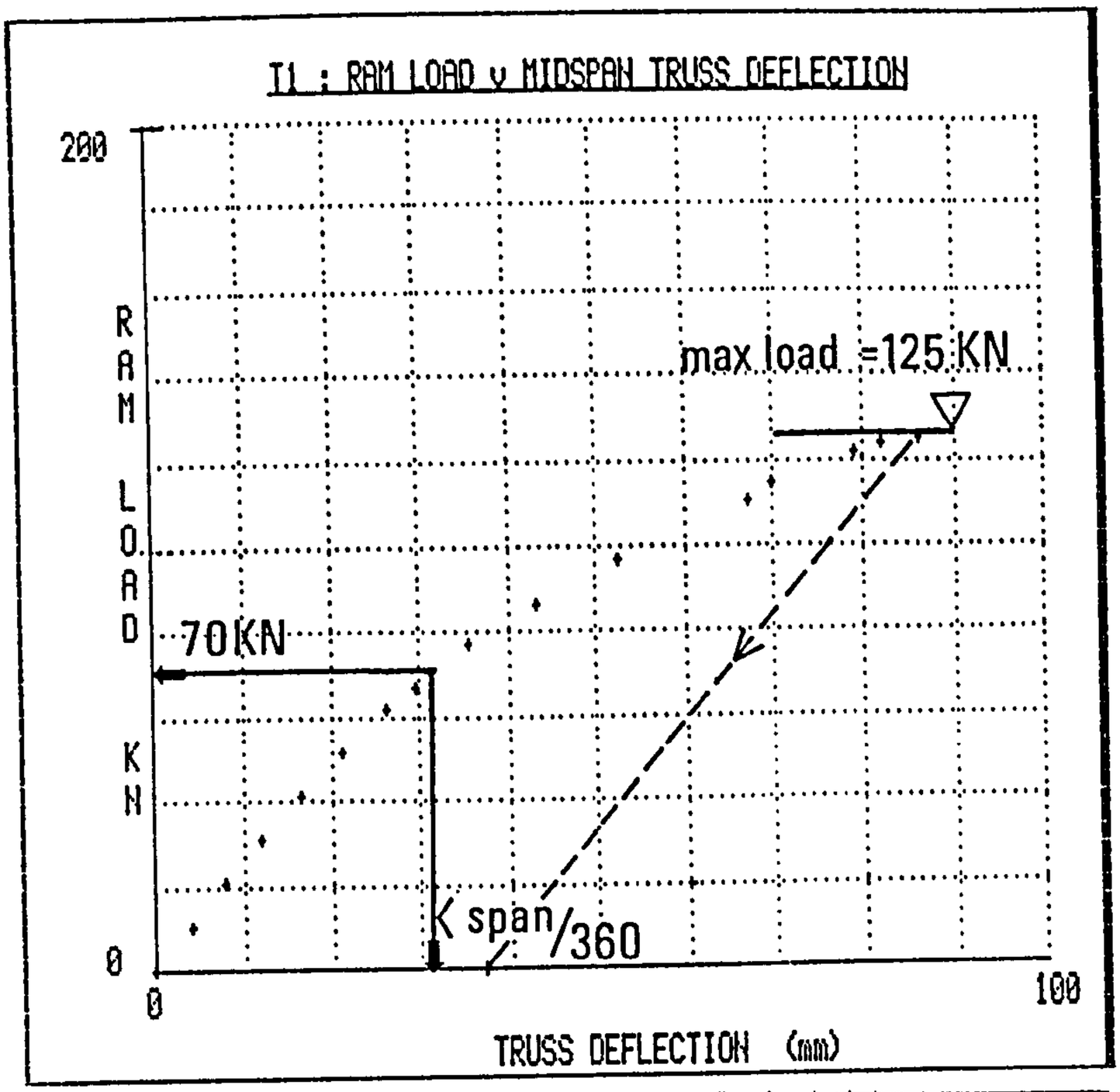

b)

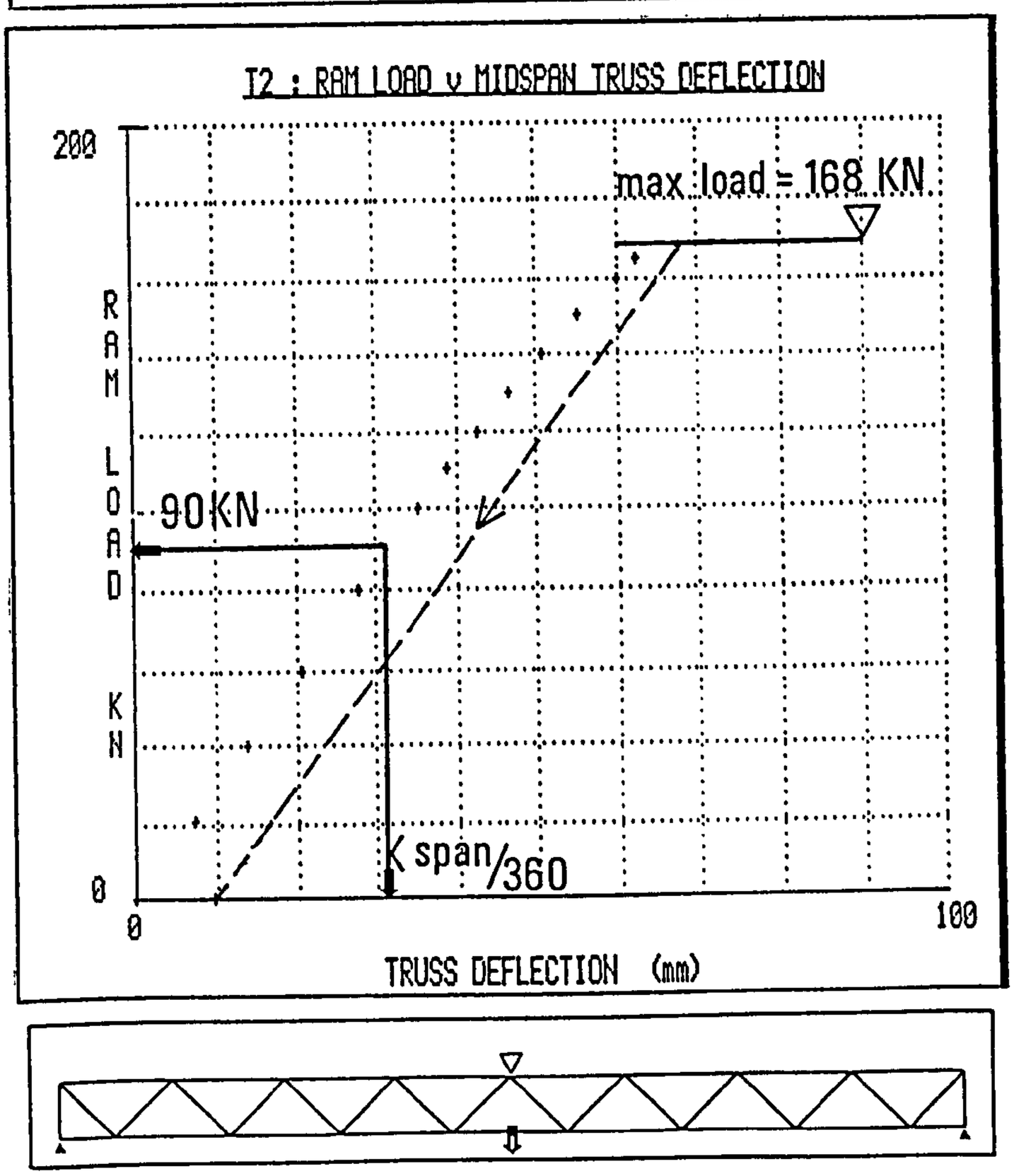

Fig 6.1 Ram load v. midspan truss deflection for trusses T1 and T2.

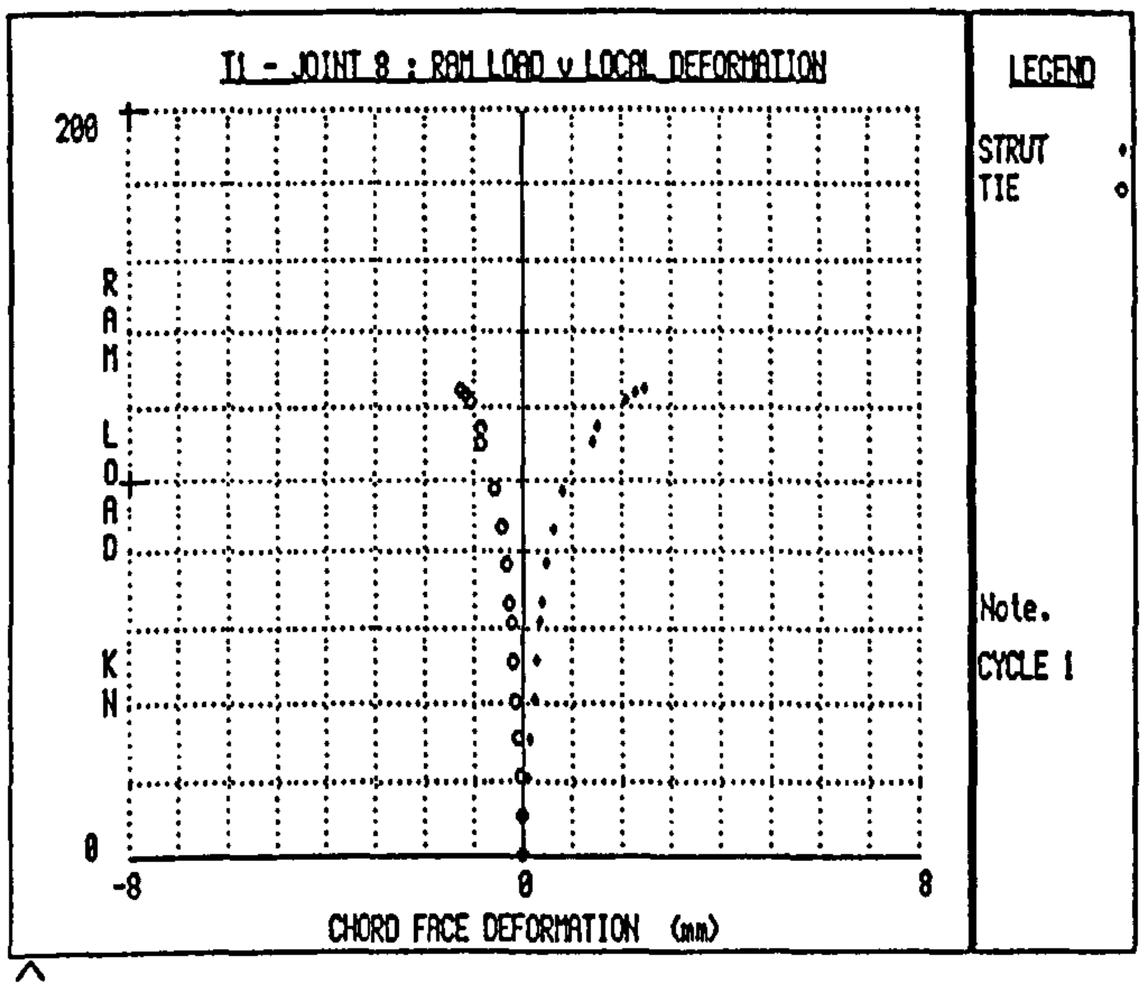

a Comp. chord (t_o = 5 mm)

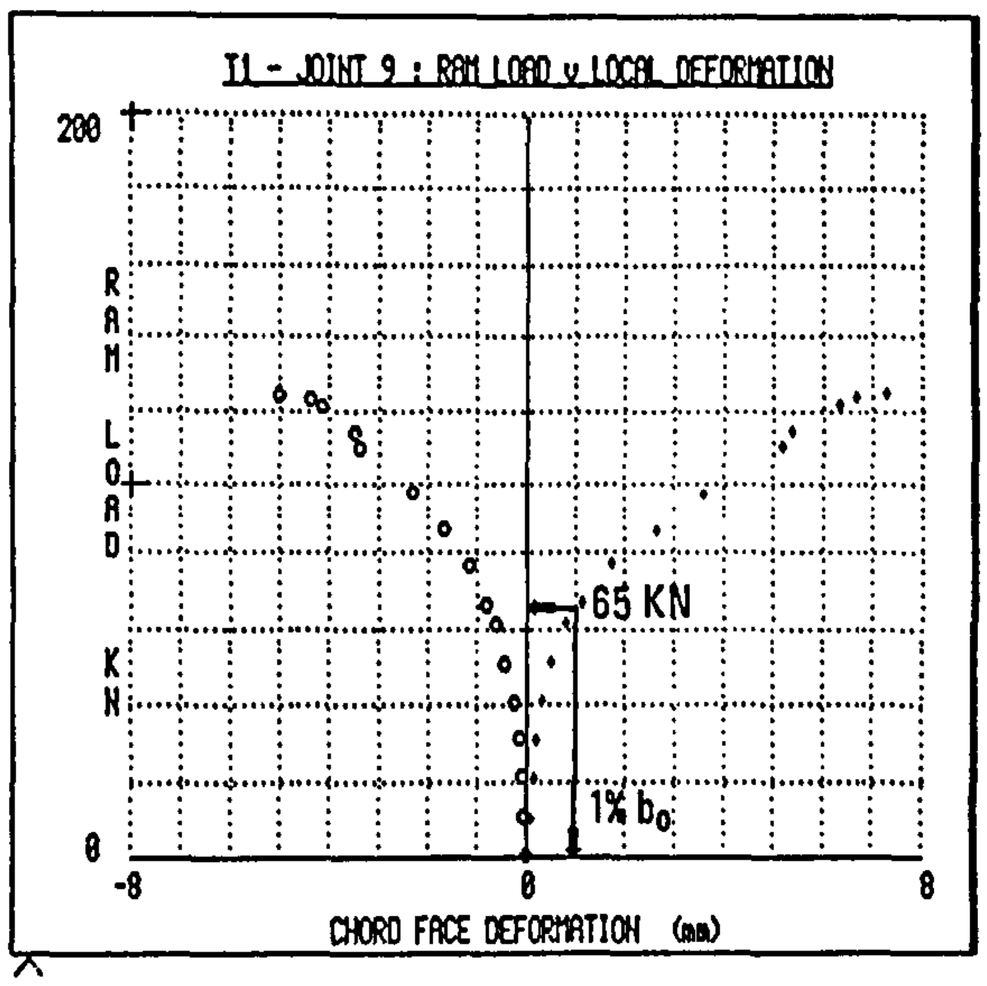

b Comp. chord (t_o = 4 mm)

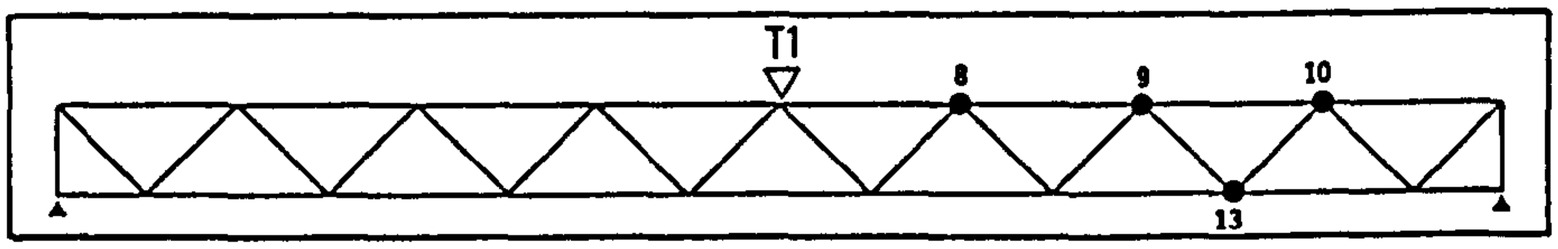

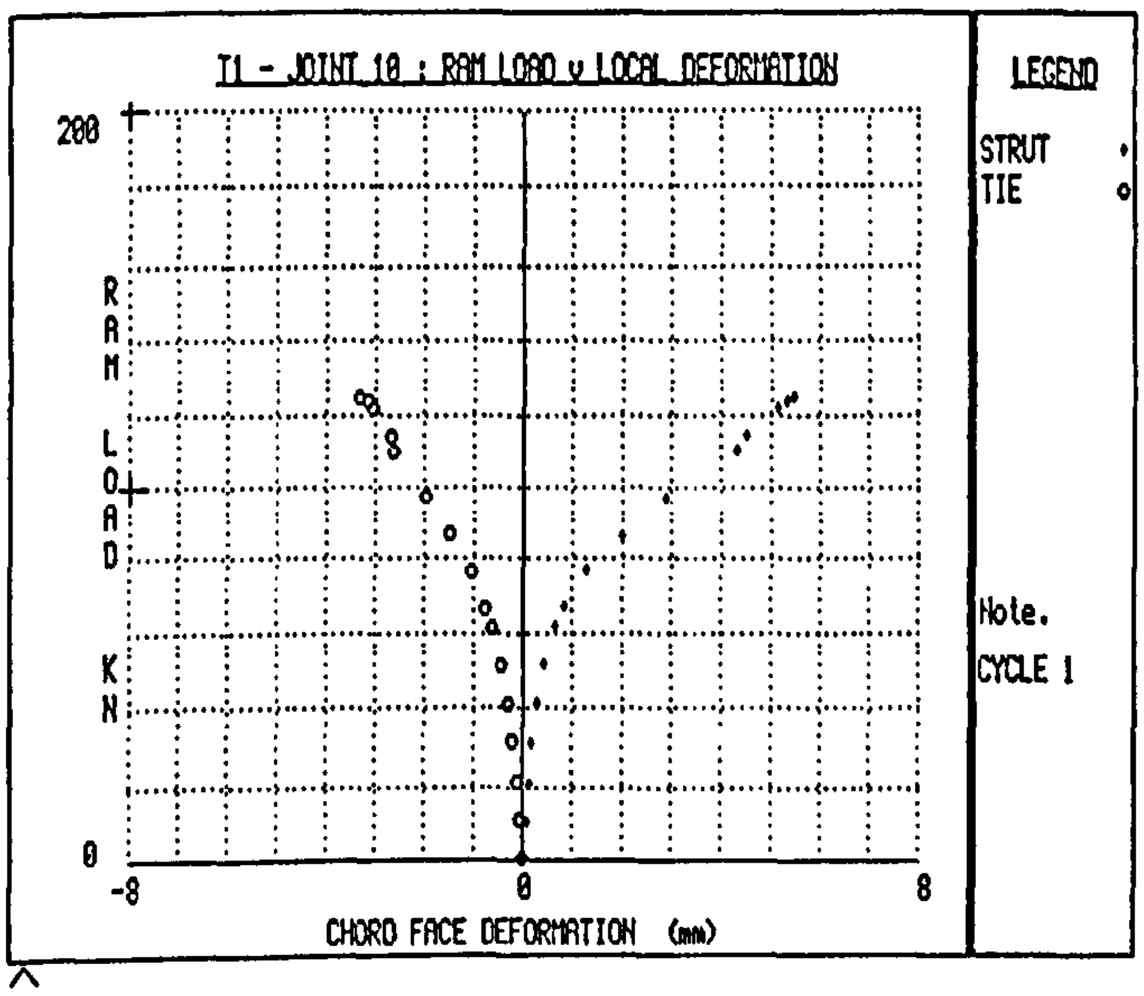

c Comp. chord (t_o = 4 mm)

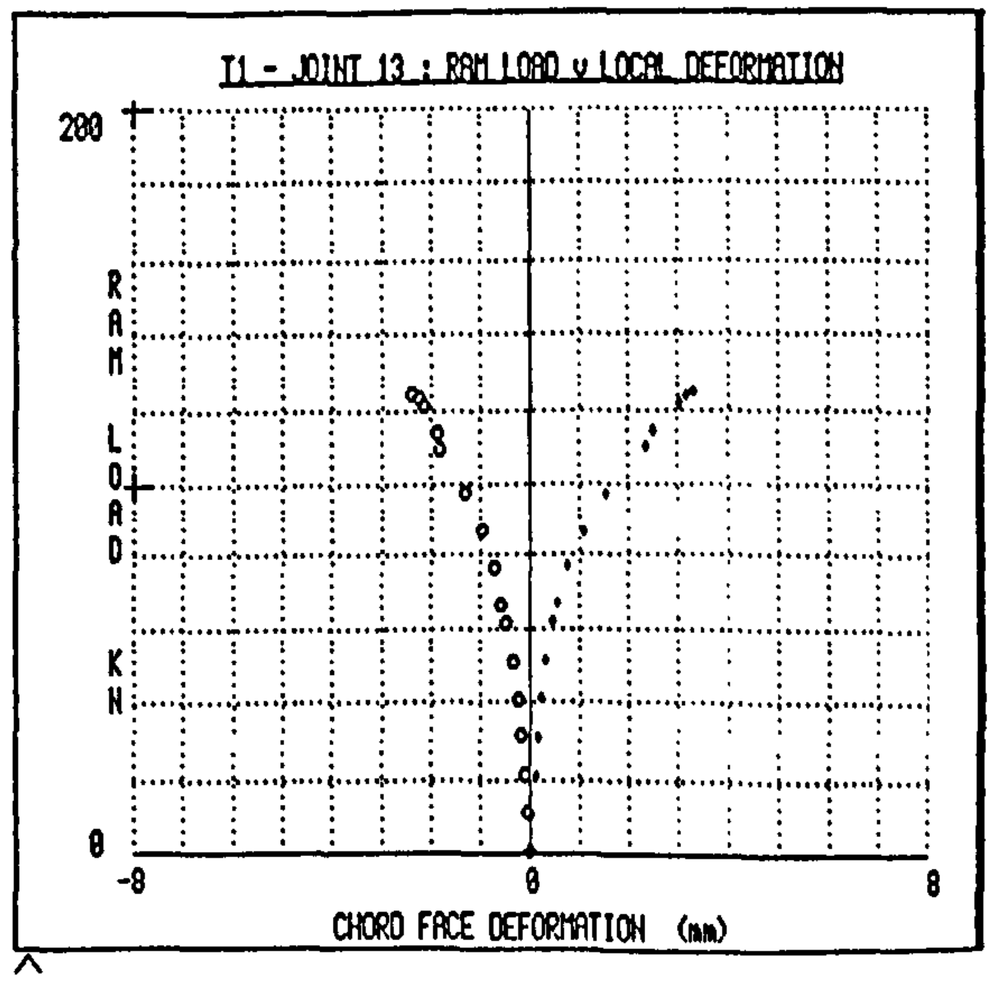

d Tens. chord (t_o = 4 mm)

Fig 6.2 Typical examples of ram load v. local joint deformation perpendicular to the chord face for truss T1.

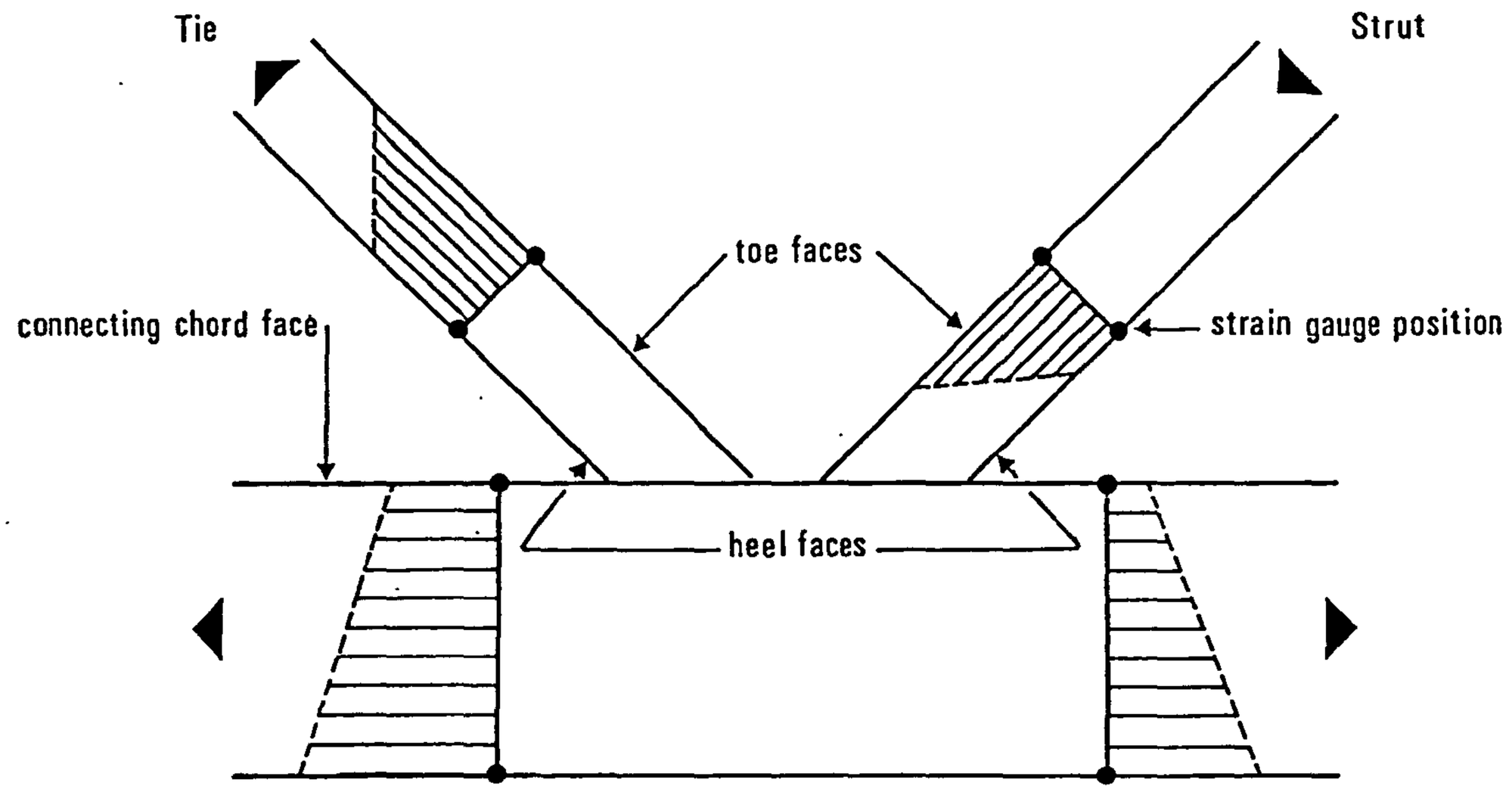

Fig 6.3 Typical example of the stress distribution, at the ram failure load, in the gap joints of truss T1. (see also Appendix E)

a)

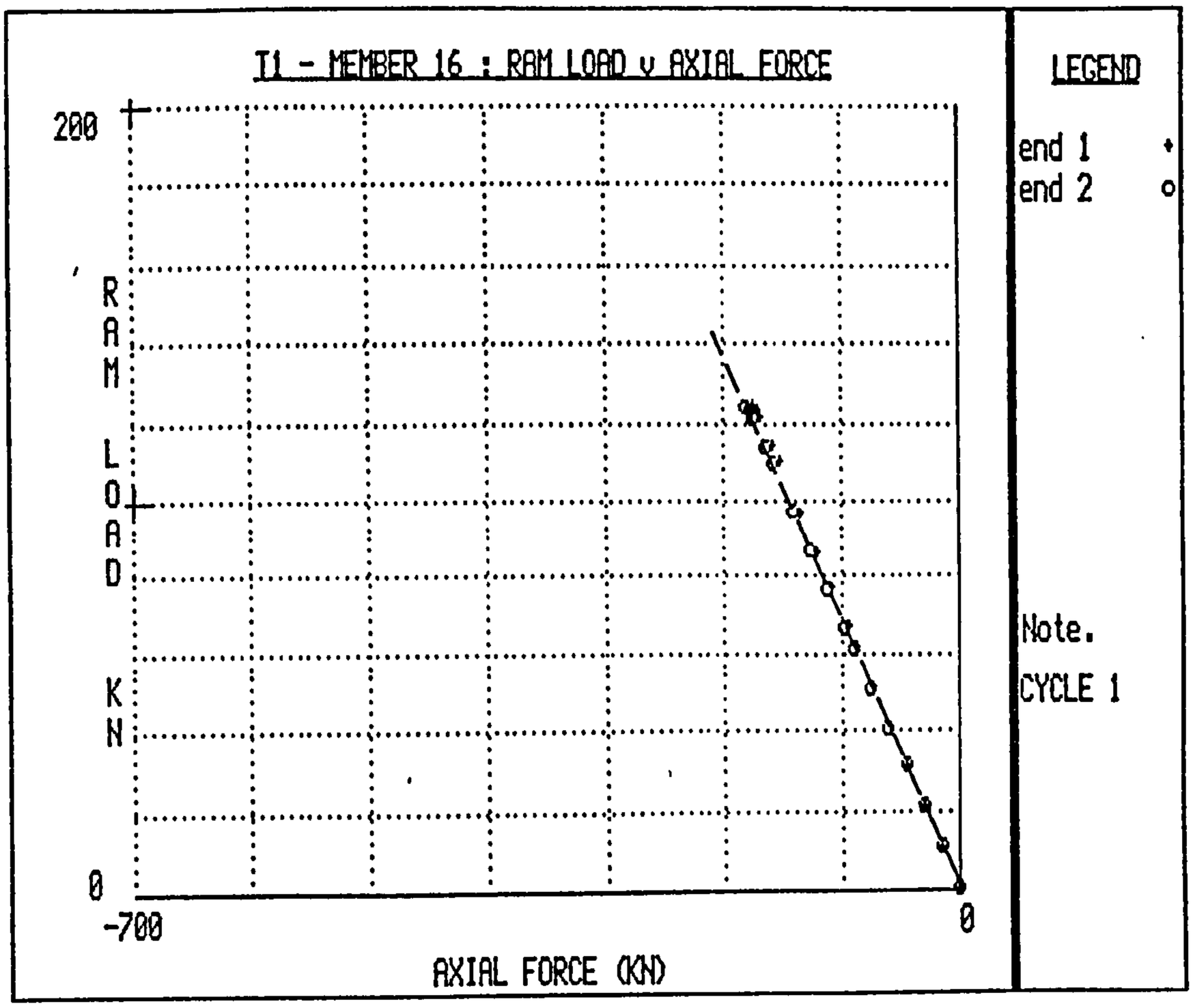

b)

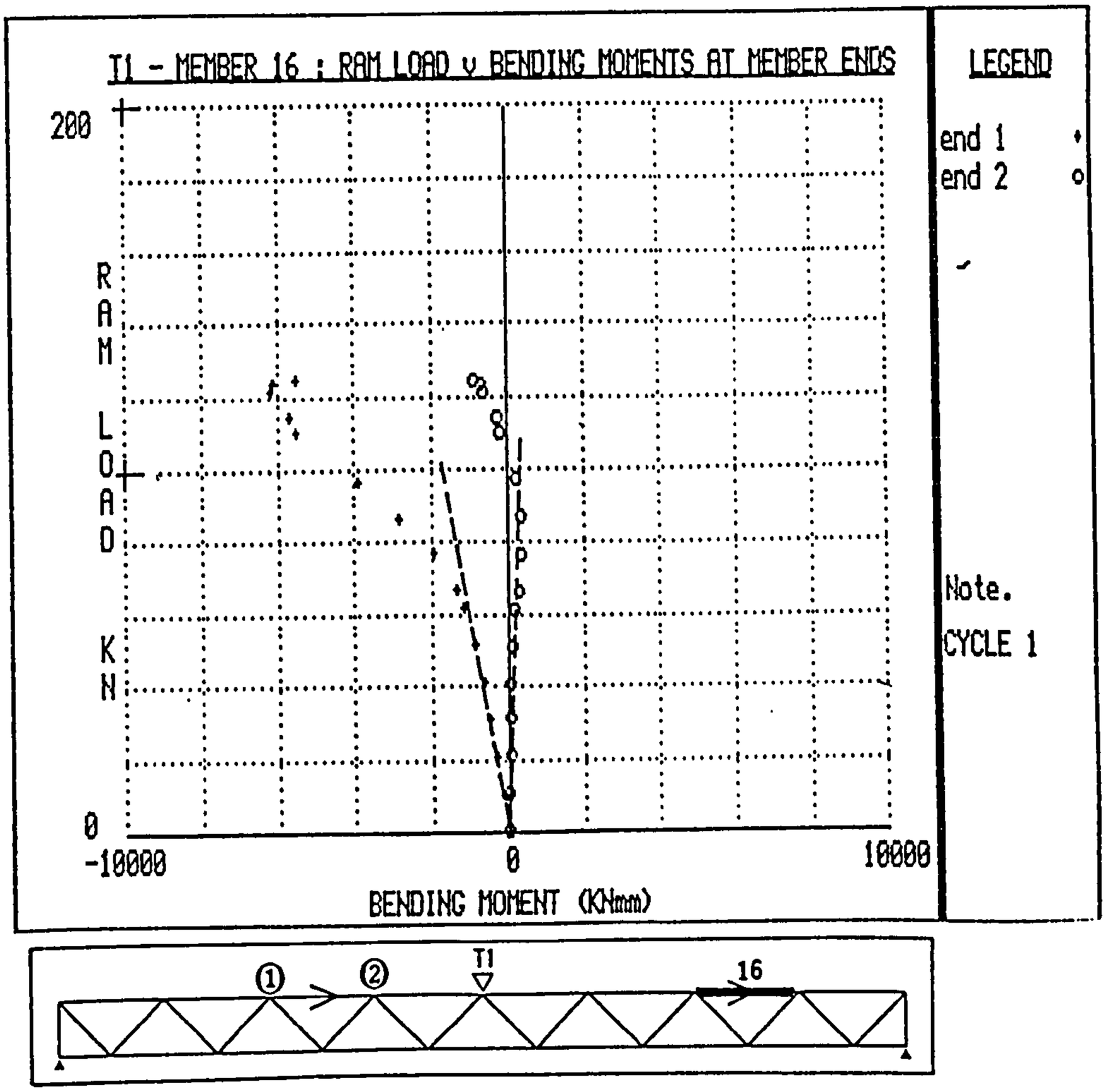

Fig 6.4 Examples of ram load v. (a) axial force, and (b) bending moment in a chord member, for truss T1.

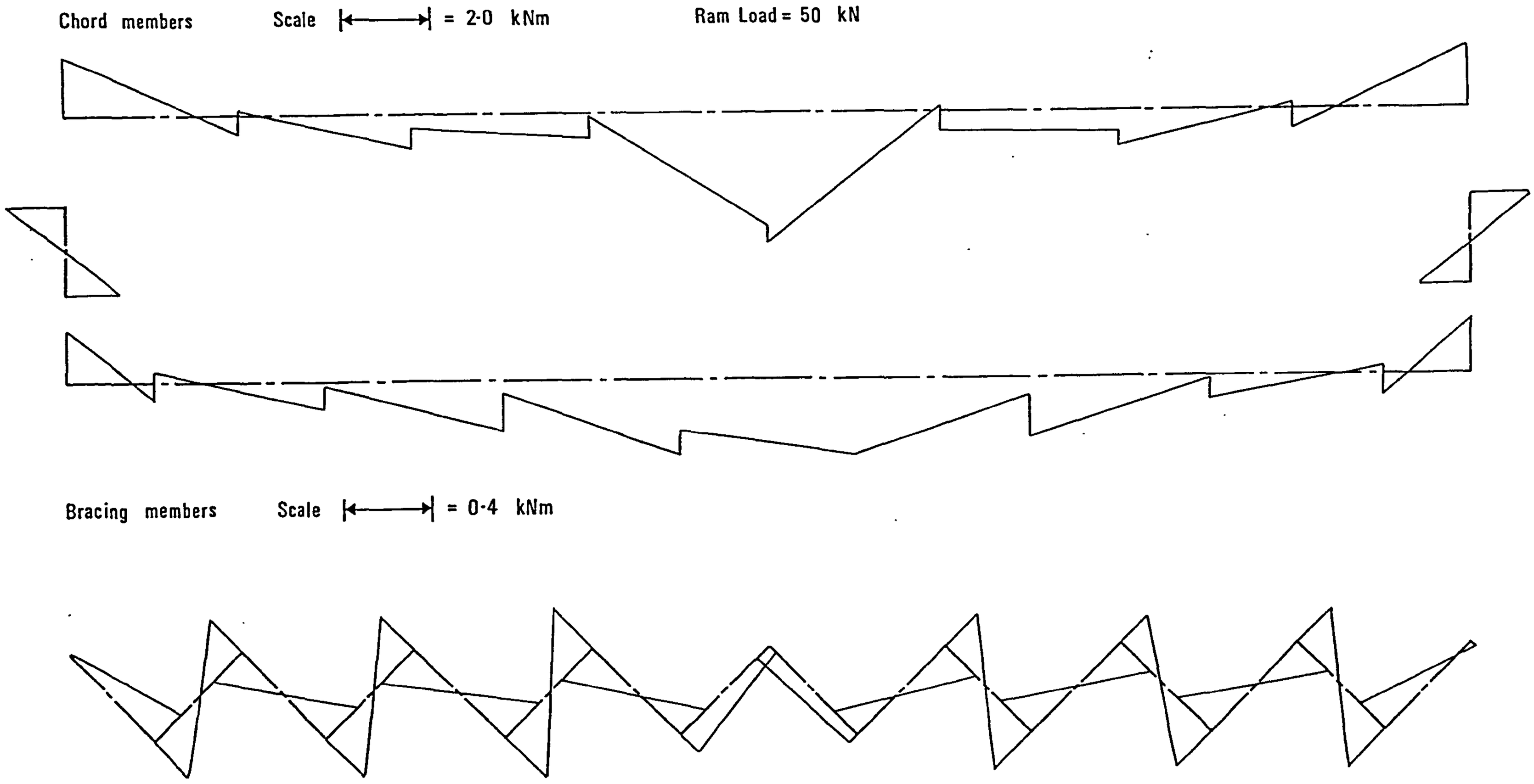

Fig 6.5 Experimental elastic bending moment distribution for truss T1.
(the bending moment diagram has been plotted on the side of the member where the stress induced by the bending moment is tensile)

a)

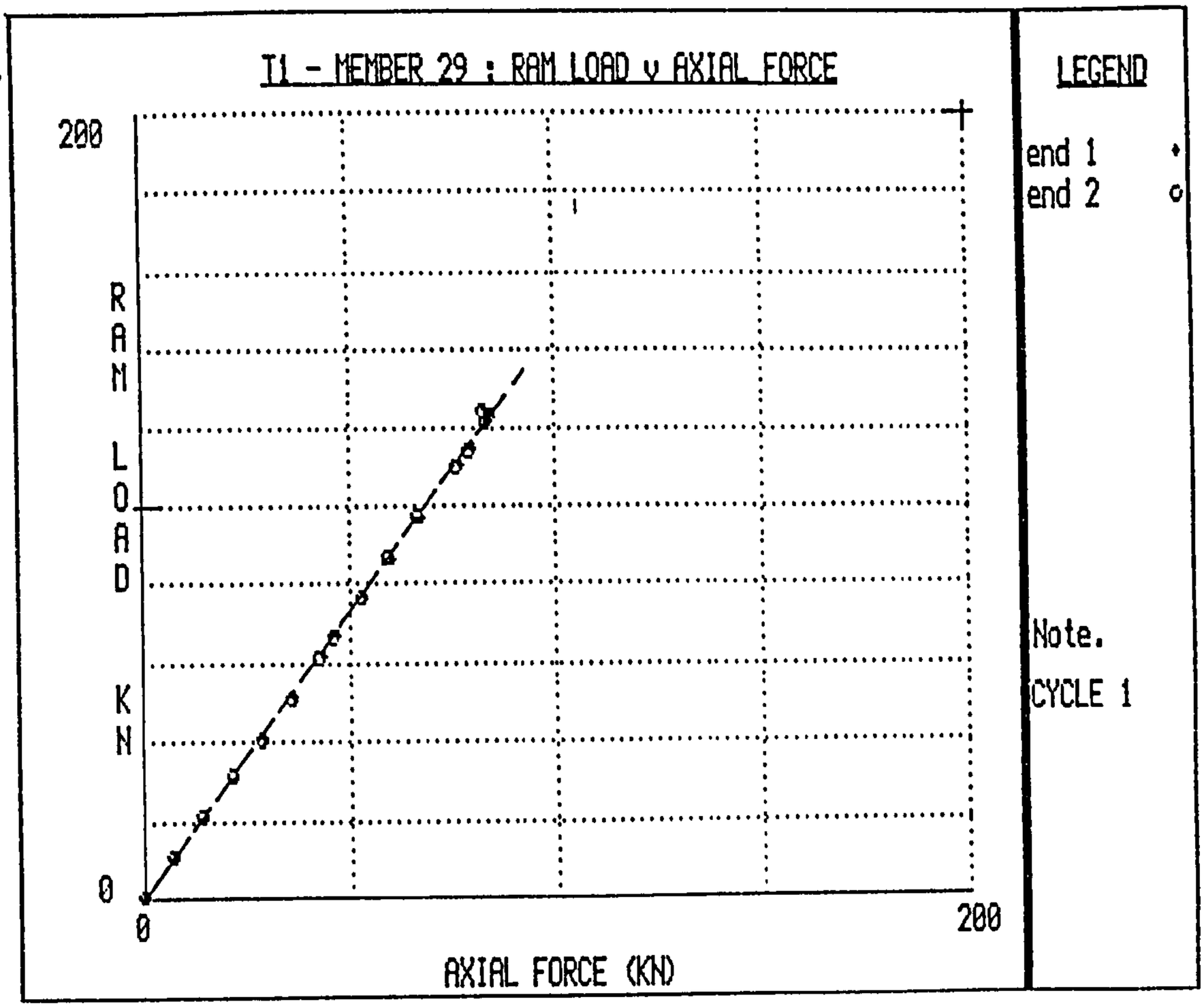

b)

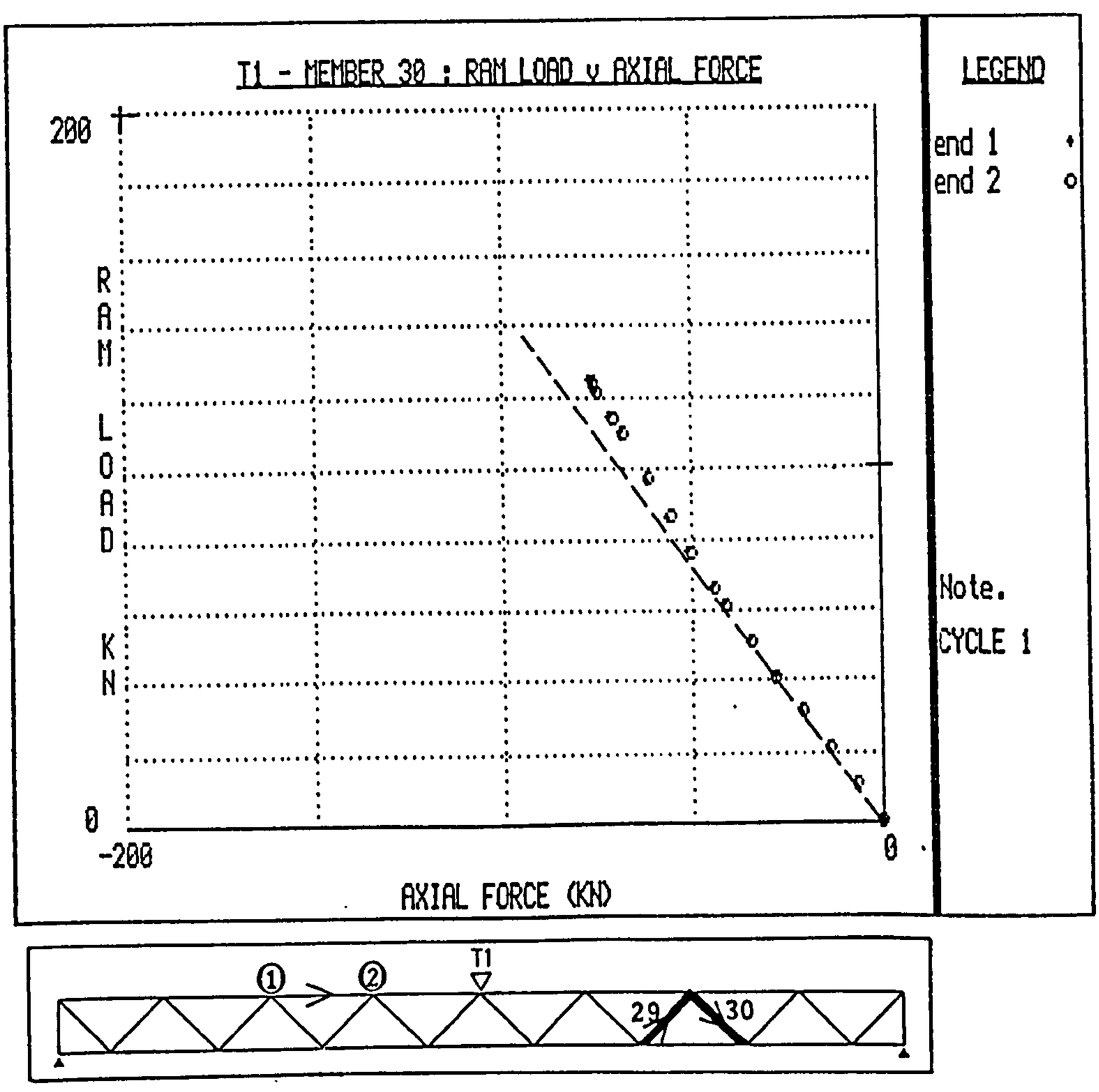

Fig 6.6 Typical example of ram load v. axial force for (a) a tension branch, and (b) a compression.branch, in truss T1.

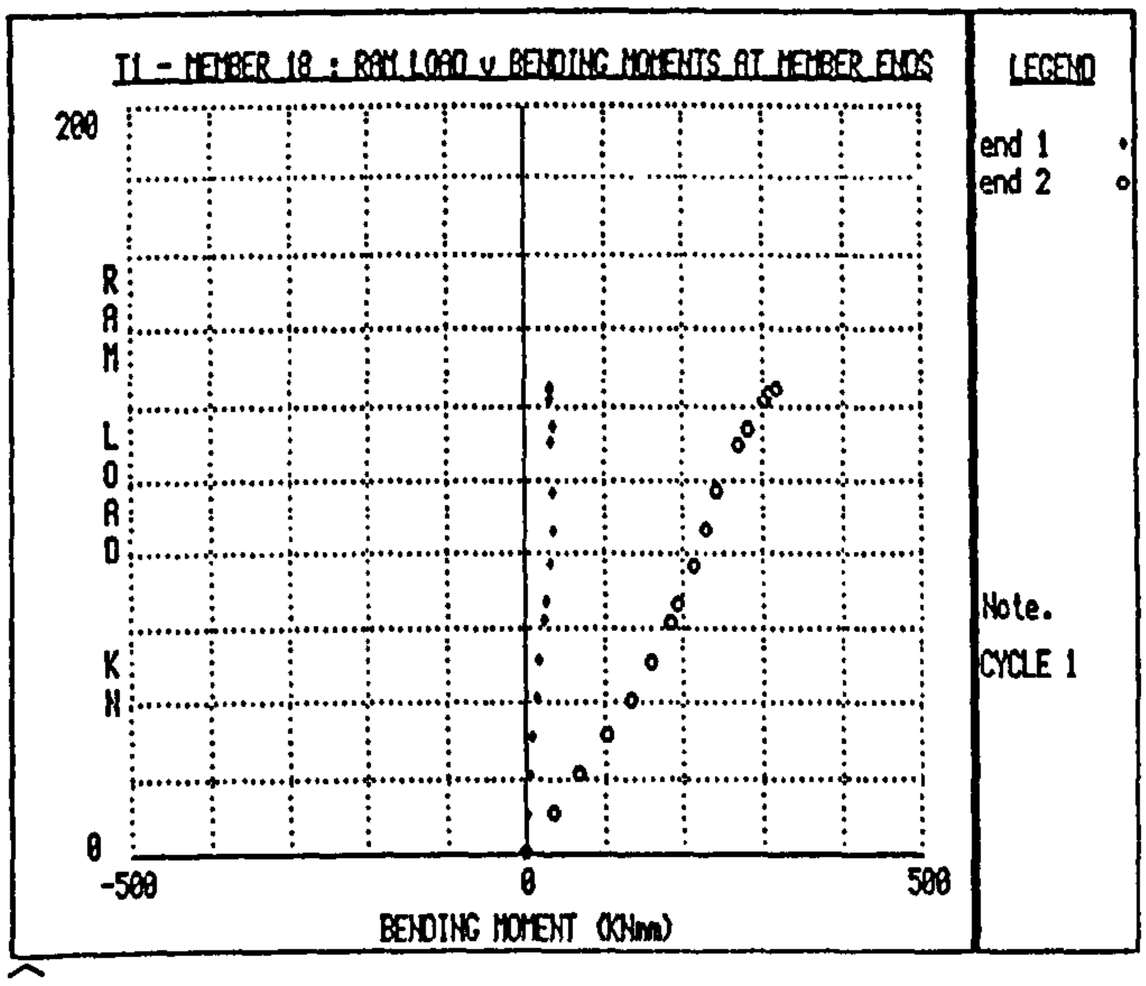

a

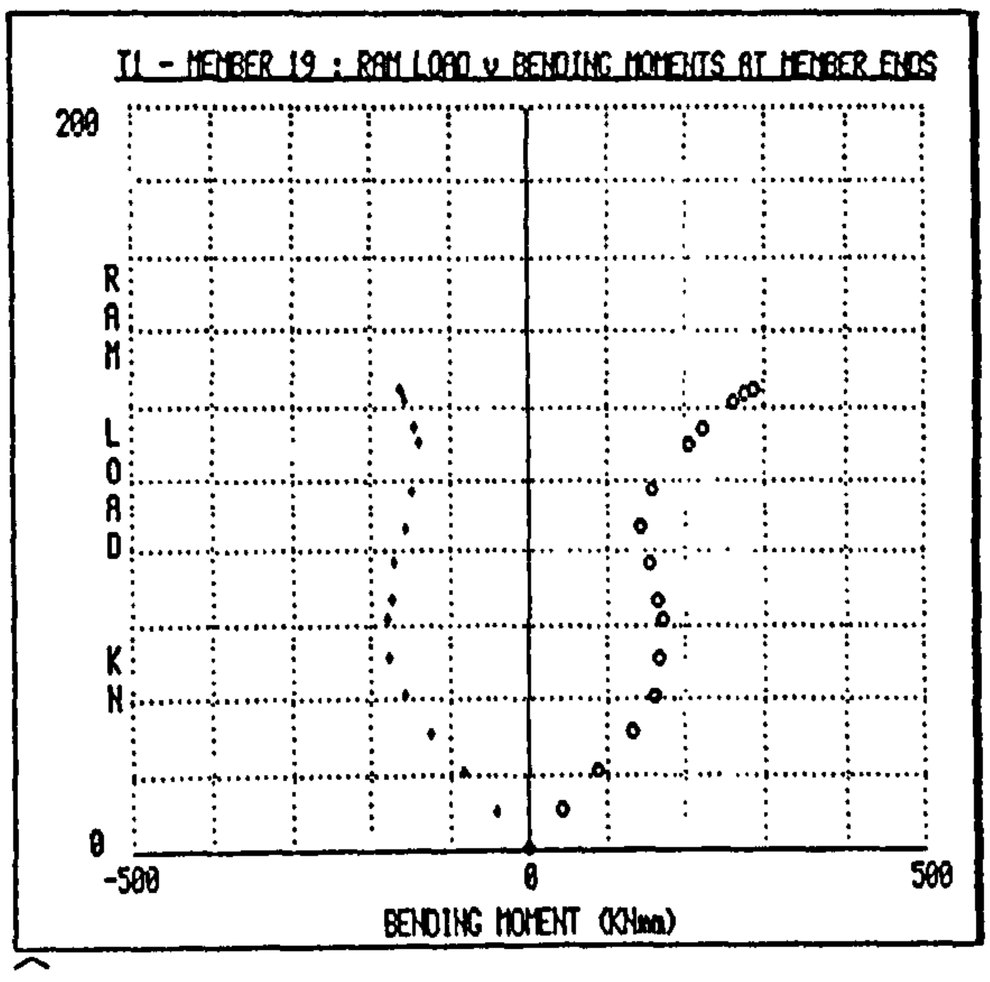

b

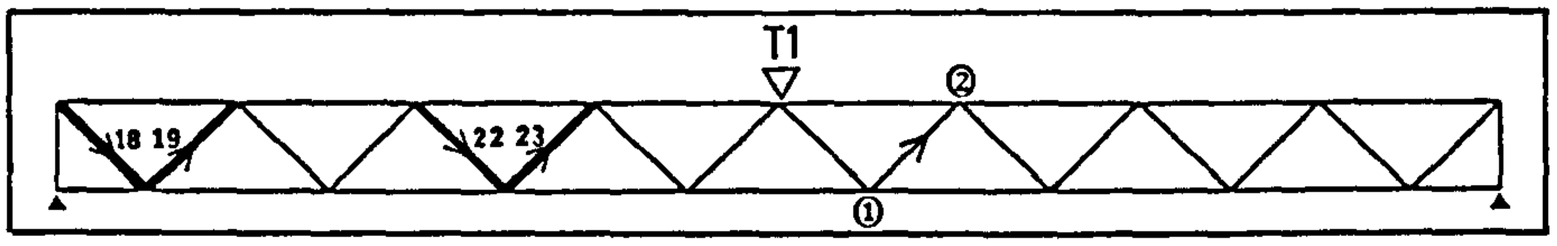

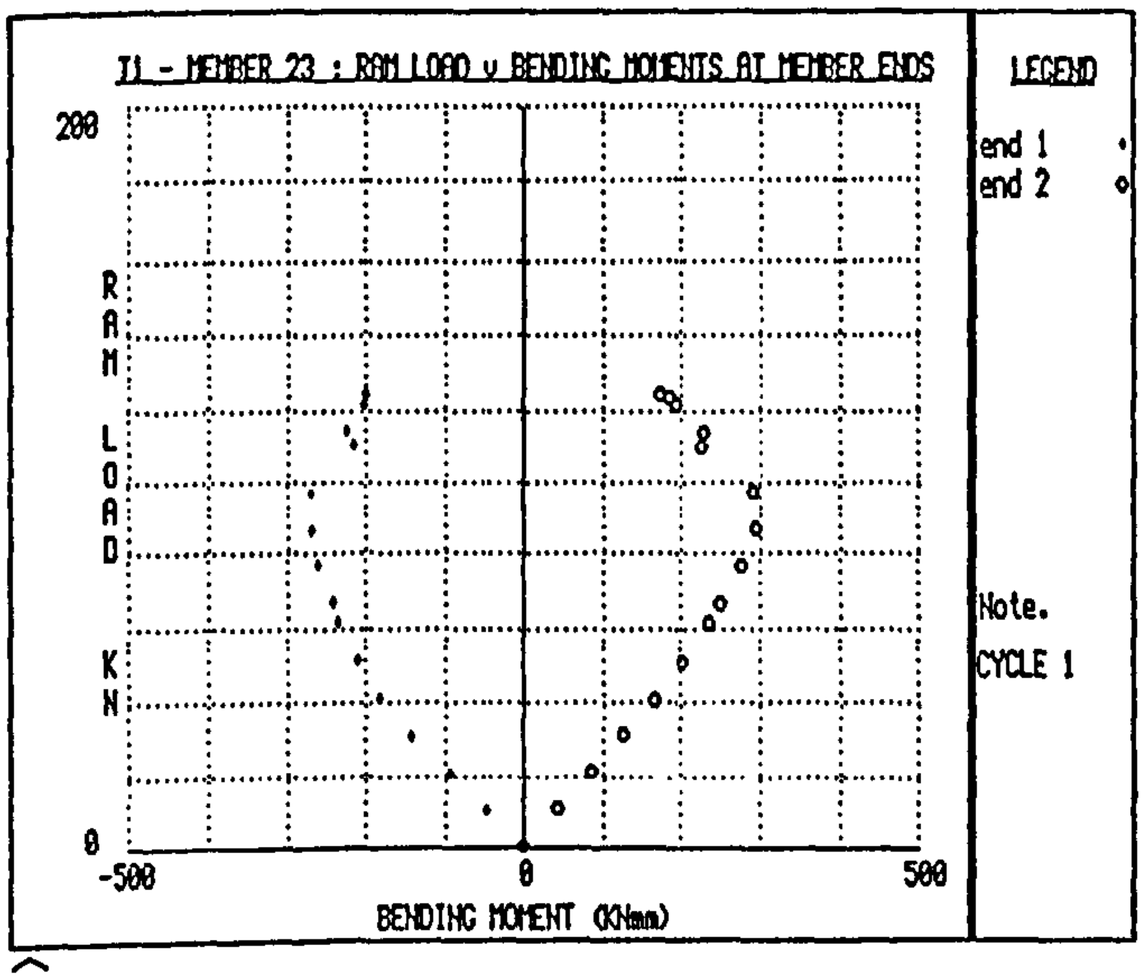

c

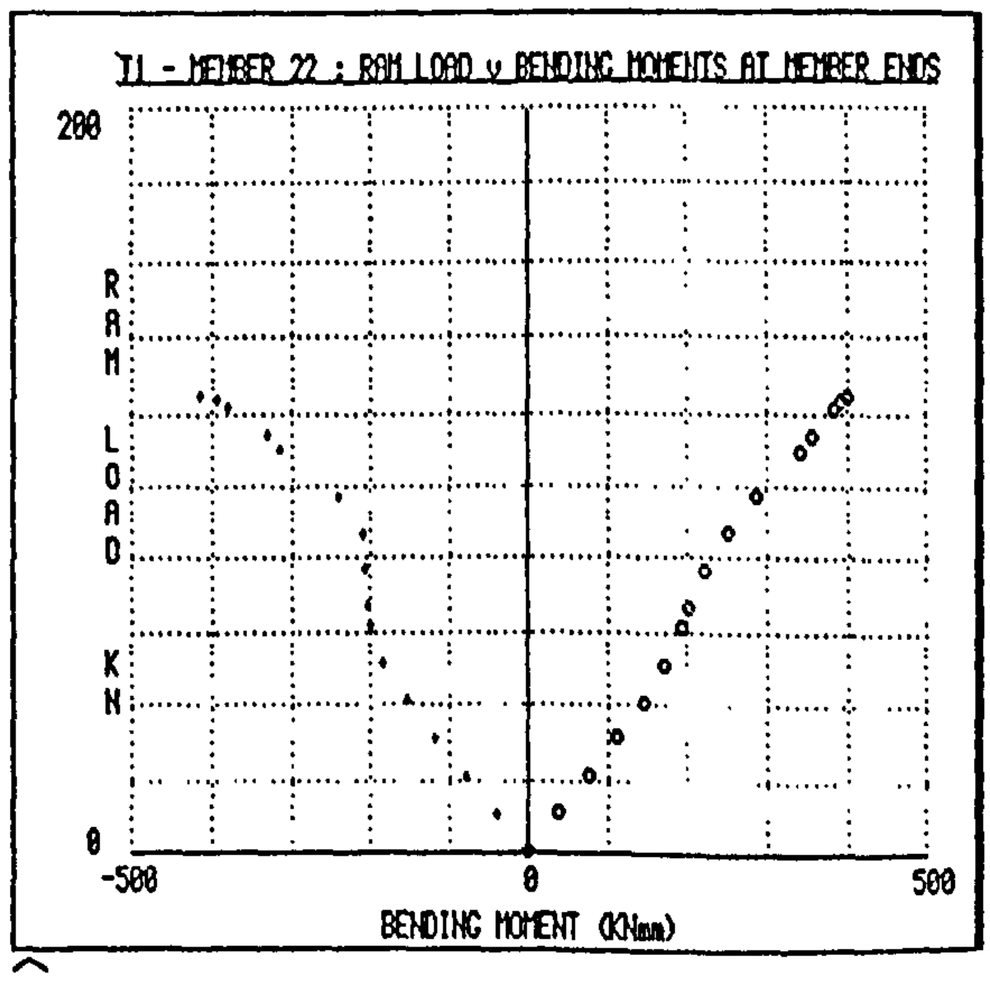

d

Fig 6.7 Examples of ram load v. bending moment in the branch members of truss T1.

a)

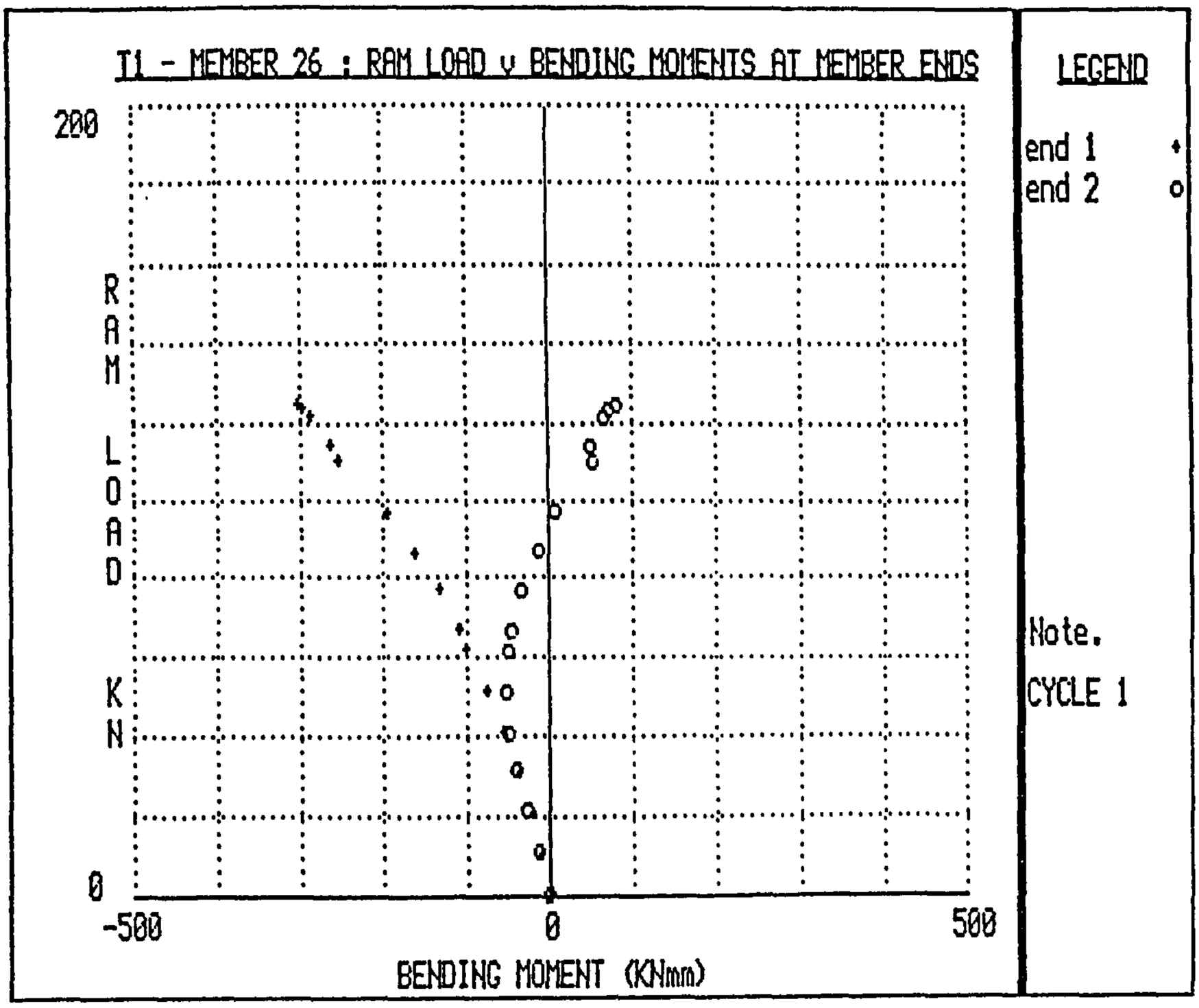

b)

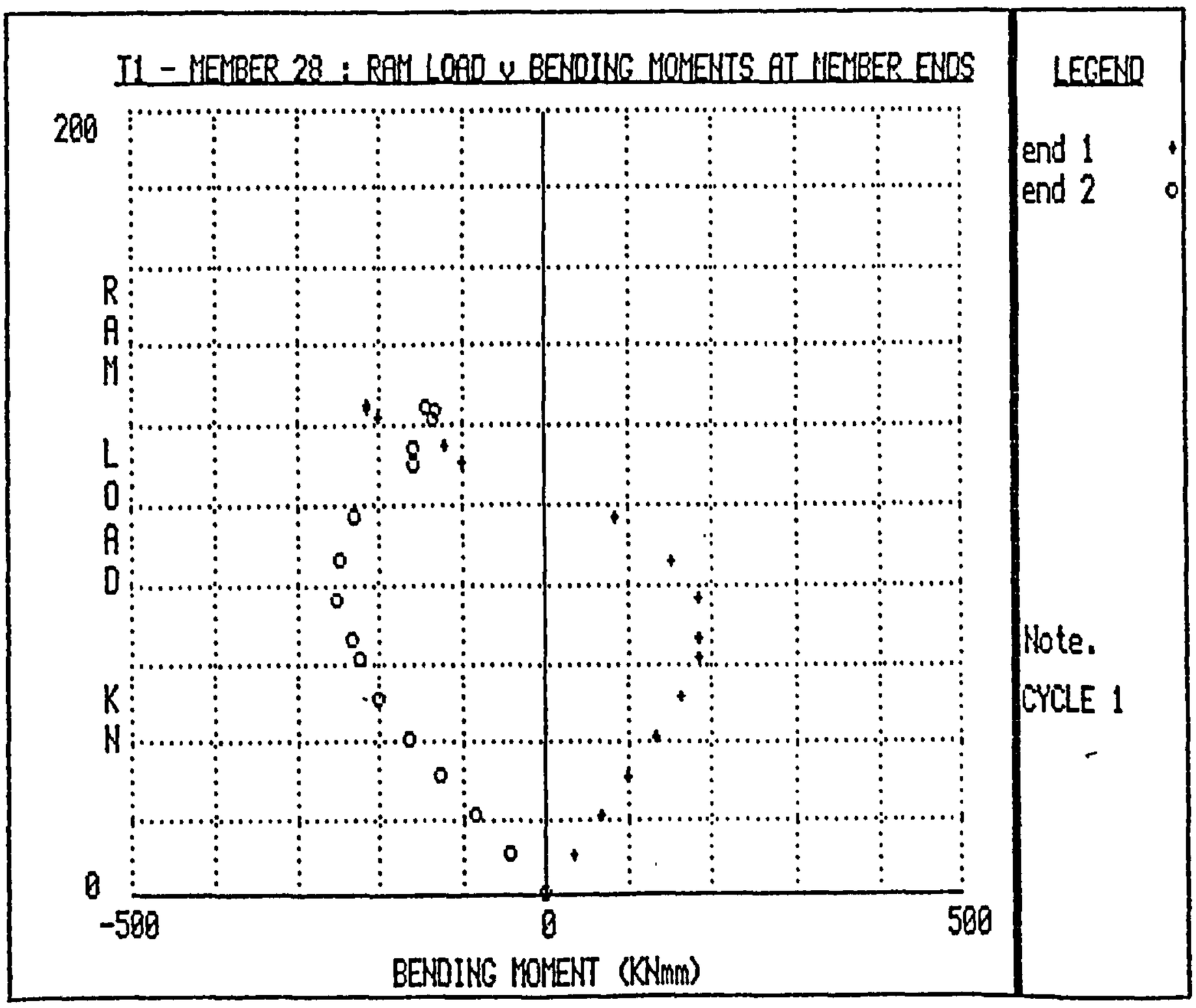

Fig 6.8 Examples of the reversal in the sense of branch member bending moments of truss T1.

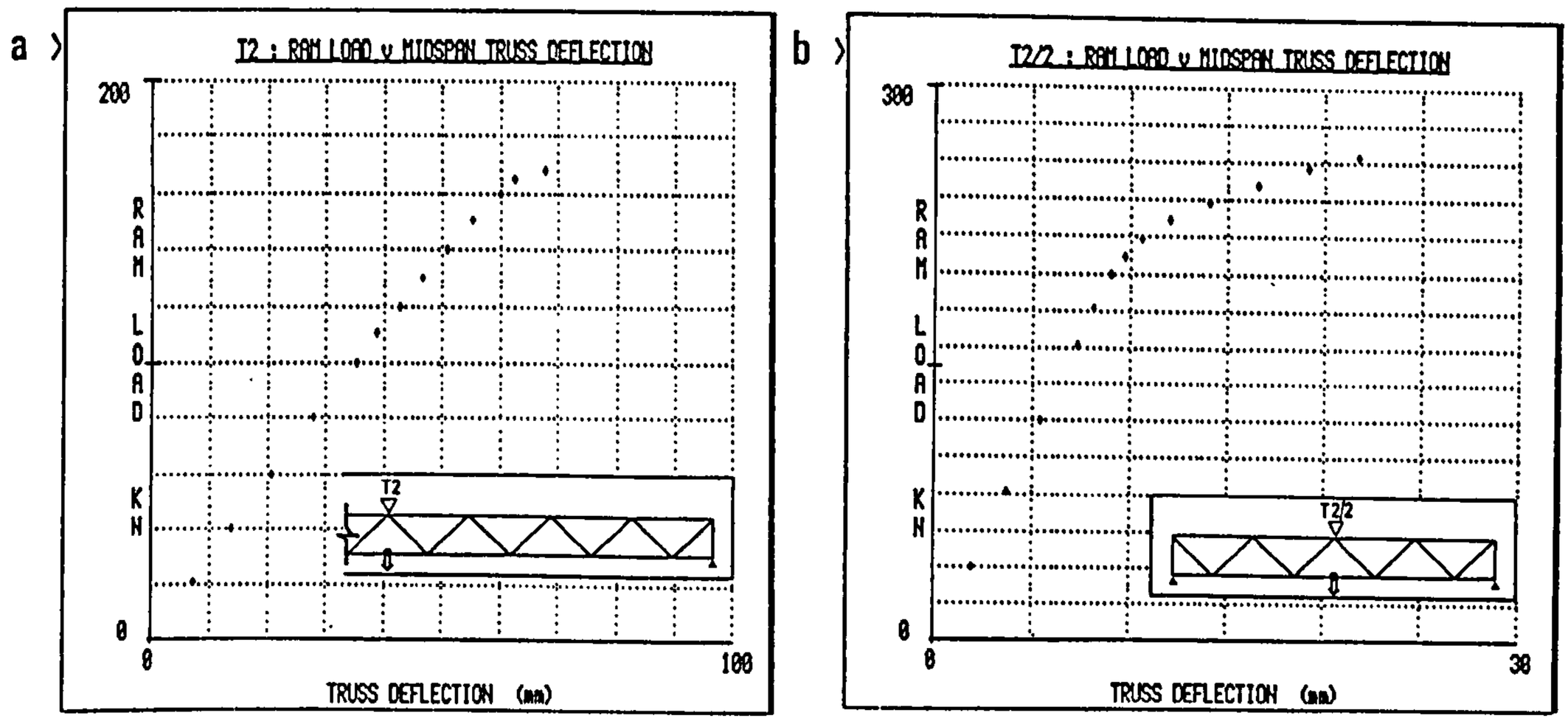

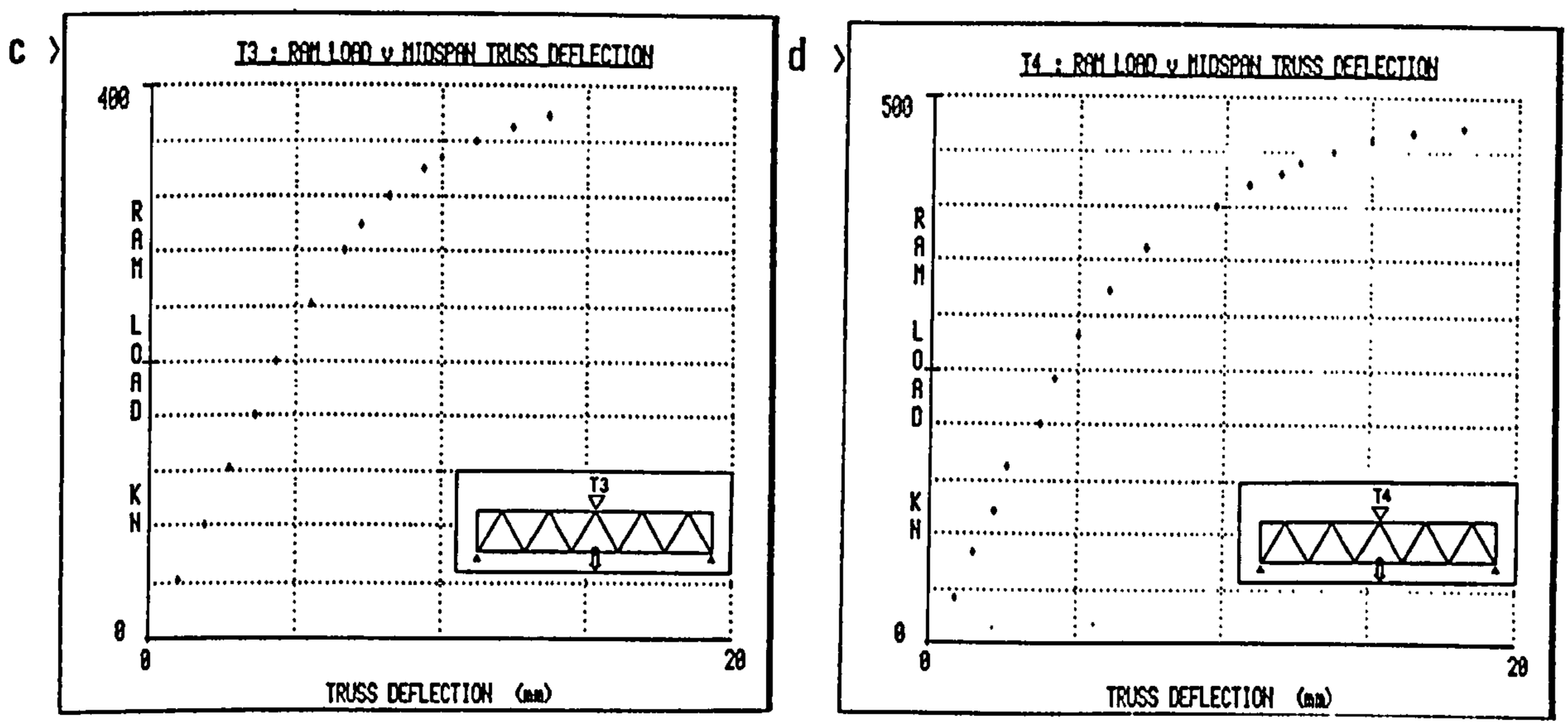

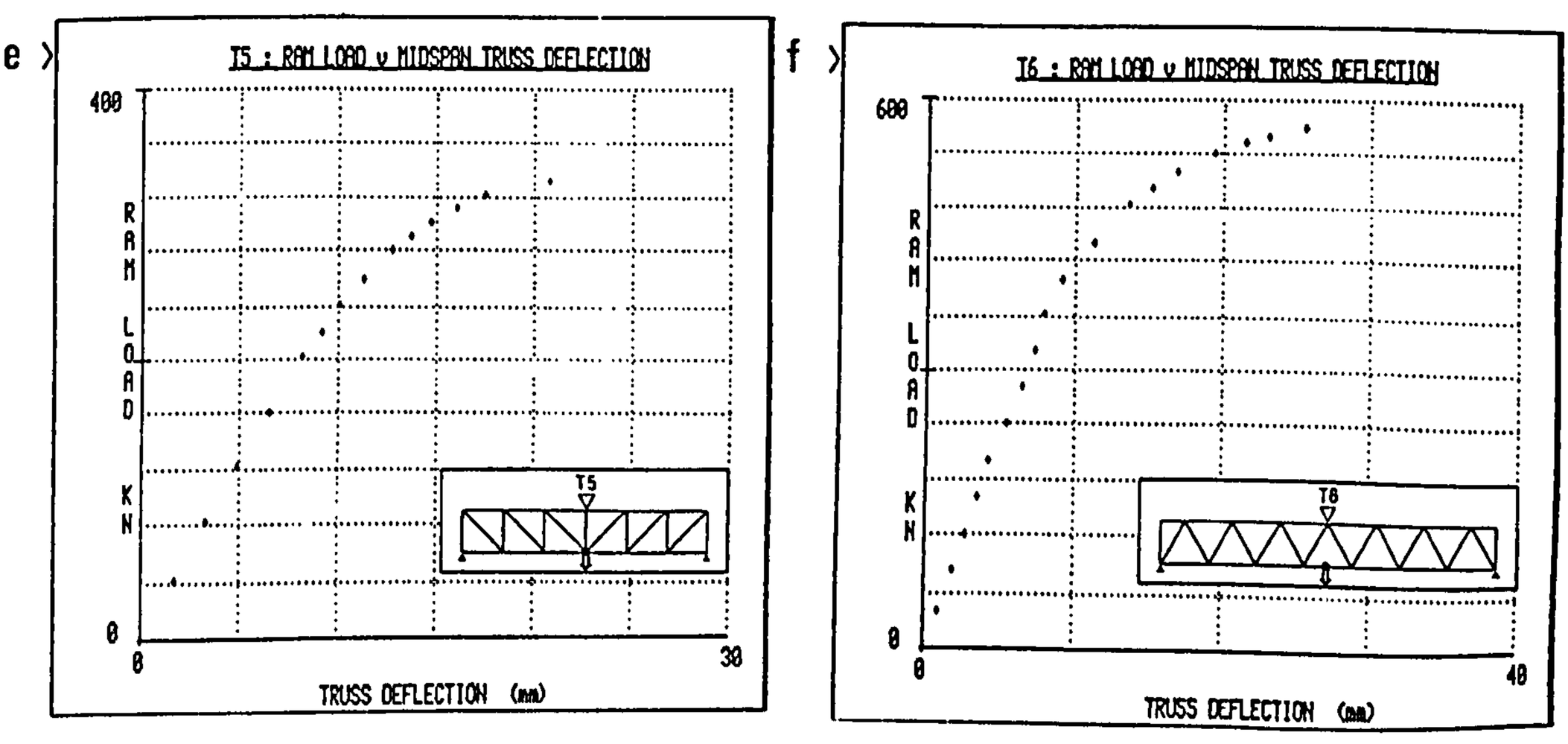

Fig 6.9 Ram load v. midspan truss deflection for the 100% overlap joint trusses.

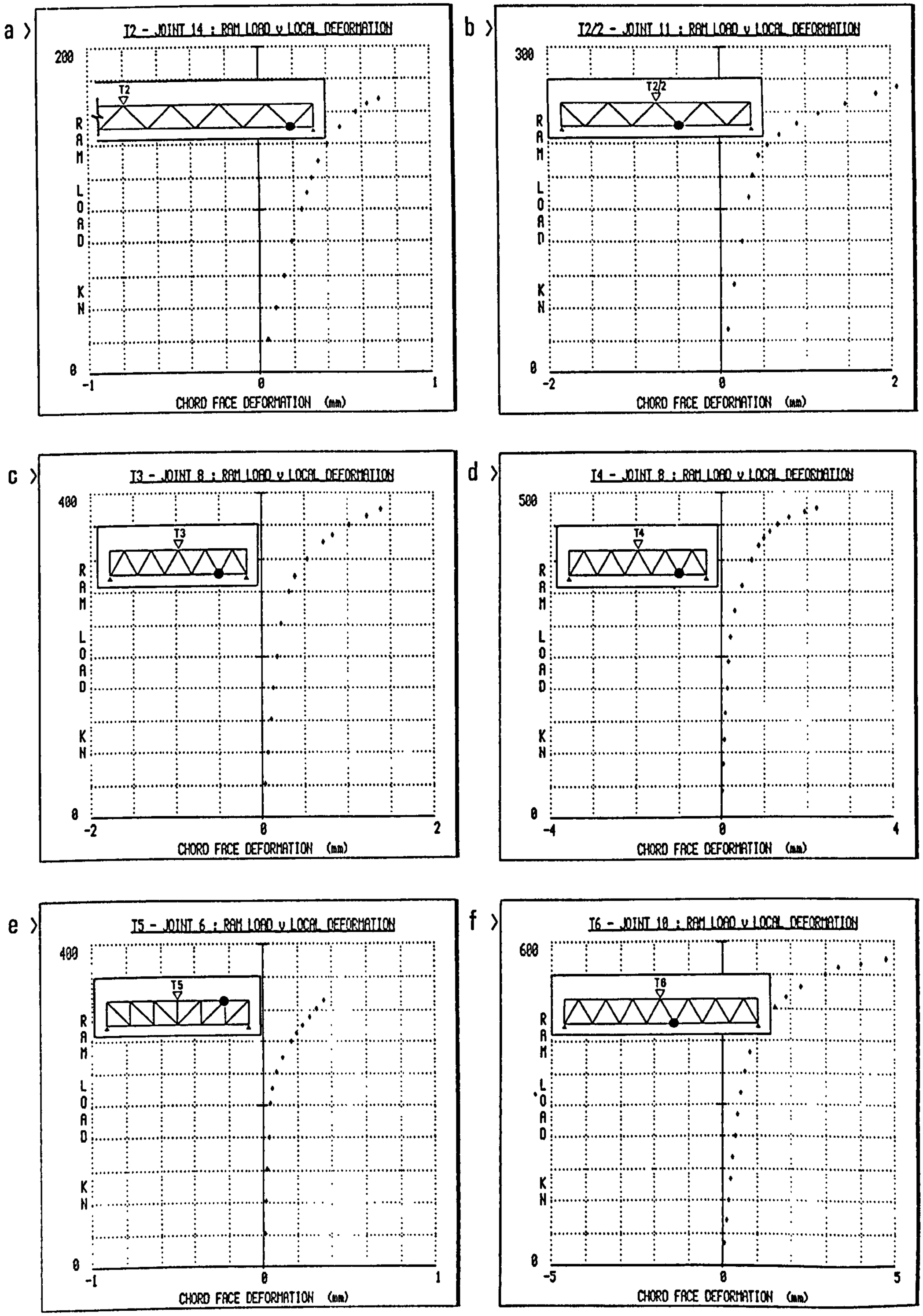

Fig 6.10 Examples of ram load v. local joint deformation perpendicular to the chord face for the 100% overlap joint trusses.
(for each truss the joint where the deformation was greatest has been selected)

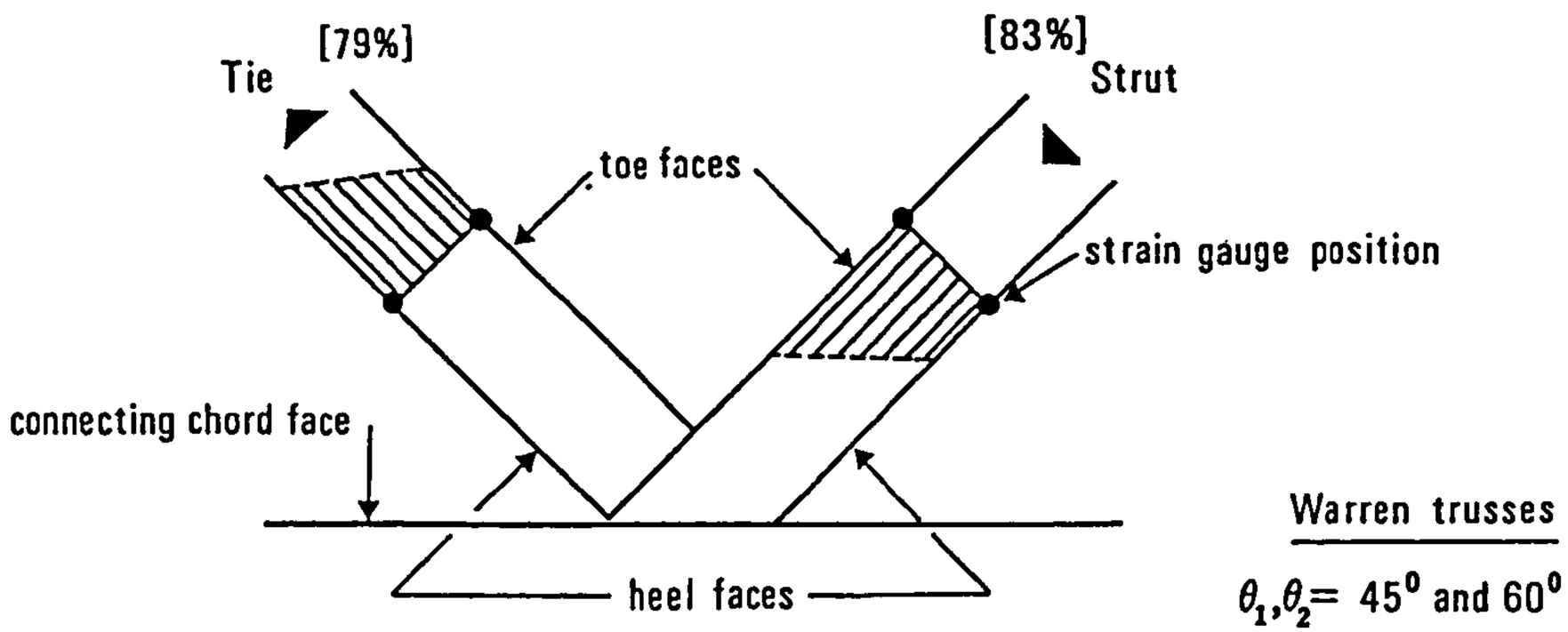

Warren trusses

$\theta_1, \theta_2 = 45^0$ and 60^0

a)

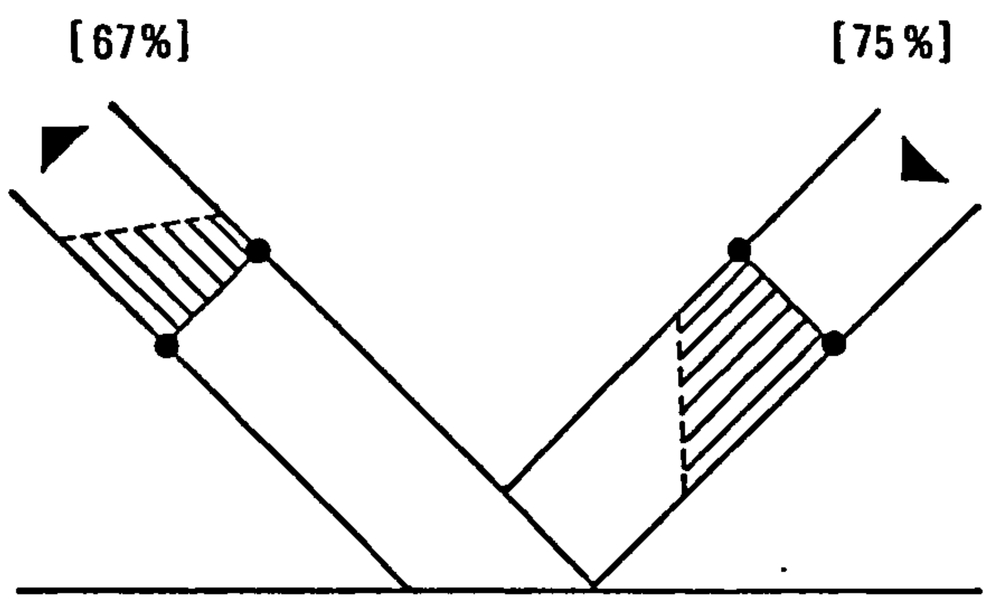

b)

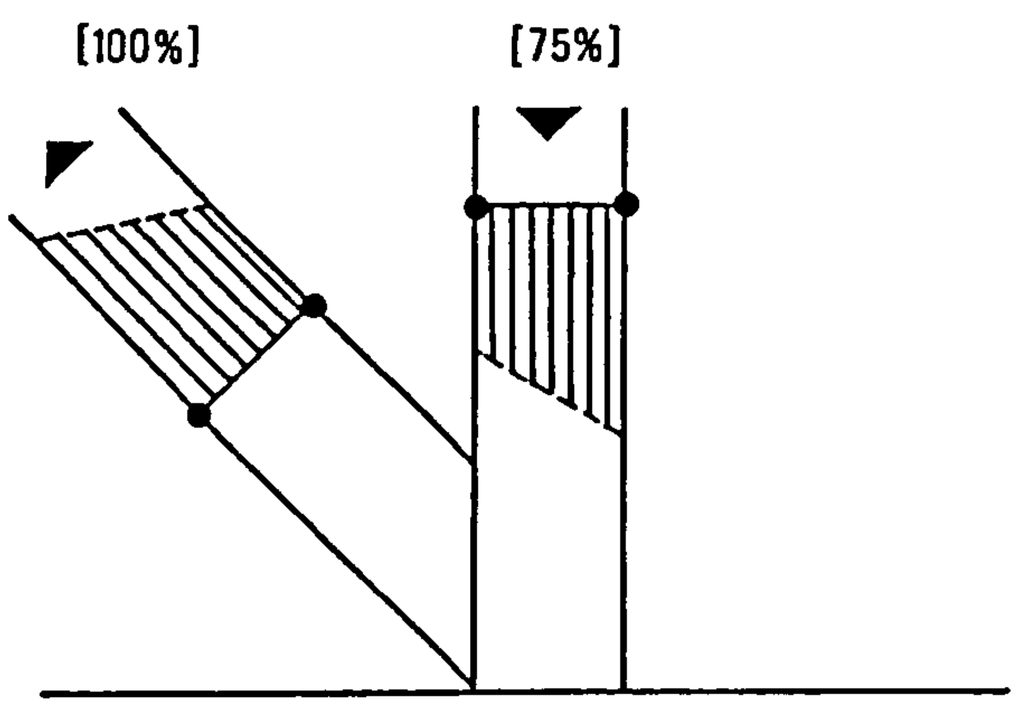

Pratt truss

c)

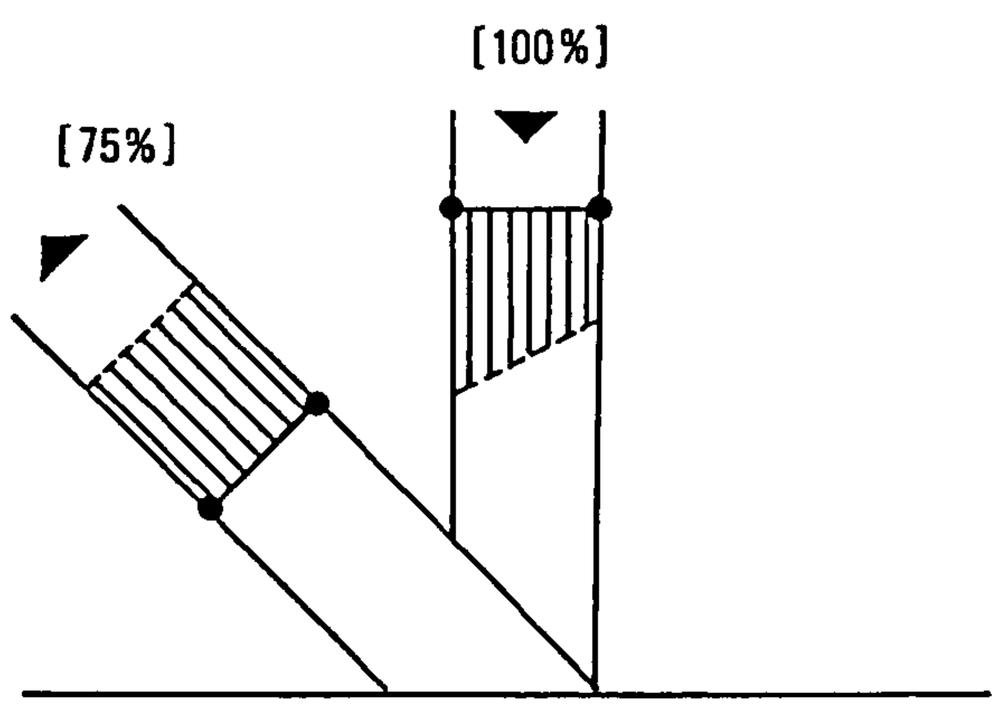

d)

Note : [Percentage] relates to total of { tie/strut joints for (a) and (c) ; strut/tie joints for (b) and (d) } ie., for overlapped warren ties, 67% were more highly stressed on the heel crosswall

Fig 6.11 Typical stress distributions, at the ram failure load, for the 100% overlap joint trusses. (see also Appendix E)

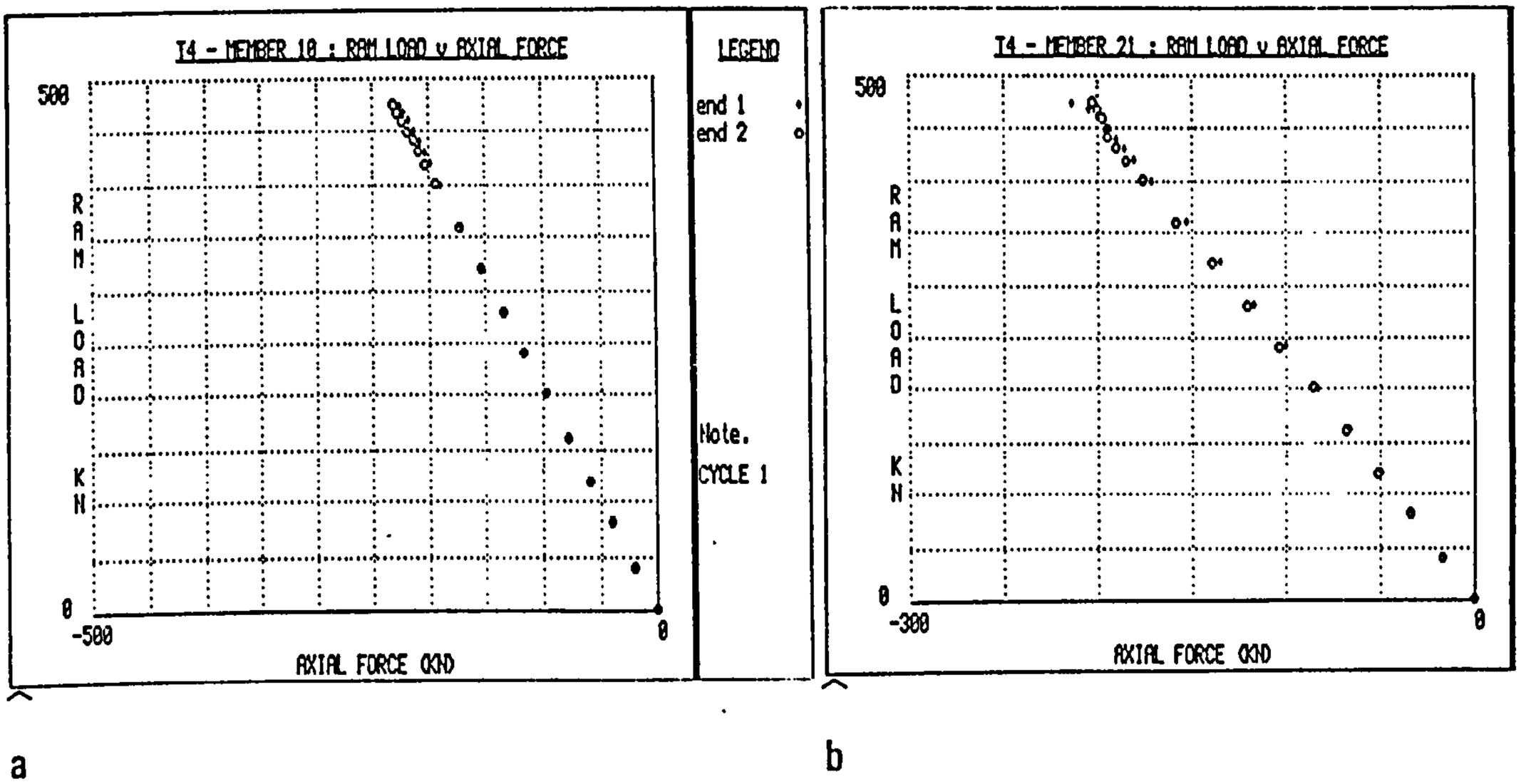

Fig 6.12 Examples of ram load v. axial force taken from truss T4 for (a) a chord member away from the ram, (b) a branch member, (c) an end post, and (d) a chord member adjacent to the ram.

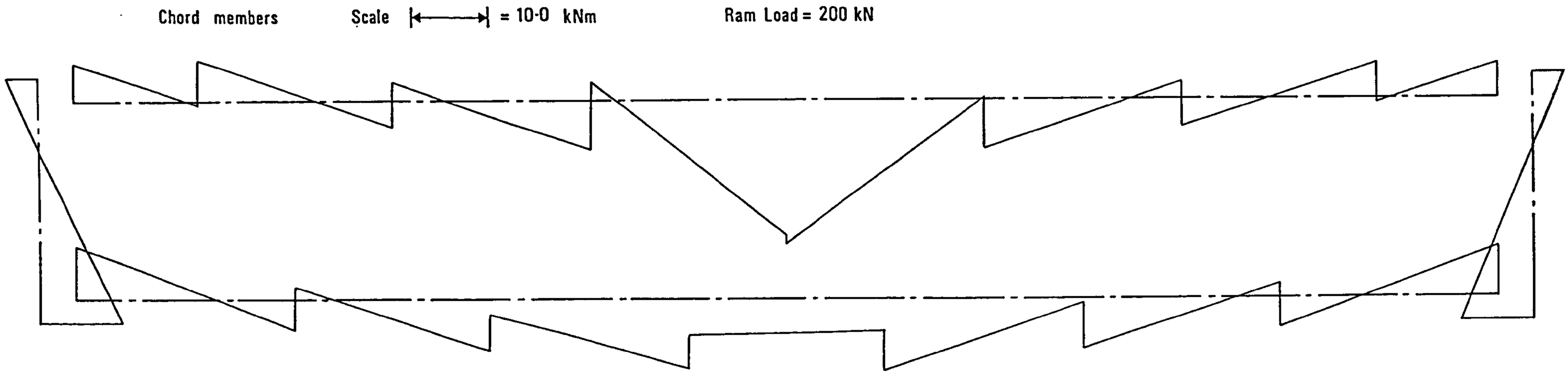

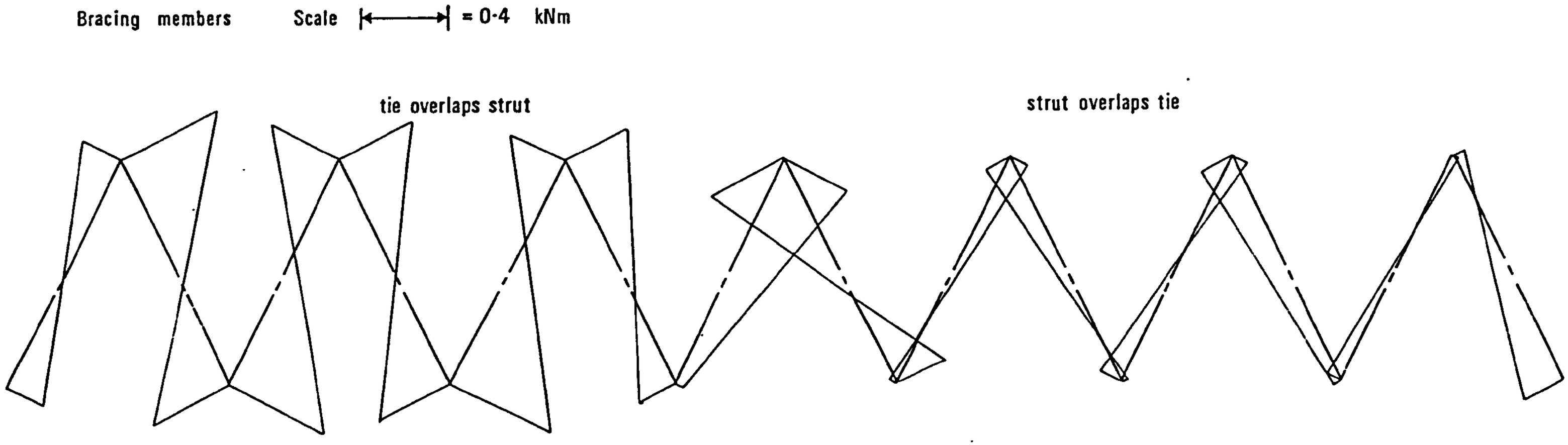

Fig 6.13 Experimental elastic bending moment distribution for truss T6.
(the bending moment diagram has been plotted on the side of the member where the stress induced by the bending moment is tensile)

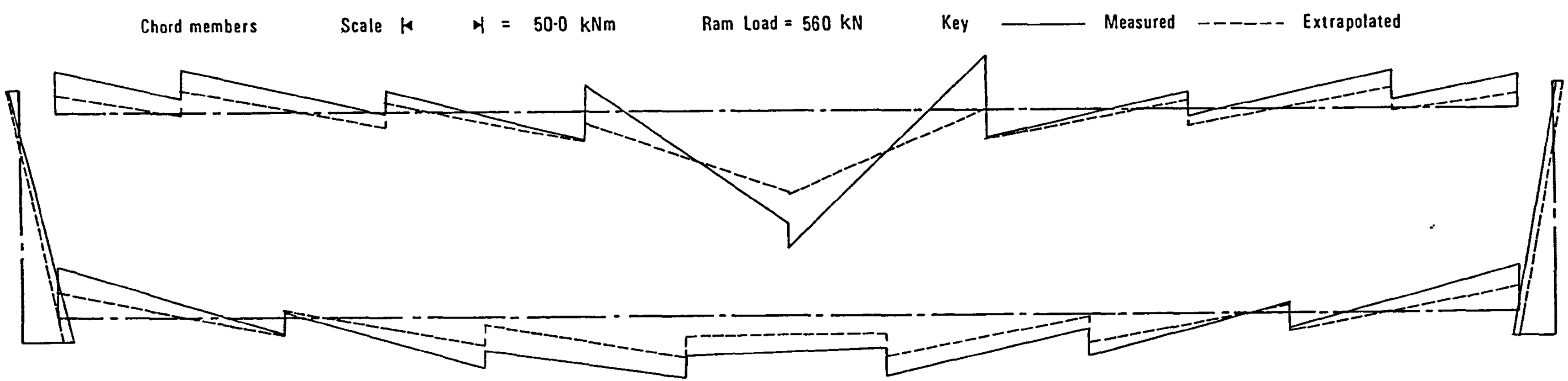

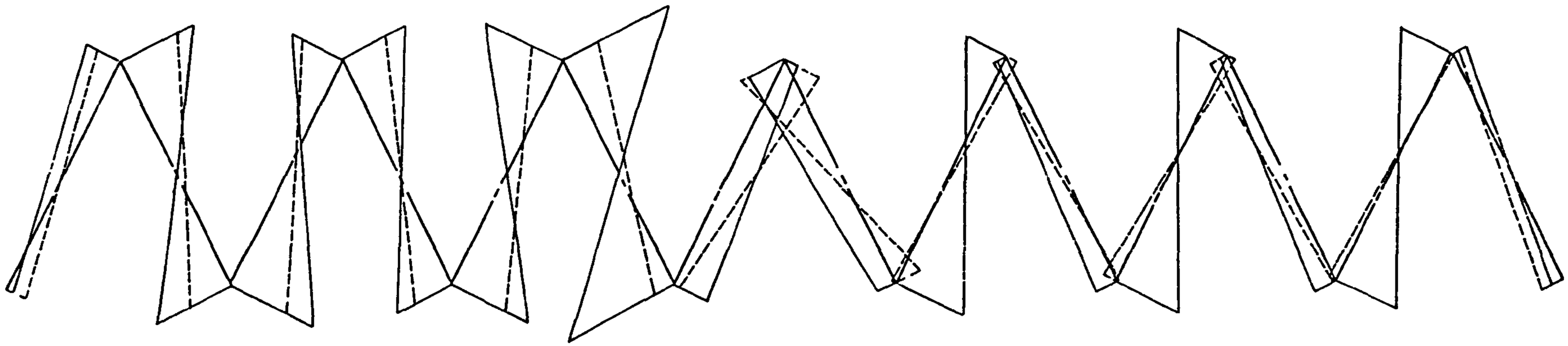

Fig 6.14 Truss T6 : Comparison of the measured bending moment distribution at truss ultimate load with the experimental elastic distribution extrapolated to the ultimate load.
(the bending moment diagrams have been plotted on the side of the member where the stress induced by the bending moment is tensile)

a)

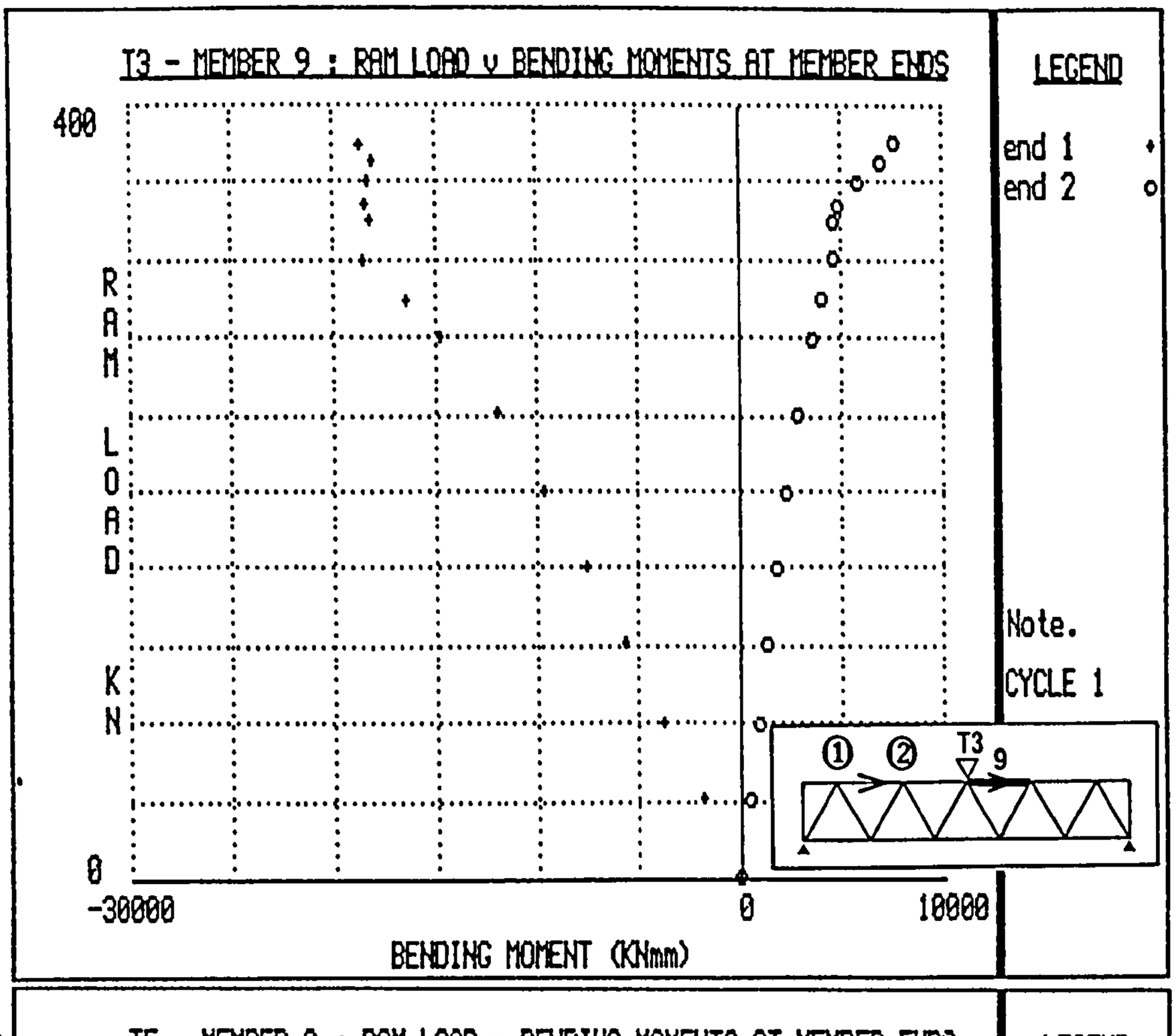

b)

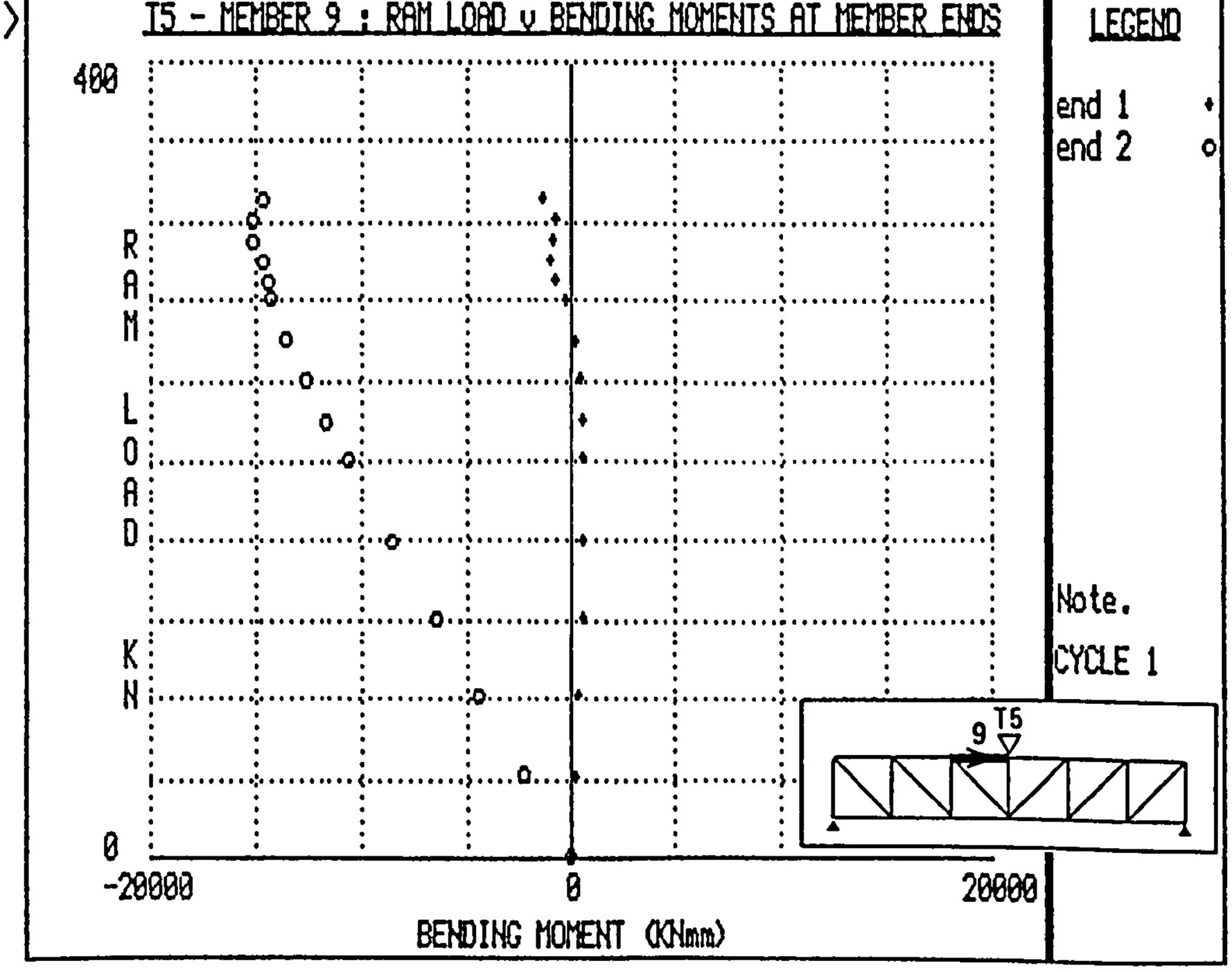

Fig 6.15 Typical examples of ram load v. bending moment for the compression chord members adjacent to the ram in the 100% overlap joint trusses.

a)

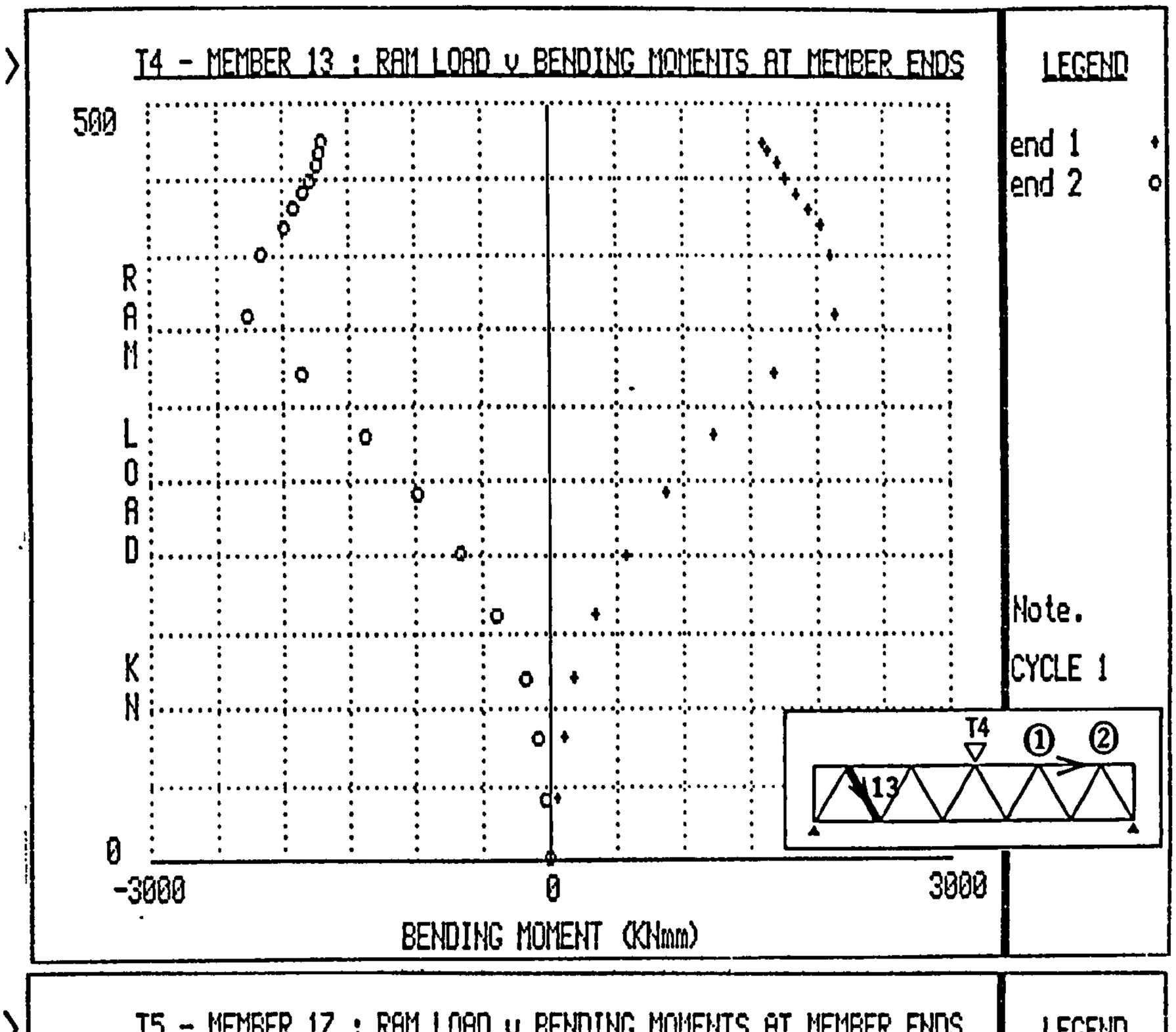

b)

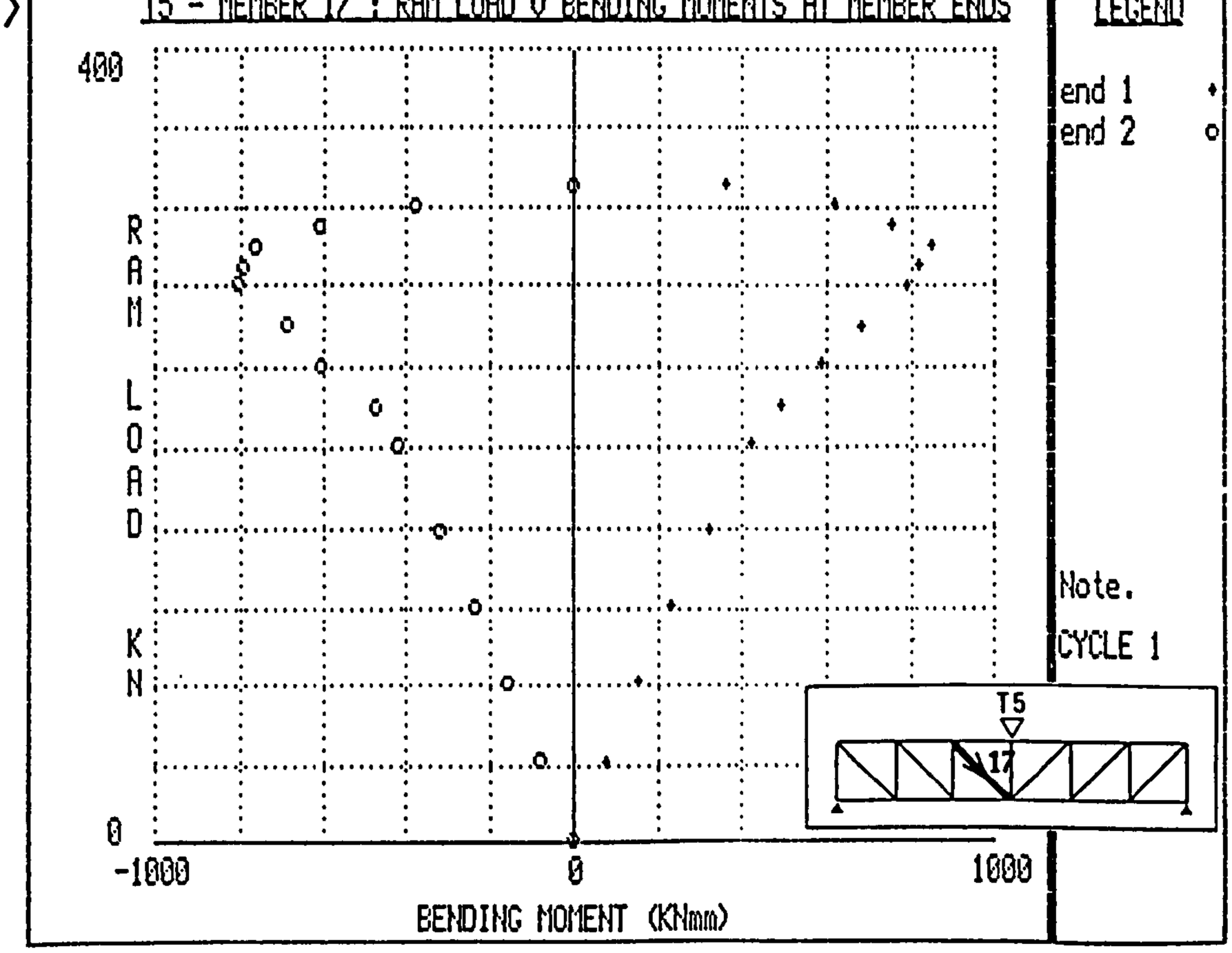

Fig 6.16 Typical examples of ram load v. bending moment in the branch members of the 100% overlap joint trusses.

a)

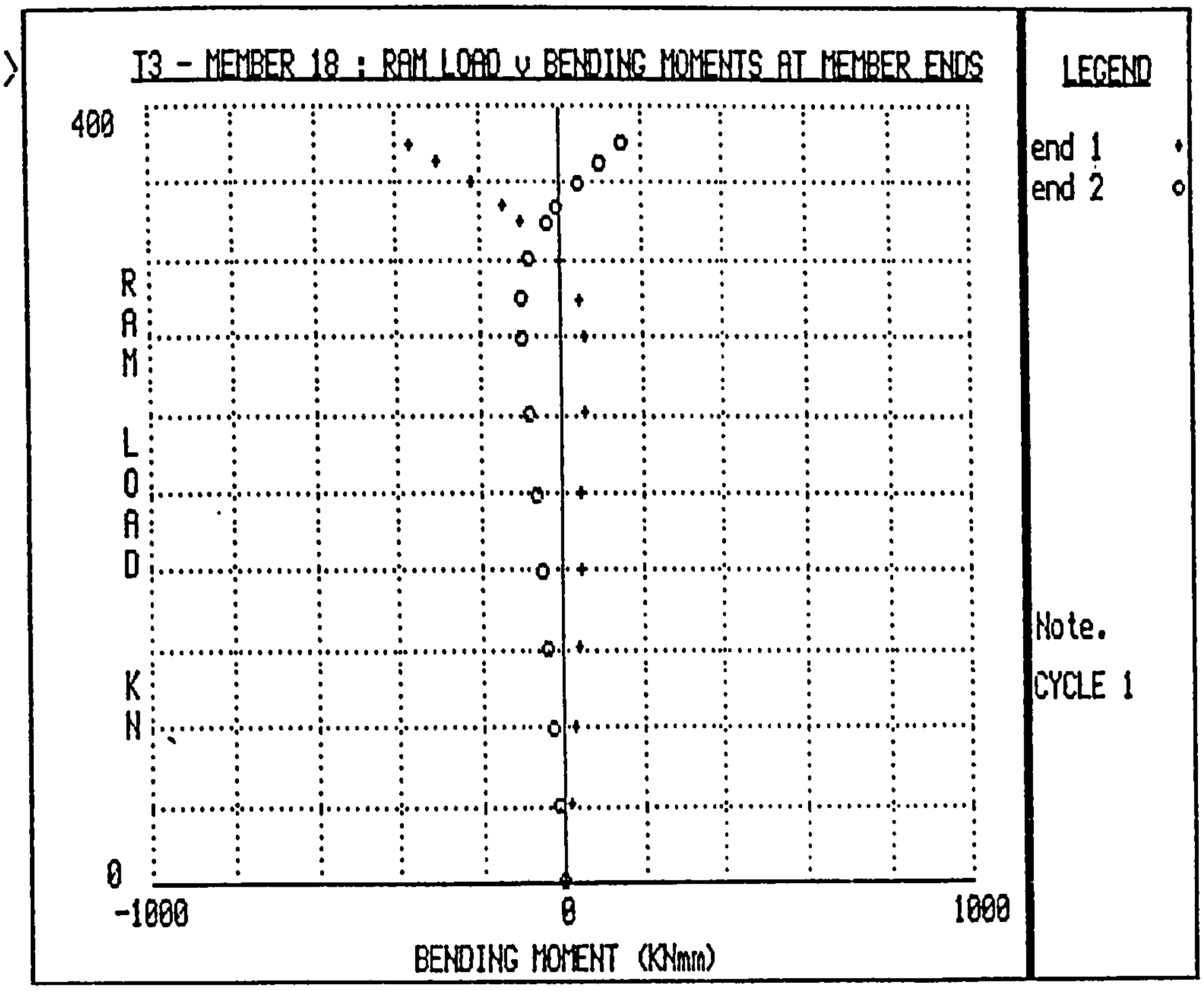

b)

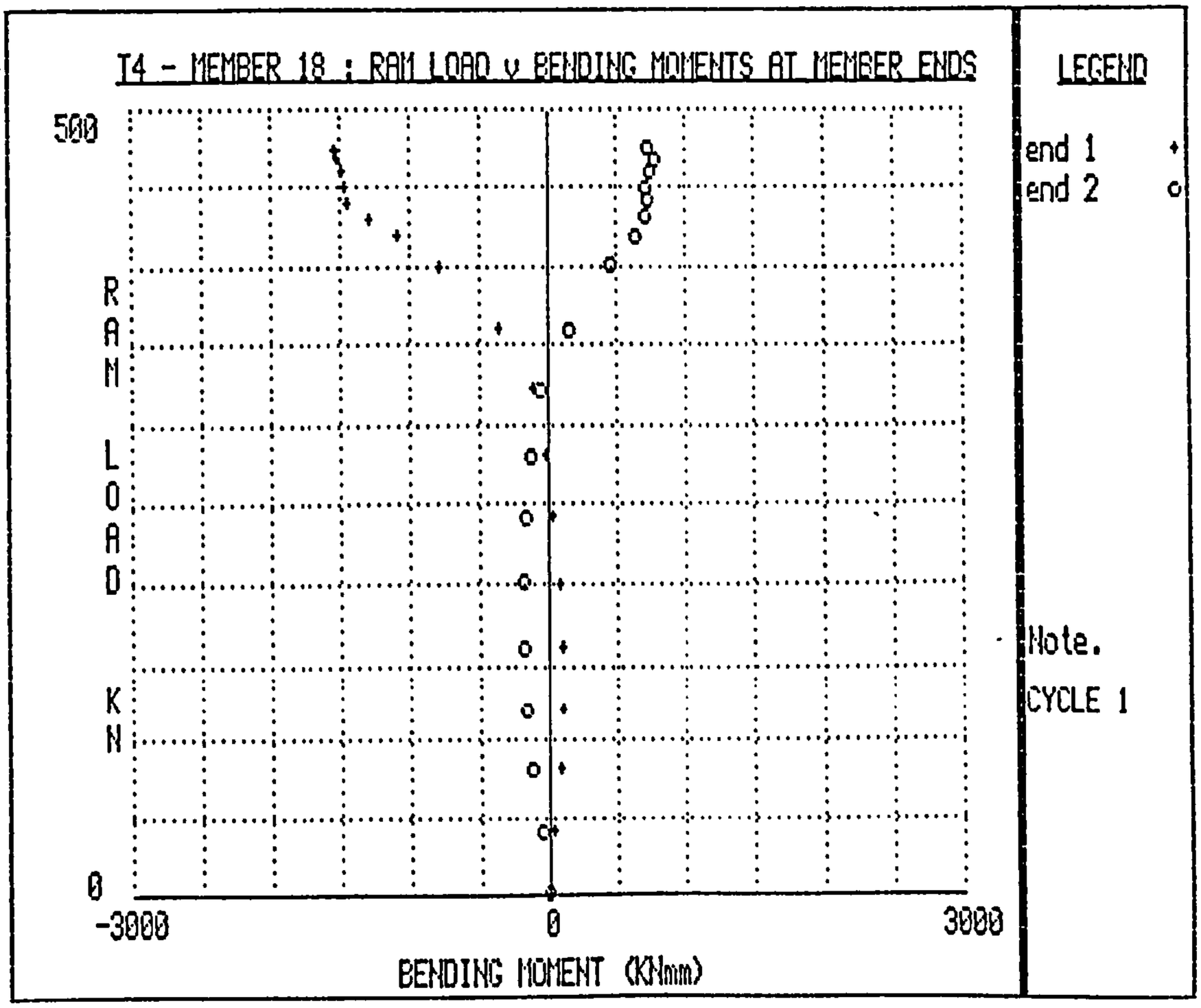

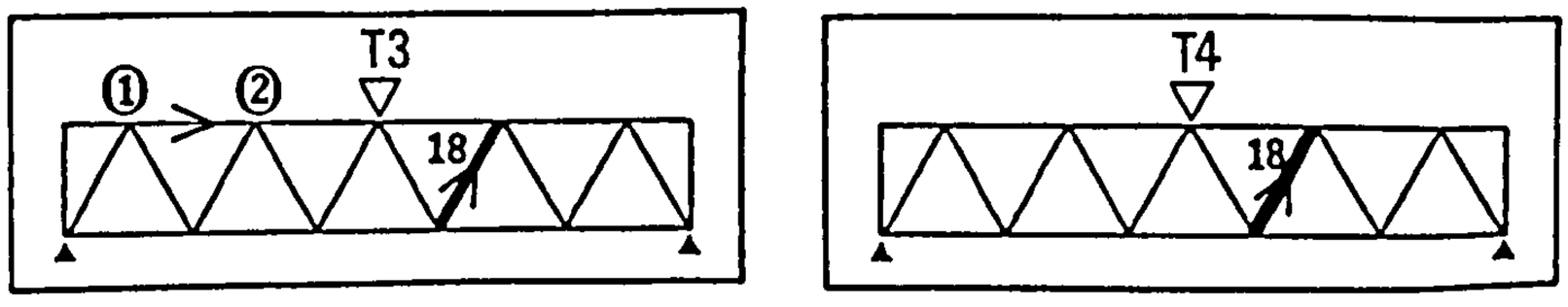

Fig 6.17 Examples of the reversal in the sense of branch member bending moments of the 100% overlap joint trusses.

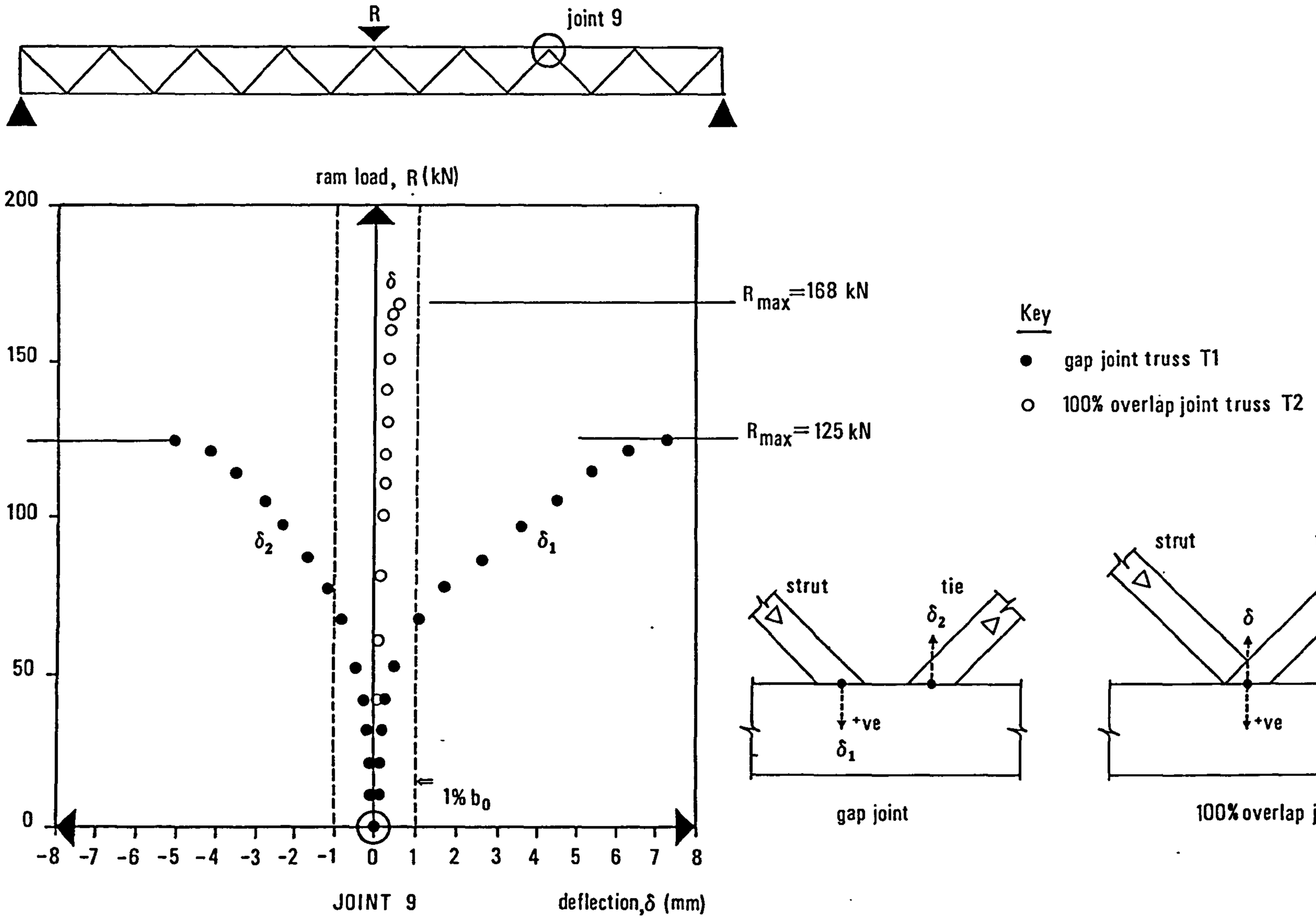

Fig 6.18 Comparison of local joint deformation.for the gap joint truss T1 and the 100% overlap joint truss T2.

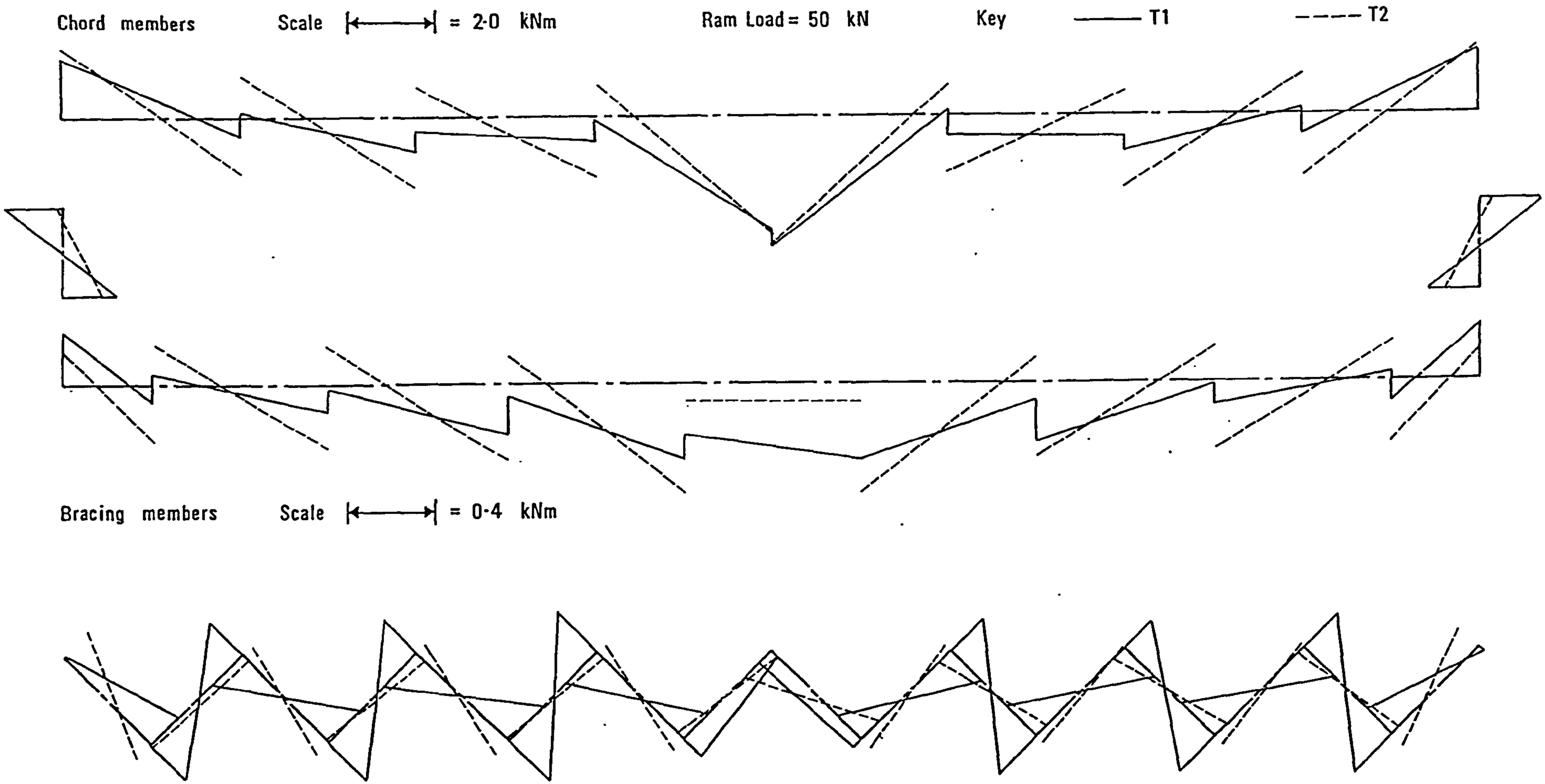

Fig 6.19 Comparison of the experimental bending moment distributions, at a ram load of 50 kN, for trusses T1 and T2.
(the bending moment diagrams have been plotted on the side of the member where the stress induced by the bending moment is tensile)

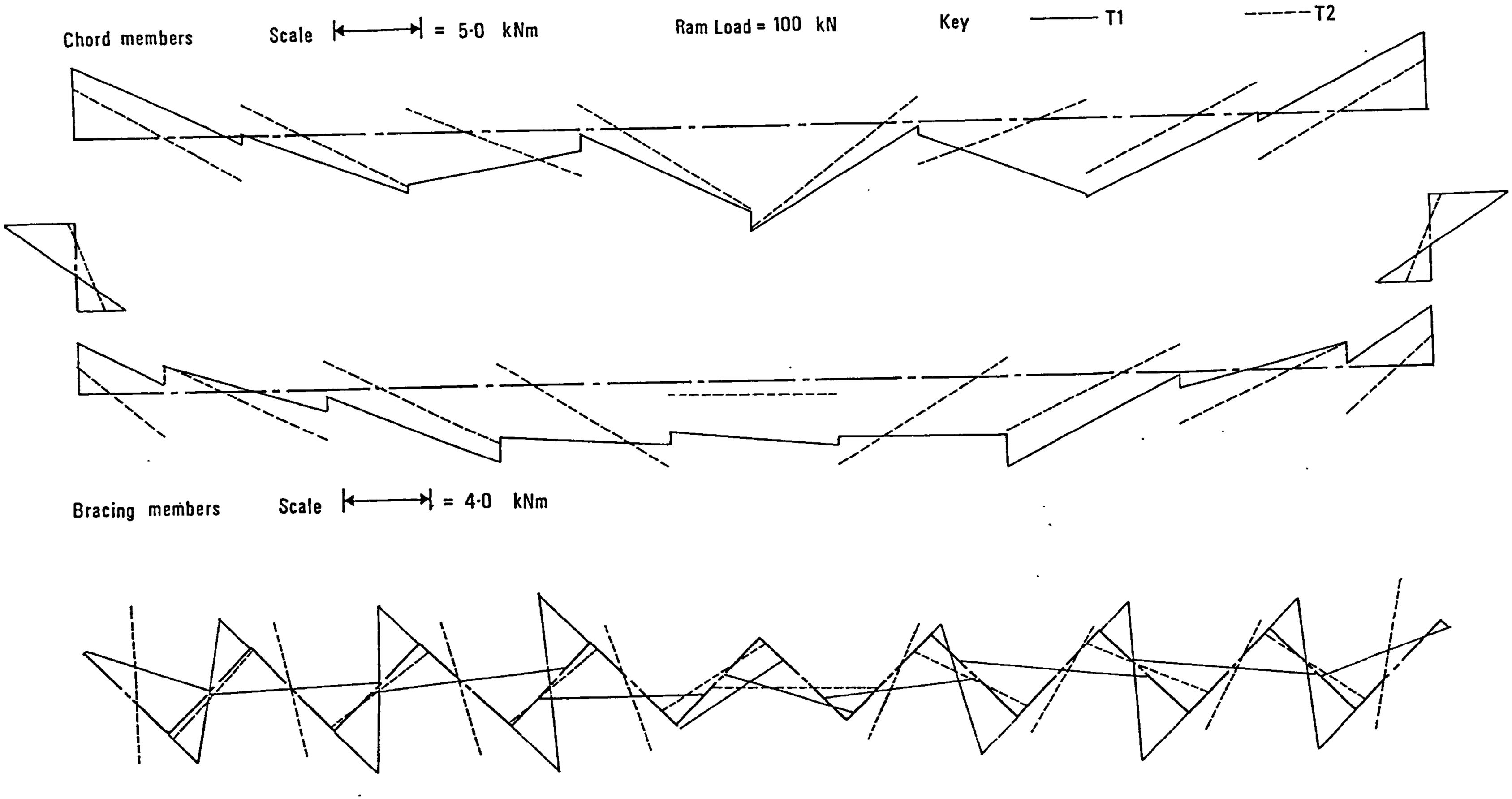

Fig 6.20 Comparison of the experimental bending moment distributions, at a ram load of 100 kN, for trusses T1 and T2.
(the bending moment diagrams have been plotted on the side of the member where the stress induced by the bending moment is tensile)

CHAPTER 7
ANALYTICAL MODELLING OF THE TEST TRUSSES

7.1 Scope of theoretical plane frame modelling

For each of the trusses the elastic behaviour has been compared to that derived from various two-dimensional theoretical models. This comparison has been carried out with respect to the distribution of axial forces and bending moments, as well as the overall truss deflection. Attention has been concentrated on the trusses formed from 100% overlap joints, however the analytical modelling of the gap joint truss has also been investigated. With respect to the test trusses the object was to derive answers to the following questions:

(i) Are the assumptions made in the conventional method of analysing the chord valid? Designers normally assume that the bending stress in the chord section can be deduced by distributing the eccentricity moment equally either side of the joint. For the critical chord section this bending stress is combined with the axial force derived from a pin-jointed frame analysis.

(ii) Does the joint stiffness need to be modeled in order to simulate the structural behaviour?

(iii) What are the limitations of elastic plane frame analyses in assessing the structural behaviour?

Essentially the objective was to define the most practical analytical approach for the 100% overlap joint trusses and to outline the problems associated with the modelling of the noded gap joint truss.

7.2 Two-dimensional pin-jointed frame models

Where reference is made to a pin-jointed analysis (P), the axial force distribution in the truss was evaluated by using the true branch to chord angle, θ. In the case of a truss formed from noded joints such as T1 it is possible to model both θ and the effective depth (see Fig. 7.1[a]). However for eccentric 100% overlap joints the branch centre-lines intersect at a distance away from the chord centre-line. By modelling the true branch angle, the actual effective depth of the structure differs from that assumed in the theoretical analysis (see Fig. 7.1[b]).

7.3 Rigid frame analytical models

The support conditions have been simulated in each of the analytical models by assuming a roller bearing at one end and a rocker at the other.

In the rigid frame models only simple beam elements have been used to model the structure. This type of element is capable of transmitting only in-plane axial, bending and shear forces. In all the analyses the measured section properties were used for each of the members (see Appendix B).

In a gap joint the end of each branch member has two in-plane degrees of freedom, namely, a translation perpendicular to the chord face and a rotation. In a 100% overlap joint the branch members intersect and form a single connection to the chord face. The in-plane degrees of freedom associated with such a connection are the same as those in the gap joint. However, for both gap and 100% overlap joints the experimental data could only be used to assess the stiffness associated with translations. Rotations were not measured.

For both gap and 100% overlap joints the local deflection in the direction perpendicular to the chord face has been simulated by the use of a short connecting element (denoted as element '1' throughout Fig. 7.2). This element was given infinite bending and shear stiffness, however, the axial stiffness was derived from the experimental data as shown in Fig. 7.3.

7.3.1 Modelling of gap joint truss, T1

For the gap joint truss two rigid frame models have been used to assess the performance, namely GS and GK (see Fig 7.2). Model GS approximately simulates the chord face deformation. The traditional form of analysis which is used for a noded truss is represented by GK. In this case the chord face flexibility has been ignored but the correct geometry of the truss has been maintained.

In model GS the deformation of the chord connecting face has been simulated, while maintaining the correct geometry. This type of theoretical model is similar to the 'micro-bar model' referred to in the Polish test programme[33]. The axial stiffness of element 1, was derived from the experimental results (see Fig. 7.3 and Table 7.1), while element 2 was given infinite axial and bending stiffness. The Polish researchers derived the axial stiffness of element 1 from a theoretical analysis, in which the chord

face was considered as a strip plate restrained at the edges by the adjacent walls. This method considered both the translational and 'rotational' degrees of freedom. However, the 'rotation' that is referred to is the effective rotation of the joint about the noding point as opposed to the rotation at the ends of individual branch members.

7.3.2 Modelling of 100% overlap joint trusses

Since the rotational stiffness of the 100% overlap joints could not be derived from the experimental data, two models have been used to assess the influence of the joint rotation, namely S1 and S2 (see Fig. 7.2). The former provides an upper bound value to the rotational joint stiffness, and the latter a lower bound. A further two models have been considered in the case of the 100% overlap joint trusses, namely Y, and K (see Fig. 7.2). In both S1 and S2 the joint translation perpendicular to the chord face has been simulated, but not in the remaining models. All the analyses have two common characteristics. Firstly, the true branch angle has been modeled and secondly the branches are rigidly connected to each other. In S1, S2, and Y the effective depth has been correctly simulated.

For S1, S2, and Y the joint eccentricity has been incorporated into the geometry of the frame analyses. This has been done by the use of a beam element (see 'connecting element' in Fig 7.2) which connects the intersection of the branch members to the chord centre-line. In S1 and S2 an axial stiffness, derived from the experimental test results, has been designated to this element (see Fig. 7.3 and Table 7.1), while the bending stiffness is assumed to be infinite. In model Y the deformation of the connecting chord face at the joints was set to zero. This was achieved by using a 'connecting element' with infinite axial and bending stiffness. S1 differs from S2 only in the method of attachment of the 'connecting element' to the branch members. In S1 it is rigidly connected, while in S2 the connection is pinned.

The K type model does not incorporate the joint eccentricity in its geometry. In this case the bending moments generated at the joints have been input as a component of the applied load. These bending moments were calculated using the axial forces derived from the pin-jointed frame analysis (P).

7.3.4 Modelling of corner joints

The methods that have been used to model the corner joints are shown in Fig 7.4. With the exception of truss T2 the branch member centre-line coincides with the

junction of vertical post and the chord. At this type of joint the deformation was identified from the tests as negligible (see section 6.3.2). Therefore the axial and bending stiffness of the 'connecting element' was assumed to be infinite. The moment connections at either end of this element are rigid.

Where stiffening plates have been used to prevent chord face deformation of a corner joint (see truss T2, Appendix A, Fig A8), the correct geometry has been used in conjunction with a 'connecting element' of infinite axial and bending stiffness.

7.3.5 Modelling of central joints

In the case of the joints where the ram load was applied a significant amount of stiffening was afforded to each structure. The extent and nature of the stiffening plates has been incorporated into each of the rigid frame models (see Fig 7.5). In trusses T1, T2, T3 and T5 stiffening plates were only provided to the top and bottom faces of the chord section. In the remaining trusses additional plates were welded to the sides of the chord. Furthermore, plates were welded to the sidewalls of the branch members to prevent the branches from punching into the connecting chord face.

In all trusses the stiffening effect of the plates welded to the top and bottom faces of the compression chord was modeled using an element of infinite axial and bending stiffness. The length of this element being equivalent to the length of the plated section.

With respect to trusses T1, T2, and T3 the S type models (GS for T1, S1 and S2 for T2 and T3) the chord face stiffness has been modeled by deriving from the experimental data the respective axial stiffnesses for element 1. Since joint deformations were not measured at the central joints, the joint stiffness was extrapolated from the corresponding truss joints. It has been assumed that the deformation of the chord face is, approximately, directly proportional to the cube of the thickness (t_0^3), of the chord face. Therefore, if the normal joint stiffness of the chord wall, t_0 is denoted by ζ and a stiffening plate of thickness $2t_0$ was welded to the connecting chord face then the combined stiffness was assumed to be $(2^3+1)\zeta$.

For T4 and T6 even the sidewalls of the chord were stiffened, and therefore deformation perpendicular to the chord face was very small. In T5 the full width T joint connection ensured that the deformation of the chord face was negligible. Therefore in T4, T5 and T6 the 'connecting element' has been given infinite axial and bending

stiffness. As far as joint rotation is concerned the plating on the connecting chord face, has been assumed to provide a rotational rigidity.

7.4 Comparison of experimental and theoretical behaviour for the gap joint truss

7.4.1 Axial force distribution

From Table 7.2[a] it can be seen that the analytical models give similar values for the axial force distribution. Each model under-estimates the magnitude of the experimentally derived axial forces. The percentage error between the theoretical and experimental values is in most members less than 5%. It was found in measuring the cross-sectional areas from specimen tubes that there was often a variation over a length from the same batch. This, in some cases, was as much as 5%. There are however members where the percentage error between the theoretical and experimental axial forces is in the region of 10% (see Table 7.2[b]). In these cases errors in the measured cross-sectional area could account for the larger difference between the theoretical and experimental values.

7.4.2 Bending moment distribution

The GS model gives a good general representation of the elastic bending moment distribution in the chord members (see Fig. 7.6). The eccentric moment generated by the joint deformation (see section 6.2.4) can be identified as a discontinuity at the joints. Generally this eccentric moment has been overestimated by the theoretical analysis as has the continuity moment. In the case of the branch members the correlation between the experimental and theoretical bending moments is very poor. The theoretical moments are double the magnitude of the experimental, but the sense of the bending is generally predicted correctly.

The bending moment distribution predicted by model GK does not correspond to the experimental in either the branch or the chord members (see Fig. 7.7). The model is only capable of defining the continuity component of the moment distribution in the chord, consequently the sense of bending has been correctly predicted. The sense of the bending is also correctly defined for the branch members, however the magnitude is significantly under-estimated.

7.4.3 Truss deflection

The Pin-jointed frame analysis (P) gives similar results to model GK, but model GS represents a more flexible theoretical structure (see Fig. 7.15[a]). Nevertheless even the latter under-estimates the true deformation behaviour. At the span/360 serviceability limit model GS under-estimates the experimental value by 15%. At ultimate load the discrepancy is of the order of 100%. The most important characteristic is the non-linear behaviour of the experimental deflection, and the fact that the load/deflection behaviour was only approximately linear even at load levels less than 50% of the ultimate load.

7.5 Implications arising from the theoretical modelling of the gap joint truss

It is clear that in order to define the structural behaviour of the noded gap joint truss it is necessary to model the chord face flexibility. Nevertheless, however good the model is in the elastic region the experimental structural performance was non-linear with respect to bending and deformation (see section 6.2). Although the behaviour was never linear for the test truss, non-linearity was more pronounced at loads in excess of 60 kN. At ultimate load the measured bending moment distribution bears little resemblance to the extrapolated experimental distribution (see Fig. 7.8). Therefore, even if the joint deformations had been defined more accurately, the theoretical results would only have been reliable at low load levels. A complex non-linear analysis would be necessary to predict the structural behaviour in the region between serviceability and ultimate load.

In a gap joint there are three ways of increasing the stiffness of a joint :

(i) By decreasing the size of the gap.

(ii) Increasing the branch to chord width ratio, β.

(iii) Decreasing the slenderness of the chord wall, b_0/t_0.

In truss T1 the bending moments and the overall truss deflection were, for ram loads greater than 60 kN, non-linear with respect to the applied ram load. The onset of non-linearity in the graphs of applied load v. local joint deformation also occurred at the 60 kN ram load. In this case the non-linearity was related to yielding of the connecting chord face at the joints. Therefore the extent of the linear region with respect to the bending moments and central deflection is likely to have been determined by the stiffness of the joints.

The conclusions from the Polish research programme[33] were that the experimental bending moments in the gap joint test trusses were greater than those predicted by the 'theoretical micro-bar model'. However, it has not been specified whether this relates to both the chord and branch members, or just the chord. Furthermore, it was found that the experimental central deflection of the trusses was closely predicted. It has not been stated, however, over what load range these deductions were applicable. Although similar conclusions have been made for the Nottingham gap joint truss T1, they only apply at modest applied load levels as indicated above.

The argument that the Polish test trusses have stiffer joints and therefore an extended linear range (ie., for applied ram load v. overall deflection and applied ram load v. bending moment) cannot be used in defending their conclusions. For the majority of the gap joint trusses tested the chord walls were more slender than for T1. Furthermore one of their trusses (K1) was similar to T1. The K1 Warren truss was fabricated from 40x40x3mm RHS branch members and 100x100x3mm RHS chords. The inclination of the branches being 45^0.

For gap joint trusses with flexible joints as in T1 the non-linear joint deformations with respect to the applied load makes any **elastic** frame analysis impractical. The choice as to whether to use 'flexible' (as opposed to 'stiff') gap joints in a truss must remain with the structural engineer. If structural efficiency with respect to strength and serviceability are primary requirements, then 'flexible' gap joints should be avoided. However, where a design calls for a lattice truss fabricated from gap joints it is important that the designer understands the behaviour and limitations of gap joints.

7.6 Comparison of experimental and theoretical behaviour for 100% overlap joint trusses

7.6.1 Axial force distribution derived from a pin-jointed frame analysis

The pin-jointed frame models (see Fig. 7.1[b]) always over-estimate the axial forces in the truss members (for a typical example see Tables 7.3[a] & [b] - taken from Appendix F). In the chord the discrepancy between the theoretical and experimental values lies in the range of 10%-25%. The error is most pronounced in the midspan chord sections. For the branches the discrepancy is greater and generally of the order of 25%-30%, however the error exceeds 50% in the midspan tie members.

By modifying the branch angles and using the true effective depth in the pin-jointed analysis, the errors with respect to the experimental axial forces are reduced. In this case the difference in the theoretical and experimental values is generally less than 5% for the chord members, but still high (less than 20%) in the branch members. The influence of the effective depth and the branch angle on the axial forces derived from a pin-jointed analysis is similar for all the 100% overlap joint trusses, (Table 7.4 relating to truss T3 is typical).

The large difference between the theoretical and experimental axial forces in the branch members is caused by the varying slope of the experimental bending moment distribution in the chord (Fig 7.9 is typical). This causes the chord shears on either side of a joint to be different (see section 6.2.2). In order to establish equilibrium in the direction perpendicular to the connecting chord face the chord shear reduces the axial forces in the branches with respect to those predicted by a pin-jointed analysis. The experimental shear forces in the branch members were negligible (less than 1%) in comparison to the experimental chord axial forces.

The distribution of errors in the theoretical branch member axial forces is greatest along the midspan section and the ends of the trusses. At these locations large changes in the slope of the experimental bending moment distribution occurred across the joint (see Fig. 7.9).

7.6.2 Axial force distributions derived from rigid frame models

For each truss the experimental elastic axial force distribution has been compared with the values derived from the theoretical models. The results are presented in Appendix F.

The S1 and S2 models give similar predictions for the member axial forces (for example see Table 7.2[b]). These theoretical values are generally less than the experimental. The error for the chord and branches is less than 5% and 10% respectively. The Y model gives similar values for the chord forces to those of the S models, but larger errors generally occur in the branch members. These errors are greatest in the branches along the midspan section. The results derived from the K model are the least accurate of all the analyses.

7.6.3 Bending moment distribution in the chord members

For each truss the experimental elastic bending moment distribution has been compared with the values derived from the theoretical models. The results are presented in Appendix G.

For the chord members the best representation of the experimental bending moment distribution is given by S1, S2 and Y (Figs. 7.10, 7.11, 7.12 are typical). The values derived from the K-model are less accurate (Fig 7.13 is typical), but the magnitude of the experimental moments is generally over-estimated.

The S models give similar values. The only difference between S1 and S2 is that there is no moment transfer between the branches and the chord section in the case of the S2. The experimental moments in the branches were small compared to those in the chord. The values of branch bending moment derived from the Y-model differ from those of the S-models only along the midspan section of the compression chord, particularly at the position of the central point load.

Differences with respect to the experimental distribution occur in all the theoretical models along the midspan section of the compression chord. However the S-models do give a more accurate representation than the Y or K models. The theoretical moment at the applied load is sensitive to the joint stiffness. This is demonstrated in Fig. 7.14, relating to truss T3. In distribution (a) the stiffness of the compression chord section under the ram has been set to the same value as the remaining chord section, while in (b) this part of the chord section has been modeled by an infinitely stiff beam element. It can be seen that the bending moment distribution is significantly affected in the compression chord, particularly at the position of the applied ram load. At this position the model in which the infinitely stiff element was used attracts extra bending. Away from the loading point the two analyses indicate better agreement with each other, and in the tension chord the distributions are similar.

This indicates that where the concentrated load was applied to the 100% overlap joint trusses the bending moment in the chord section either side of the ram was sensitive to the stiffness of the joint. Conversely, where there were no applied loads at the joints (ie., away from the midspan section) the chord bending moment distribution is similar for models S1, S2, and Y, indicating that the chord bending moment was not sensitive to the joint stiffness.

Normally trusses are subject to uniformally distributed loads (U.D.L's) from floors or roofs. This usually involves transferring the loads to the truss at the joints by some form of secondary structure such as purlins. The test trusses were loaded only at the midspan joint. It is therefore difficult to assess the influence of the joint stiffness on the chord bending moment distribution for a 100% overlap joint truss subject to a U.D.L. It is likely, however, that there is a range of b_0/t_0 and β for which a Y type model would be adequate in analysing 100% overlap trusses subject to a U.D.L.

7.6.4 Bending moment distribution in the branch members

For the branch members models S1, Y and K always over-estimate the experimental moments, while S2 under-estimates the values. Furthermore S1 and Y give similar values, while those of K are larger in magnitude.

None of the models give a reliable prediction for the sense of the branch bending moments. The sense and magnitude of the bending moments is influenced by the rotational stiffness of the joint which is sensitive to the weld detailing - this is discussed in section 6.3.3. Therefore, an accurate representation of the branch moments cannot be deduced from simple rigid frame models. However, it is encouraging that the magnitude of the bending moments is over-estimated by those analyses where the branches are rigidly connected to the chord section (namely models, S1, Y, and K).

7.6.5 Truss Deflection

Up to the serviceability limit of span/360 all the models give estimates of the central deflection which agree with the experimental to within 5% (for example see Figs. 7.15, 7.16, and 7.17). The prediction afforded by a pin-jointed analysis corresponds to that defined by the K-model. The values derived by S1, S2, and Y are similar but differ from those of the P and K-models. The S1, S2 and Y models generally under-estimate the central deflection, while the P and K models give over-estimates. The fact that all the analyses give similar results indicates that joint deformation did not significantly influence the overall deflection. Truss deflection was, therefore, governed by the axial stiffness of the members.

7.7 Implications arising from the theoretical modelling of the 100% overlap joint trusses

There was little difference in the experimental axial force, bending moment or

deflection and the corresponding theoretical values derived from models S1 and Y. For the range of parameters studied (ie., $\beta < 0.6$; $b_0/t_0 < 25$) the influence of the joint stiffness on the structural behaviour was negligible. Hence, there is little merit in simulating the deformation of the connecting chord face. However, for slender chord sections the joint stiffness may be more important.

The Y-type frame analysis provides a simple and practical tool for assessing the elastic axial forces, bending moments and overall deflection of 100% overlap joint trusses. It is important, therefore, to assess more precisely the range of parameters (β, and b_0/t_0) for which this form of analysis is applicable, particularly for 100% overlap joint trusses subject to a U.D.L.

Designers normally assume that the bending stress in the chord section can be evaluated by distributing the eccentricity moment equally either side of the joint. For the design of the critical chord section this bending stress is combined with the axial force derived from a pin-jointed frame analysis. In the test trusses there was a continuity bending moment in both the tension and compression chords which was caused by the overall truss deflection. The assumption that the bending moment in the chord is the same either side of a joint is therefore incorrect (Fig. 7.9 is typical) - this simplified design technique is not recommended.

Table 7.1 Chord face stiffness co-efficients derived from the experimental results.

Truss	Chord wall thickness t_0 mm	Stiffness Co-efficient Γ $kNmm^{-1}$	
T1	4.0	65	
	5.0	75	
T2	4.0	21	
	5.0	41	
T3	5.0	43	
T4	5.0	93	
T5	5.0	40	tie overlaps strut
		70	strut overlaps tie
T6	6.3	27	

Notes :

1) Refer to Fig 7.3 for the definitions relating to chord face stiffness co-efficients.
2) Chord face stiffness co-efficients were evaluated for each joint . For truss T1 there were two values for each joint while in the 100% overlap joint trusses only one value was derived for each joint.

The following simplifications have been made :

Gap joint truss

(i) For each joint the mean of Γ_1 and Γ_2 (see Fig 7.3) was calculated, so that the same value was used for the chord face stiffness under the tension and compression branches.
(ii) Mean values for each chord thickness were then evaluated (ie.,the 4mm and 5mm thick chord sections were considered separately). Therefore, two joint stiffness co-efficients have been derived for the gap joint truss, one for the 4mm thick chord section and another for the 5mm thick section.
(iii) The variation in chord face deformation that was observed in the test truss between corresponding tension and compression chord joints has not been incorporated into Model GS.

100% overlap joint trusses

(i) A chord face stiffness co-efficient was derived for each joint. A mean value was then calculated for each truss.
(ii) In truss T2 where there were two different chord thicknesses, a chord face stiffness co-efficient was evaluated for for each chord section thickness.
(iii) In truss T5, due to the absence of symmetry in the joint geometry, the chord face stiffness of the joints where the tie overlapped the strut was different to that where the strut overlapped the tie, therefore two different values have been derived for this truss.

Table 7.2(a) Experimental and theoretical elastic axial force co-efficients for truss T1.

Member	Axial force co-efficients (kN per 1 kN of applied load)			
	Experimental	Theoretical models		
		P	GS	GK
	X_e	X_1	X_2	X_3
1	-0.02	0.00	0.06	0.04
2	0.96	0.93	0.92	0.92
3	1.91	1.87	1.85	1.85
4	2.98	2.80	2.77	2.78
5	3.93	3.73	3.64	3.65
6	2.86	2.80	2.77	2.78
7	1.93	1.87	1.85	1.85
8	0.93	0.93	0.92	0.92
9	0.03	0.00	0.06	0.04
10	0.48	-0.47	-0.46	-0.46
11	1.43	-1.40	-1.38	-1.39
12	2.36	-2.33	-2.31	-2.31
13	3.21	-3.27	-3.20	-3.21
14	3.27	-3.27	-3.20	-3.21
15	2.36	-2.33	-2.31	-2.31
16	1.44	-1.40	-1.38	-1.39
17	0.48	-0.47	-0.46	-0.46
18	0.64	0.68	0.58	0.61
19	0.67	-0.68	-0.65	-0.67
20	0.69	0.68	0.66	0.68
21	0.69	-0.68	-0.66	-0.68
22	0.68	0.68	0.66	0.68
23	0.70	-0.68	-0.66	-0.68
24	0.64	0.68	0.61	0.64
25	0.69	-0.68	-0.64	-0.64
26	0.69	-0.68	-0.64	-0.64
27	0.65	0.68	0.61	0.64
28	0.71	-0.68	-0.66	-0.68
29	0.69	0.68	0.66	0.68
30	0.68	-0.68	-0.66	-0.68
31	0.68	0.68	0.66	0.68
32	0.72	-0.68	-0.65	-0.67
33	0.64	0.68	0.58	0.61
34	0.51	0.50	-0.45	-0.46
35	0.51	0.50	-0.45	-0.46

Notes :
1) To be read in conjunction with Fig S1.
2) Forces shown are per 1 kN of applied ram load.
3) Experimental co-efficients have been derived from the measured strain gauge values at the 50 kN ram load.
4) For definition of theoretical models see Chapter 7.

Table 7.2(b) Comparison of experimental and theoretical elastic axial forces for truss T1.

Member	Percentage difference between theoretical and experimental values $(X_n-X_e).100/X_e$		
	P	GS	GK
2	-2.9%	-4.2%	-4.5%
3	-2.5%	-3.6%	-3.6%
4	-6.0%	-6.9%	-6.8%
5	-4.9%	-7.2%	-7.1%
6	-2.1%	-3.0%	-3.0%
7	-3.5%	-4.6%	-4.6%
8	0.5%	-0.8%	-1.1%
10	-2.5%	-4.2%	-3.8%
11	-2.2%	-3.3%	-3.2%
12	-1.3%	-2.3%	-2.2%
13	1.9%	-0.1%	0.1%
14	-0.1%	-2.0%	-1.8%
15	-1.0%	-2.0%	-2.0%
16	-2.9%	-4.0%	-4.0%
17	-2.9%	-4.6%	-4.2%
18	6.2%	-9.3%	-5.3%
19	2.1%	-2.5%	-0.4%
20	-0.7%	-4.4%	-1.0%
21	-0.6%	-4.8%	-1.9%
22	0.1%	-3.2%	-0.6%
23	-1.6%	-5.5%	-2.6%
24	6.2%	-4.7%	-1.4%
25	-0.4%	-7.4%	-6.3%
26	-1.4%	-8.4%	-7.2%
27	5.7%	-5.1%	-1.9%
28	-3.7%	-7.5%	-4.6%
29	-1.4%	-4.8%	-2.2%
30	0.6%	-3.7%	-0.7%
31	0.4%	-3.2%	0.1%
32	-4.5%	-8.8%	-6.8%
33	7.7%	-8.0%	-3.9%
34	-2.7%	-13.2%	-10.3%
35	-1.8%	-12.4%	-9.4%

Notes :
1) To be read in conjunction with Figs S1.
2) Forces shown are per 1 kN of applied ram load.
3) Experimental co-efficients have been derived from the measured strain gauge values at a ram load of 50 kN.
4) For definition of theoretical models see Chapter 7.

Table 7.3(a) Experimental and theoretical elastic axial force co-efficients for truss T3.

Member	Axial force co-efficients (kN per 1 kN of applied load)					
	Experimental	Theoretical models				
		P	S1	S2	Y	K
	X_e	X_1	X_2	X_3	X4	X5
1	0.26	0.25	0.26	0.26	0.25	0.25
2	0.67	0.75	0.68	0.68	0.69	0.67
3	1.02	1.25	1.03	1.03	1.03	0.99
4	0.66	0.75	0.68	0.68	0.69	0.67
5	0.25	0.25	0.26	0.26	0.25	0.25
6	-0.06	0.00	-0.06	-0.06	-0.06	-0.08
7	-0.46	-0.50	-0.47	-0.47	-0.47	-0.46
8	-0.80	-1.00	-0.84	-0.84	-0.84	-0.82
9	-0.79	-1.00	-0.84	-0.84	-0.84	-0.82
10	-0.45	-0.50	-0.47	-0.47	-0.47	-0.46
11	-0.05	0.00	-0.06	-0.06	-0.06	-0.08
12	-0.44	-0.56	-0.44	-0.44	-0.41	-0.37
13	0.47	0.56	0.46	0.47	0.49	0.47
14	-0.47	-0.56	-0.46	-0.47	-0.48	-0.45
15	0.38	0.56	0.37	0.37	0.35	0.33
16	-0.43	-0.56	-0.42	-0.43	-0.41	-0.40
17	-0.44	-0.56	-0.42	-0.43	-0.41	-0.40
18	0.39	0.56	0.37	0.37	0.35	0.33
19	-0.46	-0.56	-0.46	-0.47	-0.48	-0.45
20	0.48	0.56	0.46	0.47	0.49	0.47
21	-0.43	-0.56	-0.44	-0.44	-0.41	-0.37
22	-0.06	0.00	-0.07	-0.06	-0.09	-0.12
23	-0.06	0.00	-0.07	-0.06	-0.09	-0.12

Notes :

1) To be read in conjunction with Fig S1.
2) Forces shown are per 1 kN of applied ram load.
3) Experimental co-efficients have been derived from the measured strain gauge values at a ram load of 200 kN.
4) For definition of theoretical models see Chapter 7.

Table 7.3(b) Comparison of experimental and theoretical elastic axial forces for truss T3.

Member	Percentage difference between theoretical and experimental values $(X_n-X_e).100/X_e$				
	P	S1	S2	Y	K
1	-2.3%	0.0%	0.0%	-3.5%	-2.0%
2	12.4%	1.5%	1.3%	2.7%	0.1%
3	22.1%	0.8%	0.9%	0.2%	-3.0%
4	13.1%	2.1%	1.9%	3.3%	0.8%
5	-0.8%	1.6%	1.7%	-2.0%	-0.4%
6		-4.9%	-5.4%	-1.6%	36.1%
7	9.9%	2.4%	2.6%	2.6%	1.5%
8	24.4%	5.0%	4.9%	4.9%	1.4%
9	26.1%	6.4%	6.3%	6.3%	2.8%
10	10.1%	2.6%	2.8%	2.9%	1.8%
11		26.1%	25.4%	30.4%	80.4%
12	28.2%	0.0%	1.3%	-6.0%	-15.6%
13	18.9%	-1.3%	0.3%	3.8%	-0.4%
14	19.7%	-1.3%	0.1%	1.7%	-3.9%
15	47.9%	-2.6%	-1.0%	-7.9%	-14.0%
16	28.8%	-3.2%	-1.9%	-5.8%	-7.8%
17	25.9%	-5.4%	-4.1%	-7.9%	-9.9%
18	44.1%	-5.2%	-3.5%	-10.3%	-16.2%
19	21.3%	0.0%	1.4%	3.0%	-2.6%
20	17.4%	-2.5%	-1.0%	2.5%	-1.7%
21	30.0%	1.4%	2.7%	-4.7%	-14.4%
22		0.0%	14.4%	65.5%	121.8%
23		1.9%	6.6%	54.2%	106.8%

Notes :

1) To be read in conjunction with Fig S1.
2) Forces shown are per 1 kN of applied ram load.
3) Experimental co-efficients have been derived from the measured strain gauge values at a ram load of 200 kN.
4) For definition of theoretical models see Chapter 7.

Table 7.4 Comparison of experimental and theoretical axial force co-efficients for two types of pin-jointed frame analysis.(truss T3)

Member	Axial force co-efficients (kN per kN of applied ram load)		
	Experimental	Pin 1	Pin 2
1	0.26	0.25	0.22
2	0.67	0.75	0.65
3	1.02	1.25	1.08
4	0.66	0.75	0.65
5	0.25	0.25	0.22
6	-0.06	0	0
7	-0.46	-0.5	-0.43
8	-0.8	-1	-0.87
9	-0.79	-1	-0.87
10	-0.45	-0.5	-0.43
11	-0.05	0	0
12	-0.44	-0.56	-0.54
13	0.47	0.56	0.54
14	-0.47	-0.56	-0.54
15	0.38	0.56	0.54
16	-0.43	-0.56	-0.54
17	-0.44	-0.56	-0.54
18	0.39	0.56	0.54
19	-0.46	-0.56	-0.54
20	0.48	0.56	0.54
21	-0.43	-0.56	-0.54
22	-0.06	0	0
23	-0.06	0	0

Notes :

1) To be read in conjunction with Fig S1.
2) Forces shown are per 1 kN of applied ram load.
3) Experimental co-efficients have been derived from the measured strain gauge values at a ram load of 200 kN.
4) Pin 1 is equivalent to the pin-jointed frame analysis shown in Fig 7.1[b]. In this model the effective depth is equivalent to the distance between the connecting chord faces. The theoretical effective depth is, therefore, less than the true effective depth, but the true branch angle, θ has been used in the calculation of the axial forces.
5) Pin 2 is equivalent to a pin-jointed frame analysis where the effective depth is equivalent to the true effective depth ie., the distance between the chord centre-lines. In this model the branch angle that has been used to calculate the axial forces is greater than the true branch angle, θ.

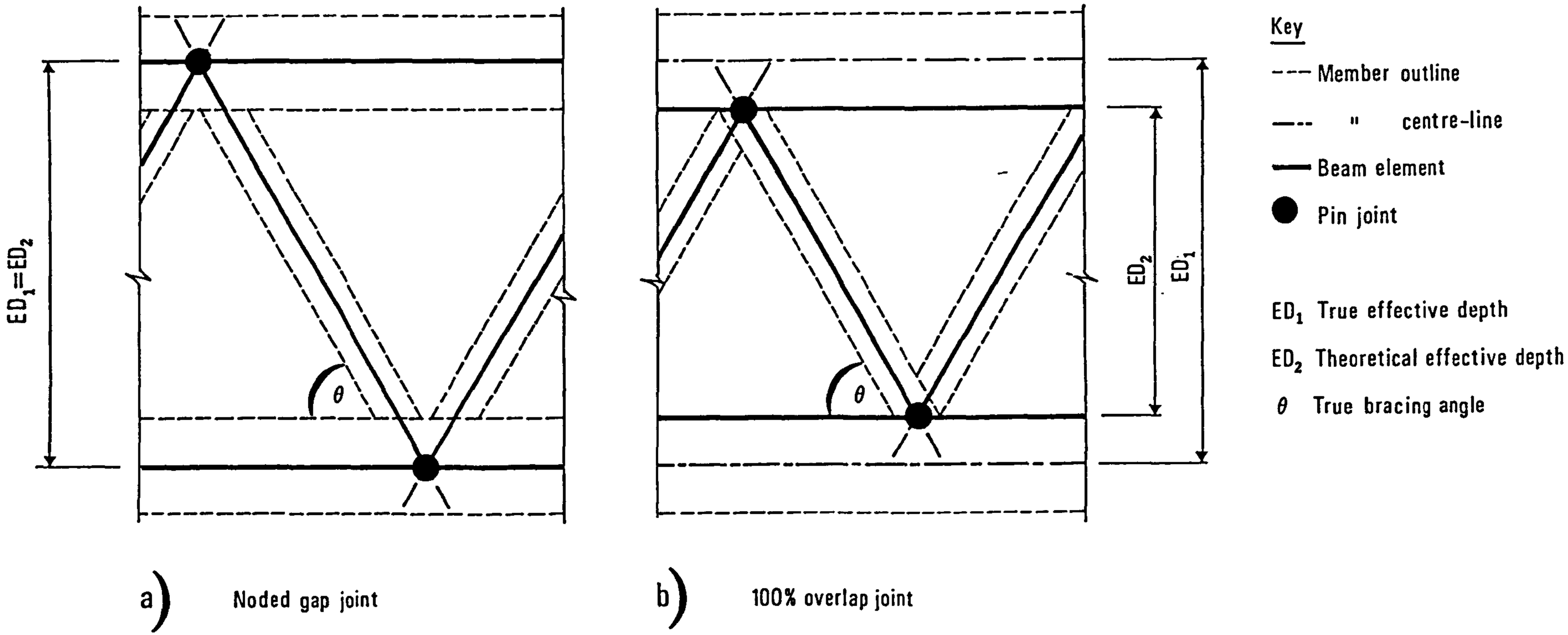

Fig 7.1 Pin-jointed frame modelling of gap and 100% overlap joints.

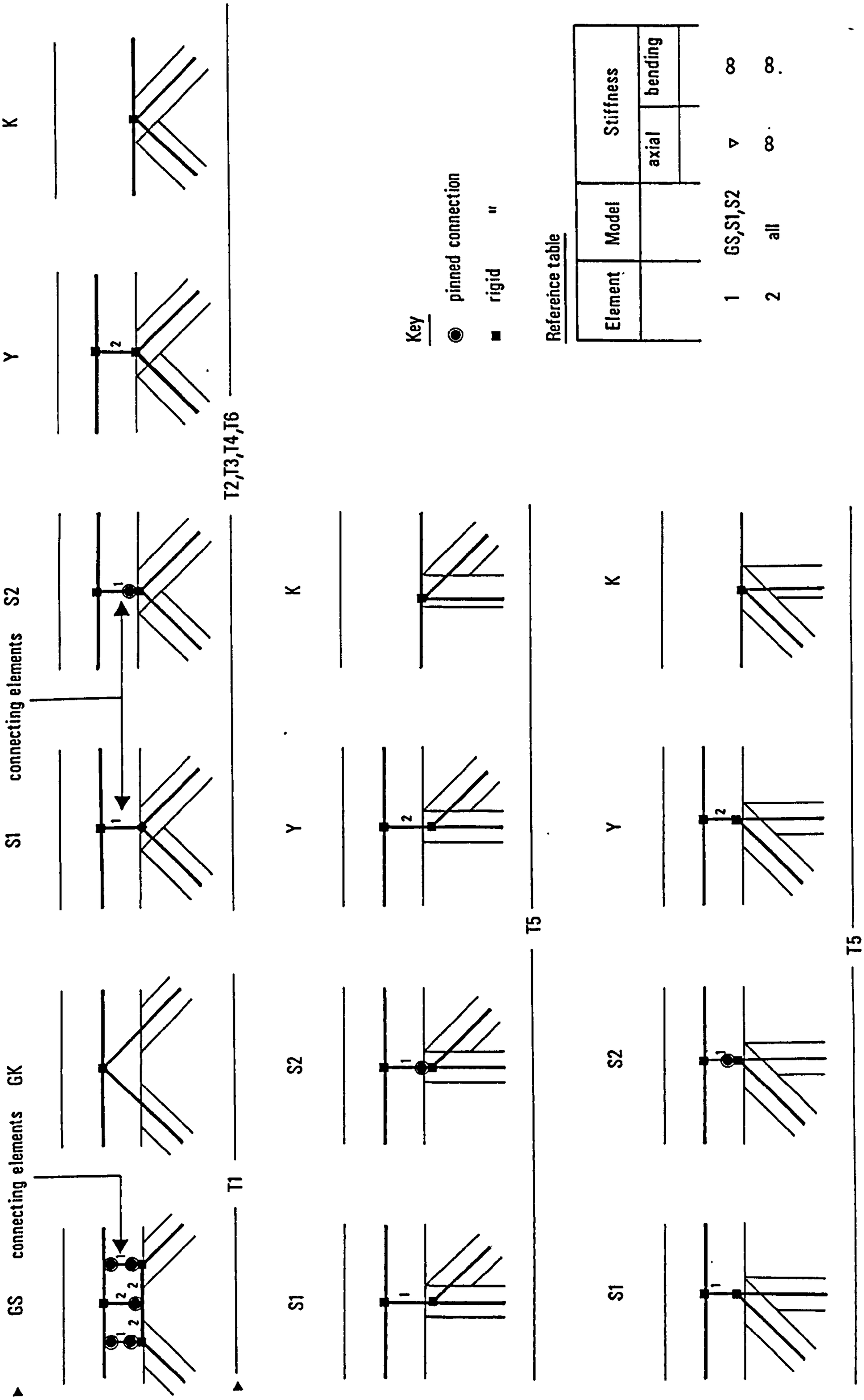

Fig 7.2 Plane frame modelling of gap and 100% overlap joints. (see also Table 7.1)

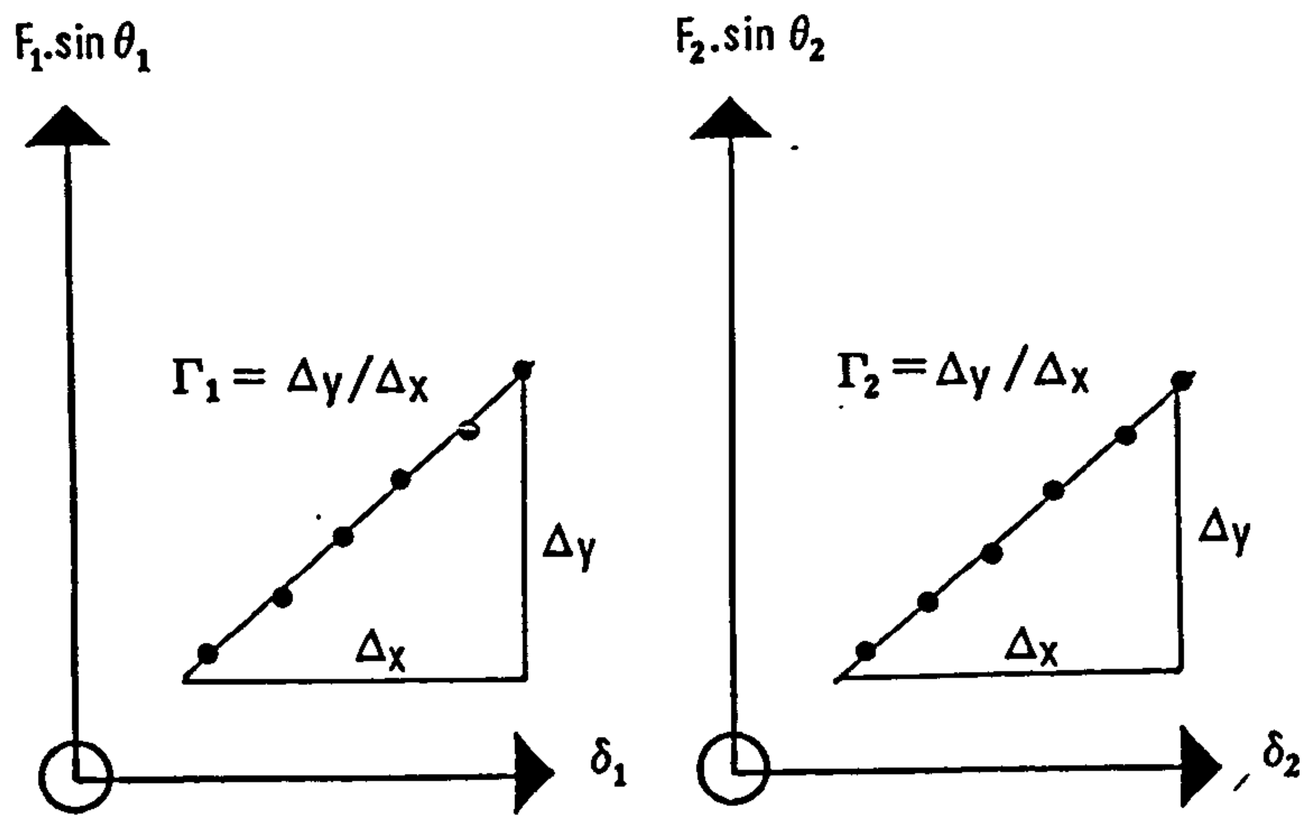

Note

Chord face stiffeness was evaluated for each joint

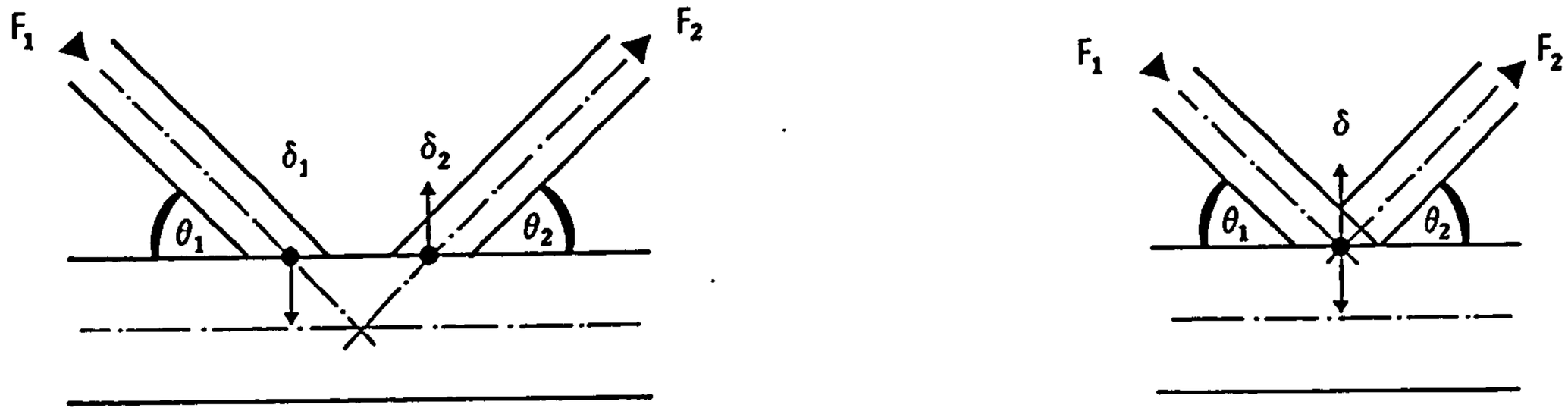

a) Gap joint

b) 100% overlap joint

Fig 7.3 Determination of chord face stiffness co-efficients from the experimental data. (see also Table 7.1)

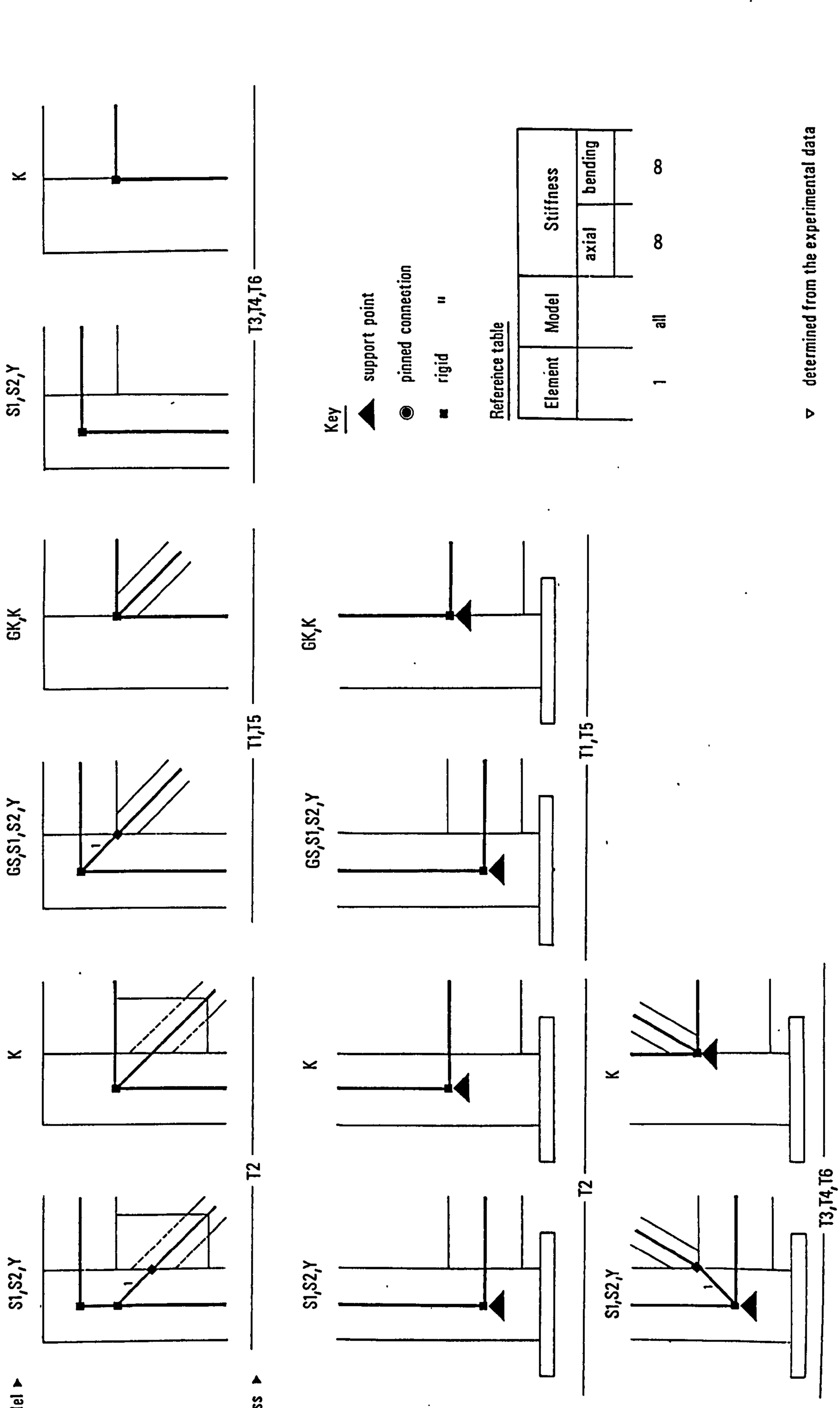

Fig 7.4 Plane frame modelling of corner joints.

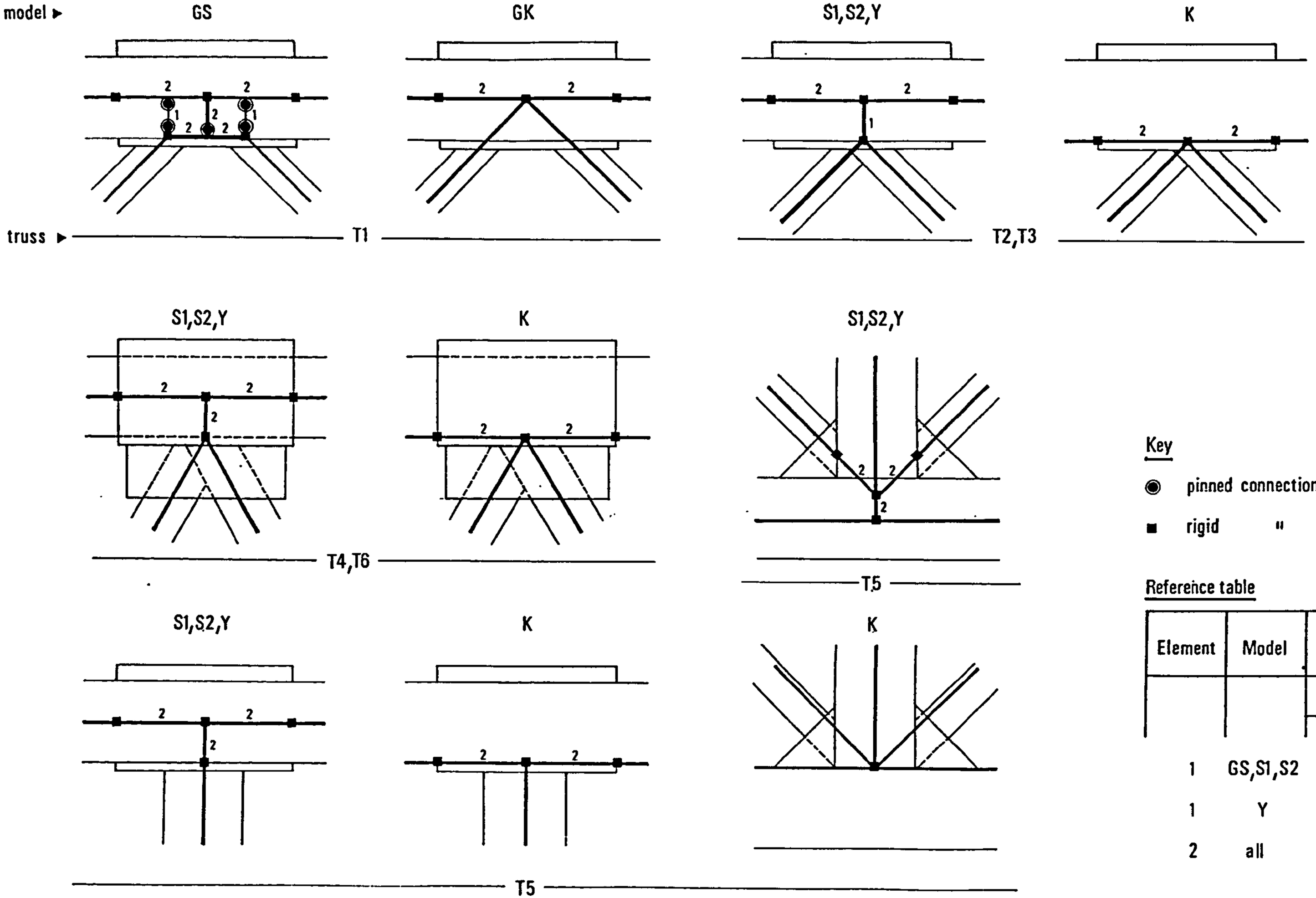

Fig 7.5 Plane frame modelling of midspan joints.

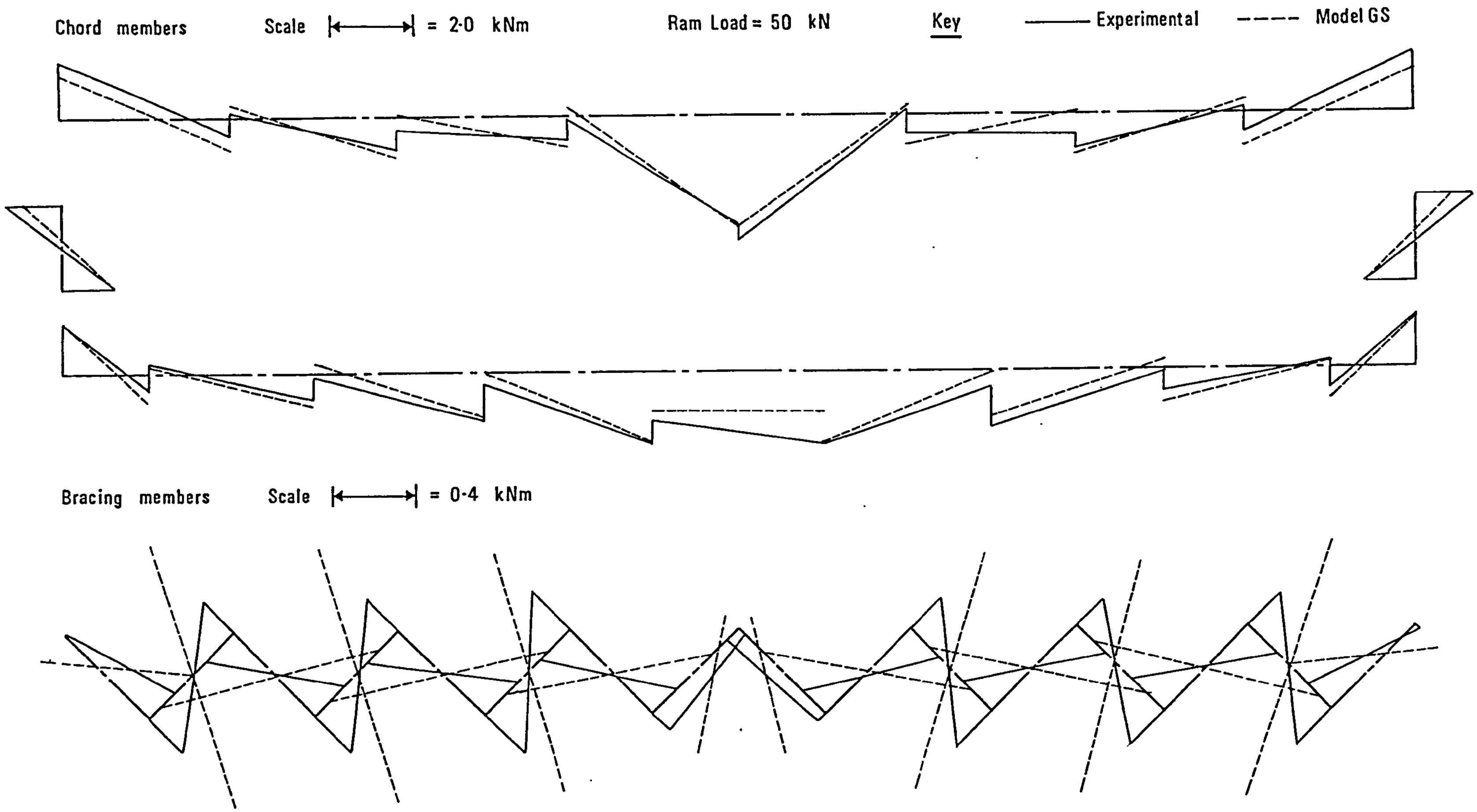

Fig 7.6 Truss T1 : Comparison of experimental and theoretical (model GS) elastic bending moment distributions.
(the bending moment diagrams have been plotted on the side of the member where the stress induced by the bending moment is tensile)

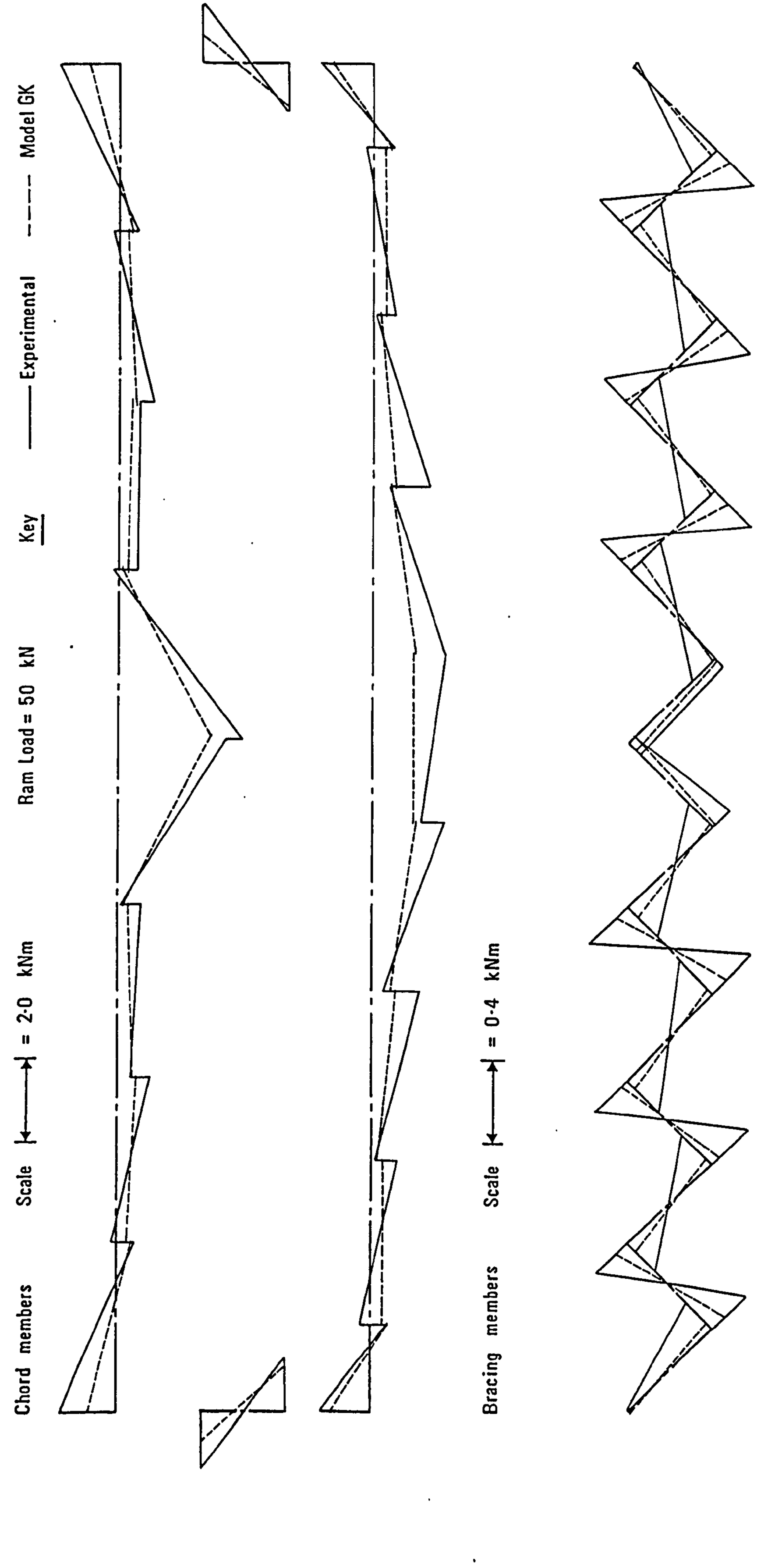

Fig 7.7 Truss T1 : Comparison of experimental and theoretical (model GK) elastic bending moment distributions.
(the bending moment diagrams have been plotted on the side of the member where the stress induced by the bending moment is tensile)

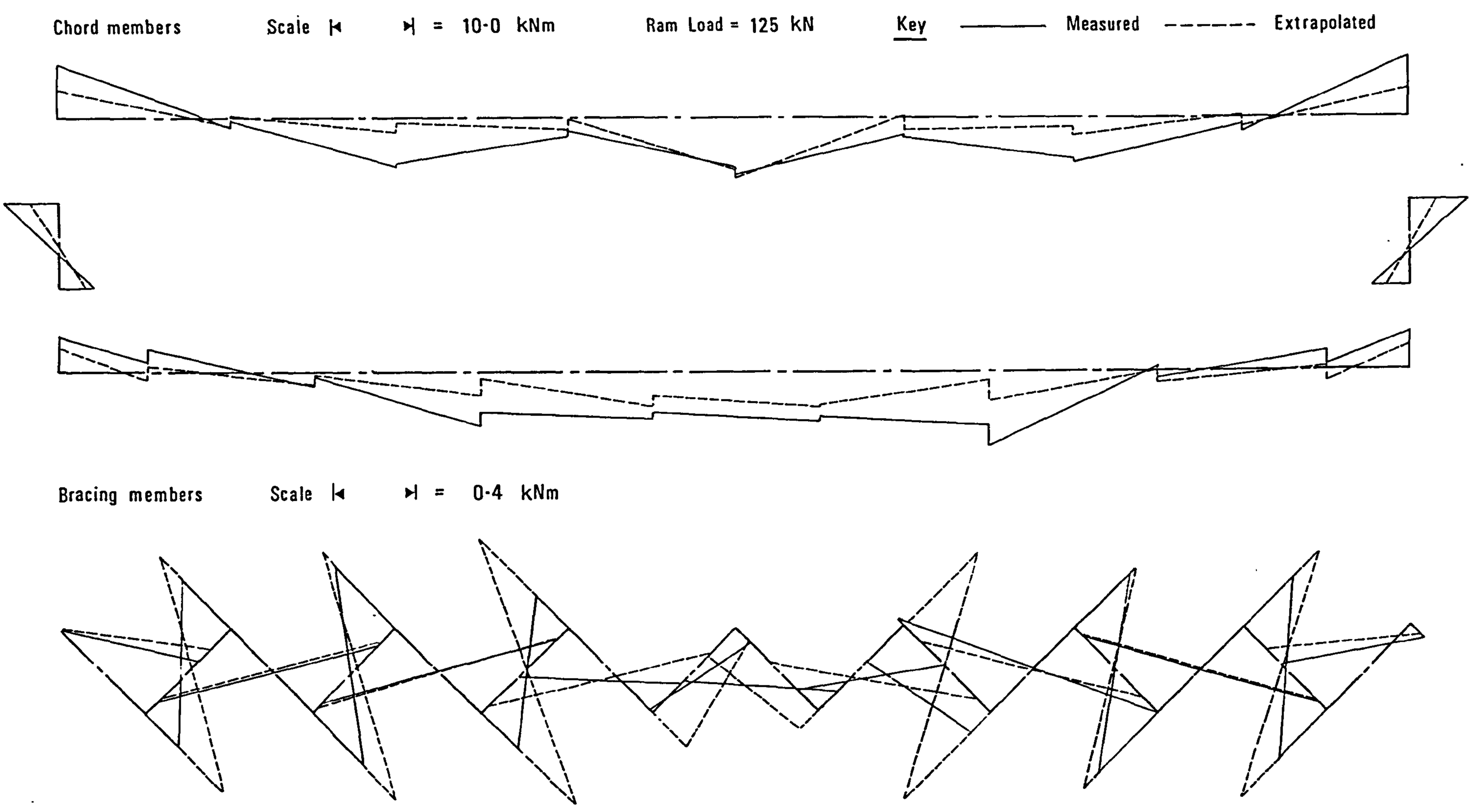

Fig 7.8 Truss T1 : Comparison of the measured bending moment distribution at truss ultimate load with the experimental elastic distribution extrapolated to the ultimate load.
(the bending moment diagrams have been plotted on the side of the member where the stress induced by the bending moment is tensile)

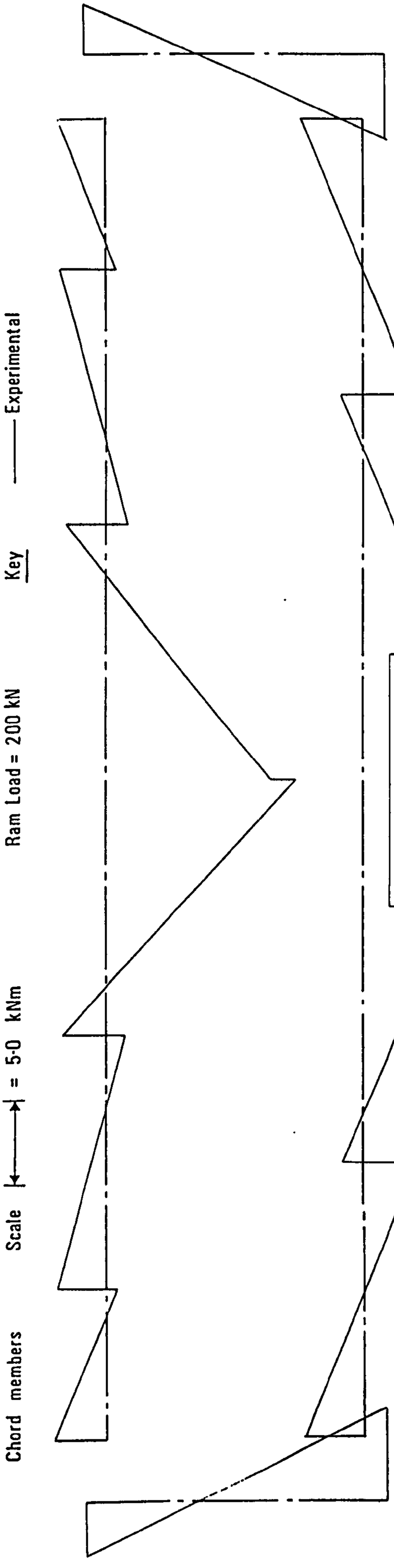

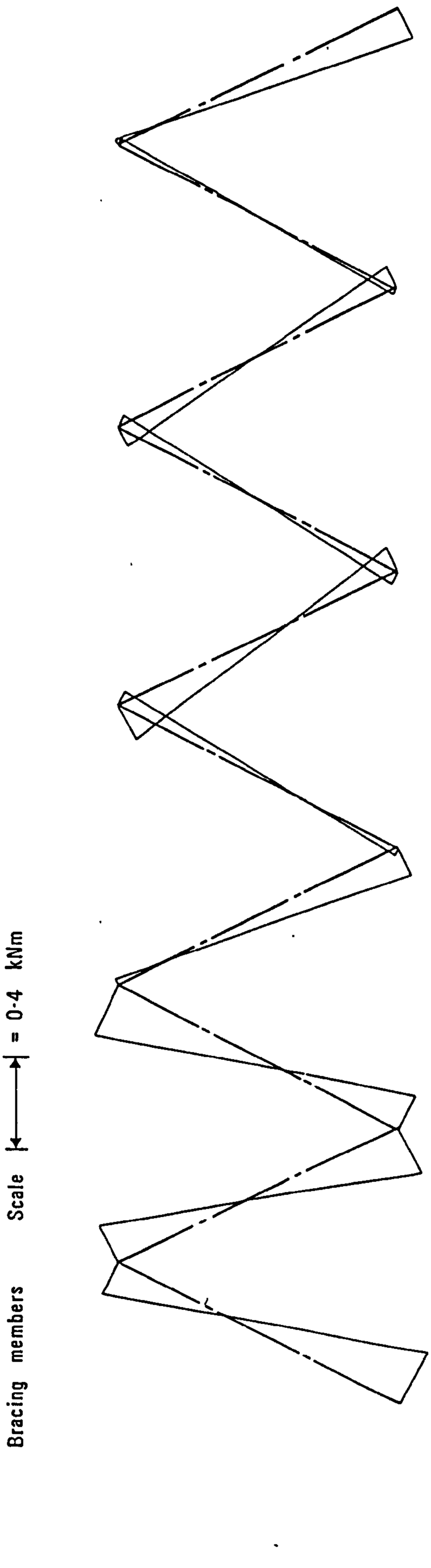

Fig 7.9 Experimental elastic bending moment distribution for truss T3.
(the bending moment diagram has been plotted on the side of the member where the stress induced by the bending moment is tensile)

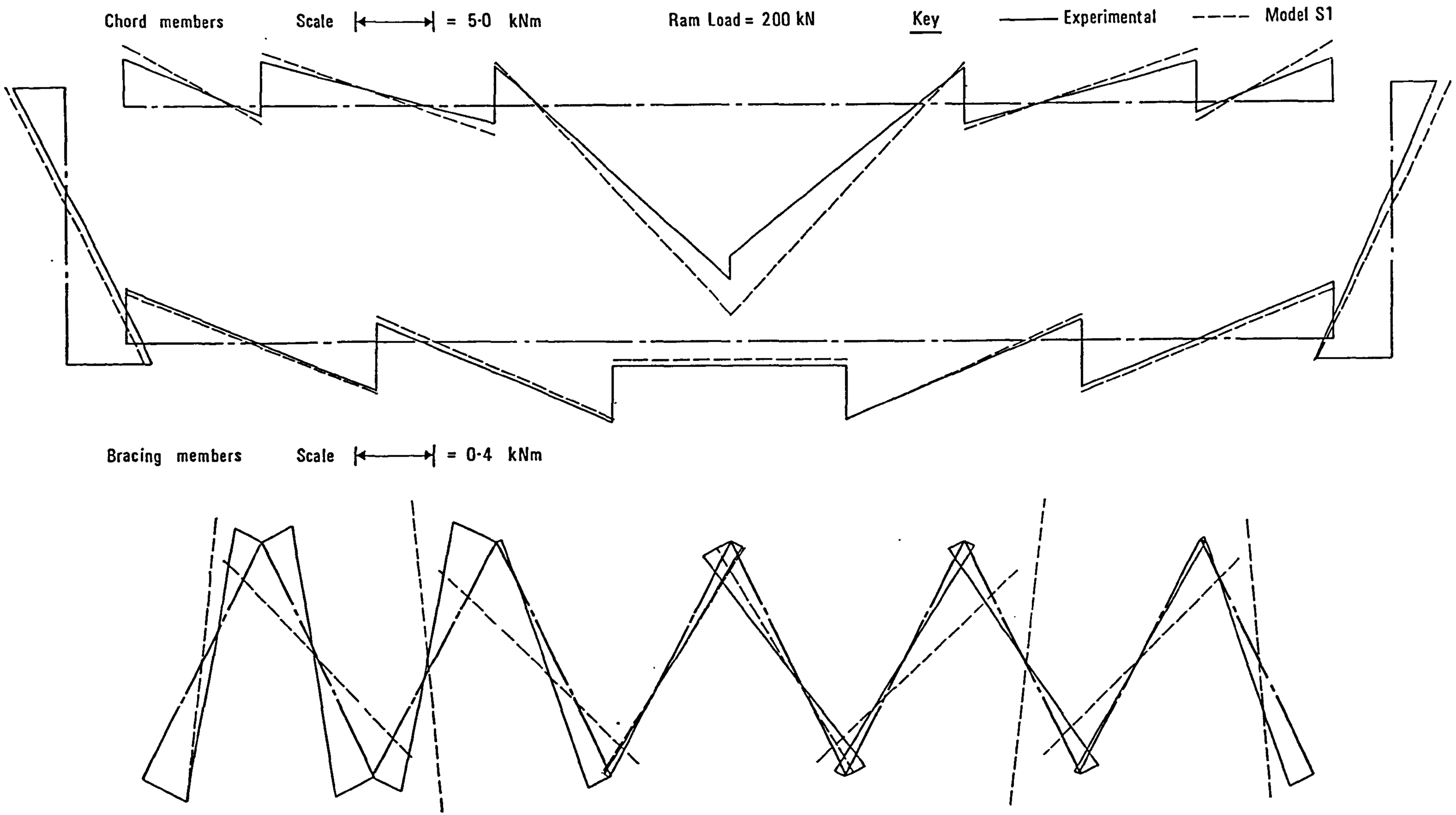

Fig 7.10 Truss T3 : Comparison of experimental and theoretical (model S1) elastic bending moment distributions.
(the bending moment diagrams have been plotted on the side of the member where the stress induced by the bending moment is tensile)

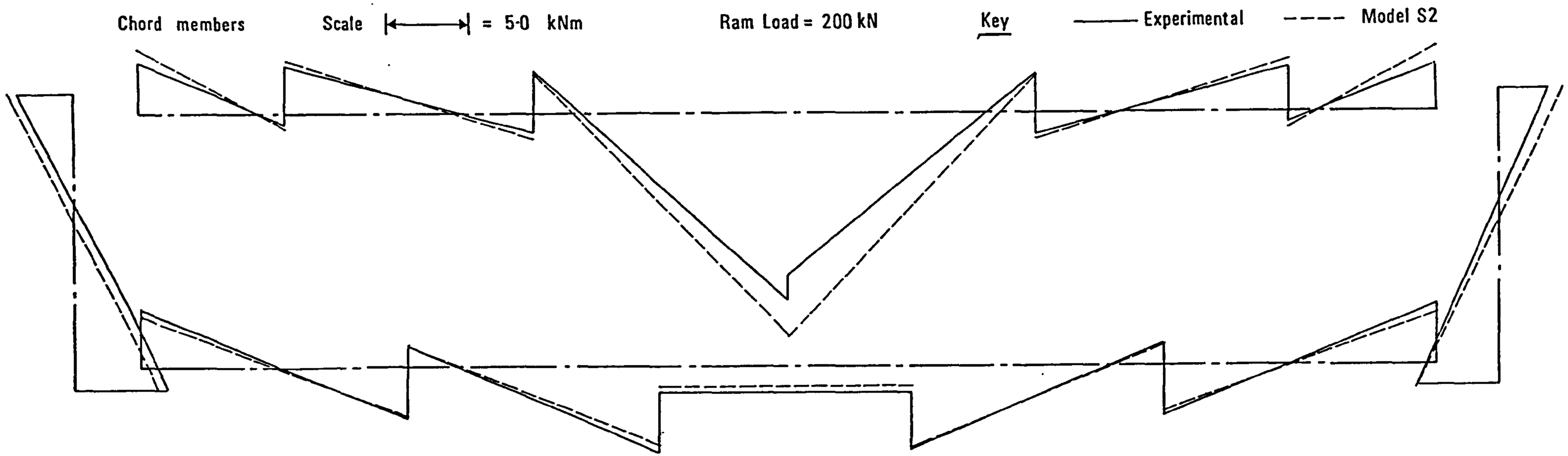

Fig 7.11 Truss T3 : Comparison of experimental and theoretical (model S2) elastic bending moment distributions.
(the bending moment diagrams have been plotted on the side of the member where the stress induced by the bending moment is tensile)

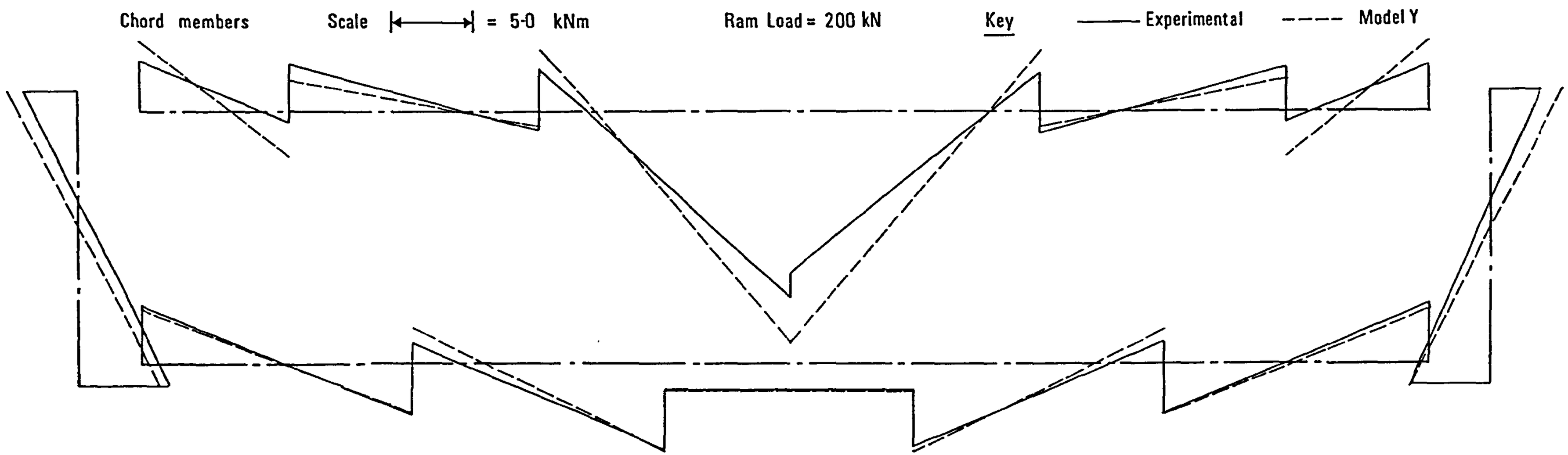

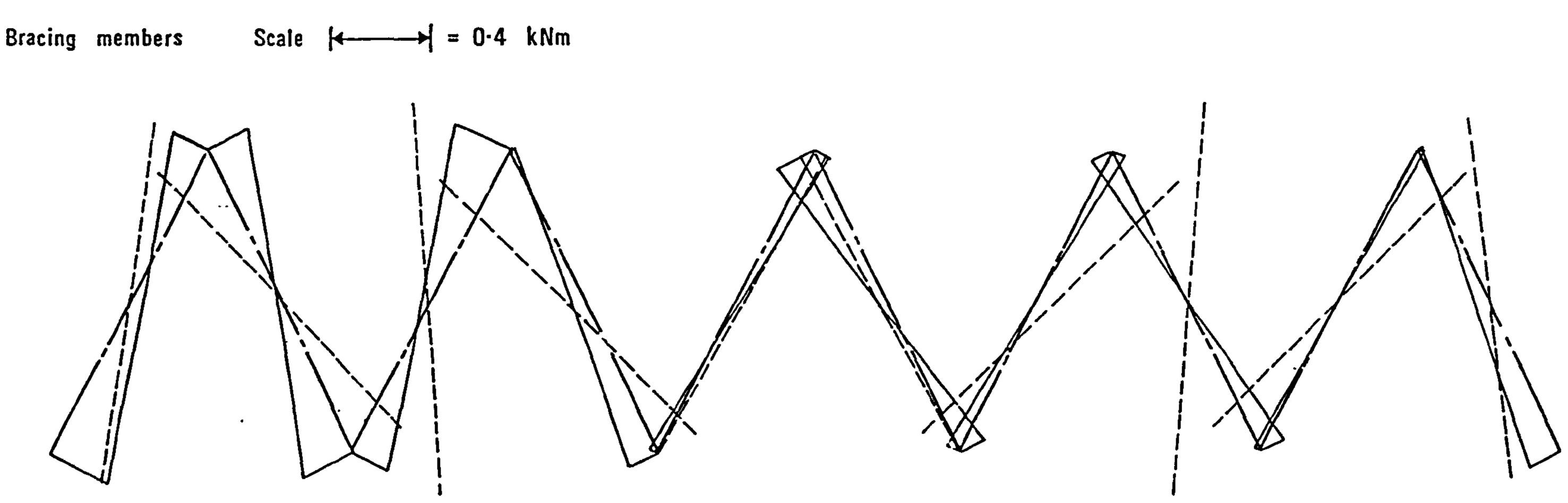

Fig 7.12 Truss T3 : Comparison of experimental and theoretical (model Y) elastic bending moment distributions.
(the bending moment diagrams have been plotted on the side of the member where the stress induced by the bending moment is tensile)

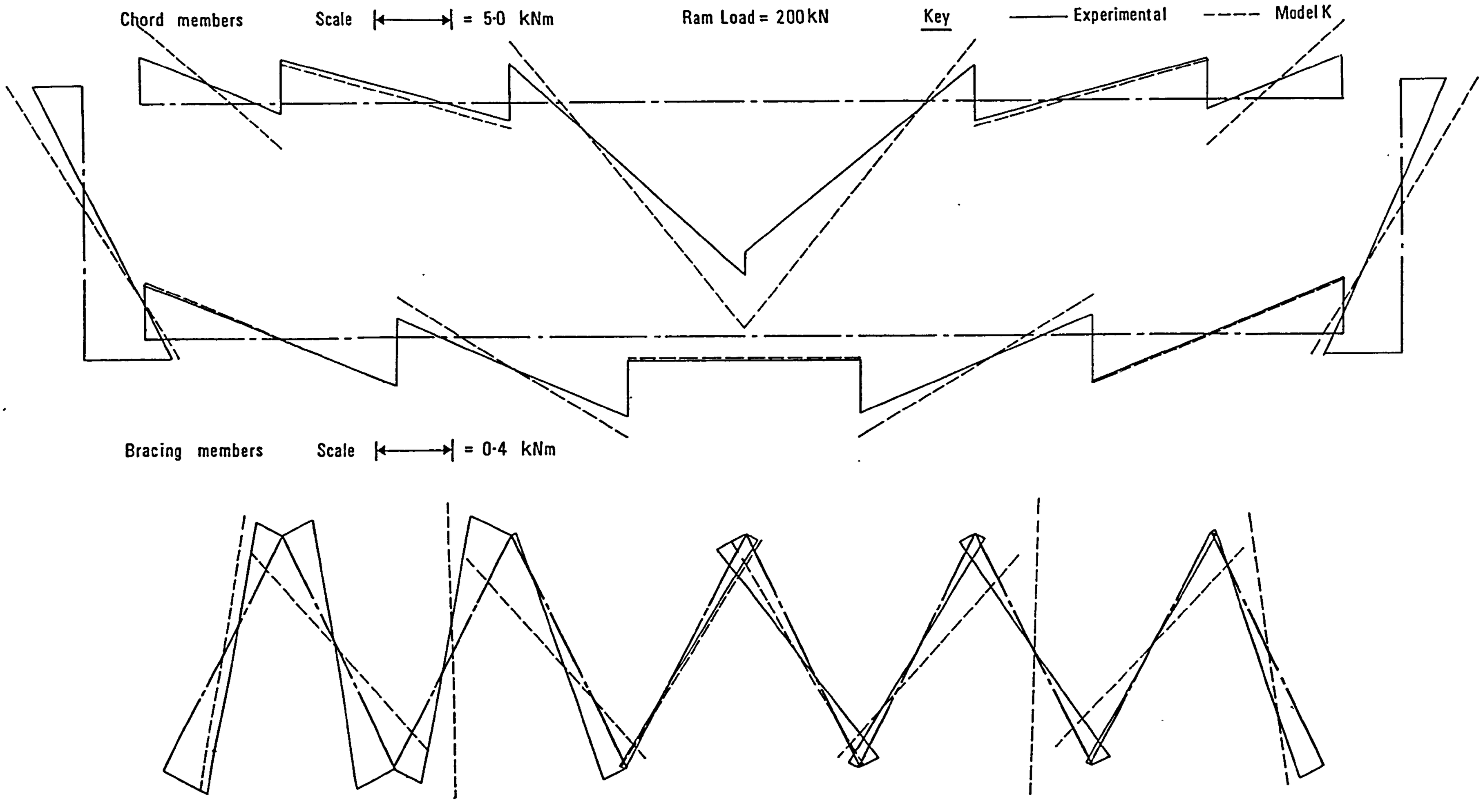

Fig 7.13 Truss T3 : Comparison of experimental and theoretical (model K) elastic bending moment distributions.
(the bending moment diagrams have been plotted on the side of the member where the stress induced by the bending moment is tensile)

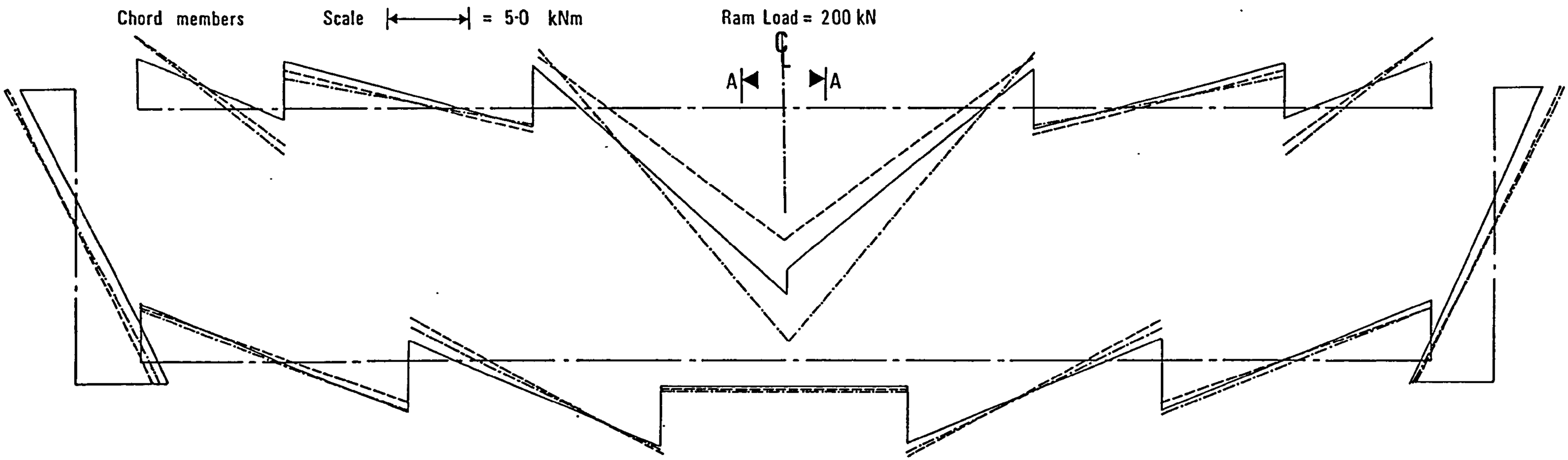

Key

—— Experimental

a – – – Model Y with axial and bending stiffness of chord length AA equivalent to chord section (AA = 250 mm)

b –·–·– " " " " " " " " " " " = ∞

Fig 7.14 Truss T3 : The effect of central joint chord bending stiffness on the theoretical chord bending moments.
(the bending moment diagrams have been plotted on the side of the member where the stress induced by the bending moment is tensile)

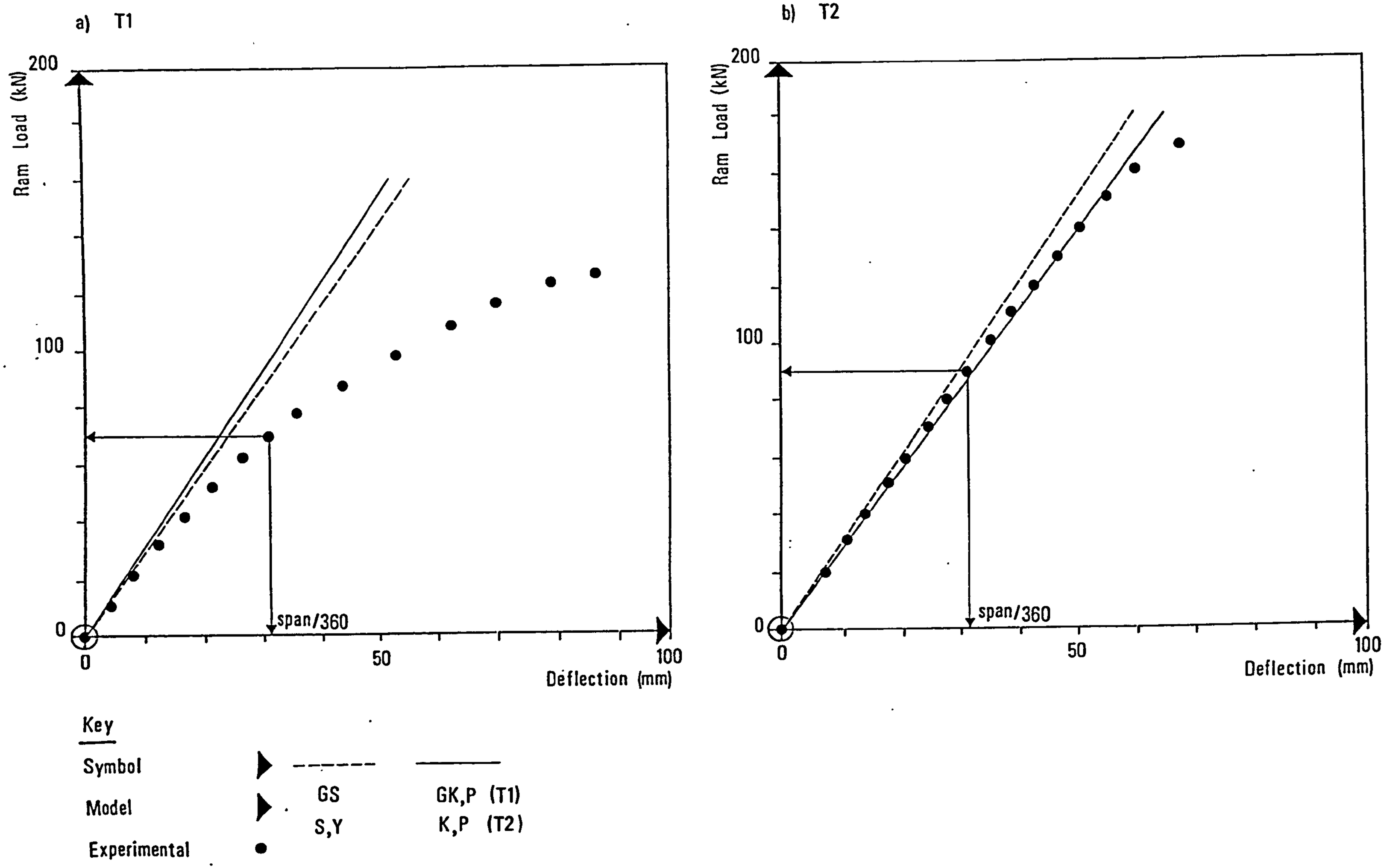

Fig 7.15 Comparison of experimental and theoretical overall deflections at midspan for trusses T1 and T2.

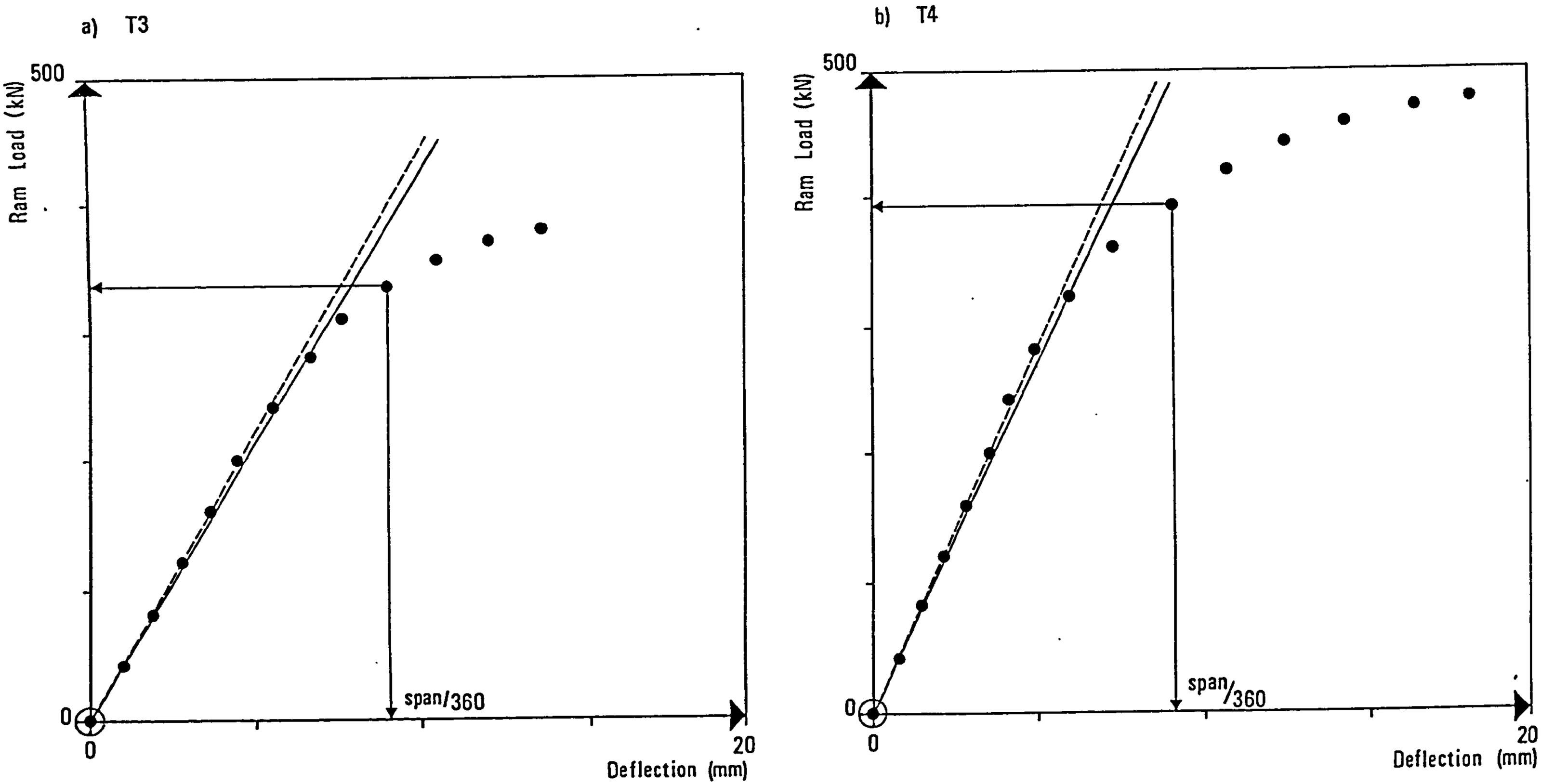

Fig 7.16 Comparison of experimental and theoretical overall deflections at midspan for trusses T3 and T4.

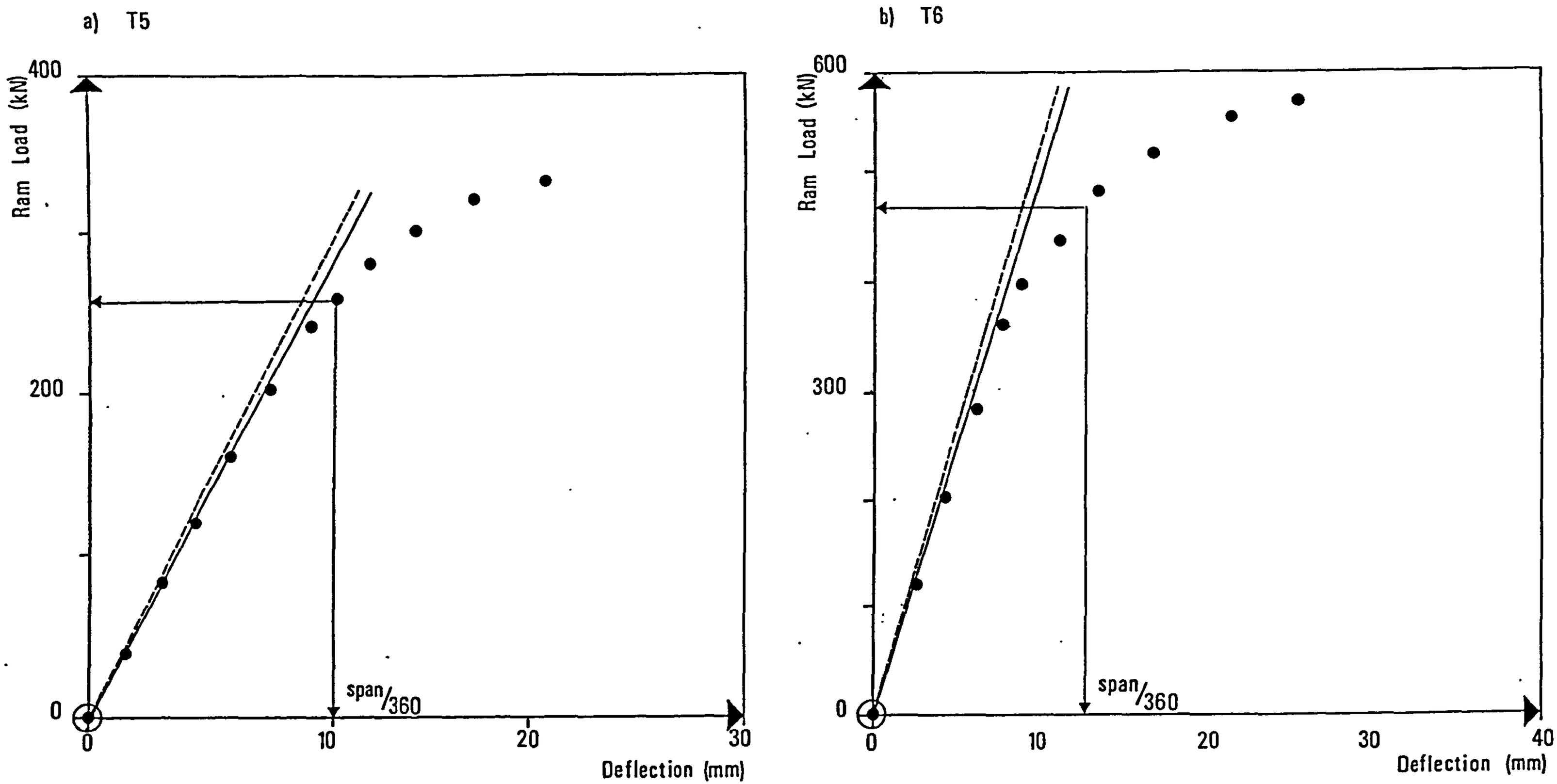

Fig 7.17 Comparison of experimental and theoretical overall deflections at midspan for trusses T5 and T6.

CHAPTER 8
JOINT ULTIMATE STRENGTH

8.1 Introduction

Different strength models and formulae have been developed for the failure modes associated with RHS gap and overlap joints - these are described in detail in CIDECT Monograph 6[43]; some have been derived theoretically while others are substantially empirical. In some cases it has been possible to predict the joint strength by only one or two governing failure modes. Normally joint ultimate strength is used as the design criterion, but the CIDECT design recommendations and limits of validity are set so that a limit state for deformation will not be exceeded at the service load.

A summary of the critical equations for determination of the mean and characteristic strengths of K and N gap joints with RHS chords and branches is given in Table I1 of Appendix I. The ultimate strength of RHS overlap joints is primarily governed by the strength of the compression and tension branches. Table I2 gives the equations that have been developed to give the mean and characteristic strength of fully or partially overlapped joints. For both gap and overlap joints, the design joint strength equations presented in Appendix I are substantially empirical and are based on the results of isolated joint testing (see CIDECT Monograph 6[43]).

The limits of validity for the equations are also presented in Tables I1 and I2. Some of these limits represent bounds for which supporting test evidence is available; others are theoretical estimates to ensure adequate joint performance, with regard to such factors as local joint deflections at the service load level, sufficient moment-redistribution capacity and prevention of premature local buckling. The reasons for their implementation are described in detail by CIDECT[43].

In this chapter the experimental and design joint strengths have been compared for the gap joint truss as well as the 100% overlap joint trusses. Although this thesis is not specifically concerned with gap joint trusses, it is felt that the observations made in the testing of truss T1 will be of use to those involved in the testing of gap joint trusses in the future. For the 100% overlap joint trusses the relationship between the results derived from the truss tests and those obtained from the testing of isolated partial and 100% overlapped joints have been reviewed in detail. Attention has been focused on the relevance of the isolated joint failure modes, and the suitability of the corresponding design joint strength equations.

8.2 Identification of joint and member failures in the test trusses

(for a detailed description see Chapter 5)

In isolated joint testing the ultimate strength has normally been defined as the maximum resistance to applied load. In this case an isolated joint is deemed to have failed when it is no longer capable of resisting further increases in load. For the gap joint truss, T1, individual joint failures were identified by studying the graphs of applied ram load v. chord face deformation (see section 5.3).

In the 100% overlap joint trusses the most common mode of failure was member yielding of the branches. Only three joint failure modes were observed:

(i) Local buckling of the compression chord, L7. This occurred only in truss T2 at joint 9.

(ii) Local buckling of the compression branch (L6). This failure mode was observed only in truss T6.

(iii) Rupture of the tension branch. This occurred on two occasions (in truss T5 at joint 2, and in truss T6 at joint 3). These ruptures always occurred in the heel crosswall directly above the weld to the chord face. The tear occurred in the 'heat affected zone' of the parent metal and not in the weld itself. This type of failure occured only at joints where the tie overlapped the strut.

For all the 100% overlap truss joints the deformation of the connecting chord face was negligible, irrespective of the failure mode. As a result joint failure was not clearly defined from the graphs of applied ram load v. chord face deformation. For the 100% overlap joint trusses joint failures were identified visually.

In the 100% overlap joint trusses it was found difficult to assess joint strength independently of the structure strength, particularly since the structures achieved higher strengths by redistribution of chord bending moments (see section 6.3.6). In the test trusses it was difficult to define whether an element (member or joint) had reached its full load carrying capacity (see section 5.7). The distribution of axial forces at truss ultimate load did not, therefore, necessarily correspond to the ultimate load carrying capacity of a particular part of the truss. In the case of the 100% overlap joint trusses, it is possible to state only the joint forces at truss ultimate load, and to indicate whether extreme fibre yielding had occurred at the strain gauges in any of the members.

8.3 Post-failure residual strains in branch and chord members

For both gap and 100% overlap joint trusses an attempt was made to measure the residual strains (see section 4.4). The most likely causes of post failure residual strains in the truss members are :

(i) Extreme fibre yielding at a section.

(ii) Axial and bending forces caused by permanent set in joint deformation and overall truss deflection.

(iii) Welding and repair work.

8.4 Residual strains in the gap joint truss, T1

During the entire loading history (seven failure cycles) of the truss it was observed that the branch members were not subject to yielding at the strain gauge positions. Therefore, the residual axial and bending forces in these members were caused by :

(i) Axial and bending forces arising from permanent set in joint deformation and overall truss deflection.

(ii) Welding and repair work.

(iii) A combination of (i) and (ii).

The residual axial forces generated in the branch members at each failure cycle varied along the length of the truss, and were highest at those positions where failure of a joint or member had occurred. The residual axial forces generated by a single failure cycle were, generally, less than 5% of the maximum branch force for that load cycle. However, the residual forces caused by each load cycle were not always additive.

For the chord members yielding did occur at the strain gauge positions. The residual forces cannot be evaluated for a section which has yielded since the amount of strain caused by extreme fibre yielding cannot be distinguished from that caused by permanent deformation set.

For both the branch and chord members the residual strains created by the repair of an element were negligible in magnitude compared to those caused either by yielding or permanent set deformations. Furthermore, these strains were always localized, affecting only those members directly adjacent to the element that was repaired.

8.5 Secondary bending stresses in the gap joint truss, T1

At truss ultimate load the secondary chord bending stresses in the gap joint truss (caused by the continuity moment) were of the same order of magnitude as the primary chord bending stresses in the corresponding 100% overlap joint truss T2 (see section 6.4.3). Therefore, in truss T1 it is likely that the secondary bending stresses influenced the mode of failure and ultimate strength of the joints. With respect to the influence of the secondary chord bending stresses on ultimate joint strength two observations have been made :

(i) For the compression chord joints the secondary bending stress was always tensile on the connecting chord face. Therefore, it was in the opposite sense to the compressive stress caused by the axial force in the chord (see Fig 8.1[a]).

(ii) For the tension chord joints the secondary bending stress was always compressive on the connecting chord face. Once more the bending stress was in the opposite sense to the tensile axial force in the chord (see Fig 8.1[b]).

A study of the residual stresses in the chord indicates that a proportion of continuity bending moment was retained on removal of the applied ram load. For multiple failure cycles, the residual bending stresses caused by the permanent set in the overall deflection were additive.

8.6 Comparison of experimental and design joint strengths for the gap joint truss, T1

The gap joint mean strength equation (Eqn. 8.1) is based on the results of isolated joint testing. In isolated joint tests the bending induced in a continuous chord section cannot be correctly simulated. However, the chord bending moments in truss T1 were significant even though the joints were noded (see section 6.2.4). Consequently the influence of observations (i) and (ii) in section 8.5 have not been considered in the formulation of the mean ultimate joint strength equation.

$$N_{1m} = 7{\cdot}7 \cdot \sigma_{e0} \cdot t_0^2 \cdot \beta \cdot \sqrt[2]{\frac{b_0}{t_0}} \cdot f\left(\frac{b_0}{t_0}\right) \cdot \mu \qquad \text{Eqn. 8.1}$$

where :

$$f\left(\frac{b_0}{t_0}\right) = \left(1+\left(\frac{1.25}{3000}\right)\right) \cdot \left(\frac{b_0}{t_0} - 30\right) \cdot (90-\theta_1-\theta_2)\ ;\ (< 1) \qquad \text{Eqn.8.1.1}$$

$$f\left(\frac{b_0}{t_0}\right) = 1 \quad \text{for } \frac{b_0}{t_0} < 30$$

$$\beta = \left(\frac{b_1+h_1+b_2+h_2}{4b_0}\right) \qquad \text{Eqn. 8.1.2}$$

$$\mu = \left(1.3 - \left(\frac{0.4}{\beta}\right)\right) \cdot \left(\frac{\sigma_0}{\sigma_{e0}}\right) \quad \text{for compression chord} \qquad \text{Eqn 8.1.3}$$

$$= 1 \quad \text{for tension chord}$$

The modes of failure that occurred in truss T1 over the six failure cycles have been categorized using the CIDECT definitions. Each joint failure mode involved deformation of the chord connecting face. The predicted joint strengths derived from the gap joint mean strength equation (Eqn. 8.1) are shown in Table 8.1. It should be noted that the residual stresses have not been considered in the determination of the experimental axial forces.

It is clear that a compressive axial load in the chord is detrimental to the joint strength (this has been found in isolated joint testing - see CIDECT Monograph 6[43]). The joints on the compression chord were weaker than corresponding joints on the tension chord. Furthermore, the compression chord joints were normally subject to buckling in the sidewalls. On the tension chord only deformation of the connecting face occurred. The inclusion of the μ function for the compression chord joints is thus justified, without it the compression chord joint strengths would be significantly over-estimated (see Table 8.1).

There was a compressive bending stress on the connecting chord face of the tension chord caused by the continuity moment (see Fig 8.1[b]) and by the residual stresses accumulated in previous load cycles. This compressive bending stress appeared to be detrimental to the strength of tension chord joints. This could explain why the gap joint mean strength equation significantly underestimates the experimental ultimate strength of joints 4, 11 and 12, which all failed by mode G1. Since these joints were at truss midspan the continuity bending moment in the tension chord was greater than for the other tension chord joints.

In a truss environment the influence of secondary bending stresses in the tension chord joints could, therefore, have a significant effect on the strength of a joint. Joints 4 and 11 failed in the third load cycle, and joint 12 in the sixth. Therefore, the accumulated residual stresses in the chord also need to be considered. After the first

load cycle the combination of accumulated residual stresses and the influence of stiffening plates and repairs make it difficult to assess the influence of secondary bending stresses on the strength of the joints. Moment redistribution in the chord section was also observed in the case of the gap joint truss. Although this may have relieved the stress concentration at chord sections subject to extreme fibre yielding, the redistributed moment would have tended to increase the bending stress at other chord sections, thus possibly reducing the the strength of joints elsewhere in the truss.

8.7 Failure modes observed after the first load cycle in the 100% overlap joint trusses

(for a detailed description see Chapter 5)

Of the 100% overlap joint trusses only trusses T2 and T3 were subject to more than one failure cycle. On the first load cycle of T2 in plane double curvature buckling of the compression chord occurred. Initially this involved yielding in the 4mm thick section adjacent to the splice. The member was subsequently repaired, as was the corresponding section on the opposite side of the truss. On re-loading the same member failed but this time in the L7 mode which has been identified in isolated joint testing (see CIDECT Monograph 6[43]). Failure of the branch members did not occur, and only a 1% increase in the ram failure load was achieved with respect to the first load cycle.

In truss T3 overall yielding of the branch members was observed in the first load cycle, however local buckling of the chord in all four walls of the central joint (joint 9) was also observed. Joint 9 was strengthened, but only the same branch members yielded on the second load cycle. For truss T3 a 4% increase in the ram failure load was achieved with respect to the first load cycle.

Truss T2/2 is unique in that it was formed by cutting truss T2, once it had failed, and reducing the span. Although it was subject to only one failure cycle. It was not possible to evaluate the residual strains caused by the cutting, welding and plating necessary to form truss T2/2. This is because the sensors had to be disconnected from the datalogger to allow the repair to take place. The experimental results of T2/2 have, therefore, been treated with caution.

With the exception of the L7 mode in truss T2, only the experimental joint strength results of the first load cycle have been considered for the 100% overlap joint trusses.

8.8 The influence of joint stiffness on 100% overlap joints

In the 100% overlap joint trusses a variation in stiffness between the heel and toe faces has been identified in both the overlapping and overlapped branches. The stress distribution in the crosswalls of the branch members appeared to be influenced by the sense of overlapping (ie., strut/tie or tie/strut), and is described in detail in section 6.3.3.

Due to the variation of stiffness in a 'partially' overlapped connection, from the flexible heel to the stiff overlapping toes of the branches, a moment is induced in the branches which increases the stress in the walls facing each other (see Fig 8.2[a]). In the testing of isolated partial overlap joints (see CIDECT Monograph 6[43]) this has led to two failure modes for the branch members :

(i) Local yielding of the toe crosswall of the tie or strut.

(ii) Local buckling of the toe crosswall of the compression branch.

The results derived from the test trusses do not conform with the results of partial overlap isolated joint testing. Although (i) was observed in the truss tests, local yielding on the heel crosswall was more common. Furthermore, the L6 local buckling mode in truss T6 was observed initially to form on the heel crosswall of the strut.

It has been concluded from isolated joint testing that the moment generated by a negative eccentricity always relieves the bending in the branches caused by the variable stiffness of the connection. The resulting change in the sign of the bending moments has been observed by De Koning and Wardenier[32] in fully overlapped joints. For the trusses this change in sign was observed mainly in the branches where the tie overlapped the strut. This can be explained by the fact that the bending moment caused by the difference in stiffness between the toe and heel crosswalls was in opposition to that caused by the joint eccentricity (see Fig. 8.2[b]). For the joints where the strut overlapped the tie the general tendency was for the heel face of the overlapped tie members to be more highly stressed than the toe face (for the reasons described in section 6.3.3). As a result the eccentricity moment added to the moment induced by the variable stiffness of the connection (see Fig. 8.2[c]).

8.9 Comparison of experimental and design joint strengths for the 100% overlap joint trusses

The CIDECT design joint strength equation (Eqn. 8.2) is presented in Table 8.2. The IIW[44] implementation is given by Equation 8.3. Both sets of equations relate

the mean ultimate joint strength to the axial forces in the branch members.

$$N_{im} = \sigma_{ei} (2h_i - 4t_i + b_i + b_{e(ov)}) \text{ where } i = 1 \text{ or } 2 \qquad \text{Eqn. 8.3}$$

$$b_{e(ov)} = \left(\frac{C}{(b_j/t_j)_{ov}}\right) \cdot \left(\frac{(\sigma_{ei}t_i)_{ov}}{(\sigma_{ei}t_i)}\right) . b_i \quad (< b_i) \qquad \text{Eqn. 8.3.1}$$

where (ov) = overlapped member

The IIW method of assessing the joint strength is the simpler of the two. Only the strength of the overlapping member is calculated, while the overlapped member is assumed to develop its full axial capacity (ie., cross-sectional area x yield stress).

The CIDECT approach is more comprehensive and strength equations are provided for both of the branches at a joint. The derivation of the equations is outlined in detail in Monograph 6[43]. The equations are based on a defined stress distribution in the walls of the branch members. This has been derived by assuming that the heel crosswall weld of the overlapping member is formed adjacent to the toe weld of the overlapped member (see Fig. 8.3[a] - detail 2). In the truss joints this type of detail was not used, no weld was provided along the toe of the overlapped branch (see Fig. 8.3[b] - detail 4). Consequently, the predicted stress distributions (at failure) in the walls of the overlapped tie branches do not always correspond to the experimental distributions at the ram failure load.

For strut overlapping tie the experimental stress (at the ram failure load) on the heel crosswall of the tie was, for the majority of Warren joints, greater than on the toe face (see Fig. 6.11[b]). The predicted tie strength is, however, based on the assumption that the opposite is true. For the strut the predicted strength equation assumes that the higher stress is on the heel crosswall. This generally corresponds to what has been identified experimentally (see Fig. 6.11[b]). Where the tie overlaps the strut the predicted stress distributions generally correspond to the experimental (see Fig. 6.11[a]). In this case the overlapping tie was always more highly stressed on the heel face, while the overlapped member was more highly stressed on the toe face.

In a truss environment it is difficult to define whether an element (member or joint) has reached its full load carrying capacity (see section 5.7). For this reason a comparison of the predicted and experimental failure loads in the branches cannot be relied upon to assess the 'accuracy' of the joint strength equations. For each of the

100% overlap joint trusses the CIDECT and IIW effective width equations have been compared to the experimental joint forces at the ram failure load (see Appendix J, Table 8.3 is typical). The branch member axial forces corresponding to the predicted joint strengths are always higher than the experimental axial forces at ram failure load, even where joint failure occurred by strut local buckling,(L6). With respect to these joint failures the CIDECT and IIW equations are unsafe. Member yielding of the tension and/or compression branches was the most common mode of failure in the test trusses. It could, therefore, be argued that where branch member yielding occurred the CIDECT and IIW equations are not unsafe, but rather that the yielding of the branch member was critical.

From isolated joint tests Haleem[59] observed that the longitudinal strains on the tie branch side of the strut (ie., on the toe crosswall) were usually significantly higher than the average value. Generally, for the Warren trusses the opposite was true, namely that the heel crosswall of the strut was more highly stressed than the toe crosswall. For the N-truss the heel crosswall of the strut was more highly stressed than the toe only where the strut overlapped the tie. On the opposite side of the N-truss where the overlapping was reversed (ie., tie overlapped the strut), the toe crosswall of the strut was more highly stressed than the heel crosswall. The experimental distribution of stresses in the Warren and N-type 100% overlap joint test trusses is described in detail in section 6.3.3. Haleem's overlap joint strength formula (Eqn. 8.4) is based on the assumption that the strength is limited to that load which produces local yield or buckling of the strut on the toe crosswall.

$$N_{1m} = A_1.\sigma_{e1}.h_1 \qquad \text{Eqn. 8.4}$$

where

$$h_1 = 1.4 \cdot \sqrt[4]{\left(\frac{b_0}{t_0}\right)\left(\frac{b_1}{b_0}\right)^2 \cdot \left(\frac{t_1}{t_0}\right)} \cdot 2 \cdot \left(\frac{\mathrm{Sin}(\phi_1+\phi_2)}{1+\mathrm{Sin}(\phi_1+\phi_2)}\right) \qquad \text{Eqn. 8.4.1}$$

and

$\phi 1 = 90^o-\theta_1$;

$\phi 2 = 90^o-\theta_2$

This formula has been applied to the joints in the test trusses with the result that the predicted strut efficiency is never less than 0.96 (see Appendix J, Table 8.3 is typical). Strut local buckling (L6) in truss T6 always occurred firstly on the heel crosswall. Haleem's equation is unsafe in predicting the L6 failures in truss T6 (see Table 8.3). This is not surprising since Eqn. 8.4 is based on the assumption that local

yield or buckling (L6) occurs on the toe face of the strut.

Haleem's equation was later modified for the mean results by dropping the angle function and including the effect of the chord axial pre-load, F_{op}. The resulting equation is deemed to apply to joints with overlap in excess of 25% and assumes that deformation of the chord connecting face occurs in conjunction with local buckling of the compression branch. For overlapped joints Packer[17] considered two mechanisms of failure. Both correspond to mode of failure L6 and again assume deformation of the chord connecting face. In truss T6 where strut local buckling did occur (see section 5.5.3) it did not involve deformation of the chord connecting face. Since deformation of the chord connecting face was negligible for the 100% overlap joint trusses, the predicted joint strengths derived from Packer's mechanisms and Haleem's modified equation are not applicable. However, in a truss where a 100% overlap joint is subject to a concentrated point load significant deformation of the connecting chord face is likely to occur. In this case the Packer mechanisms could be applicable.

The L7 type joint failure in the chord was only observed in one of the trusses, namely T2 at joint 9. In this case there is reason to suspect that it was related to the repair afforded to adjacent chord section (see section 5.5.1). The L7 mode is directly related to the build up of compressive stress in the chord connecting face behind the heel of the tie, due to joint eccentricity moment. In a continuous chord section, this stress can be relieved by :

(i) Moment redistribution in the chord. This was observed in each of the 100% overlap joint trusses (see section 6.3.6).

(ii) The continuity moment in the chord. For the test trusses this was caused by the overall deflected shape. The bending stress related to the continuity moment was always tensile on the connecting chord face of the compression chord, therefore acting against the L7 mode (see Fig. 7.1[c]).

In Warren joints an estimate of the branch force required to produce local buckling of the chord (L7) has been presented in CIDECT Monograph 6[43], namely:

$$N_{1m} = A_1.\sigma_{e1}.h_1 \qquad \text{Eqn. 8.5}$$

where

$$h_1 = \frac{[(t_0/\sigma_{e0})/(t_1/\sigma_{e1})].[(h_0/b_0)+1-(2t_0/b_0)].[1-(|F_{op}/A_0.\sigma_{e0}|)].\text{Sin}\,\theta_2}{[(h_1/b_1)+1-(2t_1/b_1)].[1+k(A_0h_0/Z_0)].(e/h_0).\text{Sin}(\theta_1+\theta_2)}$$

This equation incorporates the chord pre-load, F_{op}. For a continuous chord the moment induced by the joint eccentricity is assumed to be distributed equally on either side of the chord, ie., k=0.5. Haleem[59] noted from isolated joint tests that the measured stress distribution in the chord sidewalls due to branch shear transfer parallel to the chord is approximately triangular, irrespective of the actual geometric eccentricity, in which case

$$k \cdot \left(\frac{A_o h_o}{Z_o}\right) \cdot \left(\frac{e}{h_o}\right) = 1$$

In a truss environment, the effect of chord continuity moment and the action of moment redistribution invalidate Haleem's assumptions. The chord bending moments in the test trusses either side of a joint were never equal (see bending moment distributions in Appendices G & H).

For T2 the L7 mode occurred at a strut force of 90 kN. Use of Eqn. 8.5 predicts failure at a strut force of 70 kN. In the remaining trusses the equation gives limiting values for the strut axial force which are generally exceeded by the experimental values (see Table 8.4) However, with the exception of truss T2, the L7 failure mode was not observed in any of the other trusses.

Haleem and Packer[15] also suggested that the chord shear strength should be checked and presented an equation for this purpose. However, no such failure occurred in any of the trusses that were tested. In fact shear failure of the chord has never been observed in any isolated joint or truss tests on partial or 100% overlap joints.

8.10 Use of plane frame analyses in designing 100% overlap joint trusses

In order to design a lattice truss, a designer needs to know which frame analysis to use in conjunction with the joint strength equations. Three analytical methods have been investigated. The objective was to define the most practical approach by which to design a 100% overlap joint lattice truss.

8.10.1 Design of the branch members based on joint failure

Using the CIDECT joint mean strength equations (see Table 8.2) the predicted applied ram load corresponding to the failure of each joint, (ie., local yielding of the

branch member), has been evaluated, by considering the strut and tie strengths individually. Two calculation methods have been used, method '1' is based on the experimental elastic axial force co-efficients, and method '2' on the axial force co-efficients derived from the model-Y rigid frame analyses, described in Chapter 7.

The predicted ram load corresponding to local yielding in the branches has been evaluated by :

(i) Calculating the predicted branch forces corresponding to joint failure from the CIDECT equations - see Table 8.2.

(ii) Dividing the calculated branch force from (i) by the corresponding axial force co-efficient. (NB. The axial force co-efficient in any member is defined as the axial force caused by a 1 kN applied ram load).

The results have been tabulated with respect to individual branch members as opposed to joints. Therefore for each branch member in a truss there is a corresponding predicted ram load which causes local yielding at the joint in that member. Since each branch spans between two joints there can be two different values of predicted ram load for the same member. In such cases the critical value has been tabulated.

For each branch the experimental strain gauge values, at ram failure load, have been extrapolated to assess whether the yield stress was exceeded at the ends of the member. In the tables presented in Appendix K (Table 8.5 is typical) the asterisk denotes the occurrence of extreme fibre yielding in a branch member at the ram failure load.

The predicted ram load corresponding to local yielding in a branch member has been compared to the experimental ram failure load (see Appendix K, Table 8.5 is typical). For those branch members where extreme fibre yielding occurred the predicted ram load is always greater than the experimental ram failure load. Even for those members which failed by L6 in truss T6 the predicted ram load is always greater than the corresponding experimental ram failure load (see Table 8.5). This demonstrates that the CIDECT joint strength equations can be unsafe if used in conjunction with a rigid joint frame analysis.

8.10.2 <u>Design of the branch members based on overall member yielding</u>

This design method ('3') involves :

(i) Calculating the predicted branch forces corresponding to overall member

yielding, assuming that the member develops its full axial capacity (ie., measured cross-sectional area x measured yield stress).

(ii) Dividing the calculated branch force from (i) by the corresponding axial force co-efficient derived from the pin-jointed frame analysis, model-P described in Chapter 7.

For the members where joint failure and/or extreme fibre yielding occurred (denoted by an asterisk) the predicted ram load required to cause overall yielding of the member is, with the exception of members 29 and 33 in truss T2, less than the experimental ram failure load. In truss T2 yielding of the tie branches at joints 12 and 14 did not cause the truss to fail. When truss T2 was shortened joint 12 was included in the shortened truss (T2/2). This truss attained a ram failure load of 263 kN, as opposed to the ram failure load of T2 which was only 168 kN. The predicted ram load required to cause overall yielding of member 29, (the tie branch in joint 12 of truss T2) is only 218 kN.

Therefore, method '3' is always safe, irrespective of the mode of failure. It also follows that if the CIDECT joint strength equations are used in conjunction with the pin-jointed frame analysis then the ram failure load is once more **always** safely predicted, irrespective of failure mode.

The implication is that for all the 100% overlap joint trusses that were tested method '3' could have been used to design the branch members, and the strength of the joints need not have been assessed.

8.10.3 Design of the chord section based on extreme fibre yielding

For the chord section the theoretical combined stress due to axial forces and bending moments has been evaluated at the member ends using the model-Y rigid frame analysis. As a result it has been possible to evaluate for each chord member in a truss a predicted value for the applied ram load which causes extreme fibre yielding in that member. For each chord member this predicted ram load has been compared to the experimental ram failure load (see Appendix L, Table 8.6 is typical).

For each chord member the experimental strain gauge values, at ram failure load, have been extrapolated to assess whether the yield stress was exceeded at the joints. In Appendix L (Tables 8.6 is typical) the asterisk denotes the occurrence of extreme fibre yielding in a chord member at the ram failure load. With the exception of

member 14 in truss T2, the predicted ram load values are significantly less than the experimental ram failure load for those chord members where yielding (denoted by *) was observed. In truss T2 the predicted ram load is approximately equivalent to the experimental ram failure load for member 14.

Truss T2 differs from the other trusses in that the chord sections were spliced (see Appendix A, Fig A2), to allow the section thickness to change from 5mm to 4mm. Extreme fibre yielding occurred in the 4mm section of member 14 adjacent to the chord splice. Subsequent to the attainment of the yield stress there was little increase in applied load before the member failed by in-plane overall buckling. The splice, therefore, appeared to limit the redistribution of moments away from the position of yielding. For the remaining 100% overlap joint trusses the redistribution of moments was observed to prevent the sudden onset of instability in those chord members where extreme fibre yielding occurred (see section 6.3.6). Consequently, the ultimate load carrying capacity of trusses T3, T4, T5 and T6 was significantly higher (> 20%) than the applied load which caused extreme fibre yielding in the chord section.

The theoretical rigid frame analysis (model Y) thus provides a reliable method of defining the onset of extreme fibre yielding in the chord section. In the test trusses the redistribution of moments ensured that chord member failure occurred at loads higher than those corresponding to the attainment of the yield stress. The model-Y rigid frame analysis thus provides a safe method for designing the chord section. However, discontinuities in the bending stiffness of the chord section (ie., such as splices and local stiffening) appear to limit the extent of moment redistribution, and can therefore have a detrimental effect on the ultimate load carrying capacity of a truss.

8.11 Design against overall member buckling of the compression branch

Member buckling in the branches was observed only in truss T4. For the critical compression branch in each truss the experimental strut force at ram failure load has been compared with the predicted buckling force derived in accordance with section 4.7 of BS 5950[45], Part 1 (see Table 8.7).

In T4 the strut buckling force is accurately predicted. In the remaining trusses buckling did not occur, and the following relationships exist between predicted strut buckling and strut failure:

(i) For trusses T1, T2 and T5 the critical strut did not yield, but the predicted strut

buckling force is at least 50% greater than the experimental strut force at the ram failure load.

(ii) For truss T3 the predicted strut buckling force is 13% greater than the sustained experimental strut force, but only member yielding occurred.

(iii) For truss T2/2 the predicted strut buckling force is the same as the experimental strut force, but only member yielding occurred.

(iv) In T6 the predicted strut buckling force is higher than the experimental force but only strut local buckling (L6) occurred.

The same section size was used for the compression branches in T4 and T6 (60x60x3.2 RHS). In T4 the strut to chord width ratio was greater than in T6, thus affording more restraint against local buckling and member instability. This is reflected in the higher experimental strut efficiency of T4, at the ram failure load (see Table 8.7). In truss T6 local buckling of the compression branches was critical - overall buckling of the compression branches did not occur. In the other trusses the section used was a 40x40x4 RHS. Trusses T3 and T4 were identical in all respects apart from the size of the branch members. A comparison of the bending moments in corresponding branch members indicates that they were significantly larger in T4, where the branches were stiffer.

Although the elastic bending moment distribution in the branches was double curvature, where overall buckling occurred in truss T4 (members 16 & 17) the mode was single curvature. It was observed that local yielding in these branch members at the joints was responsible for a change from double to single curvature bending.

Local yielding at the joints was a characteristic which occurred in all branch members prior to their failure. This was irrespective of the mode of failure. At many joints it was observed the compression branch section became fully plastic before the truss reached the ram failure load. For those compression branches subject to local yielding at the joints it is unlikely that the joints provided any significant rotational restraint against member buckling. There are examples where this yielding led to the complete loss of bending in a branch member (see section 6.3.8). In these cases only axial force was sustained by the branch and the end restraint afforded by the joints at either end was significantly reduced. It would be logical, therefore, to assume an effective length equivalent to the actual length of the branch. This makes the assumption that at ultimate load the branch member is pinned at both ends.

8.12 Shear strength of branch member sidewalls

According to BS 5950 Part 1[45] (clause 4.2.3) only the sidewalls should be assumed to be effective in transferring the shear force from the branches to the chord face (see Fig. 8.4). Extensive yielding in the sidewalls of the branches was observed in the area of overlapping where the transfer of shear into the chord takes place. There was evidence of the formation of a shear plane in the sidewalls of the connecting branch member and it was thought that a mode of failure associated with this shear transfer might occur. However, tearing of the sidewalls was never observed (see section 5.5.2). No gross deformation took place and the shear transfer was well in excess of that which could be carried by the branch sidewalls in shear.

In BS 5950 the Von Mises criterion of pure shear is assumed such that there is no direct stress across the critical shear plane (see Fig. 8.5). The shear stress in the sidewalls at the ram failure load has been compared with the allowable shear stress for all joints in each of the trusses (see Appendix M, Table 8.8 is typical). The allowable shear stress was exceeded in most instances.

It appears that the presence of the transverse weld at the stiff point where both branch crosswalls meet greatly assists in transferring the horizontal shear. It is likely that the other crosswall also made some contribution to this action. It is also possible that residual stresses induced by fabrication welding affected the shear strength of the sidewalls. A residual direct stress in a direction perpendicular to the shear plane would tend to increase the shear capacity of the sidewalls (see stress field in Fig. 8.5).

It is possible that shear failure in the overlapped branch member of a 100% overlap joint is never critical. This could explain why it has never been observed in isolated joint testing. Further truss testing is necessary before a definitive conclusion can be drawn. However, it is possible (for all 100% overlap joints) that the shear stress in the sidewalls of the overlapped branch need not be considered with respect to the joint design.

For trusses T2, T2/2, T3, and T5 , the joints where the strut overlapped the tie were critical with respect to the shear capacity. This is because a thinner walled section was used for the tie member. In the remaining trusses T4, and T6 the same section size was used for both of the branch members. For the strut overlapping tie joints in trusses T2, T2/2, T3, and T5 and all joints in T4 and T6 the following observation has been made (see Appendix M) : **BS 5950, clause 4.2.3 always underestimates the**

shear strength of the joints by at least 50%. This implies that it would be safe to multiply the allowable shear capacity of the branch sidewalls defined by BS 5950 by a factor of 1.5.

It is also worth emphasizing that the distress in the sidewalls, due to shear transfer to the chord, was always more pronounced where the thinner branch was used as the overlapped member. Therefore, the thicker walled branch should always be used as the overlapped member, as it affords greater shear strength.

8.13 Weld Detailing

The weld details for the joint connections are shown in Fig. 3.3. Cracking in the welds did not occur although rupture of tension branch adjacent to the welds was observed in two 100% overlap joints (truss T5-joint 2 and truss T6-joint 6). In both cases fracture occurred in the 'heat affected zone' of the heel branch wall. The failures did not appear to correspond to defective welding in these instances.

It is significant that cracking was always in the parent metal and not in the weld, indicating that the welds were not defective. It is common knowledge among structural engineers that welding reduces the yield stress in high yield members directly adjacent to welds. Where cracking did occur it was in conjunction with member yielding of the branch. It appears, therefore, that the welding did not have a detrimental effect on the ultimate load carrying capacity of the tension branches. The weld details that were used were thus satisfactory, ensuring ease of fabrication without compromising the strength of the joints.

8.14 100% overlap isolated joint testing at Corby

In order to supplement the truss testing programme, joints identical to those used in truss T6 were tested in isolation at Corby (British Steel Corporation - tubes division). The objective was to investigate to what extent isolated joint testing of 100% overlap joints correctly reflects the behaviour of identical joints in a truss environment.

Four joints were tested in all, three were formed by the tie overlapping the strut and the remaining joint was fabricated with the strut overlapping the tie. Two loading patterns were investigated. The first involved holding the tie and pushing the strut, while in the second the strut was held in position and the tie was pulled. The results of this programme are outlined by Marniche[37]. The relative performance of the isolated

and truss joints have been compared below. Particular attention has been paid to the modes of failure and the ultimate load capacity of the joints.

The failure mode that was obtained in the isolated joints where the tie overlapped the strut was similar to that observed in the truss. In the isolated joint test failure was by local buckling of the strut (L6), however this occurred only on the heel adjacent to the chord connecting face. In the truss environment local buckling was observed both on the toe and the heel faces. In the isolated joint tests local buckling was followed by overall member buckling of the strut. On each occasion no evidence of yielding was observed in the tie member.

In the case where the strut was being pushed and the tie held buckling of the compression branch was always more pronounced. This indicates the difficulty in controlling the compression ram with the onset of instability. By pulling the tie member more control was afforded during testing.

Only one joint was tested with the strut overlapping the tie. Failure was by local buckling of the strut on both the toe and heel faces, this subsequently initiated overall buckling in that member. Only local buckling of the strut heel occurred in the corresponding truss joints.

Significant deformations occurred at the ends of the isolated joint members, both in and out of plane of the joint. Furthermore, the measured in-plane bending moments in the branch and chord section were of the same order as the out of plane moments. Nevertheless, only in-plane buckling occurred. In the truss out-of-plane bending was not monitored, and therefore no comparisons can be made in this respect.

The measured strut efficiencies at ram failure load compare favourably. For the tie overlapping the strut the experimental strut efficiencies from the isolated joint tests were 0.82, 0.85 and 0.90. The corresponding values from the truss test were in the range 0.74 to 0.88. For the strut overlapping the tie the value derived from the isolated joint test was 0.88, and from the truss test in the range 0.75 and 0.86. Agreement is good, however, it should be noted that the values obtained for the truss joints do not necessarily correspond to the joint ultimate strength (see section 5.7).

In the isolated joint tests conducted by Marniche[37] only failure of the branch members was observed, and in each case this did not involve deformation of the chord connecting face. In this respect the isolated joint testing appears to simulate the main

failure mode characteristics of the 100% overlap joints in truss T6. Nevertheless, the method of loading and the end restraint of the isolated joints can never correctly reflect the situation in a truss. This largely influences the distribution of bending moments at the joint. Consequently, the in-plane bending moments in the isolated joints differ from those of the truss joints.

At Nottingham Ben Salem[38] performed isolated joint tests on 100% overlap joints with joint parameters different to those of the test trusses. The majority of joints tested by Ben Salem failed by L7, chord local buckling. The advantages of chord continuity as well as plastic redistribution of moments have been observed to prevent the occurrence of chord local buckling in a truss environment.

It appears that results[37 & 38] obtained from isolated joint tests relating to the branch members agree with those obtained from the truss tests, both with respect to strength and failure mode. However in an isolated joint test it is difficult to simulate the bending moment in the chord section to coincide with that of a chord in a truss environment. It is likely, therefore, that isolated joint testing is unreliable in assessing the strength of the chord in 100% overlap joints. Further testing is necessary before a definitive conclusion can be drawn with respect to the reliability of isolated 100% overlap joint testing for indicating the strength of 100% overlap joints in a truss environment.

8.15 Ultimate strength capacity of truss corner joints

A number of configurations are possible for the end bays of a truss (see Fig. 8.6), however only two types were used in the test programme, namely [a] and [c]. The arrangements shown in Figures 8.6[b] & [d] would be subject to considerable joint deformation and were avoided for this reason.

As a direct consequence of the truss tests it was realized that the most efficient force transfer mechanism to use with respect to corner joints is that shown in Fig. 8.7[e]. No failure was observed at these joints. Subsequently on completion of each truss test the corner joints were flame cut from the truss and tested in isolation by pulling on the branch member. The results of these isolated joint tests have been presented by Marniche[37].

It was found that the branch always attained the squash load (Cross-sectional area x yield stress). Failure was by tearing of the branch adjacent to the welds

connecting it to the chord sections .

It is likely that for any type of corner joint the maximum efficiency of the branch member is attained by ensuring that the centre-line of the branch intersects the interface of the post and the chord (see Fig 8.7[e]). This is irrespective of the angle of inclination of the branch. Corner joint eccentricity was found not to be detrimental to the joint strength.

The strength of the corner joint appears to be defined by the geometry, namely that one of the branch cross-walls is connected to the post and the other to the compression or tension chord. This produces a joint with high axial stiffness and low rotational stiffness. Deformation of the connecting chord sections, due to axial force in the branch member, is therefore small. If both the branch member crosswalls are connected to either the post or the chord (see Fig 8.7), then a gap type joint is obtained and deformation of the connecting chord face results. With the exception of [e] in Fig. 8.7 the remainder, [a,b,c, & d] involve deformation of the connecting chord face which is likely to be detrimental to the joint strength.

Table 8.1 Comparison of experimental joint strengths with the predicted mean ultimate joint strengths (truss T1).

Joint	Load cycle at which joint failed	Mode of Failure (see Figure 5.2)	Measured strut force corresponding to ram failure load	Predicted joint strengths (Eqn. 8.1)			
				Strut force (without μ factor)	Ratio	Strut force (with μ factor)	Ratio
			N_1 kN	N_{1m} kN	N_{1m}/N_1	$N\mu_{1m}$ kN	$N\mu_{1m}/N_1$
1	3	G8	99	173	1.7	102	1.0
2	2	G4	91	106	1.2	78	0.9
3	5	G2b	97	106	1.1	94	1.0
4	3	G1	113	183	1.6		
5	6	unfailed	111	182	1.6		
6	5	G1	116	116	1.0		
7	6	unfailed	104	116	1.1		
8	3	G8	97	173	1.8	102	1.1
9	1	G4	76	112	1.5	82	1.1
10	6	G8	109	112	1.0	100	0.9
11	3	G1	115	183	1.6		
12	6	G1	120	182	1.5		
13	6	G1	116	116	1.0		
14	6	G1	109	116	1.1		

Notes :

1) To be read in conjunction with Fig S2.
2) For joint properties see Table B8, Appendix B ; For modes of failure see Table D2, Appendix D.
3) The mean ultimate joint strength has been evaluated using Eqn. 8.1, this equation assumes failure by chord face plastification.
4) For the compression chord joints two strength values have been calculated, one including the factor μ and the other excluding the effect of μ.
5) **For values of N_{1m}/N_1 & $N\mu_{1m}/N_1$ less than, or equal to unity the joint strength is safely predicted.**

Table 8.2 RHS overlap joint strength design equations

GENERAL EQUATION FOR BRACING STRENGTH				PARAMETER DEFINITIONS			
Eqn., 8·2 $N_{im} = \sigma_{ei} \cdot t_i \left[(A+B) b_i + C h_i - D t_i \right]$; $N_{ik} = N_{im}$				$k_{01} = \sigma_{e0} t_0 / \sigma_{e1} t_1$ $k_{02} = \sigma_{e0} t_0 / \sigma_{e2} t_2$	$k_{12} = \sigma_{e1} t_1 / \sigma_{e2} t_2$ $k_{21} = \sigma_{e2} t_2 / \sigma_{e1} t_1$	$q_1' = q \sin\theta_1 / h_1$ $q_2' = q \sin\theta_2 / h_2$	q is defined in fig 1-2
Eqn 8·2·	JOINT TYPE	MEMBER	A ● (≯1)	B ● (≯1)	C ● (≯2)	D ● (≯4)	$\gamma_m \gamma_c$
1	Strut O'laps Tie Overlap >80%	Strut	● $12{\cdot}5(t_2/b_2)\,k_{21}$	1	2	4	1·25 in A
2		Tie	$\sqrt{\sigma_{u2}/\sigma_{e2}}$ (≯1·25)	● $12{\cdot}5(t_0/b_0) \cdot k_{02}/\sin\theta_2$	A+B	2A+2B	1·25 in B
3	Tie O'laps Strut Overlap >80%	Strut	1	● $12{\cdot}5(t_0/b_0) \cdot k_{01}/\sin\theta_1$	2B	2B	1·25 in B
4		Tie	● $12{\cdot}5(t_1/b_1)\,k_{12}$	1	2	4	1·25 in A
5	Strut O'laps Tie Overlap >25% <80%	Strut	● $12{\cdot}5(t_2/b_2)\,k_{21}$	● $12{\cdot}5(t_0/b_0) \cdot k_{01}/\sin\theta_1$	● $B(2-q_1') + k_{21} q_1'$; $k_{21} \nearrow 1$	● $3B + k_{21}$; $k_{21} \nearrow 1$	1·25 in A&B
6		Tie	1	● $12{\cdot}5(t_0/b_0) \cdot k_{02}/\sin\theta_2$	1+B	2+2B	1·25 in B
7	Tie O'laps Strut Overlap >25% <80%	Strut	1	● $12{\cdot}5(t_0/b_0) \cdot k_{01}/\sin\theta_1$	2B	4B	1·25 in B
8		Tie	● $12{\cdot}5(t_1/b_1)\,k_{12}$	● $12{\cdot}5(t_0/b_0) \cdot k_{02}/\sin\theta_2$	● $k_{12}(1+q_2') + B(1-q_2')$; $k_{12} \nearrow 1$	● $3k_{12} + B$; $k_{12} \nearrow 1$	1·25 in A&B
GENERAL LIMITS	$0{\cdot}25 \le \beta \le 1{\cdot}0$; $30^\circ \le \theta \le 90^\circ$; $b_0/t_0 \nearrow 40$; $b_1/t_1 \nearrow 1{\cdot}24\sqrt{E/\sigma_1}$ $b_2/t_2 \nearrow 35$; $0{\cdot}5 \le h_0/b_0 \le 2{\cdot}0$; $b_1/b_2 \nearrow 1{\cdot}33$; $\sigma_{e0} \nearrow 360\ N/mm^2$ $\sigma_e/\sigma_u \nearrow 0{\cdot}8$							

Table 8.3 Comparison of measured branch member forces at ram failure load with the predicted mean ultimate joint strengths (truss T6).

Ram failure load = 560 kN ; (load cycle =1).

Joint	Member yielding		Measured member forces at ram failure load		Predicted strengths (see notes below for interpretation) (CIDECT Eqn. 8.2)		(IIW Eqn. 8.3)		(Haleem Eqn. 8.4)
	Strut	Tie	Strut	Tie	Strut	Tie	Strut	Tie	Strut
	* = yield	* = yield	N_1	N_2	N_{1m}/N_1	N_{2m}/N_2	N_{1m}/N_1	N_{2m}/N_2	$N_{1m}/A_1\sigma_{e1}$
	F = failure	F = failure	kN	kN					
(1)	(2)	(3)	(4)	(5)	(6)	(7)	(8)	(9)	(10)
1	F	*	-224	207	1.30	1.33	1.30	1.33	1.00
2		* & F	-217	202	1.34	1.37	1.34	1.21	1.00
3	F	*	-209	189	1.39	1.46	1.39	1.29	1.00
4	* & F	*	-257	207	1.13	1.33	1.13	1.33	1.00
5	* & F	*	-224	202	0.93	1.37	1.30	1.21	1.00
6	F		-217	189	1.34	1.46	1.34	1.29	1.00
7	F		-239	201	1.15	1.45	1.15	1.45	1.00
8	F		-220	223	1.25	1.30	1.25	1.30	1.00
9	F		-218	218	1.27	1.33	1.27	1.33	1.00
10	F		-251	201	1.10	1.45	1.10	1.45	1.00
11	F		-239	223	1.15	1.30	1.15	1.30	1.00
12	F		-220	218	1.25	1.33	1.25	1.33	1.00

Notes :

1) To be read in conjunction with Section 8.9 and Fig S2.
2) For joint properties see Table B13, Appendix B. For modes of failure see Table D8, Appendix D.
3) Columns (2) and (3) indicate by an asterisk, '*' whether extreme fibre yielding has occurred at the strain gauge positions, at the ram failure load.
4) Columns (2) and (3) indicate by an 'F' whether a joint has failed by local yielding in either the tension or compression branch.
5) Columns (4) and (5) indicate the measured axial forces in the branch members, at the ram failure load.
6) Columns (6), (7), (8), & (9) are predicted failure loads expressed as a proportion of the measured forces at the ram failure load.
7) Column (10) is a predicted failure load expressed as a proportion of the strut squash force (ie., yield stress x cross-sectional area).
8) **Joint strength is safely predicted where member yielding and/or member failure, [columns (2) & (3)] coincides with values of less than, or equal to unity in columns (6), (7), (8) & (9).**

Table 8.4 Comparison of measured strut force at critical joint with the predicted strut force required to cause chord local yielding.(L7).

Truss	Critical Joint	Measured Strut force at ram failure load N_1 kN	Predicted strut force required to cause L7 local yielding in the chord N_{1m} kN	Ratio N_{1m}/N_1
T2	9	113	67	0.59
T2/2	8	179	94	0.53
T3	1	184	173	0.94
T4	1	211	234	1.11
T5	5	119	151	1.27
T6	1	224	256	1.14

Notes :

1) To be read in conjunction with Section 8.9 and Fig S2.
2) The measured strut force at ram failure load relates to the first failure cycle for each truss.
3) The critical joint has been selected for each truss, and the predicted strut force has been derived from Eqn. 8.5.
4) The value of K in Eqn. 8.5 has been taken as 0.5.
5) Chord local yielding at a joint did not occur in any of the trusses during the first load cycle.
6) The only occurrence of L7 was in truss T2 (at joint 9). This was during load cycle 2 at a strut force, N_1= 115 kN.

Table 8.5 Comparison of experimental and predicted ram failure loads based on branch member failure (truss T6).

Experimental ram failure load, (R_{exp}) = 560 kN (load cycle = 1).

Branch Member	Predicted ram failure load			Yielding	Ratio of Experimental/Predicted		
	Method 1 R_{p1} kN	Method 2 R_{p2} kN	Method 3 R_{p3} kN	(see note 3)	R_{exp}/R_{p1}	R_{exp}/R_{p2}	R_{exp}/R_{p3}
16	752	843	520	*	0.74	0.66	1.08
17	621	591	446	*	0.90	0.95	1.26
18	674	711	520	*	0.83	0.79	1.08
19	595	552	446	*	0.94	1.01	1.26
20	703	667	520	*	0.80	0.84	1.08
21	824	1140	520	*	0.68	0.49	1.08
22	715	898	520	*	0.78	0.62	1.08
23	688	852	520	*	0.81	0.66	1.08
24	858	1202	520	*	0.65	0.47	1.08
25	665	633	520	*	0.84	0.88	1.08
26	700	658	520	*	0.80	0.85	1.08
27	667	675	520	*	0.84	0.83	1.08
28	703	705	520	*	0.80	0.79	1.08
29	701	800	520	*	0.80	0.70	1.08

Notes:

1) To be read in conjunction with Fig S1.
2) For description of Methods 1, 2, and 3 see Section 8.10.
3) For each branch the experimental strain gauge values, at ram failure load, have been extrapolated to determine whether the measured yield stress was exceeded at the ends of the member. An asterisk '*' has been used to indicated the members where the measured yield stress was exceeded at one or both ends.
4) **Branch member failure is safely predicted where yielding '*' coincides with values of R_{exp}/R_p which are greater than, or equal to unity.**

Table 8.6 Comparison of experimental ram failure load with the predicted ram failure loads based on chord member failure (truss T6).

Experimental ram failure load, (R_{exp}) = 560 kN (load cycle = 1).

Chord member	Predicted ram failure load Rp kN	Yielding (see note 3)	Ratio of Experimental/Predicted R_{exp}/Rp
1	1347		0.42
2	984		0.57
3	637		0.88
4	717		0.78
5	637		0.88
6	984		0.57
7	1347		0.42
8	1356		0.41
9	1279		0.44
10	1117		0.50
11	396	*	1.41
12	396	*	1.41
13	1117		0.50
14	1279		0.44
15	1356		0.41
30	1259		0.44
31	1259		0.44

Notes:

1) To be read in conjunction with Fig S1.
2) For description of method for calculating the predicted ram failure load see Section 8.10.
3) For each chord member the experimental strain gauge values, at ram failure load, have been extrapolated to determine whether the measured yield stress was exceeded at the ends of the member. An asterisk '*' has been used to indicated the members where the measured yield stress was exceeded at one or both ends.
4) **Chord member failure is safely predicted where yielding '*' coincides with values of R_{exp}/R_p which are greater than, or equal to unity.**

Table 8.7 Comparison of the measured compression branch force at ram failure load with the predicted buckling force for the critical members.

Truss	Critical member	Member length	Measured strut force at ram failure load	Failure mode	Slenderness ratio	Predicted strut buckling force	Ratios	
		L mm	N_1 kN	* = yielding b = buckling	λ kN	N_{b1}	N_{b1}/N_1	$N_1/A_1.\sigma_{e1}$
T1	21	889	79		61	170	2.15	0.43
T2	21	955	91		65	163	1.79	0.37
T2/2	16	955	179	*	65	178	1.00	0.34
T3	14, 19	727	184	*	49	207	1.13	0.58
T4	16, 17	727	226	b & *	31	230	1.02	0.95
T5	20	650	119		42	176	1.50	0.71
T6	22	650	257	*	31	276	1.07	0.94

Notes :
1) To be read in conjunction with Fig S1.
2) The theoretical buckling force has been derived according to BS 5950, Part 1 clause 4.7.
3) Critical member is either i) the member which buckles first.
   or ii) the strut which had the greatest axial force at the ram failure load.
4) The effective length is equivalent to the length of the member, L.
5) Overall buckling of the compression branch occurred only in truss T4.
6) Member yielding (denoted by an asterisk - *) has been defined as the occurrence of extreme fibre yielding at one or more of the strain gauges.

Table 8.8 Comparison of experimental and allowable shear stress in branch member sidewalls at ram failure load (truss T6).

Ram failure load = 560 kN ; (load cycle = 1).

Joint	Shear force	Sidewall lengths		Sidewall thicknesses		Yield Stress	Shear stresses Test	Allow	Ratio
		L_1	L_2	T_1	T_2	σ_e	τ_{test}	τ_{max}	τ_1/τ_{max}
	kN	mm	mm	mm	mm	Nmm^{-2}	Nmm^{-2}	Nmm^{-2}	
1	194	67.2	5.0	3.2	3.2	421	423	243	1.7
2	188	67.2	5.0	3.2	3.1	421	412	243	1.7
3	179	67.2	5.0	3.2	3.1	421	391	243	1.6
4	209	67.2	5.0	3.2	3.2	421	455	243	1.9
5	191	67.2	5.0	3.2	3.1	421	419	243	1.7
6	182	67.2	5.0	3.2	3.1	421	399	243	1.6
7	198	67.2	5.0	3.2	3.2	421	432	243	1.8
8	199	67.2	5.0	3.2	3.2	421	435	243	1.8
9	196	67.2	5.0	3.2	3.2	421	428	243	1.8
10	203	67.2	5.0	3.2	3.2	421	444	243	1.8
11	208	67.2	5.0	3.2	3.2	421	454	243	1.9
12	197	67.2	5.0	3.2	3.2	421	430	243	1.8

Notes :

1) To be read in conjunction with Figs 8.4, 8.5 and S2.
2) For joints 1 - 4 the tie overlaps the strut.
3) For joints 5 - 8 the strut overlaps the tie.
4) For all calculations it has been assumed that the horizontal shear force ($N_1 \cos\theta_1 + N_2 \cos\theta_2$) at an overlapped joint is transferred to the chord face via the sidewalls ($L_1 + L_2$), see Fig 8.4.
5) The calculated shear stress at ram failure load (τ_{test}) has been evaluated along Section A-A, directly above the line of the weld (taken as 5mm above the chord face).
6) From the Von-Mises stress field (Fig 8.5) the direct stress across the shear plane A-A has been assumed to be zero (ie., $\sigma_0 = 0$), this corresponds to a maximum allowable shear stress (τ_{max}) of $\sigma_e/\sqrt{3}$.
7) The permissible shear stress according to BS 5950, Part 1 (clause 4.2.3) is based on the assumption that $\sigma_0 = 0$; $\tau_{max} = \sigma_e/\sqrt{3}$.

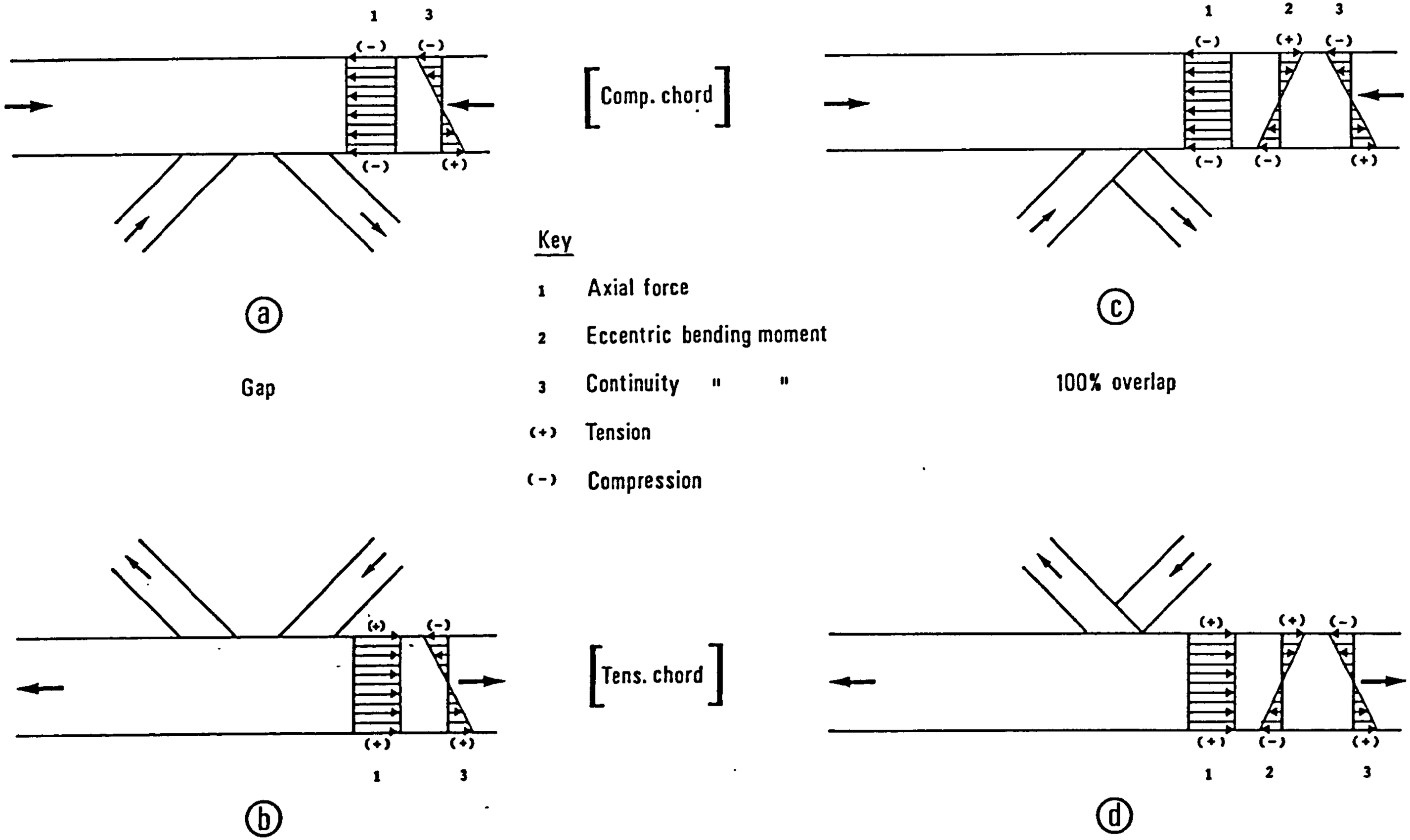

Fig 8.1 Components forming the stress distributions in the chord sections of the gap and 100% overlap joint trusses.

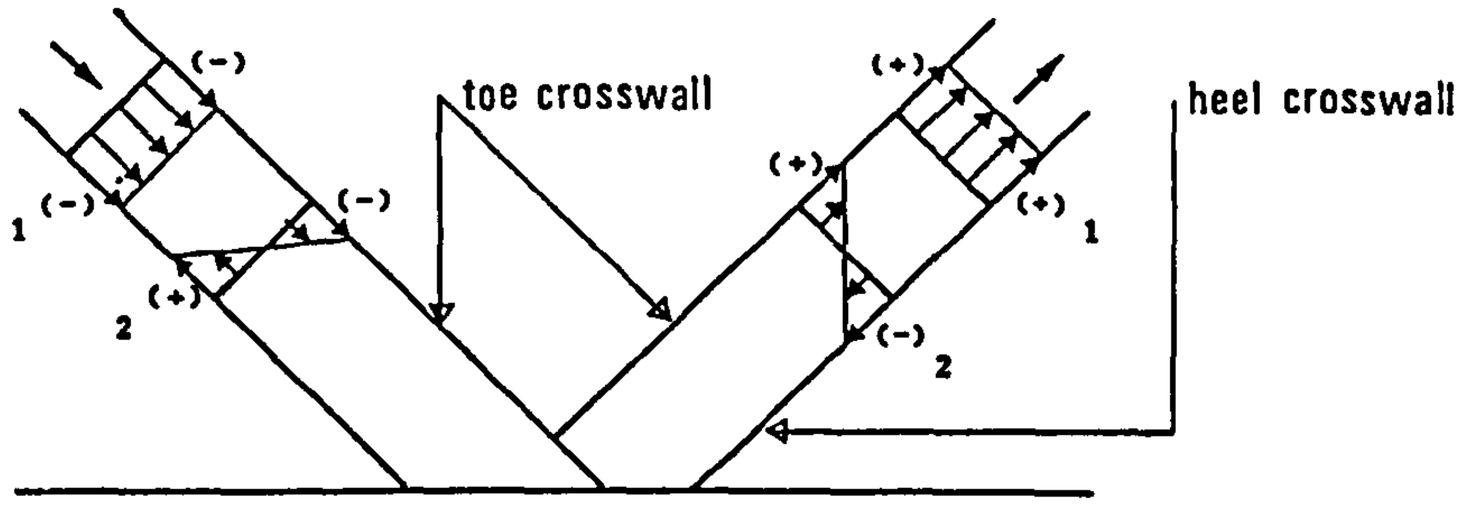

ⓐ Partial overlap

ⓑ 100% overlap [tie/strut]

ⓒ 100% overlap [strut/tie]

Key

1 Axial force.

2 Bending moment due to difference in stiffness between toe and heel crosswalls.

3 " " " " eccentricity bending moment.

(+) Tension.

(-) Compression.

Fig 8.2 Components forming the stress distributions in the branch members of overlap joints.

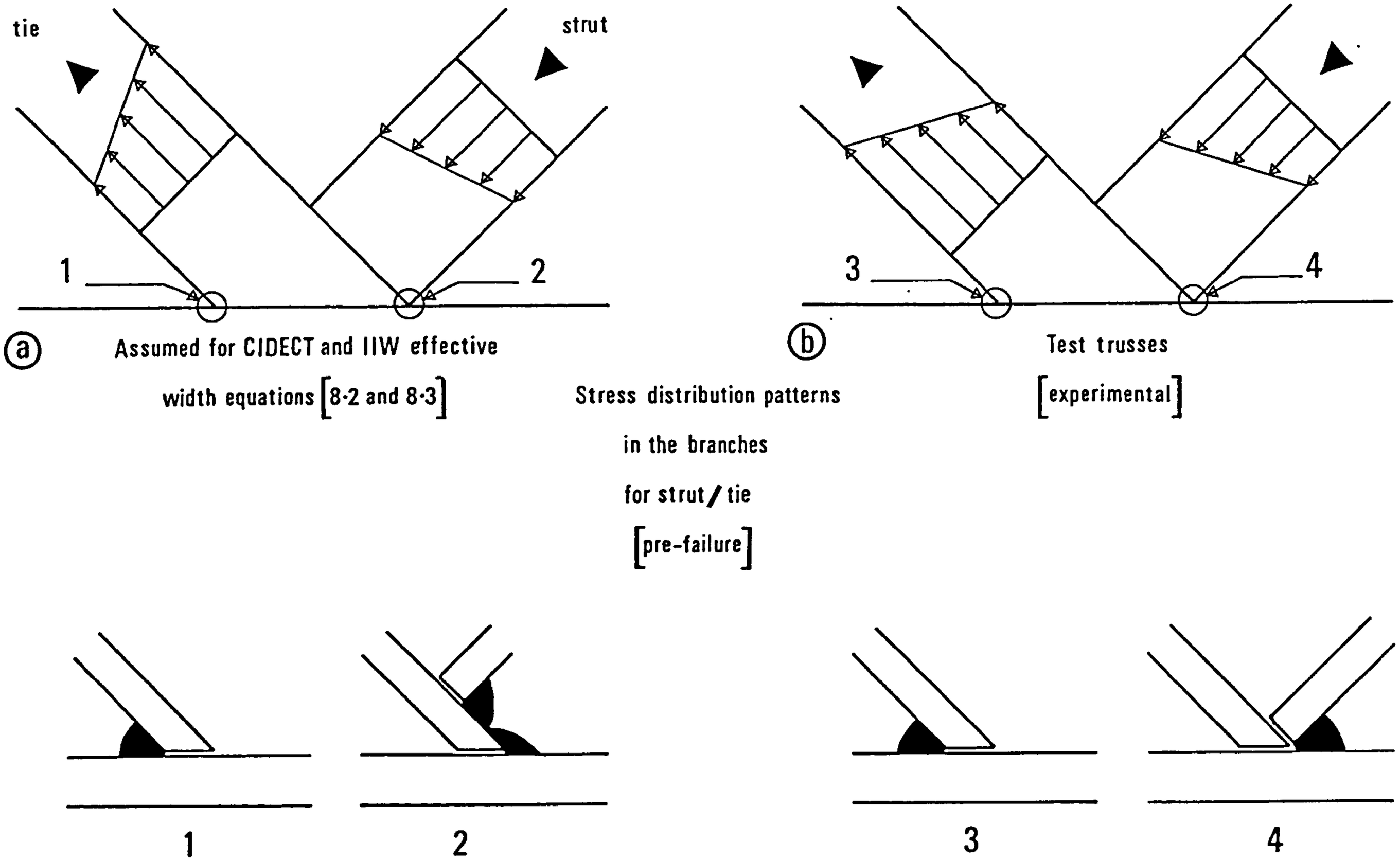

Fig 8.3 Relationship between the weld details in 100% overlap joints and the stress distribution in the branch members. (for joints where the strut overlaps the tie).

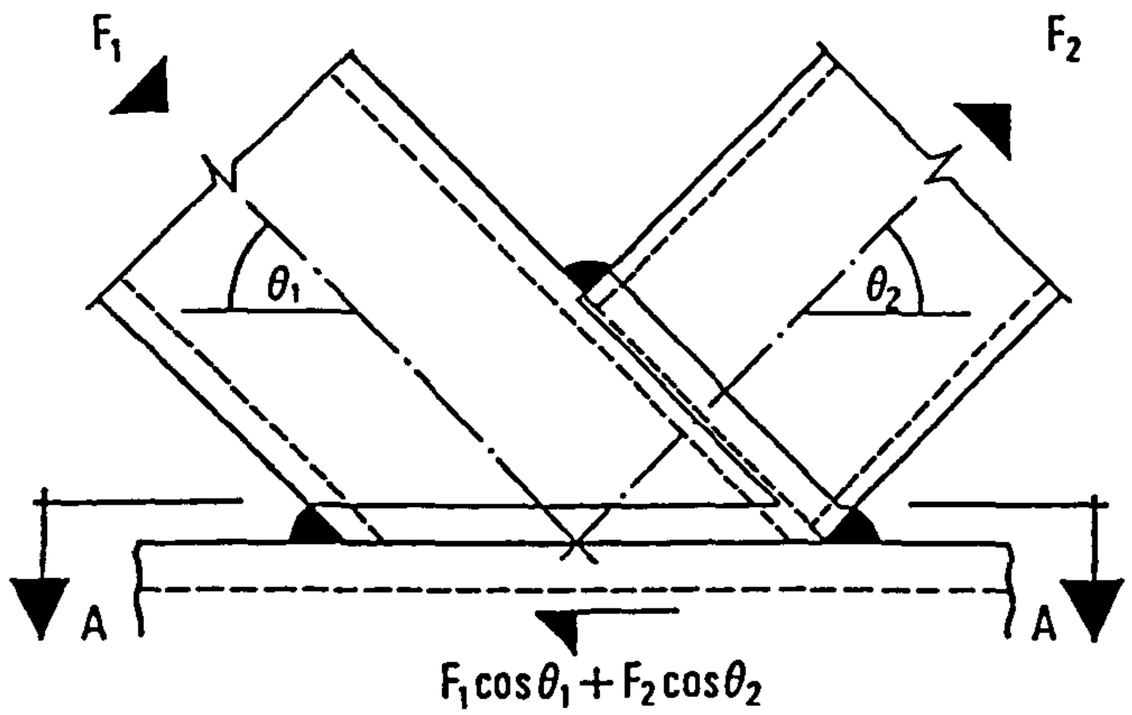

side elevation of 100% overlap joint

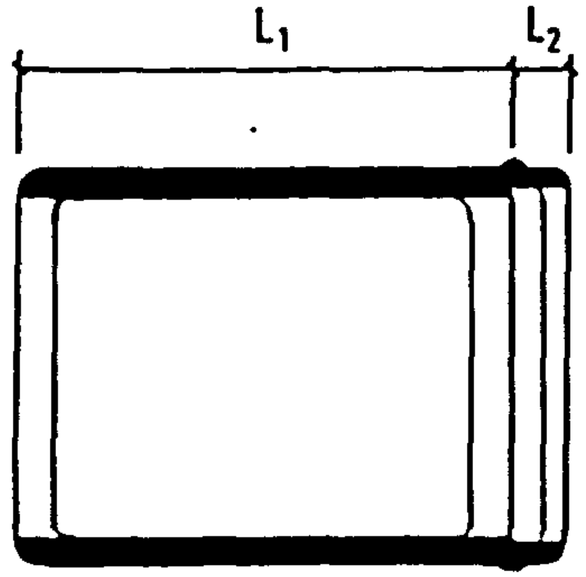

A – A

only sidewalls are assumed to be effective in transferring shear according to BS 5950 (clause 4·2·3)

Fig 8.4 The transfer of shear force between the branch members and the connecting chord face.

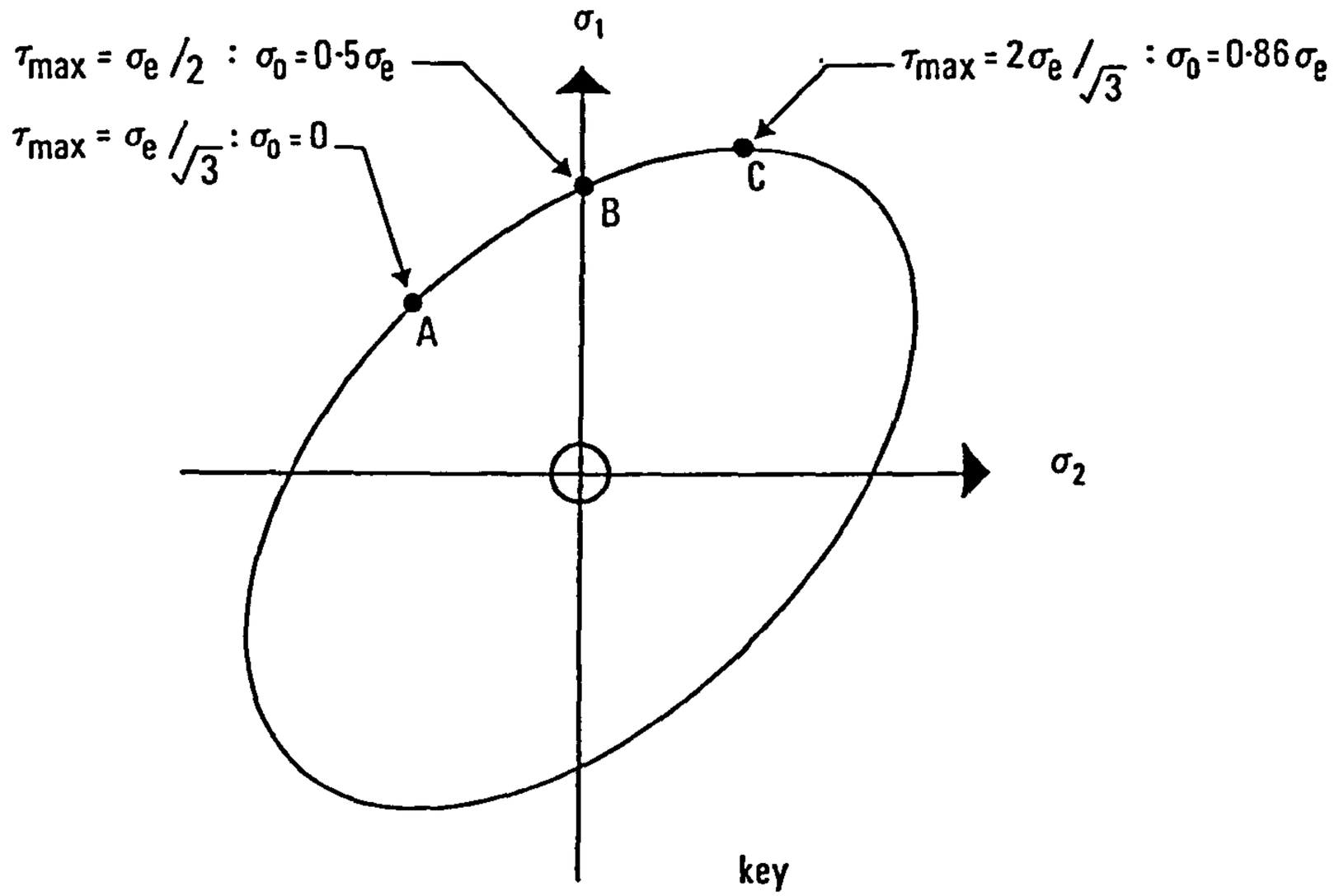

key

σ_1, σ_2	principal stresses
σ_0	direct stress on shear plane A-A
τ_0	shear " " " " "
σ_e	yield stress
τ_{max}	allowable shear stress

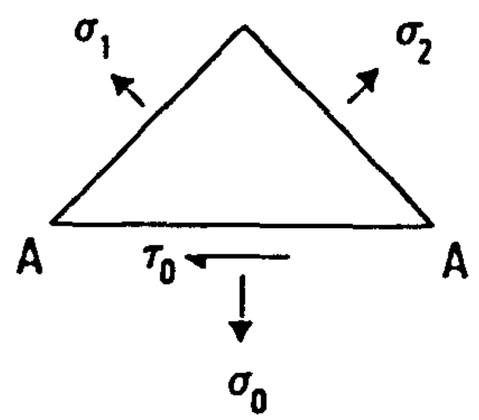

Fig 8.5 Allowable shear stress based on the Von Mises stress field.

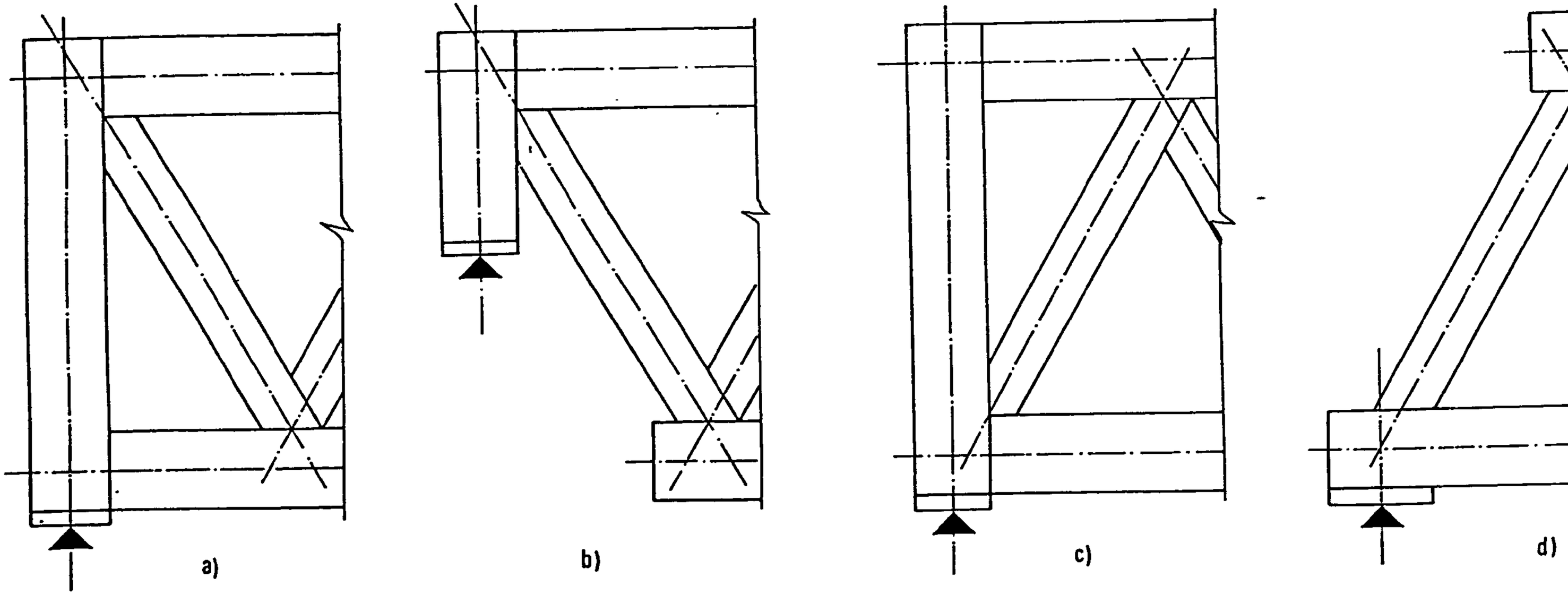

Fig 8.6 Possible end bay configurations.

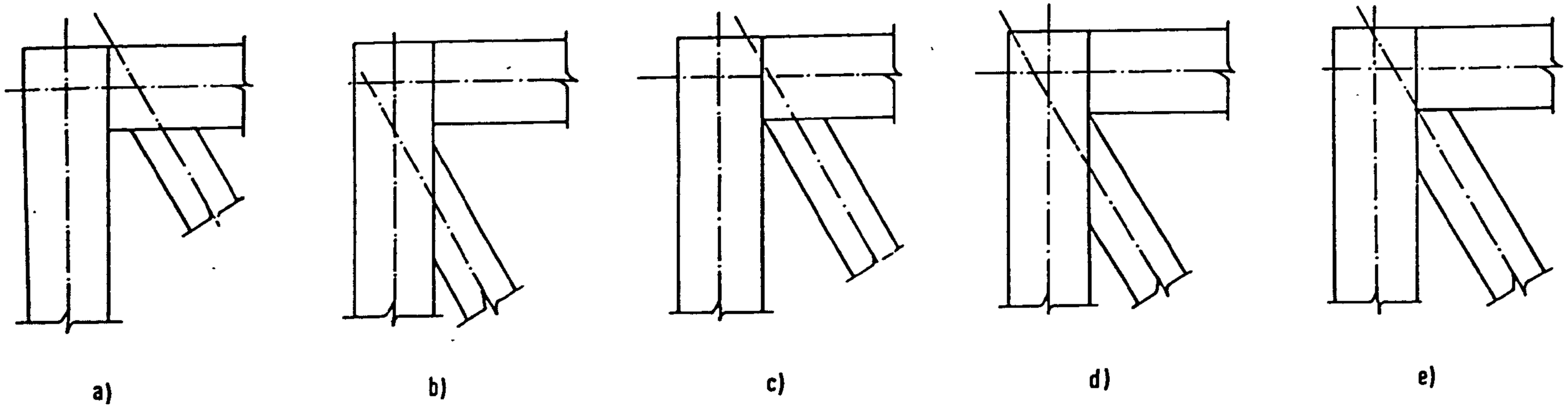

Fig 8.7 Possible corner joint configurations.

CHAPTER 9
CONCLUSIONS AND RECOMMENDATIONS

9.1 Comments

9.1.1 Material variation

Some difficulty was found in obtaining steel of consistent properties. For normal design a specification giving minimum values (as in BS 4360) is adequate. However, for researchers material having consistent properties between samples is all important. In this investigation the wide range of material properties found in material, all supplied at grade 43 caused delays in fabrication, and considerable difficulty in interpretation of results.

9.1.2 Elastic truss behaviour

Various methods of elastic analysis were used in modelling the non-noding trusses including :

(i) simple pin jointed approach which either involved
  (a) an assumed modification of the branch angle to ensure noding, or
  (b) modification of chord centre line to ensure noding
(ii) simple calculations allowing for pin-ended branches, but continuous chords
(iii) stiffness analysis allowing for a range of connection details from rigid joint assumptions to various degrees of axial and rotational flexibility in the joints

For the gap joint truss T1, good agreement was obtained for axial force for the pin jointed assumption - agreement being within 5%.

For the overlapped joint trusses T2 - T6, neither of the pin joint models (i) above gave good results for the branches although the chord forces were predicted to within 5% by (i(b)) above. It was found that branch forces could be over predicted by as much as 20% indicating that the shear forces generated in the chord by the joint eccentricity moments can have a significant effect, by relieving the axial forces in the branches. The agreement between measured axial forces for members of the test trusses and those derived from stiffness analysis where allowance for eccentricity was made was usually within 5%.

The theoretical distribution of moments based on rigid connections for the gap

joint truss (T1) was an indication of the level of the secondary moments. As predicted this test showed that the sense of the chord moments for the six middle bays was single curvature, but the numerical agreement was relatively poor. The predicted moments in the branch members fell well below those obtained in the test. This shows that severe bending moments can occur at the end of branch members in practice, and that more careful modelling of the joint is needed to successfully predict these.

For the 100% overlap joint trusses the agreement of the test results with the rigid jointed model was good where allowance was made for the lack of noding, and points of contra-flexure were clearly seen along the length of most chord bays. It should be noted that in the case of T2, the bending moments in the branches were not only lower than in the corresponding gap joint truss T1 (and were more accurately predicted by rigid joint frame analysis) but were opposite in sense.

In much of the isolated joint testing on overlap joints, failure was found to be associated with local buckling of the connecting chord face adjacent to the heel of the branch tie (failure mode L7). The measured bending moments in the 100% overlap joint trusses showed these to be relieved by the secondary moment shifting the maximum chord moment to the side of the joint with the lower chord axial force. This effect is likely to be particularly advantageous to the 100% overlap joint, and will reduce the incidence of L7 type failures in real trusses compared to isolated joints.

The large moment in the top chord at the truss loading point is of particular interest and is mainly associated with secondary effects. This is typical of such trusses under symmetric loading which produces zero slope at the loading point. It is likely that redistribution of moments at failure can take place for stocky sections but care is required if more slender sections are to be used. This may well be the reason for premature failure in some of the Pisa trusses [5].

9.1.3 Overall truss performance

Load/central deflection graphs for the trusses were obtained. In the T1 gap joint truss departure from linearity occurred at an early stage, and agreement with the theoretical deflections was poor. In the overlap joint trusses linearity was retained nearly up to the point where member yielding occurred. Furthermore there is good agreement with the theoretical truss deflections for most of the range.

9.1.4 Local joint deflection

The difference between gap and 100% lap joints in ram load - local joint deflection curves was immediately obvious. It is clear that local joint deflections under service conditions are unlikely to be a problem with 100% overlap joints where there are no external purlin loads. This is not necessarily the case with large gap joints as seen for the T1 joints. Gap joints are normally designed on the basis of strength, service behaviour being usually considered acceptable if the local deflection is less than 1% of the chord width (=1%b_0).

9.1.5 Joint ultimate strength

It was difficult to assess joint strength independently of the structure strength in the test trusses, particularly when the structures achieved higher strengths by plastic redistribution of moments. Gap joint strengths were assessed according to the CIDECT rules. The best estimates of gap joint strength have been compared with the predicted strength, with and without the chord axial load factor, μ, which was found to be of great importance. Generally the CIDECT approach predicts the joint strengths for gap joints to within 10% of the actual member forces. However the failure load of several tension chord joints was significantly underestimated - this is thought to be due to secondary bending moments in the chord, caused by chord continuity and the build up of residual stresses from successive load cycles.

In the overlap joints design strengths were predicted according to the CIDECT design recommendations and compared with the experimental strengths. Generally the predicted strengths were in excess of the maximum branch member forces achieved, even where joint failure occurred by failure mode L6. This indicates that the CIDECT equations can be unsafe. L7 failure loads have also been tabulated and compared. It was observed that sufficient redistribution took place for failure loads to exceed those predicted, sometimes quite significantly.

9.1.6 Modes of Failure

In the gap joint truss failure occurred when axial force in the critical branch member was less than 50% of the squash force. The majority of failures occurred at the joints and involved deformation of the chord connecting face. For the compression chord local buckling of the chord sidewalls was also evident.

In the 100% overlap joint trusses full joint failures did not occur, i.e. deformation of the chord connecting face was not apparent. The most common mode of failure was overall yielding of the branch members. L6 type strut failure occurred only in truss T6 and L7 chord buckling was observed only once, in truss T2. It is thought that the L7 mode in truss T2 was related to the close proximity of stiffening plates which had been used to repair the chord section which had failed in the previous load cycle. Only two fractures occurred, both in the heat affected zone of the branch wall. Apart from this, weld cracking was not observed in any of the overlap joints.

Extensive yielding of the sidewall of the branches was observed in the area of overlapping for the 100% overlap joints, where the transfer of shear into the chord takes place, and it was thought that a mode of failure associated with this shear transfer might occur. However, no gross deformation took place and the shear transfer was well in excess of that which could be carried by the branch sidewalls in shear. It appears that the presence of the transverse weld at the stiff point where both branch crosswalls meet greatly assists in transferring the horizontal shear. It is likely that the other crosswall also makes some contribution to this action.

9.2 Conclusions

(i) The inherent eccentricity of the 100% overlap joint is not as detrimental to the strength and efficiency of the connection, as traditionally anticipated. Although some chord moment redistribution did occur it did not generally reached the value associated with fully plastic interaction in the chord.

(ii) Elastic plane frame analyses can be successfully used to predict the structural behaviour of overlap joints provided allowance is made for the eccentricity. However, great difficulty arises in deriving a suitable model to describe the behaviour of trusses with gap joints.

(iii) A comparison of the structural behaviour of two almost identical gap and 100% lap joint trusses indicates the latter's considerably improved behaviour in all ways - under elastic and failure conditions. Local joint deflections were much reduced, and linear behaviour observed up to near a much improved collapse load. Although this may not be true for all parameters, it is likely to be so when compared with low values of β and large gaps.

(iv) In the trusses, up to 20% of the load was carried by shear action in the

continuous chords. When this effect is taken into account the branch forces did not usually reach the joint failure values predicted by the CIDECT and IIW joint strength equations, but it was not usually apparent that failure occurred in the joint.

(v) The parameters previously identified appear to be the important ones, although the effect of slenderness (b/t) and angle (θ) have been clarified, as well as the sense of overlapping. The capacity of 100% overlap joints to transfer shear wall in excess (> 50%) of the values allowed in BS 5950 (clause 4.2.3) has been clearly demonstrated for square and rectangular branches (h/b <1) - but is dependent on good quality transverse welds.

(vi) The structural behaviour of 100% overlap joints in trusses compared favourably with that predicted from isolated joints. The low local joint deformation was particularly noticeable. The effect of chord continuity was however particularly noticeable in restricting local chord failure, which had occurred in a large number of previously tested isolated joints. The boundary conditions imposed in isolated joint tests can be very important, particularly when associated with particular modes of failure.

The truss tests showed large chord secondary moments (not associated with chord eccentricity) at the centre point of loading which could cause early failure in slender sections.

(vii) Although the elastic bending moment distribution in the branches was double curvature, where overall buckling occurred the mode was single curvature (in-plane). It was observed that local yielding in the branch members at the joints was responsible for a change from double to single curvature bending. Subsequently, at several joints the branch section became fully plastic before the truss reached the ram failure load. For those compression branches subject to local yielding at the joints it is unlikely that the joints provided any significant rotational restraint against member buckling. This is contrary to the recommendations regarding effective length criteria outlined in clauses 4.7.2 and 4.10[b] of BS 5950 Part 1.

(viii) Simple and safe design recommendations have been identified although care has to be taken with their application.

9.3 General recommendations

> The CIDECT joint strength equations should always be used in conjunction

with a pin-jointed frame analysis (for both gap and 100% overlap joints). This ensures that the joint strength is safely predicted.

> For 100% overlap joints the thinner branch member should always overlap the thicker member in order to utilize the greater shear capacity of the thicker walled section in transferring horizontal shear to the chord face.

> The weld details shown in Fig. 3.3 should be used for gap and 100% overlap joints. For 100% overlap joints the absence of weld along the toe face of the overlapped branch is not detrimental to the strength of the joint. These weld details ensure both ease and economy in the fabrication of 100% overlap joint trusses, without compromising their strength.

> For RHS joints which have both low brace to chord width ratios ($\beta < 0.6$), and slender chord sections ($b_0/t_0 > 20$), 100% overlap joints should be used in preference to gap joints.

9.4 Method for designing the members in a 100% overlap joint truss

The following ('Limit State') design approach is intended for use only in the parameter range that was studied (see Tables 3.1 & 3.2). It is both simple and safe.

Branch members

> Derive the distribution of axial forces in the branch members from a pin-jointed frame analysis.

> Design the tension branches assuming that they develop the full axial capacity based on the specified minimum yield stress (= minimum yield stress x cross-sectional area). However, the compression branches should be designed against overall buckling.

> Design the compression branches against single curvature buckling assuming an effective length equivalent to the true length of the member.

Chord section

> For eccentric joints designers normally assume that the maximum bending stress in the chord section can be evaluated by distributing the eccentricity moment equally either side of the joint. This simplification will lead to the maximum bending stress in a chord member being under-estimated .

> Continuity bending moments in the chord members of 100% overlap joint trusses are significant. Therefore, the distribution of axial and bending forces in the chord sections should be derived from a rigid frame analysis - allowing for joint eccentricity.

> Locate the critical section with respect to the combined axial and bending stresses and design the section according to the specified minimum yield stress.

It should be noted that the design approach outlined above does conflict with certain aspects of the recommendations outlined in clause 4.10 of BS 5950.

(i) For the purpose of calculating the forces in the chord members a rigid frame analysis should be used which allows for joint eccentricity. This is in conflict with clause 4.10[a]. A designer may be tempted to evaluate the bending moment in the chord section of a 100% overlap joint by distributing the eccentricity moment equally either side of a joint. As indicated previously this is not advisable, since it can lead to the maximum bending stress in a chord member being under-estimated .

(ii) For the branch members it has been suggested from the results of this research that the fixity of the connections should not be considered as providing rotational restraint against buckling ie., the effective length of a branch member should be taken as equivalent to the true length of the member. This is in conflict with clause 4.10[b].

9.5 Recommendations for further research

(i) The parameter range needs to be extended in order to assess whether the recommendations outlined in section 9.4 are more generally applicable.

(ii) The influence of concentrated point loads on the strength of 100% overlap joints in a truss environment needs to be assessed.

(iii) For reasons of aesthetics some Architects are now favouring the use of partial overlap joints as opposed to gap or 100% overlap joints. It is therefore

necessary to study the structural behaviour of trusses formed from such joints with the aim of producing simple design guide-lines.

REFERENCES

1 EASTWOOD. W & WOOD. A.A 1970: Welded joints in tubular structures involving rectangular sections. Conference on Joints in Structures, Session A, Paper 2. University of Sheffield.

2 MANNESMANN RESEARCH INSTITUTE 1968: Tests on RHS joints.

3 CIDECT PROGRAMME 5EC : Research into the strength of welded lattice girder joints in structural hollow sections.

4 WARDENIER. J & STARK. J.W.B 1978: The static strength of welded lattice girder joints in structural hollow sections. *Parts 1-10.* CIDECT Final Report 5Q/78/4. Delft University of Technology, Delft, Netherlands.

5 BRITISH STEEL CORPORATION 1977a: Tests on complete girders. CIDECT Draft Report CE 73/95. Tubes Division, Corby, England.

6 BRITISH STEEL CORPORATION 1977b: Tests on isolated joints. CIDECT Report CE 73/96/D. Tubes Division, Corby, England.

7 COUTIE. M.G & DAVIES. G 1981 : The strength of welded gap joints with RHS members. International Conference on Joints in Structural Steelwork. Teeside Polytechnic, Middlesborough, preprint pp. 4.80-4.98.

8 WARDENIER. J, DAVIES. G & INTERNATIONAL INSTITUTE OF WELDING 1981: Design recommendations for hollow section joints - predominantly statically loaded. International Institute of Welding Annual Assembly, Oporto, XV-491-81, revised.

9 WARDENIER. J & DAVIES. G 1981: The strength of predominantly statically loaded joints with square or rectangular hollow section chord. International Institute of Welding Annual Assembly, Oporto, Doc XV-492-81.

10 CIDECT PROGRAMME 5M: Failure load tests on large size RHS Warren joints.

11 MANG. F, BUCAK. O, & HAMMEL. T 1978: Investigations into the behaviour of high tensile steel joints of rectangular hollow sections. University of Karlsruhe, west Germany, IIW Doc XV-416-78.

12 CIDECT PROGRAMME 5T:

13 WARDENIER. J & DE KONING. C.H.M: Rig Comparison Tests. TNO/Stevin Laboratory. INO-IBBC Report No. BI-76-90-35-3-51210, Stevin Report No. 6-26-20, CIDECT Report No. 76-24(5S).

14 GIDDINGS. T.W 1981: Welded joints in tubular construction. International Conference on Joints in Structural Steelwork. Teeside Polytechnic, Middlesbrough, preprint pp. 4.3-4.24.

15 PACKER. J.A & HALEEM. A.S 1981: Ultimate strength formulae for statically loaded welded HSS joints in lattice girders with RHS chords. Proceedings, Annual Conference, Canadian Society for Civil Engineering. Frederiction, Vol 1 pp.331-343.

16 DE KONING. C.H.M & WARDENIER. J 1976: Supplement test results of welded joints in structural hollow sections with rectangular boom. CIDECT Report 76/11/5Q. Delft University of Technology, Delft, Netherlands.

17 PACKER. J.A 1978: A theoretical analysis of welded steel joints in rectangular hollow sections. Ph.D, thesis, University of Nottingham, England.

18 PACKER. J.A 1979: A Computer program for the structural analysis of welded tubular joints with RHS chords. Advances in Engineering Software, 1(4), pp. 153-164.

19 PACKER. J.A 1982: Ultimate strength of overlapped joints in rectangular hollow section trusses. Proceedings- The Institution of Civil Engineers, Part 2, 73, pp.329-350.

20 PACKER. J.A & DAVIES. G 1977: Strut local buckling in trusses of rectangular hollow sections. Proceedings, egional Colloquium on Stability of Steel Structures, Budapest-Balatonf'red, pp.365-371.

21 PACKER. J.A & DAVIES. G 1982: Ultimate strength of of overlapped joints in rectangular hollow section trusses. Proceedings, The Institution of Civil Engineers, Part 2, 73, pp. 329-350.

22 PACKER. J.A 1983: Developments in the design of welded HSS truss joints with RHS chords. Canadian Journal of Civil Engineering, Vol 10, pp.92-103.

23 STELCO INC 1981: Hollow structural sections - design manual for connections. 2nd ed, Hamilton, Ont.

24 PACKER J.A, BIRKENMOE. P.C & TUCKER. W.J 1984: Canadian implementation of CIDECT Monograph No.6. CIDECT Report No. 5AJ-84/9-E.

25 PACKER. J.A, BIRKENMOE. P.C & TUCKER. J.T 1986: Design Aids and Design Proceedures for HSS Trusses. Canadian Journal of Structural Engineering, Vol. 112, No.7.

26 PACKER. J.A 1986: Design examples for HSS trusses. Canadian Journal of Civil Engineering, Vol. 13, No.4, pp. 460-473.

27 BLOCKLEY. D.I 1967: Joints between structural hollow sections in plane frameworks. PhD Thesis, Department of Civil and Structural Engineering, University of Sheffield.

28 SHINOUDA. M.R 1967: Stiffened tubular joints. PhD Thesis, Department of Civil and Structural Engineering, University of Sheffield.

29 MEE. B.L 1969: The structural behaviour of joints in rectangular hollow sections. PhD Thesis, Department of Civil and Structural Engineering, University of Sheffield.

30 DE KONING. C.H.M & WARDENIER. J 1983: The static strength of welded K-joints with rectangular chord. CECA Convention No. 7210 SA 6.606, Stevin Report No. 6-83-4.

31 DASGUPTA. A 1970: The behaviour of joints in tubular trusses. PhD Thesis, Department of Civil Engineering, Nottingham University.

32 DE KONING C.H.M & WARDENIER. J 1979: Tests on welded joints in complete girders made of square hollow sections (CIDECT Programme 5Qg). TNO-IBBC Report No. BI-79-19/0063-3471, Stevin Report No. 6-79-4, CIDECT Report No. 5-Q/79.

33 CZECHOWSKI. A, GASPARSKI. T, ZYCINSKI. J & BRODKA. J 1984: Investigation into the static behaviour and strength of lattice girders made of RHS. IIW Doc. Xv-562-84. 34. Draft Documents at Corby.

34 WARDENIER, J. 1982 : Hollow Section Joints. Delft University Press, Delft, The Netherlands.

35 EDWARDS, M. AND GIDDINGS, T.M. 1974: The behaviour of welded joints in complete lattice girders with RHS chords (Design and Fabrication). CIDECT Report No. 74/3/E.

36 DE KONING, C.H.M, AND WARDENIER, J. 1979: Tests on welded joints in complete girders made of square hollow sections. TNO-IBBC Report No. BI-79-19/0063.4.3471.

37 MARNICHE. M 1988: (N.B title to be determined). M. Phil, thesis, University of Nottingham, England. To be submitted in the summer of 1988.

38 BEN-SALEM. K 1988: (N.B title to be determined). M. Phil, thesis, University of Nottingham, England. To be submitted in the summer of 1988.

39 PACKER. J.A, DAVIES. G & COUTIE. M.G 1978: Gap joint strength of rectangular hollow section trusses. Final Report, International Association for Bridge and Structural Engineering Symposium, Moscow, Vol 2, pp. 177-185.

40 PACKER. J.A, DAVIES. G & COUTIE. M.G 1980: Yield strength of gapped joints in rectangular hollow section trusses. Proceedings, The Institution of Civil Engineers, Part 2, 69, pp. 995-1013.

41 PACKER. J.A, DAVIES. G & COUTIE. M.G 1982: Ultimate strength of gapped joints in RHS trusses. Journal of the Structural Division, ASCE, 108(ST2), pp.411-431.

42 COUTIE. M.G, DAVIES. G, PHILIASTIDES. A, YEOMANS, N 1987: Testing of full-scale lattice girders fabricated with RHS members.pp 98-105 Structural Assessment- The use of full and large scale testing. Butterworths, 1987.

43 CIDECT MONOGRAPH NO. 6 1986: The strength and behaviour of statically loaded welded connections in structural hollow sections, Sections 1-10. Prepared and printed by the British Steel Corporation, Tubes Division Technical Centre, Corby, England.

44 IIW : Design recommendations for hollow section joints predominately statically loaded. International Institute of Welding Document XV-491-81 (Rev).

45 BRITISH STANDARDS INSTITUTION 1985 : BS 5950 Part 1 - Structural use of steelwork in building. British Standards Institution, 2 Park St, London W1A 2BS.

46 BRITISH STANDARDS INSTITUTION 1985 : BS 5135 - Metal arc welding of carbon and carbon-manganese steels. British Standards Institution, 2 Park St, London W1A 2BS.

47 BRITISH STANDARDS INSTITUTION 1972: CP110 - Code of Practice for the structural use of concrete. British Standards Institution, 2 Park St, London W1A 2BS.

48 SOLATRON INSTRUMENTS : Orion delta Data logger ; operating manual for 3530 D & F.

49 T.M.L: Catalogue reference - TML pam E-101 G.

50 KINGSBURY. C.H & ASSOCIATES 1985: Interfacing the Orion Delta with the BBC microcomputer for saving and graphing the logged results. 6 Lea Wood Croft,

Holloway, Matlock, Derbyshire, DE4 5BD.

51 PHILIASTIDES, A. 1988 : Results from the testing of truss T1 - Test programme : Design of rectangular hollow section, overlap joints in a truss environment. SERC Co-operative Research grant no. GR/D/09576., 1984.

52 PHILIASTIDES, A. 1988 : Results from the testing of truss T2 - Test programme : Design of rectangular hollow section, overlap joints in a truss environment. SERC Co-operative Research grant no. GR/D/09576., 1984.

53 PHILIASTIDES, A. 1988 : Results from the testing of truss T2/2 - Test programme : Design of rectangular hollow section, overlap joints in a truss environment. SERC Co-operative Research grant no. GR/D/09576., 1984.

54 PHILIASTIDES, A. 1988 : Results from the testing of truss T3 - Test programme : Design of rectangular hollow section, overlap joints in a truss environment. SERC Co-operative Research grant no. GR/D/09576., 1984.

55 PHILIASTIDES, A. 1988 : Results from the testing of truss T4 - Test programme : Design of rectangular hollow section, overlap joints in a truss environment. SERC Co-operative Research grant no. GR/D/09576., 1984.

56 PHILIASTIDES, A. 1988 : Results from the testing of truss T5 - Test programme : Design of rectangular hollow section, overlap joints in a truss environment. SERC Co-operative Research grant no. GR/D/09576., 1984.

57 PHILIASTIDES, A. 1988 : Results from the testing of truss T6 - Test programme : Design of rectangular hollow section, overlap joints in a truss environment. SERC Co-operative Research grant no. GR/D/09576., 1984.

58 MANG. F, BUCAK. O, HAMMEL. T 1978: Investigation into the behaviour of high tensile steel joints of rectangular hollow sections. Versuchsanstalst fur stahl, holz und steine. University of Karlsruhe, West Germany. IIW Document XV-416-78.

59 HALEEM. R 1977: Determination of ultimate joint strength for statically loaded SHS welded lattice girder joints with RHS chords. Report to CIDECT welded joints group 77/37.